CENOMANIAN–TURONIAN PLATFORM EVOLUTION AND RECORDS OF OAE 2 ON THE DROWNED NORTHERN ARABİAN CARBONATE PLATFORM (SE TURKEY): INTEGRATION OF BIOSTRATIGRAPHY, SEQUENCE STRATIGRAPHY, SEDIMENTOLOGY, AND STABLE ISOTOPES

A THESIS SUBMITTED TO
THE GRADUATE SCHOOL OF NATURAL AND APPLIED SCIENCES
OF
MIDDLE EAST TECHNICAL UNIVERSITY

BY

OĞUZ MÜLAYİM

IN PARTIAL FULFILLMENT OF THE REQUIREMENTS
FOR
THE DEGREE OF DOCTOR OF PHILOSOPHY
IN
GEOLOGICAL ENGINEERING

SEPTEMBER 2020

Approval of the thesis:

CENOMANIAN–TURONIAN PLATFORM EVOLUTION AND RECORDS OF OAE 2 ON THE DROWNED NORTHERN ARABİAN CARBONATE PLATFORM (SE TURKEY): INTEGRATION OF BIOSTRATIGRAPHY, SEQUENCE STRATIGRAPHY, SEDIMENTOLOGY, AND STABLE ISOTOPES

submitted by **OĞUZ MÜLAYİM** in partial fulfillment of the requirements for the degree of **Doctor of Philosophy** i**n Geological Engineering, Middle East Technical University** by,

Prof. Dr. Halil Kalıpçılar
Dean, Graduate School of **Natural and Applied Sciences** _____

Prof. Dr. Erdin Bozkurt
Head of the Department, **Geological Engineering** _____

Prof. Dr. İsmail Ömer Yılmaz
Supervisor, **Geological Engineering, METU** _____

Examining Committee Members:

Prof. Dr. Uğur Kağan Tekin
Geological Engineering, Hacettepe University _____

Prof. Dr. İsmail Ömer Yılmaz
Geological Engineering, METU _____

Assoc. Prof. Dr. Kaan Sayıt
Geological Engineering, METU _____

Prof. Dr. Bilal Sarı
Geological Engineering, Dokuz Eylül University

Prof. Dr. Kemal Taslı
Geological Engineering, Mersin University _____

Date: 20.09.2020

I hereby declare that all information in this document has been obtained and presented in accordance with academic rules and ethical conduct. I also declare that, as required by these rules and conduct, I have fully cited and referenced all material and results that are not original to this work.

Name, Last name : Oğuz Mülayim

Signature :

ABSTRACT

CENOMANIAN–TURONIAN PLATFORM EVOLUTION AND RECORDS OF OAE 2 ON THE DROWNED NORTHERN ARABİAN CARBONATE PLATFORM (SE TURKEY): INTEGRATION OF BIOSTRATIGRAPHY SEQUENCE STRATIGRAPHY SEDIMENTOLOGY AND STABLE ISOTOPES

Mülayim, Oğuz
Doctor of Philosophy, Geological Engineering
Supervisor: Prof. Dr. İsmail Ömer Yılmaz

September 2020, 280 pages

The evolution of the Cenomanian–Turonian (C–T) carbonate platform (northern Arabian Platform) in southeastern Turkey has been embraced with special emphasis on the sedimentology, biostratigraphy, lithostratigraphy, sequence stratigraphy, and stable–isotope geochemistry. The interplay of different sedimentologic features on the ramp type platform is deciphered on the basis of field and subsurface observations, detailed stratigraphic sections, macrofacies, and microfacies analyses, stable $\delta^{13}C$ and $\delta^{18}O$ isotope ratios, and fossil distribution patterns. A new multibiostratigraphic framework is based on planktonic foraminifera, rudists, and calcareous nannofossils supplemented by benthic foraminifera, pithonellids, and roveacrinids. The sequence stratigraphic framework of the Cenomanian–Turonian boundary was constructed and recorded in the transition of the transgressive systems tract (TST) to highstand systems tract (HST), coinciding with a maximum flooding surface. There are three sedimentary sequences that are separated by the C–T sequence boundary. The studied sections indicate a change from TST to HST in shallow to deeper marine deposits. Furthermore, comparisons between the ramp type platform successions and sequence patterns of SE Turkey and those from neighbouring areas allow us to differentiate local, regional, and

global controlling factors of platform evolution within the study area. The microfacies analyses, multibiostratigraphic datings, and paleoenvironmental interpretations suggest that the platform was drowned near the Cenomanian–Turonian Boundary Event (CTBE) into shallow–water environments.as a result of changing environmental conditions. A filament event is also recorded around the boundary. On a global scale, the filament event beds illustrate sea–level rise related to eustacy and/or climatic change. The abundance of filaments close to the C–T boundary is a biological marker of high organic productivity resulting in a climatic change to warmer conditions. The prevailing higher sea–level conditions were then favourable to the accumulation and preservation of organic–rich facies, characteristic of the Oceanic Anoxic Event 2 (OAE 2). Regional/local subsidence and a coeval sea–level rise during the late Cenomanian to early Turonian interval were the cause of the drowning of the platform, including regional anoxia at the northern Arabian Platform linked to the OAE 2. Carbon–isotope stratigraphy of these successions in shallow–water environments revealed a positive shift $\delta^{13}C$ (V–PDB) values that reached between 0.21‰ and 2.15‰ and represent the CTB interval excursion pointing to the presence of OAE 2. These results spotlight the potential use of carbon isotopes as a dating and high–resolution correlative tool in shallow–water carbonate rocks and help to elucidate the timing of oceanographic events affected the area that we studied. In particular, it is suggested that the highest rate of a relative, possibly tectono–eustatic sea–level rise took place during the latest Cenomanian, that was followed by the global oceanic anoxic event (OAE 2) around the CTB interval, and that peak transgression or maximum flooding was achieved during the early Turonian in this region. The time difference between the end of the OAE and the establishment of a shallow platform is attributed to the Turonian sea–level rise and tectonic effect.

Keywords: Cenomanian–Turonian, Carbonate Ramp Platform, Northern Arabian Platform, Oceanic Anoxic Event 2, Integratted Biostratigraphy, Sequence Stratigraphy, Stable Isotopes ($\delta^{13}C$ and $\delta^{18}O$)

ÖZ

SENOMANİYEN–TURONİYEN YAŞLI BOĞULMUŞ KUZEY ARAP KARBONAT PLATFORMU'NDA (GÜNEYDOĞU ANADOLU), OAO 2 KAYITLARI VE EVRİMİ: BİYOSTRATİGRAFİ SEKANS STRATİGRAFİ SEDİMANTOLOJİ VE DURAYLI IZOTOP JEOKİMYA BÜTÜNLEŞİMİ

Mülayim, Oğuz
Doktora, Jeoloji Mühendisliği
Tez Yöneticisi: Prof. Dr. İsmail Ömer Yılmaz

Eylül 2020, 280 sayfa

Bu çalışmada Türkiye'nin güneydoğusundaki Senomaniyen–Turoniyen yaşlı yokuş tipi karbonat platformunun (kuzey Arap Platformu) evrimini, sedimantoloji biyostratigrafi litostratigrafi sekans stratigrafi ve duraylı–izotop jeokimyasını kapsamaktadır. Karbonat platformundaki farklı sedimantolojik ve jeodinamik özelliklerin birbiri ile olan etkileşimi, saha ve yeraltı gözlemleri, detaylı stratigrafik kesitler, makrofosil ve mikrofosil analizler, $\delta^{13}C$ ve $\delta^{18}O$ izotop değerleri ve fosil dağılım modelleri temelinde açıklanmıştır. Biyostratigrafik çerçeve, başlıca planktonik foraminiferler, rudistler ve kalkerli nannofosiller üzerine kuruludur. Ancak elde edilen veriler bentik foraminiferler, pithonellidler, algler ve roveakrinidler ile de desteklenmiştir. Senomaniyen–Turoniyen sınır birimlerinin transgresif sistem çökelleri (TSÇ) ile yüksek deniz seviyesi sistem çökelleri (YSÇ) geçişinde, ve bir maksimum sellenme yüzeyine denk gelecek şekilde çökeldiği belirlenmiştir. İstif Senomaniyen–Turoniyen sekans sınırı ile ayrılan üç tortul sekans paketini içermektedir. Çalışma alanı sığ deniz çökellerinden, göreceli derin deniz çökellerine, YSÇ'den TSÇ'ye bir değişimi göstermektedir. Ayrıca, Türkiye'nin güneydoğusundaki ve komşu bölgelerden karbonat yokuş tipi platformlar arasındaki karşılaştırmalar, çalışma alanındaki platform evriminin yerel, bölgesel ve küresel kontrol faktörlerini

ayırt etmemize de olanak tanımaktadır. Mikrofasiyes analizleri, çoklu–biyostratigrafik yaşlandırma ve eski ortam yorumları, platformun Senomaniyen–Turonyan Sınır Olayı (CTBE) yakınlarında değişen çevresel koşulların bir sonucu olarak sığ su ortamlarında boğulduğunu göstermektedir. Ayrıca, S–T sınırında bir filaman olayı da kaydedilmiştir. Küresel ölçekte, filaman olayı, östatik ve/veya iklim değişikliği ile ilgili deniz seviyesindeki yükselişi göstermektedir. STSO'ya yakın filamanların bolluğu, iklim değişikliğine bağlı olarak ortamın daha da ısınması sonucunda yüksek organik üretkenliğin biyojenik bir göstergesidir. Hakim olan yüksek deniz seviyesi koşulları, okyanusal anoksik olayı 2' nin (OAO 2) karakteristik özelliği olan, organik maddece zengin fasiyeslerin birikmesi ve korunması için elverişlidir. Bölgesel/yerel tektonizmanın etkisi, Senomaniyen'in sonundan Turoniyen başlarına kadar deniz seviyesindeki yükseliş, Senomaniyen–Turoniyen okyanusal anoksik olayı 2'ye bağlı kuzey Arap platformundaki bölgesel anoksiznasının de dahil olduğu platformun boğulmasının ana nedenidir. Sığ sularda yer alan bu istiflerde yapılan karbon–izotop stratigrafisinde, ‰ 0.21 ile ‰ 2.15 arasında değişen değerlere ve Senomaniyen–Turoniyen Sınırı (STS) aralığında oluşan OAO 2 temsil eden pozitif bir değişim ^{13}C (V–PDB) değerleri saptanmıştır. Bu sonuçlar, sığ su karbonat kayaçlarının karbon izotopları ile yaşlandırması ve yüksek çözünürlüklü karşılaştırılarak bir araç olarak potansiyel kullanımını vurgulamakta ve çalıştığımız alanı etkileyen okyanusal olayların zamanlamasının aydınlatılmasına yardımcı olmaktadır. Özellikle, göreceli ve muhtemel tektonik–östatik bir deniz seviyesi artışının en yüksek oranının erken Turoniyen sırasında deniz yükselmesi veya en fazla sellenme gerçekleştiği ortaya konmuştur. OAE 2 'nin sonu ile sığ bir platformun kurulması arasındaki zaman farkı, Turoniyen deniz seviyesinin yükselmesine ve tektonik etkiye bağlanmaktadır.

Anahtar Kelimeler: Senomaniyen–Turoniyen, Yokuş Tipi Karbonat Platform, Kuzey Arap Platformu, Okyanusal Anoksik Olayı 2, Bütünleşik Biyostratigrafi, Sekans Stratigrafi, Duraylı İzotoplar ($\delta^{13}C$ ve $\delta^{18}O$

To my “the one and only” wife, Gülden and “pretty little son”, Gencer İlber

“Research is to see what everybody else has seen, and to think what nobody else has thought.”

Albert Szent–Gyorgi

ACKNOWLEDGMENTS

I would like to express my sincere gratitude to Prof. Dr. İsmail Ömer Yılmaz, my supervisor, for his patient guidance, enthusiastic encouragement, immense knowledge, numerous discussions, and helpful suggestions for this research work. His guidance helped me in all time of research and writing of this thesis. Besides my supervisor, I would like to thank my committee members: Prof. Dr. Uğur Kağan Tekin, Prof .Dr. Bilal Sarı, Prof. Dr. Kemal Taslı, and Assoc.Prof. Dr. Kaan Sayıt, for their encouragement, insightful comments, hard questions, and providing me with a lot of suggestions to improve my research work.

Thanks are due to Prof. Dr. Sacit Özer (DEU retired, İzmir/Turkey), who specified rudists and reviewed part of the manuscript and for his guidance, advice, criticism, encouragements, and insight throughout the research.

I am grateful to Dr. Remzi Aksu (retired, TPAO) for sharing his experiences during the fieldwork.

I am grateful to Prof. Dr. Bruno Ferre (Saint Étienne du Rouvray, France), for his valuable contributions and introduction to roveacrinids and his help in roveacrinids specification. I furthermore thank the him for his guidance, critical reading, careful recommendations, and constructive criticism that greatly improved this thesis.

I would also like to thank Prof. Dr. Michael Wagreich (Vienna University, Austria), for his contributions to the calcareous nannofossils. Prof. Dr. Jens Wendler to thanked (Bremen University, Germany), for his contributions to the pithonellids.

Special thanks go to Zeynep Macide Yücel (Director of Sedimentology) in Research Center (ARGEM) and her team for their supports in Ankara, and their valuable help in the laboratory.

I owe to thank Adıyaman District Management (Geology Department), Murat Sargınalp, Mahmut Utmanoğulları, and Recep Tofan for their help and for logistic support in during my field studies.

I appreciate thanking Dr. Selin Suer for helping in performing the stable isotope analysis and grateful to Center Laboratory of the Middle East Technical University for stable isotope analyses.

I wish to thank my colleague and friend Ali Rıza Çığrı, in Adıyaman for his help with fieldwork for helping me get through the difficult times, and the care he provided.

I would also like to thank my colleague and friend Tufan Tığlı, in Ankara for his help in Petrel software.

This work is partially funded by the Scientific and Technological Research Council of Turkey under grant number TUBİTAK 118Y425 and supported by the BAP (Scientific Research Projects) of Middle East Technical University with Project Number: 2844. TPAO is lso acknowledged for providing the subsurface data.

I am most grateful to my friends for their friendships, favors and endless encouragement during my studies. My special thanks are for Tufan Tığlı, Aycan Yıldırım, Seren Sert, Osman Merey, Özkan Kaya and Dekant Kıran for their patience and tolerance during my studies. Finally, I would like to acknowledge everybody who was important to the successful realization of the thesis, as well as expressing my apology that I could not mention personally one by one.

As always it is impossible to mention everybody who had a contribution to this work however there are those whose spiritual support is even more important. I would like to express my special thanks to my wife Gülden Mülayim for her understanding, patience, and endless support. I feel a deep sense of gratitude for her who formed part of my vision and taught me good things that really matter in life.

TABLE OF CONTENTS

ABSTRACT……...v

ÖZ.....vii

ACKNOWLEDGMENTS.....x

TABLE OF CONTENTS xx

LIST OF TABLES xvixviii

LIST O F FIGURES.....xix

LIST OF ABBREVIATIONS xxxix

CHAPTERS

1. INTRODUCTION.....1

1.1 Purpose and Scope…...……..……..…….....1

1.2 Geographic Setting…….……..…….…… ……..5

1.3 Methods of Study…….……..…….…… ……....5

1.4 Previous Studies…….……...……...…….……...…11

1.4.1 Previous Studies About the Cretaceous Autochthonous Sequences in the SE Turkey 11

1.4.2 Previous Studies in the Cenomanian–Turonian Anoxic Event (OAE 2) Studies and OAE 2 in Turkey and Arabian Platform……..……14

2. GEOLOGICAL SETTING AND STRATIGRAPHY…… …….17

2.1 Cenomanian–Turonian Paleogeography……...……....……18

2.2 Regional Tectonic Setting…...……..…….……....21

2.3 Regional Stratigraphy…….……...…… ……25

2.4 Stratigraphy of Cretaceous Rock Units……...…….…….....…..25

2.4.1 Mardin Group.. 27
2.4.1.1 Areban Formation 28
2.4.1.2 Sabunsuyu Formation……..……..…...28
2.4.1.3 Derdere Formation.....28
2.4.1.4 Karababa Formation……...……..……..…… ……..29
2.4.2 Adıyaman Group……...…...…… ……....29
2.4.2.1 Karaboğaz Formation 29
2.4.2.2 Sayındere Formation 30
2.4.3 Şırnak Group 30
2.4.3.1 Kastel Formation 30
2.4.3.2 Terbüzek Formation 31
2.4.3.3 Besni Formation 31
2.4.3.4 Germav Formation.....31
2.5 Lithostratigraphy……...…...……..……..…….....32
2.5.1 Revision of Cenomanian–Turonian Lithostratigraphic Depositional Units in the SE Turkey……..……..…..……..…32
2.5.2 Lithostratigraphic Nomenclature……....…… .……32
2.5.2.1 Derdere Formation……..…… .……...36
2.5.2.2 Karababa–A Member……..……..……...39
2.5.3 Isopach Maps…… ..…..…....41
2.6 Lithostratigraphy of the Stratigraphic Sections…… ..…….44
2.6.1 Sabunsuyu Stratigraphic Section…….…….. ...……..44
2.6.2 İnişdere Stratigraphic Section……..…… ...…...…..52
2.6.3 Türkoğlu Stratigraphic Section……..…… ...……...…57

3. BIOSTRATIGRAPHY……...……..…63

3.1 Macro– and Microfossil Assemblages……...……...…63

3.1.1 Roveacrinids……...…….....64

3.1.2 Rudists..... 73

3.1.3 Planktonic Foraminifera..... 85

3.1.4 Benthic Foraminifera……...…… ……..102

3.1.5 Calcareous Nannofossils…...…… ……....112

3.1.6 Pithonellids.…….…….....113

4. MICROFACIES ANALYSES AND SEDIMENTOLOGY...……...117

4.1 Results of Point–Counting and Measurements…….…….…… ……..118

4.2 The Determination of Ramp Microfacies Types (RMF types)……..…124

4.1.1 Microfacies of the Derdere–A Member (Derdere Formation).....126

4.1.1.1 Mf–1: Non–Laminated, Silt–Bearing Pelagic Lime Mudstone 126

4.1.1.2 Mf–2: Pithonellid–Planktonic Foraminifera Ws–Ps 127

4.1.1.3 Mf–3: Pithonellid–Roveacrinid Wackestone–Packstone 130

4.1.1.4 Mf–4: Bioclastic Roveacrinoidal Wackestone 130

4.1.2 Microfacies of the Derdere–B Member (Derdere Formation)…… ...132

4.1.2.1 Mf–5: Bioclastic Dolowackestone 132

4.1.2.2 Mf–6: Peloidal Dolowackestone–Dolopackstone 133

4.1.2.3 Mf–7: Benthic Foraminiferal Dolowackestone 135

4.1.2.4 Mf–8: Dolomudstone..... 136

4.1.2.5 Mf–9: Fine Crystalline Planar–s Dolomite Mosaic..... 137

4.1.2.6 Mf–10: Medium Crystalline Planar–e–s Dolomite Mosaic..... 138

4.1.2.7 Mf–11: Coarse Crystalline Planar–e–s Dolomite Mosaic 139

4.1.3 Microfacies of the Derdere–C Member (Derdere Formation)……...139
4.1.3.1 Mf–12: Bioturbated Wackestone.....140
4.1.3.2 Mf–13: Rudist Floatstone–Rudstone.....141
4.1.3.3 Mf–14: Intraformational Breccia 142
4.1.3.4 Mf–15: Poorly Sorted Intraclastic Peloidal Ps–Gs……. 143
4.1.3.5 Mf–16: Bivalve–Roveacrinid Floatstone 145
4.1.3.6 Mf–17: Benthic Foraminifera Bioclastic Silty Ws–Ps.....145
4.1.3.7 Mf–18: Peloidal Packstone.....147
4.1.3.8 Mf–19: Bioclastic Wackestone–Packstone 148
4.1.3.9 Mf–20: Peloid Bioclastic Silty Packstone.....150
4.1.3.10 Mf–21: Ooidal Grainstone 151
4.1.3.11 Mf–22: Non–Burrowed Lime Mudstone. 152
4.1.4 Microfacies of the Karababa–A Member (Karababa Formation).…...153
4.1.4.1 Mf–23: Finely Laminated, Silt–Bearing Pelagic Lime Ms.....153
4.1.4.2 Mf–24: Planktonic Foraminifera Bearing Ws–Ps……154
4.3 Diagenesis…….……...……..……155
4.3.1 Micritization.…….…… ……..…..….....155
4.3.2 Dissolution.……..… ……..…..... 156
4.3.3 Cementation…… …..…..…..... 157
4.3.4 Neomorphism…….. …..…..... 158
4.3.5 Dolomitization.……. ……..…..…..... 159
4.3.6 Stylolites and Dissolution Seams.……...……...….....159
5. DEPOSITIONAL ENVIRONMENTS…….…….. .…….161
5.1 Depositional and Palaeoenvironmental Scenario…….……..…….....161

5.1.1 Middle–Late Cenomanian……..…… .……..……162

5.1.2 Latest Cenomanian…… ……..……...163

5.1.3 Early Turonian…….…… ……...166

5.2 Palaeoenviromental change Across the Cenomanian–Turonian boundary..167

6. SEQUENCE STRATIGRAPHY…….…… .…....171

6.1Sequence Stratigraphic Framework of the Sabunsuyu Section.…… ……..171

6.1.1 Depositional Sequence–1……..……..… ……172

6.1.2 Depositional Sequence–2……..…… …….174

6.1.3 Depositional Sequence–3…….……..... .....….175

6.2 Sequence Stratigraphical Comparison for Sabunsuyu Section…… ……...176

6.3 Sequence Stratigraphic Framework of the İnişdere Section…….....…...178

6.4 Sequence Stratigraphical Comparison for İnişdere Section…… .……...180

7. RECORDS OF CRETACEOUS OCEANOGRAPHIC ANOXIC EVENTS ON THE DROWNED ARABIAN PLATFORM…….…… .……..183

7.1 Drowning Platform…..…….. …….....183

7.1.1 Drowning Unconformity…….…… .. ……184

7.1.2 Anoxia…….…… .. ……186

7.2 Stable Isotope Analyses and OAE 2…….…….…….……... …….187

7.2.1 Türkoğlu Stratigraphic Section–Upper Part…… ... ……...193

7.2.2 Türkoğlu Stratigraphic Section–Lower Part….……..…….... ……195

7.2.3 İnişdere Stratigraphic Section...…….…… .. ….……196

7.2.4 Sabunsuyu Stratigraphic Section...…….…… .. ……198

7.2.5 CM–14 Borehole Section…… ... ……...199

7.3 Timing and Correlation Based on the $\delta^{13}C$ Excursion…..…… ... ……..200

7.4 Diagenetic Effect……..……...……...202

7.5 Biostratigraphy Versus Isotope Stratigraphy……..…… ……203

7.6 Possible mid–Cenomanian Anoxic Event in SE Turkey…..…… ...……...206

7.7 Biotic Contributions to Records of Anoxic Events……..…….…….207

8. PALAEOECOLOGICAL TAPHONOMIES FOR PALEOENVIRONMENTAL PROXIES AND CORRELATION TO ADJACENT AREAS.…… ….....208

8.1 Palaeoenvironmental Significance of Pithonellids……..…..…. ...…….208

8.1.1 Nutrient Availability and Water Depth…..……..……..209

8.1.2 Upwelling Relations…..……..…..210

8.2 Palaeoenvironmental Significance of Filament Marker Beds..… ...….....211

8.2.1 Petrographic Characteristics..…… .……...215

8.2.2 Filaments, Depositional Environment, and OAE 2…… ……..219

8.2.3 Filament Event and Carbon–Isotope Correlation……..……..…..221

8.3 Stratigraphic Meaning and Palaeogeographic Potential of Roveacrinid.. ..226

8.3.1 Palaeoecological Proxies and Correlation to Adjacent Areas…..….226

8.4 Rudist Shell Concentrations……...……..…...227

8.4.1 Taphonomic Aspects of Rudists…….....… …….....228

9. CONCLUSIONS……..……..…229

REFERENCES…… .…….233

APPENDICES…… ……..273

A.Abstracts of Published Papers……..……..273

CURRICULUM VITAE……279

LIST OF TABLES

TABLES

Table 1.1 Location and GPS coordinates of all stratigraphic sections 5

Table 4.1 Petrographic and point counted data of the outcrop and borehole samples……...118

Table 4.2 Percentage data of the quantitative analysis using point count data fort he measured outcrop and borehole sections……...120

Table 4.3. Grain size measurement of some samples of the outcrop and borehole sections……...123

Table 7.1 $\delta^{13}C$ and $\delta^{18}O$ data from this study. # indicates negative $\delta^{13}C$ values and * indicates samples with relatively lower $\delta^{13}C$ values than those of adjacent samples, displaying as spikes in the carbon isotope curve……189

Table 7.2 Cross–plot of $\delta^{13}C$ and $\delta^{18}O$ values of all the samples from this study…192

LIST OF FIGURES

FIGURES

Figure 1.1. Location map of the study area. A; showing tectonic units in SE Anatolia, (after Mülayim et al. 2016), location of outcrops and boreholes sections in the study area B; Geographical map of SE Turkey on the Arabian platform (after Sharland et al. 2001)……..4

Figure 1.2. Dolomite textures and classification from Machel (2004) after Gregg and Sibley (1984), Sibley and Gregg (1987)…….……...8

Figure 1.3. Cretaceous trends and excursions in carbon stable isotopes and 87Sr/86Sr and Oceanic Anoxic Events (OAE) (after Gradstein et al. 2004)……..16

Figure 2.1. The palaeogeographic maps of the Cenomanian (96.6 Ma) and Turonian (91.1 Ma) (Scotese, 2014)..……...19

Figure 2.2. The palaeotectonic maps of the Middle East–northern margin of the Arabian Plate–Cenomanian (99.6–93.5 Ma) (Barrier and Vrielynck, 2009).…...…20

Figure 2.3. Late Early Permian palinspatic reconstruction map (after Stampfli and Borel, 2002). The modifications include the illustrations for the incipient faults of NeoTethys rifts as accommodative structures to lengthening related to progressive shortening caused by the collision between Gondwana and Laurussia and for the formation of sporadic uplifts located at the Northern Arabian Plate…….. 22

Figure 2.4. Simplified geological map of the northwestern part of Turkey (after Şenel, 2002 and Mülayim et al. 2019b). A. Tectonic map of Turkey showing the major sutures and continental blocks (after Okay and Tüysüz, 1999), B. The geographic location of SE Turkey in the northernmost part of the Arabian Platform (after, Sharland et al. 2001).…..……...24

Figure 2.5. Generalized stratigraphic section of the southeast Turkey. (Güven et al. 1991).……...26

Figure 2.6. Generalized stratigraphic section of the study area and surroundings in SE Anatolia (after Mülayim et al. 2016) 27
Figure 2.7. The correlation chart of the Cenomanian–Turonian formations in the SE Turkey 34
Figure 2.8. Generalised lithological log of the Boreholes with gamma–ray in Derdere Members A, B and C respectively and Karababa–A Member..... 35
Figure 2.9. Isopach map of the Derdere Formation in SE Turkey..... 42
Figure 2.10. Isopach map of the Karababa–A Member in SE Turkey..... 43
Figure 2.11. Geological map of the study area including the position of the Sabunsuyu stratigraphic section (after Şenel, 2002)..... 44
Figure 2.12. (A) General field view of the Sabunsuyu strtatigraphic succession (B) Field view of the contact between the Derdere and Karababa formations (C) Pre–drowning rudist–rich limestone beds belong to the top of the Derdere Formation. (D) The Derdere–C Member where host carbonate facies are mainly mud– to wackestone, including many bivalve clasts. (E) Bioclastic limestones in the upper part of the Derdere Formation..... 45
Figure 2.13. Outcrop evidence of intercalation of dolomitic limestone and shale beds at the base of the Derdere Formation. Exogyrine oysters are observed in shale layers, which are indicated in the area (red square, A), just below the hammer..... 47
Figure 2.14. Log of the Sabunsuyu stratigraphic section and sampling levels. Showing the distribution of fossils and lithological changes in composition (after Mülayim et al., 2020)..... 50
Figure 2.15. Geological map of the study area including the position of the İnişdere stratigraphic section. (after Sungurlu, 1974)..... 52
Figure 2.16. (A) Field view of the contact between the Derdere and the Karababa formations. (B) The Karababa–B Member includes irregular chert nodules and

horizons where host muddy carbonate facies are mainly lime mudstone and fine–bioclastic wackestone. (C) Pre–drowning well–bedded (light grey), limestone beds belonging to the Derdere Formation, and post–drowning thinly bedded pelagic condensed carbonates (dark grey) belonging to the Karababa–A Member which lie parallel to the drowning surface. (D) The upper unit where host carbonate facies are mainly mud– to wackestone, including many bivalve clasts. (E) Well–bedded Derdere Formation limestone includes thin–bedded dolomitic beds……....53

Figure 2.17. Log of the İnişdere stratigraphic section and sampling levels. Showing the distribution of fossils and lithological changes in composition……...56

Figure 2.18. Geological map of the study area including the position of the Türkoğlu stratigraphic section. (after Usta et al. 2015)…….57

Figure 2.19. A. Field view of the contact between Derdere Formation, and Karababa–A Member. B. The Derdere–A Member includes organic–rich thin–bedded limestone. C. Nodular cherty limestone in the Karababa–B Member. D. General view of the contact between the Areban, Sabunsuyu and Derdere formations. E. Rudist remains in the Derdere–C Member. F. Laminated dolomudstone in the Derdere–B Member……58

Figure 2.20. Log of the Türkoğlu stratigraphic section and sampling levels. Showing the distribution of fossils and lithological changes in composition…….…61

Figure 3.1. Morphological reconstitution of a complete roveacrinid individual with orientation of possible section planes (after Ferré and Berthou, 1993, 1994; Ferré and Granier, 1997a, b, 2001; Mülayim et al. 2018).……66

Figure 3.2. The thin–section photographs of roveacrinid ossicles, lower–middle Cenomanian, Adıyaman area, SE Turkey. A. *Roveacrinus communis* Douglas *(= R. derdereensis* Manni, in Farinacci and Manni), Obl/sub–TS–Rad and OblS–NBrn, core sample B–1–1484.1; B. *Roveacrinus communis* Douglas TS–Rad, Tg/LgS–Rad, and Lg/TgSRad, core sample S–2–2204.1; C. *Roveacrinus* cf. *alatus* Douglas OblS–Rad, core sample Bz–1–4–8; D. *Roveacrinus* cf. *alatus* Douglas, (TS–Rad) and

Roveacrinidae indet. (TS–NBrn), core sample S–2–2202.3; E. accumulation of roveacrinoidal brachial plates (*Roveacrinus* cf. *alatus*), core sample D–1–2552.2; F. *Roveacrinus* sp., TS–Rad and Obl/TS–IBr2, core sample Bz–1–4–7.1; G. *Roveacrinus* sp., TS–Theca and OblS–I/IIBrn, core sample Bz–1–4–9.1; H. *Roveacrinus* sp., OblS–Theca, core sample Bz–1–4–10.1 (after Mülayim et al. 2018)……68

Figure 3.3. The thin–section photographs of roveacrinid ossicles, lower middle Cenomanian, Adıyaman area, SE Turkey. A. *Roveacrinus spinosus* Peck, Lg/TgS–IBr1 and OblS–NBrn, core sample S–2–2202.4; B. *Roveacrinus spinosus* Peck bearing typical spinose ornamentation (Lg/TgS–NBrn), and Roveacrinidae indet. (TgS–IBr1), core sample S–2–2202.5; C. *Applinocrinus* sp. (Lg/TS–Rad) and Saccocomidae indet. (TgSIBr2; OblS–NBrn), core sample Bz–1–4–7.3 (ex Bz–1–4.7); D. Saccocomidae indet., indeterminable plates, core sample Bz–1–4–7; E. Saccocomidae indet., Obl/TSN/ IIBrn/Rad, core sample B–1–1508.1; F. Roveacrinidae indet., TgS–IBr2, core sample Bz–1–4–7.2; G. Roveacrinidae indet., TgSIBr1 and TgS–IBr2, core sample Bz–1–4–9.2 (ex Bz–1–4.9.10x); H. Roveacrinidae indet., brachial plates, core sample Bz–1–4–10 (after Mülayim et al. 2018)……....68

Figure 3.4. The thin–section photographs of roveacrinid ossicles, lower–middle Cenomanian, Adıyaman area, SE Turkey. A. Roveacrinidae indet., TS–NBrn and TgS–IBr1, core sample B–1–1484.1; B. Roveacrinidae indet., TS–NBrn, core sample D–1–2488.1; C. Roveacrinidae indet., accumulation of broken brachial plates (NBrn), core sample D–1–2488.2; D. Roveacrinidae indet., TS–Theca and Lg/TgS–NBrn, core sample G–1–2980; E Roveacrinidae indet., OblS–IBr2, core sample G–1–2992; F. Roveacrinidae indet.,TgS–IBr1, OblS–NBrn and TgSIBr2, core sample S–2–2202_5x; G. Roveacrinidae indet. (sturdy morphology), OblS–NBrn, core sample S–2–2206; H. Roveacrinidae indet. (sturdy morphology), OblS–NBrn, core sample S–2–2206_5x (after Mülayim et al. 2018)……...….71

Figure 3.5. The thin–section photographs of roveacrinid ossicles, lower–middle Cenomanian, Adıyaman area, SE Turkey. A. Roveacrinidae indet. (sturdy morphology), OblS–NBrn, core sample S–2–2206–10x; B. Roveacrinidae indet., TS–NBrn, core sample S–2–2202.1; C. Indeterminable roveacrinoidal sections, core sample S–2–2274.1; D. Roveacrinidae indet., IBr2 and NBrn, core sample B–1–1484.2; E. Roveacrinidae indet., accumulation of brachial plates (OblSNBrn), core sample Bk–1–1962.4; F. Roveacrinidae indet., accumulation of brachial plates NBrn, core sample D–1–2552; G. Roveacrinidae indet., TS–NBrn and TgS–IBr2, core sample D–1–2492; H. Roveacrinidae indet., TgS–IBr2, core sample K–1–1630 (after Mülayim et al. 2018)……..….71

Figure 3.6. Distribution of rudists and some bivalvia in the Sabunsuyu stratigraphic section (after Mülayim et al. 2020)……...…74

Figure 3.7. Rudist–bearing limestones of the Derdere Formation in the Sabunsuyu stratigraphic section. A. Field view showing thickness (white bar equals 2.90 m) of lower rudist–bearing limestones of unit IV. B, D. Close up of previous photograph showing transverse and oblique sections of rudist fragments (BeC. *Biradiolites* sp.; *D. Durania* sp.), scale bar equals 10 mm. E, J. Field views of upper rudist bearing limestones of unit IV. E. Rudist–bearing limestones alternating with limestones (white bar equals 40–50 cm, indicating rudist–bearing limestones. F, H. Close up of previous photograph showing transverse sections of monospecific *Durania acuticostata* Caffau. Note thin outer shell layer and strong and acute ribs limited by wider sinuses (scale bar equals 10 mm). I. *Neithea fleuriausiana* d'Orbigny (n) and small radiolitidis (thin black arrows) in life position (scale bar equals 10 mm). J. Transverse sections of right valves of *Sauvagesia sharpei* Bayle (thin black arrows). Note thick outer shell layer, small, triangular ligamental ridge (L) and presence of *Neithea fleuriausiana* d'Orbigny (n) (scale bar equals 10 mm) (after Mülayim et al. 2020)……77

Figure 3.8. A, C. Radiolitid valve fragment lithosome in the Sabunsuyu stratigraphic section. A, B. This lithosome consist mainly of the radiolitid fragments, however some radiolitid transverse and oblique sections (probably *Durania/Sauvagesia, Biradiolites*) are rarely observed (arrows). C. Some echinid moulds preserving the spicules are also present. D. *Bournonia* sp. transverse sections. E,G. Ichthyosarcolitid–Bivalvia lithosome. Small Ichthyosarcolitid undetermines Bivalvias. Scale bar indicates 10 mm (after Mülayim et al. 2020)……....78

Figure 3.9. Rudist–bearing limestones of the Derdere Formation, outcrop photographs in the Sabunsuyu stratigraphic section. A. *Sauvagesia sharpei* Bayle, two right valves in growth position. B. *Sauvagesia sharpei* Bayle, transverse section of right valve showing thick outer shell layer, short triangular ligamental ridge (L), flat and slightly protruding radial structures separated by a concave interband (Ib). Cellular structure seems to be partially preserved (thin black arrows). C. *Bournonia?* sp., transverse section of right valve; radial structures showing some similarities to those of the genus. D. Stalk elements of crinoids. E. Field views of rudist–bearing limestones of unit VI (scale bar equals 2 m). F, G. Close up of previous photograph. F. Poorly preserved transverse section of right valve of a canaliculated rudist fragment showing very thin internal shell layer with one or two rows of small rounded pallial canals in posterior part (white arrows), as in *Caprinula sharpei*. G. *Biradiolites* sp., transverse section of right valve showing acute ribs (scale bar equals 10 mm in all photographs, except E (after Müülayim et al. 2020)……79

Figure 3.10. A. Field view showing rudist–bearing limestones of Derdere (unit VII) and Karababa (units VIII and IX) formations in the Sabunsuyu stratigraphic section. BeI. Rudists of the Derdere Formation, outcrop photographs (scale bar equals 10 mm). B,F. *Ichthyosarcolites monocarinatus* Slišković. B,E. Transverse sections of right valve with single flange on anteroeventral side (black arrow), internal shell layer consisting of dense, ovaloid and round pallial canals, a single very thin tabula (yellow arrow) and elongated teeth sockets of left valve. F. Curved left valve (umbo to right) showing pallial canals in eroded part, some parts may be belong to right

valve (black arrow). G,I. *Ichthyosarcolites triangularis* Desmarest, triangular transverse sections of right valve with single projecting flange on dorsal side (white arrow). Teeth sockets of left valve may be present in part. Concave tabulae observed in internal moulds of body cavity (yellow arrow, in G). J. Field view showing thickness of lower (a) and upper (b) rudist–bearing limestones of unit IX (hammer for scale). K,O. Rudists of the Karababa Formation, outcrop photographs (scale bar equals 10 mm). K–M. *Bournonia excavata*, transverse sections of small right valves showing subrounded dorsal side, ventral radial band (black and white arrows) better developed than posterior one and concave interband. N,O. *Apricardia* sp., small valves, strongly coiled left valve and conical, slightly capuloid right valve (after Mülayim et al. 2020)…….80

Figure 3.11. A,E. *Ichthyosarcolites triangularis* lithosome in the Sabunsuyu stratigraphic section A) Field view of the lithosome showing. the bed thickness of the Derdere and Karababa A contact, (white bar is approximately 310 cm). B. *Ichthyosarcolites triangularis* Desmarest, transverse section of the right valve. C,E. general view of the monospecific lithosome and transverse section of the right valve of *Ichthyosarcolites triangularis* Desmarest. Scale bar indicates 10 mm. (after Mülayim et al. 2020)……..…82

Figure 3.12. A,E *Bournonia excavata* lithosome in the Sabunsuyu stratigraphic section. A,D Note radial bands (arrows) and in growth position of the valves. B,C Rare, small *Bournonia excavata* (thick white arrows), *Apricardia* sp. (thick red arrows) and undeterninable bivalvia are present. E. general view of the lithosome showing the transverse sections and moulds of the species and also radial bands on the surface of the right valve (arrows). Scale bar is 10 mm (after Mülayim et al. 2020)……84

Figure 3.13. Distribution of planktonic foraminifera in the İnişdere stratigraphic section (after Mülayim et al. 2019a)…….87

Figure 3.14. Thin–section images of the planktonic foraminifera observed in the Karababa–A Member. (A–L) İnişdere stratigraphic section; A. *Dicarinella* cf. *primitiva* (Dalbiez), sample IND–22; B. transitional from *H. praehelvetica* to *H. helvetica*, sample IND–22; C. *Helvetoglobotruncana praehelvetica* (Trujillo), sample IND–25; D. *Dicarinella* cf. *marianosi* (Douglas), sample IND–22; E. *Marginotruncana* cf. *paraconcavata* Porthault, sample IND–25; F. *Marginotruncana renzi* (Gandolfi), sample IND–27; G. *Marginotruncana schneegansi* (Sigal), sample IND–24; H. *Marginotruncana* cf. *sigali* (Reichel), sample IND–23; İ. *Marginotruncana tarfayaensis* (Lehmann), sample IND–22; J. *Whiteinella aprica* (Loeblich and Tappan), sample IND–22; K. *Whiteinella* cf. *archaeocretacea* Pessagno, sample IND–22; L. *Whiteinella baltica* Douglas and Rankin, sample IND–24. (after Mülayim et al. 2019a)…….88

Figure 3.15. Distribution of planktonic foraminifera in the Sabunsuyu stratigraphic section (after Mülayim et al. 2020)……...90

Figure 3.16. Thin–section images of the planktonic foraminifera taxa observed in the Sabunsuyu stratigraphic section. A,C. *Asterohedbergella asterospinosa* Hamaoui ,MU, samples 19, 79 and 79, respectively; DeL. Hedbergellidae indet., MU, samples 79, 1D, 1A, 1D, 19, 19, 79, 63 and 63, respectively; M. Hedbergellidae indet. (left) and *Globigerinelloides* sp. (right), MU, sample 86; Q. Hedbergellidae indet., MU, sample 80; R. *Globigerinelloides* sp., MU, sample 63; S. Heterohelicidae indet., MU, sample 1A (after Mülayim et al. 2019a)……...97

Figure 3.17. Distribution of planktonic foraminifera in the upper part of the Türkoğlu stratigraphic section (after Mülayim et al. 2019b)……....94

Figure 3.18. Stratigraphic distribution of planktonic foraminifera in the A–1 borehole section. (after, Mülayim et al. 2020b)……97

Figure 3.19. Stratigraphic distribution of planktonic foraminifera in the BS–1 borehole section. (after Mülayim et al. 2019a)…….…98

Figure 3.20. Stratigraphic distribution of planktonic foraminifera in the KM–1 borehole section. (after Mülayim et al. 2019a)……..…99

Figure 3.21. Stratigraphic distribution of planktonic foraminifera in the CM–14 borehole section. (after Mülayim et al. 2019a)……100

Figure 3.22. Thin–section images of the planktonic foraminifera taxa observed in the four borehole sections. A. *Archaeoglobigerina* cf. *cretacea*, Sample BS 1–7, BS–1 section; B. *Dicarinella concavata*, Sample K– 11/3–1, A–1 section; C. *Dicarinella* cf. *hagni* Sample KM 1– 8, KM–1 section; D. *Dicarinella primitiva*, Sample K–12/4–1, A–1 section; E. *Dicarinella primitiva*, Sample K–12/4–1, A–1 section; F. *Helvetoglobotruncana* aff. *helvetica*, Sample BS 1–2, BS–1 section; G. *Helvetoglobotruncana helvetica*, Sample K–11/6–1, A–1 section; H. *Helvetoglobotruncana* cf. *helvetica*, Sample K–12/12, A–1 section; I. *Helvetoglobotruncana* cf. *helvetica*, Sample K–11/6–2, A–1 section; İ. *Helvetoglobotruncana* cf. *helvetica*, Sample K–13/4–1, A–1 section; J. *Helvetoglobotruncana* cf. *helvetica*, Sample KM 1–10, KM–1 section; K. *Helvetoglobotruncana* cf. *praehelvetica*, Sample BS 1–2, BS–1 section; L. *Helvetoglobotruncana praehelvetica*, Sample BS 1–2, BS–1 section; M. *Helvetoglobotruncana praehelvetica*, Sample K–12/5–1, A–1 section; N. *Helvetoglobotruncana praehelvetica*, Sample KM 1–1, KM–1 section; O. *Marginotruncana* cf. *coronata*, Sample 14–4, CM–14 section; P. *Marginotruncana marginata*, Sample KM 1–9, KM–1 section; R. *Marginotruncana* cf. *pseudolinneiana*, Sample BS 1–4, BS–1 section; S. *Marginotruncana renzi*, Sample K– 12/9, A–1 section……..101

Figure 3.23. Thin–section images of the planktonic foraminifera taxa observed in the four borehole sections. A.*Marginotruncana* cf. *sigali*, Sample K–12/4–1, A–1 section; B. *Praeglobotruncana algeriana*, Sample K–11/1–1, A–1 section; C. *Praeglobotruncana algeriana*, Sample 14–7, CM–14 section; D. *Whiteinella aprica*, Sample BS 1–2, BS–1 section E. *Whiteinella aprica*, Sample K–12/11, A–1 section;; F. *Whiteinella aprica*, Sample KM 1–7, KM–1 section; G. *Whiteinella aprica*,

Sample 14–2, CM–14 section; H. *Whiteinella* cf. *archaeocretacea*, Sample BS 1–6, BS–1 section; I. *Whiteinella baltica*, Sample K– 12/8, A–1 section; İ. *Whiteinella baltica*, Sample K– 11/3–1, A–1 section; J. *Whiteinella inornata*, Sample K–12/1–2, A–1; K. *Whiteinella* cf. *paradubia*, Sample K–12/4–1, A–1 section (after Mülayim et al. 2019a)……102

Figure 3.24. Stratigraphic distribution of benthic foraminifera in the İnişdere stratigraphic section. (after Mülayim et al. 2019a)……..103

Figure 3.25. Thin–section images of the benthic foraminifera and dasycladalean algae observed in the Derdere Formation in the İnişdere stratigraphic section; (A, B) (C, F) dasycladalean algae, samples IND–5.33; IND–5,89. (D) *Cuneolina pavonia*, d'Orbigny, sample IND–5.33 (E, H, G) *Nezzazatinella picardi*, Henson samples IND–2.84; IND–5.33……104

Figure 3.26. Thin–section images of the benthic foraminifera observed in the Derdere Formation. (A, G) Sabunsuyu stratigraphic section; benthic foraminifera: T, U. *Meandrospira* sp., MU, samples 53 and 84, respectively; V. Gavelinellidae, MU, sample 8……..105

Figure 3.27. Stratigraphic distribution of benthic foraminifera and dasycladalean algae in the upper part of the Türkoğlu stratigraphic section. (after Mülayim et al. 2019b)……....106

Figure 3.28. Thin–section images of the benthic foraminifera and dasycladalean algae observed in the Derdere Formation of the Türkoğlu section; A. *Thaumatoporella parvovesiculifera*, Raineri, sample TRK–40,37, B. *Marinella lugeoni*, Pfender sample TRK–41,00, C. *Spiroloculina cretacea*, Reuss, sample TRK–41,00, D. *Ovalveolina maccagnoae*, De Castro, sample TRK–41,00…..…107

Figure 3.29. Stratigraphic distribution of benthic foraminifera in the A–1 borehole section……...….108

Figure 3.30. Thin–section images of the benthic foraminifera and dasycladalean algae observed in the Derdere Formation of the A–1 borehole section; A,G *Sellialveolina viallii*, Colalongo, sample 4890, B, E *Nezzazata simplex*, Omara, samples 4380 and 4620, C. *Cuneolina pavonia*, d'Orbigny, sample 4380, D. dasycladalean algae, sample 16/5, F. *Biplanata peneropliformis*, Hamaoui & Saint–Marc, sample 4700, B. *Marinella lugeoni*, Pfender, sample 15/1, I. *Dicyclina schlumbergeri*, Munier–Chalmas, sample 15/2, İ. Discorbidae, sample 17/6…….109

Figure 3.31. Stratigraphic distribution of benthic foraminifera in the Y–3 borehole section……110

Figure 3.32. Thin–section images of the benthic foraminifera and dasycladalean algae observed in the Derdere Formation of the Y–3 borehole section; A. dasycladalean algae, samples 3/3, C, E Discorbidae, samples 3/1 and 3/2 B, F *Nezzazatinella picardi*, Henson, samples 3/1 and 3/2, D *Cuneolina pavonia*, d'Orbigny, sample 3/6……....111

Figure 3.33. Light microscope photographs of calcareous nannofossil species from the Karababa–A Member in the CM–14 and BS–1. All figures were taken under cross–polarized light. A. *Lucianorhabdus maleformis* Reinhardt, sample CM–14–2; B. *Eiffellithus eximius* Stover, sample BS–1–4; C. *Quadrum gartneri* Prins and Perch–Nielsen, sample BS–1–7 (after Mülayim et al. 2019a)……..…113

Figure 3.34. Thin–section photographs of pithonellids in BZ–1 borehole section, lower–middle Cenomanian, Adıyaman area, SE Turkey. A. a cone–shaped form, *Bonetocardiella conoidea*, Bonet, Bc, core sample 370039. B. thick–walled spherical form with typical pithonelloid crystal–orientation–*Pithonella sphaerica*, Kaufmann, Ps; right middle and upper corner: organic walls are preserved, core sample 370034. C. center–*Pithonella ovalis*, Kaufmann, Po, core sample 370025. D. left (10 o'clock above center) and others on the left: *Pithonella sphaerica*, Kaufmann, Ps, core sample 370030. E. left = very clear *Pithonella sphaerica* Kaufmann, with crystal orientation nicely seen core sample 370022. F. a multi–layered form,

possibly from the *Pithonella lamellata* Keupp, form spectrum, core sample 370021. G. the multi–layered type, core sample 370019. H. *Pithonella ovalis*, Kaufmann, core sample 370005……...….114

Figure 3.35. SEM photographs of the pithonellids in the BZ–1 borehole section, lower–middle, Cenomanian, Adıyaman area, SE Turkey. A. The typical pithonellid wall type. One sees on the left and the right side of the sphere that the crystals are uniformely inclined towards a point of the sphere at around 11 o'clock, sample 2023. 2003. B: *Pithonella sphaerica* Kaufmann, with a spiral crystal arrangement, sample 2011. C and D. *Pithonella sphaerica* Kaufmann, with blocky cement infillings (the parallel lines are cleavage lamellae) samples, 2002……115

Figure 3.36. Thin–section images of the pithonellids observed in the Derdere Formation. (N, P) Sabunsuyu stratigraphic section: N. *Pithonella ovalis*, Kaufmann MU, sample SAB–7; O. *Bonetocardiella conoidea*, Bonet, MU, sample SAB–53; P: *Pithonella sphaerica*, Kaufmann, MU, sample SAB–19……116

Figure 4.1. Generalized distribution of microfacies types in different parts of a homoclinal carbonate ramp (Flügel, 2004)……..…125

Figure 4.2. Photomicrographs of microfacies types. Mf–1: Non–laminated silt–bearing lime mudstone, A. sample 1.1, SSS and B. sample 7.1. SSS……..127

Figure 4.3. Photomicrographs of microfacies types. Mf–2: Pithonellid–planktonic foraminifera wackestone–packstone A. sample–2270, S–2 borehole section B. sample–4.9, B–1 borehole section C. sample–1700, K–1 borehole section, D. sample–2570, G–1 borehole section……...128

Figure 4.4. Thin–section photographs of pithonellids in the BZ–1 borehole section, lower?–middle, Cenomanian, Adıyaman area, SE Turkey. A: a cone–shaped form, *Bonetocardiella conoidea*, Bonet Bc, core sample 370039. B: thick–walled spherical form with typical pithonelloid crystal–orientation–*Pithonella sphaerica*, Kaufmann Ps; right middle and upper corner: organic walls are preserved, core sample 370034

C: center–*Pithonella ovalis*, Kaufmann Po, core sample 370025. D: left = very clear *Pithonella sphaerica* with crystal orientation nicely seen core sample 370022. Bc: *Bonetocardiella conoidea*, Po: *Pithonella ovalis*, Ps: *Pithonella sphaerica*. (Scale bar: 100μm and 200μm)…….129

Figure 4.5. Photomicrographs of microfacies types. Mf–3: Pithonellid–**r**oveacrinid wackestone–packstone. A. sample–4.9, BO–1 borehole section; sample–2900, G.K–1 borehole section, sample–1404.1, BA–1 borehole section,, sample–2206, S–2 borehole section. Rovea. Roveacrinid, pit. Pithonellid……...131

Figure 4.6. Photomicrographs of microfacies types. Mf–4: Bioclastic roveacrinoidal wackestone, calcareous benthic foraminifera (*Lenticulina* sp.) with bioclasts in the S–2 borehole section, sample 2274.2, and a transverse section of an echinoid spine in the S–2 borehole section, sample 2274, respectively……..……131

Figure 4.7. Photomicrographs of microfacies type. Mf–5: Bioclastic dolowackestone with medium crystalline dolomite mosaic, sample 2194, S–2 borehole section……..133

Figure 4.8. Photomicrographs of microfacies types. Mf–6: Peloidal dolowackestone, A. sample 970, AK–1, borehole section. B. sample 2145 El–1 borehole section. C. sample 2472, D–1 borehole section, D. sample 1372, Al–1 borehole section sample Pe: Pellet…….134

Figure 4.9. Photomicrographs of microfacies type. Mf–7: Benthic foraminiferal dolowackestone, sample 2518, G–1 borehole section. .b: Benthic foraminifera….135

Figure 4.10. Photomicrographs of microfacies types. Mf–8: Dolomudstone. A. sample 2822, Gö–1 borehole section, B. sample 1122, Ya–1 borehole section, C. sample 752, Be–1 borehole section D. sample 6860 Ka–1 borehole section……..137

Figure 4.11. Photomicrographs of microfacies types. Mf–9: Fine crystalline planar–s dolomite mosaic. A. sample 1886, GB–1 borehole section. B. sample 6870, Ka–1 borehole section……...138

Figure 4.12. Photomicrographs of microfacies types. Mf–10: Medium crystalline planar–e–s dolomite mosaic. A. sample 2972, G.K–1 borehole section, B. sample, 6940 Ka–1 borehole section……...139

Figure 4.13. Photomicrographs of microfacies types. Mf–11: Coarse crystalline planar–e–s dolomite mosaic. A. sample 2032, G.B–1 borehole section, B. sample 2508, B–1 borehole section……....139

Figure 4.14. Photomicrographs of microfacies types. Mf–12: Bioturbated wackestone, A, B 17–1; 17–4.2 sample, A–1 borehole section. bioturb. Bioturbated……140

Figure 4.15. Photomicrographs of microfacies types. Mf–13: Rudist floatstone/rudstone, A,B, samples IND–0.17.1–3, İSS, C,D, samples SAB–70.2–3, SSS. Rd: Rudist……..141

Figure 4.16. Photomicrographs of microfacies types.. Mf–14: Intraformational breccias, A. sample IND–1,04, İSS. B. sample 880,4, Ak–1 borehole section, C–D. sample 728.3–732, Be–1 borehole section. Ext: Extraclast, sty: Stylolites…….143

Figure 4.17. Photomicrographs of microfacies types. Mf–15: Poorly sorted intraclastic peloidal packstone–grainstone. A. sample 16.4, A–1 borehole section, B, C samples 2964 and 2976, respectively, G.K–1 borehole section, D sample 2194, Y–3 borehole section, E. sample 3410, Y–1 borehole section , F sample 896, E–1 borehole section .pe: Pellet, int: Intraclast……..144

Figure 4.18. Photomicrographs of microfacies types. Mf–16: Bivalve and roveacrinid floatstone, samples, A,B samples,72.3 and 72.4 respectively, SSS. b. Bivalve, r. Roveacrinids……..…145

Figure 4.19. Photomicrographs of microfacies types. Mf–16: Benthic foraminifera bioclastic silty wackestone–packstone,, A sample 858.3, A–1 borehole section, B. sample 1028.2, E–1 borehole section, C–D samples 2186.3 and 3.4,2 respectively. Y–3 borehole section..pe: Pellet, b: Benthic foraminifera……..146

Figure 4.20. Photomicrographs of microfacies types. Mf–18: Peloidal packstone A, sample 882, E–1 borehole section. B. sample 3.7, Y–3 borehole section, C,D samples 16–3 and 16–4 respectively. A–1. borehole section pe: Pellet, bv: Bivalve……148

Figure 4.21. Photomicrographs of microfacies types. Mf–19: Bioclastic wackestone–packstone, A,B samples, TRK–48.82 TSS, B. sample 880, Ak–1 borehole section. D, sample 3320, Y–1 borehole section .bv. Bivalve, g. Gastropod……...149

Figure 4.22. Photomicrographs of microfacies types Mf–20: Peloid bioclastic silty packstone A,B samples 1–12 and 1410 respectively. Ba–1 borehole section, bv. Bivalve, pe. Pellet……...……150

Figure 4.23. Photomicrographs of microfacies types. Mf–21: Ooid grainstone. A. sample 3300, Y–1 borehole section, B, sample 2610, K–9 borehole section, .o. Oolite……..…151

Figure 4.24. Photomicrographs of microfacies types. Mf–22: Non–borrowed, lime mudstone A sample 13.1, Ba–1 borehole section , B. sample 16–1, A–1 borehole section, C, sample 6770, K–1 borehole section, D, sample 1064, Ç–1 borehole section……....152

Figure 4.25. Photomicrographs of microfacies types. Mf–23: Finely laminated, silt–bearing lime pelagic mudstone A,B sample 3a, SSS……..153

Figure 4.26. Photomicrographs of microfacies types. Mf–24: Planktonic foraminifera bearing wackestone/packstone, samples, A sample 11.8, A–1 borehole section, B, sample k1, K–1 borehole section, C sample 1874, G.B.–1 borehole section, D sample 6740, Ka–1 borehole section…….....154

Figure 4.27. Diagenetic modifications in the carbonate succession of the Derdere Formation and Karababa–A Member in the studied sections……..…155

Figure 5.1. Distribution of microfacies types and depositional environments of the Derdere, and Karababa–A Member in the carbonate ramp model…….….162

Figure 5.2. Block diagram showing the interpretation of the Cenomanian depositional environments in the study area in SE Turkey in the northwestern part of the Arabian Carbonate Platform……...……..166

Figure 5.3. Cenomanian–Turonian palaeoecological evolution of the northwestern part of the Arabian Carbonate Platform. A. The establishment of open marine conditions are reflected by the abundance of pithonellids and planktonic foraminifera. B. Short and limited subaerial exposure reduced benthic habitat and might have led to the extinction of several groups of large benthic foraminifera. C. Carbonate sedimentation is represented by the abundance of benthic foraminifera, mollusc and calcareous algae. The restricted open marine condition led to the progressive eutrophication of the shallow environment. D. Extinction and eradication of carbonate producers reduced the sedimentation rate. A relative rise in sea–level led to the deeper of the environment and the deposition of pelagic facies. E. Oligotrophic conditions were established as indicated by the presence of keeled planktonic foraminifera at middle–late Turonian……..…..170

Figure 6.1. Sequence stratigraphical construction of the Sabunsuyu stratigraphic section showing systems tracts, sedimentary packages and important surfaces (from Mülayim et al., 2019a)……..…..173

Figure 6.2. Comparison between sequence boundaries of the present study with others in neighbouring areas and with the global eustatic scheme of Haq (2014)…177

Figure 6.3. Sequence stratigraphical construction of the İnişdere sttratigraphic section showing systems tracts, sedimentary packages and important surfaces…..179

Figure 6.4. Correlation of the Cenomanian–Turonian of the study area with that of SE Turkey, global and Arabian Plate sea–level curve (Sharland et al. 2001; Haq and Al–Qahtani 2005; Haq 2014) and comparison of ages assigned to calcareous nannofossil (CC; Sissingh 1977) and planktonic foraminifer biozones used in Geologic Time Scale (GTS) 2012 (Gradstein et al. 2012). Underscored names to the right are for planktonic foraminifer zonal markers whose ages (in parentheses) are

calibrated using biostratigraphic occurrence data from Caron et al. (2006) (from Mülayim et .al., 2019a)……...182

Figure 7.1. The species ranges of planktonic/benthic foraminifera and drowning model in the İnişdere stratigraphic section (after Mülayim et .al. 2019a)……185

Figure 7.2. Cenomanian–Turonian, stratigraphic correlation of the Derdere Formation and the Karababa–A Member (SE Turkey) with the northern margin of the Arabian Carbonate Platform for Syria and Iraq areas (after Jaff et al. 2015; Mülayim et .al. 2019a)……186

Figure 7.3. Lithostratigraphic section sampled at upper part of the Türkoğlu succession (SE Turkey) with accompanying carbon– and oxygen–isotope data. The position of Cenomanian–Turonian boundary (CTB), according to carbon–isotope values are also indicated (after Mülayim et al. 2019b)……...193

Figure 7.4. Lithostratigraphic section sampled at lower part of the Türkoğlu succession (SE Turkey) with accompanying carbon– and oxygen–isotope data….194

Figure 7.5. Lithostratigraphic section sampled at İnişdere succession (SE Turkey) with accompanying carbon– and oxygen–isotope data. The position of the Cenomanian–Turonian boundary (CTB), according to carbon–isotope values is also indicated (after Mülayim et al. 2019a)……...….196

Figure 7.6. Lithostratigraphic section sampled at Sabunsuyu succession (SE Turkey) with accompanying carbon– and oxygen–isotope data. The position of the Cenomanian–Turonian boundary (CTB), according to carbon–isotope values is also indicated…….……197

Figure 7.7. Lithostratigraphic section sampled at CM–14 borehole section (SE Turkey) with accompanying carbon– and oxygen–isotope data. The position of the Cenomanian–Turonian boundary (CTB), according to carbon–isotope values is also indicated (from Mülayim et al., 2020b)…….….198

Figure 7.8. Correlation of C–isotope curve of Türkoğlu stratigraphic section with the curves obtained from the Cenomanian–Turonian Eastbourne and Pueblo reference sections and Brac succession. Letters a, b, and c mark the characteristic peaks of Pearce et al, 2009. (after Mülayim et al. 2019b)……200

Figure 7.9. Correlation of the C–isotope curve of İnişdere stratigraphic section with the curves obtained from the Cenomanian–Turonian Eastbourne and Pueblo reference sections and Brac succession. Letters a–c mark the characteristic peaks of Pearce et al. (2009) (after Mülayim et al. 2019a)……....201

Figure 7.10. Tentative correlation of the $\delta^{13}C$ and $\delta^{18}O$–curves in the studied areas……...204

Figure 7.11. Correlation of the gamma–ray curves and possible mid–Cenomanian event (MCE) zone in the borehole sections……....205

Figure 8.1. Schematic and tentative semi–quantitative distribution of pithonellids in the fossil record and its relationship to global sea–level fluctuations. (after Dias–Brito, 2000). Chronostratigraphy and eustatic curves after Haq, (2014)……....210

Figure 8.2. Stratigraphic column of the A–1 borehole succession showing the stratigraphic distribution of the planktonic foraminifera and filaments in the Karababa–A Member…….212

Figure 8.3. Stratigraphic correlations between three borehole sections including the Cenomanian–Turonian boundary in the Adıyaman district. Stratigraphic distribution of some planktonic foraminifera, calcareous nannofossils and filaments are given on the right– hand side of each log. (after Mülayim et al. 2019a)……...214

Figure 8.4. Microfacies photographs of the Karababa–A Member, A–1 core section, Adiyaman district, SE Turkey. A. Slightly deformed and diagenetically compressed, smooth bivalve shell valve, sample P1011637. B. Most probably scattered fragments of a smooth bivalve shell valve, sample P1011681. C. ‘Large’ fragments of prismatic bivalve shell valve (possibly some inoceramid relative), sample P1011636. D.

Diagenetically compressed, smooth bivalve shell valve, sample P1011642. E. Possibly some inoceramid relative, sample P1011645. F. Diagenetically compressed bivalve shell, sample P1011704. G. The thicker 'filament' resembles a transverse section of some echinoid plate test, the thinner ones are definitely transverse sections of smooth bivalve shell valves, sample P1011647. H. Diagenetically compressed huge fragments of smooth bivalve shell valve, sample P1011668. bv: bivalve pl: planktonic foraminifera……..….216

Figure 8.5. Microfacies photographs of the Karababa–A Member, Adiyaman district, SE Turkey. A. In the lower–left corner an isolated ostracode valve. In the upper right corner a transverse section of a smooth bivalve shell (with a hint of a hinge), sample P1011848, CM–14 borehole section. B. Many transverse sections of smooth bivalve shell fragments lying conformably to bedding, distal outer–ramp environment, sample P1011850, CM–14 borehole section. C. Right in the middle a transverse section of a smooth bivalve shell (bow–like), from outer–ramp environment, sample P1011814, KM–1 borehole section. D. In the lower–left corner a longitudinal axial section of a juvenile valve of *Bairdia* sp. In the lower middle part a transverse section of an ostracode valve (*Cytherella* sp.). In the upper left corner a transverse section of a thecal plate (TS–Theca) of a saccocomid (*Applinocrinus* sp.) and smooth bivalve shell debris, sample P1011775, KM–1 borehole section. E. Right in the middle of the photograph a complete ostracode shell with both valves connected (*Cytherella parallela*). Interspersed in the facies some small and thin fragments/debris of smooth bivalve shell conformable to bedding from an outer–ramp environment, sample P1011296, İnişdere stratigraphic section. F. Five bivalve shell valves: the central one may be attributed to buchiids, but the lower two show some crenulation, sample P1011753, BS–1 borehole section. bv: bivalve pl: planktonic foraminifera, os: ostracod……..217

Figure 8.6. A relative abundance of the filaments in the Cenomanian–Turonian successions at global correlation……221

Figure 8.7. Correlation of the studied section with the various sections with first and last occurrences of zone marker taxa, filament events, sea–level variations, and carbon isotope peaks……...224

Figure 8.8. Geographic distribution of roveacrinid facies over SE Turkey……..…226

LIST OF ABBREVIATIONS

ABBREVIATIONS

ARGEM: Research and Development Center

BRH: Borehole section

CTAE: Cenomanian–Turonian Anoxic Event

CTBE: Cenomanian–Turonian Boundary Event

CTB: Cenomanian–Turonian Boundary

C–T: Cenomanian–Turonian

GR: Gamma Ray

HO: highest occurence

HST: Highstand Systems Tract

IND: İnişdere

ISS: İnişdere Stratigraphic Section

LO: lowest occurrence

MF: Microfacies

MSS: Measured Stratigraphic Section

OAE 2: Oceanic Anoxic Event 2

OMZ: Oxygen Minimum Zone

PRZ: Partial Range Zone

RMF: Ramp Microfacies

SE: Southeastern

SEM: Scanning Electron Microscope

SAB: Sabunsuyu

SSS: Sabunsuyu Stratigraphic Section

TL: Transmitted Light

TST: Transgressive Systems Tract

TPAO: Turkish Petroleum Corporation

TRK: Türkoğlu

TSS: Türkoğlu Stratigraphic Section

VPDB: Vienna Per Dee Belemnite

CHAPTER 1

INTRODUCTION

Despite an upsurge in research over the last 20 years, including extensive hydrocarbon exploration, the geology of the SE Turkey is still poorly known. There is virtually no publication of the Cenomanian–Turonian carbonate deposits in SE Turkey areas. This study considers various aspects of the biostratigraphy, sequence stratigraphy, stable isotope stratigraphy, and sedimentology of the Cenomanian–Turonian ramp carbonates of SE Turkey. These data sets have been integrated into detailed depositional and palaeoenvironmental models, which provide correlation on the Arabian Carbonate Platform (SE Turkey), with adjacent areas, and with global schemes as well.

1.1 Purpose and Scope

The main targets of the present thesis are to;

- understand to Late Cretaceous (Cenomanian–Turonian) carbonate platform evolution of the northern part of the Arabian Platform (SE Turkey),
- identify the platform drowning and relationship with Cretaceous Oceanic Anoxic Event (OAE 2),
  reveal the palaeoenvironmental significance of pithonellid assemblages from the Cretaceous Tethyan realm of the SE Turkey,
- define the rudist and roveacrinid associations of the Derdere and the Karababa formations and to compare them of the other sites of the Arabian Platform,

- establish a sequence stratigraphic framework for the Cenomanian–Turonian for SE Turkey and correlate to the rest of the Arabian Platform,
- give a detailed description and comprehensive sedimentological analysis of the studied sections,
- determine the palaeoenvironmental changes and correlation potential of filament marker beds in the C–T boundary,
- evaluate the application of stable isotope stratigraphy as a stratigraphic tool for local, regional and global correlation,

This study addresses the genesis of the Cenomanian–Turonian carbonate system of SE Turkey, in the light of these factors and the particularities of its development on the northwestern part of the Arabian platform, an important part of the Cretaceous Tethyan palaeoceanographic system. This study intends to improve the geological understanding of the Cenomanian–Turonian carbonate system that may serve as a model for SE Turkey.

Efforts to meet the above–mentioned objectives have developed a perspective on the Cenomanian–Turonian carbonate platform of SE Turkey. This perspective comes along with research questions as below:

Lithostratigraphy and biostratigraphy a basic premise is to provide a chronostratigraphic framework of the sections measured. However, as reliable biostratigraphic data are generally rare in shallow carbonate platform settings, the need for an integrated lithostratigraphic and biostratigraphic approach in SE Turkey is evident. Important questions are: Which of the fossil groups recovered from the stratigraphic sections enable the best possible biostratigraphic resolution? Are the stratigraphic assignments of the investigated index fossils consistent compared to adjacent regions and global concepts? Does the combination and inter–correlation of biostratigraphic concepts allow precise biostratigraphic assignments or are the occurrences of the investigated index species stratigraphically inconsistent? Which lithostratigraphic units can be recognized and how do their lithologies vary throughout SE Turkey? Which lithologic units, marker beds, and distribution patterns of

characteristic biota are synchronous or diachronous with respect to the stratigraphic framework achieved?

Sequence stratigraphy is a useful tool for the determination of the factors controlling lateral and stratigraphic facies evolution and palaeogeography. The interpretation of relative sea–level changes and sequence architectures enables us to reconstruct varying accommodation and it improves integrated stratigraphic correlations on the platform. Important questions are: How many sequences and sequence boundaries will be established for SE Turkey? Can they be correlated with schemes from adjacent platform areas and with global models? Will a sequence stratigraphic scheme enable us to recognize local, regional, and global controlling mechanisms on platform development?

Detailed investigations of benthic and planktonic fossil groups (benthic and planktonic foraminifera, pithonellid calcitarchs, rudists, roveacrinids, calcareous nannofossils) are needed to highlight the impact of the different faunal groups as carbonate producers, to detect faunal differences between Cenomanian and Turonian assemblages and to reconstruct in which way these assemblages are influenced by carbonate ramp. How is the lateral zonation of the carbonate platform characterized with respect to the lateral distribution of skeletal and non–skeletal components? Which components reacted sensitively to changing platform organization and relative sea–level changes? Which long–term palaeoenvironmental changes controlled facies composition, biotic turnover across the C–T boundary?

A shift from neritic to pelagic deposition may be related to the drowning of the platform near the Cenomanian–Turonian boundary. Carbon isotope stratigraphy could be correlated with the platform drowning and the Cenomanian–Turonian Oceanic Anoxic Event. Geochemical, paleontological, and sedimentological data are then evaluated in order to interpret the environmental conditions that resulted in the drowning of the platform. Which environments prevail during Cenomanian and Turonian times on the platform and which controlling factors triggered the differences? Are abrupt changes from shallow to deeper water conditions in C–T boundary related to a global sea–level rise, and are comparable changes during other

time–intervals observable? Do these events relate to the same mechanisms that induced the global Cenomanian–Turonian Oceanic Anoxic Event (OAE 2)?

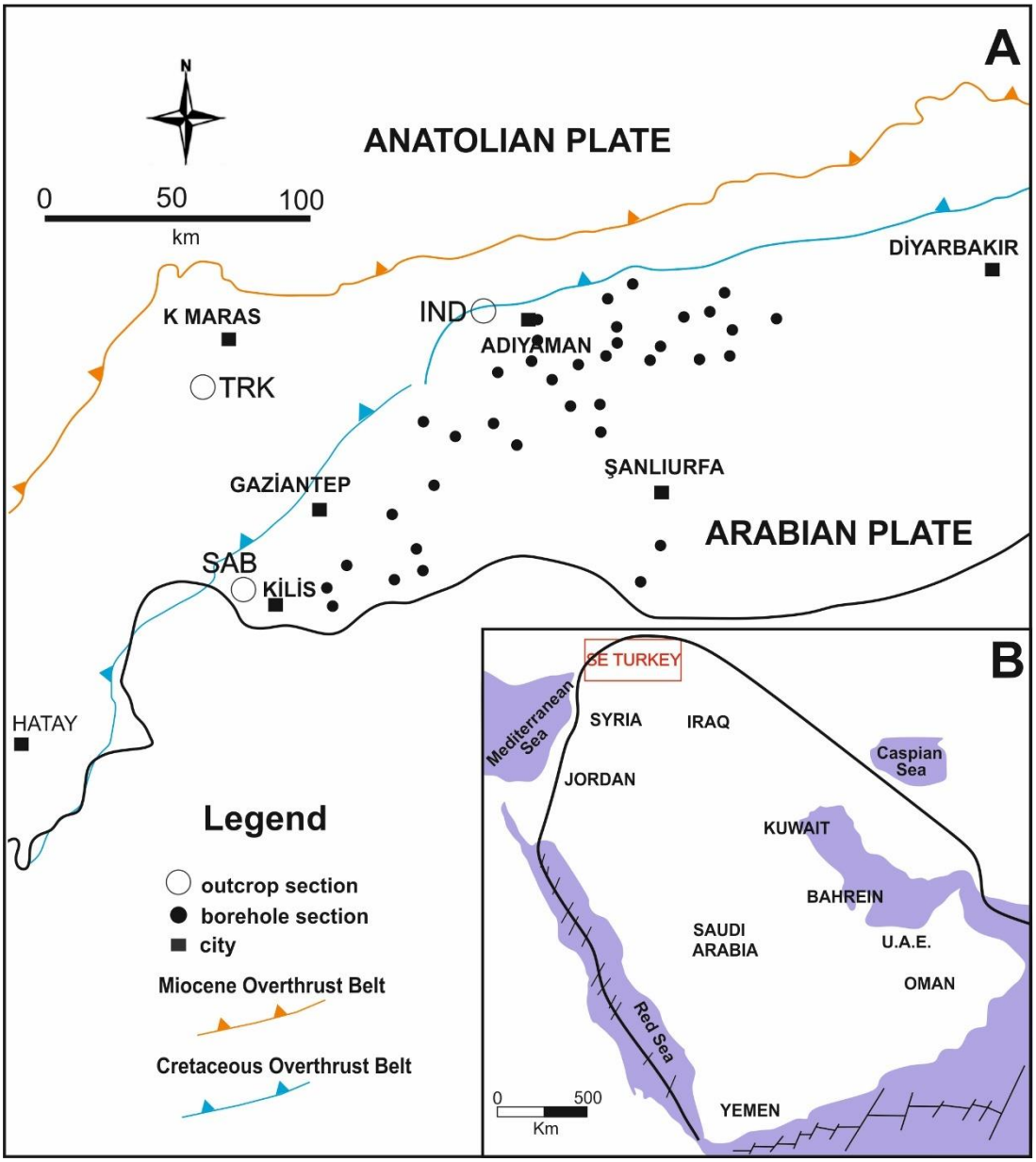


Figure 1.1. Location map of the study area. A; showing tectonic units in SE Anatolia, (after Mülayim et al. 2016), location of outcrops and boreholes sections in the study area B; Geographical map of SE Turkey on the Arabian platform (after Sharland et al. 2001).

1.2 Geographic Setting

This study has been carried out in three different regions located in the northwestern part of the Arabian platform (SE Turkey) including characteristic features of carbonate platform and comprising continuous and largely exposed upper Cretaceous limestone deposits. The sample material of this study was collected from three stratigraphical sections measured in three regions: İnişdere–Adıyaman; Sabunsuyu–Kilis and Türkoğlu–Kahramanmaraş respectively and 28 boreholes sections (Figure 1.1).

The İnişdere stratigraphic section is located 35 km southeast of Adıyaman city center along the İnişdere valley, in the north of Ünlüce village are exposed (Figure 1.1). The Sabunsuyu stratigraphic section is located 28 km northwest of Kilis city center along the Sabunsuyu stream. Antakya–Kilis main road is cut in the carbonate sequences up to the Sabunsuyu bridge (Figure 1.1). The Türkoğlu stratigraphic section is located 25 km south of Kahramanmaraş around the old quarry in Türkoğlu location (Table 1.1).

Table 1.1 Locations and GPS coordinates of all stratigraphic sections.

Section	Locality	Topographic Map (1/25.000)	Starting Position	Ending Position
IND	İnişdere–Adıyaman	M39–b3	410293.00 E 4183957.00 N	410266.00 E 4183893.00 N
SAB	Sabunsuyu–Kilis	O37–b3	312234.00 E 4077800.00 N	312250.00 E 4078080.00 N
TRK	Türkoğlu–K. Maraş	N37–b1	308431.00 E 4139304.00 N	308488.00 E 4139197.00 N

1.3 Methods of Study

This section describes the various analytical methods employed during the course of the study and outlines the rationale for conducting them. Specifically, it illustrates the outcrop procedures, sampling strategies and laboratory analyses. The combination of the petrographic, and geochemical dataset, in addition to outcrop/borehole

information, detailed microfacies descriptions of the predominantly carbonates of the Derdere and the Karababa formations present the outputs of the study.

Outcrop and Core Procedures

Outcrop sections and subsurface cuttings and limited core materials from borehole sections of Cenomanian–Turonian successions in the SE Turkey were utilized for this study. Data from these locations allowed us a comprehensive study on the Cenomanian–Turonian sediments. In order to describe, 3 different outcrop sections, 5 subsurface core sections, and 28 subsurface borehole sections were studied and samples (cuttings) were collected along them. These include outcrops such as Adıyaman (İnişdere), Kilis (Sabunsuyu), and Kahramanmaraş (Türkoğlu) and comprehensive wireline log suites are available from boreholes. The logs record information on the lithology, layer thickness, sedimentary structures, macrofossil types and content, and extent of bioturbation and diagenetic features as well as sample locations. The logs are complemented by detailed notes, diagrams, sketches, and relevant exposure and core photographs. The locations of the measured outcrop sections were chosen for best accessibility to the exposure and the quality and completeness of the Cenomanian–Turonian succession. In cored boreholes, the Derdere and Karababa–A were cored that resulted in 100% recovery. When working with the core material, housed at the core shed of the Research and Development Center (ARGEM) of TPAO, the surface of the core was washed to improve observation and measurement. These cores were also studied from high–resolution digital images. The digital images were enhanced by modifying the brightness and contrast on a specialist program (either Adobe Photoshop CS2 or Microsoft Office Picture Manager). Overall, all sampled sections were used for a detailed study of biostratigraphical distribution. All of the field and core work was carried out during four periods (June 2014, July 2015, August 2016, May 2017), around eight weeks.

Sampling Strategy

A total of 211 samples were collected from the studied sections (Figure 1.1). The majority of the samples were collected from outcrops to reduce the effects of surficial weathering. Nevertheless, the collection of weathered samples in the field was minimized by digging small trenches to excavate less weathered samples. 53 core samples were collected systematically (every 0.1 to 0.5 m) from the Derdere Formation and the A–member of the Karababa Formation. The location and character (at hand–specimen scale) of each gathered sample were recorded on the sedimentary logs. From the 211 samples gathered, large (~40 x 60 mm), thin–sections (≤ 30 μm thick) were prepared for petrographic investigations. Prior to thin–section preparation, the samples were sliced and slabbed, and macro–sedimentary features at hand–specimen scale were documented. The thin–sections were chosen to best lithofacies present both in the core and exposure. All the prepared thin–sections were scanned and investigated optically (normal transmitted light [TL] polarizing microscopy). From these thin–sections, 1195 samples were examined, and 26 were investigated for detailed micropaleontological analysis for calcareous nannofossils. These methods and their rationales are described in more detail as below.

Petrographic Methods

All thin–section preparations and petrographic analyses for this study were performed at the Department of the Geological Engineering laboratories of the Middle East University and the ARGEM of the TPAO. Detailed descriptions of the thin–sections preparation technique and their petrographic analyses are discussed in the following subsections. A detailed microfacies studies were carried out in the laboratory. The semi–quantitative analysis was carried out by the point–counting method using the James Swift apparatus that is mounted to the microscopic stage. This point–counting data was used in order to obtain the percentage and numbers of the components. 600–1100 points were counted per thin–section (Flügel, 2004). The point–counting data and visual estimation observation of different components of the microfacies are used to generate a graph and ternary diagrams to interpret the depositional environment and

component variation within the microfacies at the different intervals and through the measured section.

Microfacies analysis was applied here for the limestones, dolomitic limestones, and dolostones lithologies. Nomenclature for depositional texture are followed Dunham (1962); Embry and Klovan (1971) and descriptions were correlated with the Standard Microfacies Types of Flügel (2004), using visual estimation chart of Baccelle and Bosellini, (1965). Facies types and depositional settings were interpreted on the basis of matrix types/cement and grain contents, compositional and textural fabrics, fossil contents, energy index, and sedimentary data and depositional environments (Flügel, 2004). Textural description of dolomite and terminology is conducted following Sibley (1982), Sibley and Gregg (1987) as reviewed by Machel (2004) (Figure 1.2). For crystal size classes, the scheme of Lucia (1995) is adopted as follows: < 20 μm is fine, 20–100 μm for medium crystalline, and > 100 μm for coarse crystalline dolomite. Calcareous nannofossil data are based on the qualitative examination of smear slides using a polarized light microscope (100× oil immersion objective).

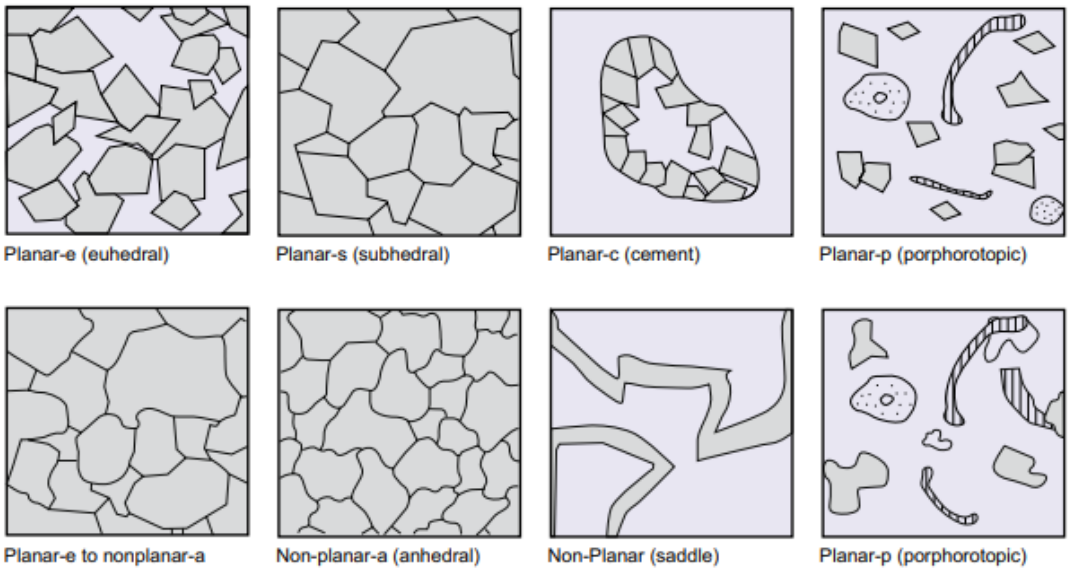


Figure 1.2. Dolomite textures and classification from Machel (2004) after Gregg and Sibley (1984), Sibley and Gregg (1987).

Thin–Section Preparation

All thin–sections of the most promising the Derdere and the A–member of the Karababa Formation samples were prepared to utilize standard procedures. One side of the sample slice was then mechanically ground flat utilizing a carborundum abrasive paper. Finer grades of abrasive were gradually applied to the same surface. When flat, the ground slice surface was then attached to a microscope slide with epoxy–resin adhesives that possess suitable refractive index properties. The mounted slice was finally ground to the desired thickness ($\leq$ 30 μm) utilizing a carborundum abrasive. All the prepared thin–sections were left uncovered in order to allow various petrographic and geochemical analyses.

Transmitted–Light Microscopy

The thin–sections were then examined optically at low to medium resolution under transmitted light (both planes polarised and cross polarised) using a binocular petrographic microscope (Nikon Optiphot2–Pol), attached to a digital camera (Jenoptik Jena D–07739). A set of photomicrographs were captured from selected thin–sections at magnifications of × 2, × 4, × 10, and × 20. This standard petrographic investigation helped to obtain lithological, textural, and compositional information.

Stable Isotope Analyses

82 samples for isotope analyses were obtained from small pieces of limestone from outcrop sections and a borehole section by micromill drilling (Dremel 4000) with care being taken to avoid diagenetic vein sparite and large skeletal grains in the Sedimentology laboratory in the Middle East Technical University. 82 powdered samples were collected from polished hand specimens. For each stable isotope analysis, at least 3.0 mg of powdered fine–grained matrix was extracted with a steel needle from identified portions of cut rock faces. Dolomitized samples were not collected for stable isotope analyses and also it is very difficult to separate dolomite from calcite and other components due to the fine–grain size. Determination of $\delta^{13}C$ and $\delta^{18}O$ isotope ratios in carbonate samples was performed by using Gas Bench–

Continuous Flow Isotope Ratio Mass Spectrometry (DeltaPlus XP Isotope Ratio Mass Spectrometer–Thermo Finnigan) in the Central Laboratory of the Middle East Technical University. Carbonate samples were weighed on a precision balance of 0.2–0.4 mg and placed in sample wells. Each sample was allowed to react with Ortho–Phosphoric acid – 99% (MERCK) (about 0.1 ml) for a period (about two hours) in an autosampler tray maintained at about 70 ° C. The CO_2 gas produced by this reaction is sent to the mass spectrometer to be separated into isotopes after purification by the Gas Bench interface. Ion ratios of CO_2 gas are converted to raw isotopic ratios by ISODAT software. In the analysis, the standard "NBS19 Limestone (NIST)" ($\delta^{13}C$: 1.95 ‰ and $\delta^{18}O$: –2.20 ‰) as the main standard was analyzed in each experiment set and used to convert the raw isotope ratios of the samples determined by the device to true isotopic values. The results are determined in terms of permil –VP according to VPDB (Vienna Pee Dee Belemnite). The 1σ error margins for $\delta^{13}C$ and $\delta^{18}O$ isotope ratios do not exceed 0.2 ‰.

SEM

The borehole section core is stored at the core archive of the TPAO Research Center as number 1024867. Raw sample materials processed 16 samples and SEM stubs of all analyses are stored at the Sedimentology Laboratory of Geological Engineering Department at the Middle East Technical University. Pithonellids were picked from weighted splits (1.2–4 mg) of the 20–75 μm fraction, using a Zeiss binocular microscope Stemi2000 at 100x magnification. The determinations of the species were carried out using a Scanning Electron Microscope (SEM).

Gamma–ray Logging

The gamma–ray log is one of the most useful logs and is run in all wells in the study area. The GR log is a record of the formation's radioactivity. The radiation emanates from naturally occurring uranium, thorium, and potassium (Rider, 1996). The radioactivity of the rock measured by the GR log tool is generally a direct function of the clay mineral content and depositional environment. They are often used to infer

changes in depositional energy, with increasing radioactivity reflecting increasing clay content with decreasing depositional energy (Rider, 1990). Pure carbonate rocks such as packstones, grainstones, rudstones, and boundstones, which are formed in high energy environments commonly indicate only very low amounts of radioactive elements, because they normally contain only low amounts of clay minerals which are concentrated in the micritic matrix. Matrix–rich carbonate rocks such as mudstones, wackestones, and floatstones reveal higher gamma–ray readings, depending on the amount of matrix and incorporated clay minerals. Thus, gamma–ray well–logging can also be used to interpret the lithology of single strata and separate them through the definition of different log shape patterns.

1.4 Previous Studies

1.4.1 Previous Studies About the Cretaceous Autochthonous Sequences in the SE Turkey

Many researchers have studied the Mardin Group of the southeast Anatolian region in terms of palaeogeography, palaeontology, lithostratigraphy, petrography, and stratigraphy. Some researchers proposed palaeogeographic models for different parts of the Mardin Group in SE Turkey and also general models and concepts.

Rigo de Righi and Cortesini (1964) were first to establish the stratigraphy and structural setting of southeast Turkey.

Tuna (1974) first provided that in terms of the common use of terms in petroleum exploration by performing the formation of a common formation by using the name of the formation has been provided.

Köylüoğlu (1986) were examined the chronostratigraphy, microfacies, and microfossils of autochthonous units in SE Anatolia.

Wagner and Pehlivan (1987) suggested that the distribution of the Cretaceous carbonates reservoirs and source rocks in the northern part of the Adıyaman region is

controlled by sea–level changes, depositional settings, and palaeoclimate. The sea–level changes affected the Derdere and the Karababa reservoirs.

Görür et al. (1991) identified cyclicity in the Mardin Group carbonates and established that the sedimentary environment of the Karababa–A member of the Mardin Group is favorable for oil generation.

Çelikdemir et al. (1991) believed that the Mardin Group carbonates were deposited on a shelf and in an intra–shelf basin of the passive continental margin of the Arabian plate during Aptian to early Campanian time intervals. Sea–level changes in the Cretaceous time intervals have resulted in three main cycles and several sub–cycles in the Mardin Group carbonates. The three main cycles are separated from each other by unconformities. Each unconformity at the top of each cycle is a product of lowstands of sea–level. When sea–level rise, the highstand deposits covered the lowstand unconformities. The first cycle shows a shallowing upward character but displays a stationary character in some places. Each of the second and third cycles is a shallowing upward sequence, indicating sea–level falls during the late Cretaceous. The first and second cycles are regionally distributed. The third cycle developed only locally, being deposited mainly in intra–shelf basins.

Tardu (1991) interpreted that the erosional and non–depositional surfaces have also been identified within the Group by sequence–stratigraphic analysis.

Perinçek et al. (1991) stated that organic–rich limestones at the base of the overlying the Derdere Formation were deposited in relatively deeper–marine, anoxic conditions, and pass up into a shallowing upward sequence consisting of lagoonal to tidal–flat carbonates.

Cater and Gillcrist (1994) suggested that the Mardin Group shallow–marine carbonate sequences in SE Turkey developed in response to regional transgressive and regressive episodes. The most widespread transgressions are thought to correlate with known or postulated global sea–level rises during the mid–to–late Cretaceous.

Coşkun (1996) suggested that two brittle deformation stages controlled the porosity evolution in the Cretaceous Mardin Carbonates in the Adiyaman region. These stages are 1) obduction of the allochthonous Koçali–Karadut complex from north to south in

the Late Cretaceous (Maastrichtian) which mainly affected the northern oil fields and 2) the Miocene–Pliocene Adıyaman wrench fault system which affected mainly the southern oil fields in the region.

Çoruh et al. (1997) studied the biostratigraphic characteristics of autochthonous units in SE Anatolia. This study has been put forward various findings but, the studies concerning biostratigraphy are limited.

Demirel and Güneri (2000) identified three potential source rock intervals in the Cretaceous time interval. Two of these, the Derdere and Karababa formations of the Mardin Group, are composed of shallow–water carbonates, deposited on the northern margin of the Arabian Platform.

Mülayim (2013) conducted a detailed study of the depositional environments and sequence stratigraphy of the Derdere and Karababa formations in the Çemberlitaş oil field, SE Turkey.

Robertson et al. (2016) emphasized that the Derdere Formation deposited in stable shelf carbonate accumulation. The microfacies of the Derdere Formation indicated in a low–energy shallow–marine setting, and a low–energy inner platform setting. On the other hand, the microfacies of the Karababa Formation is likely to have accumulated in an open–marine, mid–ramp setting.

Özkan and Altıner (2018) investigated that three measured stratigraphic sections, Türkoğlu, Derik, and İnişdere, were studied to establish the stratigraphic framework of the Mardin Group in southeast Anatolia. Based on stratigraphic distributions of the benthic and planktonic foraminifera, the Mardin Group succession is constrained to have been deposited in a time interval from early Aptian to Santonian. Late middle Albian–late middle Turonian was assigned to the Derdere Formation and the late middle Turonian–late Santonian to the Karababa Formation in their study. Their analysis was not detailed enough to characterize the parasequences and to determine the exact system boundaries along the sections.

Mülayim et al. (2018) stated that the Derdere Formation material from wells in the Adıyaman region has yielded roveacrinid fragments Here, the Derdere Formation is thought to be early – middle Cenomanian, in part based on the roveacrinids present.

Mülayim et al. (2019a and b) studied the Derdere Formation and overlying Karababa–A Member at an outcrop at İnişdere (Adıyaman) and Türkoğlu (K.Maraş), in the region. Here, the authors were able to demonstrate that the base of the Karababa–A Member corresponds to the Cenomanian–Turonian Boundary Event, where anoxia and sea–level rise contributes to the demise of the Derdere carbonate ramp platform.

Mülayim et al. (2020) investigated that rudist associations of the Derdere and Karababa formations are documented to allow comparisons with those of the Arabian Platform.

1.4.2 Previous Studies in the Cenomanian–Turonian Anoxic Event (OAE 2) Studies and OAE 2 in Turkey and Arabian Platform

Over the last decades, the Cenomanian–Turonian boundary has been the subject of international research interest. By the end of the Cenomanian and beginning of the Turonian significant global palaeoceanographic and climatic changes occurred, as shown by the widespread deposition of organic–rich rocks. The deposition of organic–rich matter strata occurs in numerous basins in the Middle East as well as in deep–sea basins of other oceans during Lower (Weissert OAE, Faroni OAE, (Selli) OAE 1a, (Paquer) OAE1b, (Amedeus) OAE1c, OAE1d,) and Late Cretaceous times (MCE) Mid Cenomanian Oceanic Anoxic Event, (Bonarelli) OAE 2, OAE3) (Figure 1.3) (Schlanger and Jenkyns, 1976; Drzewiecki and Simo, 1997: Spain; Kuhnt et al., 1997: Morocco; Robaszynski et al., 1993: Tunisia. These organic–rich strata are generally linked to eustatic sea–level rises, positive peaks in the $\delta^{13}C$–isotope record, and to marine anoxic events. The Cenomanian–Turonian Anoxic Event is determined as the CTAE 2 or Bonarelli Event (OAE 2) (Arthur, 1987; Schlanger et al., 1987; Jenkyns et al., 1994). Trigger and dating of the Upper Cretaceous anoxic events are still under discussion, despite extensive research of these topics. Several models have been suggested to explain the factors causing an Oceanic Anoxic Event. Most authors assume a coastal upwelling which lead to increased productivity and an intensified oxygen–minimum–zone (OMZ) (Schlanger and Jenkyns, 1976; Arthur et al., 1987; Schlanger et al., 1987; Jarvis et al., 1988). Some authors postulate that the early Turonian was marked by a peak transgression caused by a worldwide high sea–level

stand (Figure 1.3). (e.g. Hancock and Kauffman, 1979; Arthur et al., 1987; Haq et al., 1987; Peryt and Wyrwicka 1991; Haq, 2014). The association of sea–level peaks with anoxic events has been rejected by Hancock (1993), who explained this hypothesis as a result of misdating the Turonian boundary (e.g. by means of foraminifera or ammonite–inoceramid zonations). According to Arthur et al. (1987) the increase in shelf–sea areas caused by transgressions led to enhanced production of warm saline waters, which sank to bottom water masses. This process led to an increase in the rates of oceanic turnover because the Cretaceous oceanic circulation was salinity driven. This increased circulation created enhanced upwelling, which triggered the OAE. A different model is favoured by Summerhayes (1987). According to his model, the upwelling was caused by an influx of nutrient–rich oxygen–deficient bottom waters from the northern South Atlantic, triggered by the separation of Africa from South America. However, the dynamics of the Cenomanian–Turonian upwelling event remain poorly understood and few current models adequately explain all the characteristics of the sedimentary deposits of that time (e.g. Jenkyns, 1999). Nevertheless, it is generally accepted that the event did lead to widespread anoxia in the oceans (Jarvis et al., 1988).

The Cenomanian–Turonian carbonate successions of the Arabian Carbonate Platform are well exposed and have been mapped and investigated in detail over the past 30 years in Jordan, Oman, Israel, Iraq and Iran in Arabian Plate (Alsharhan and Nairn, 1997). In particular, numerous studies have depicted how the Cenomanian–Turonian Boundary Event is recorded in most countries of the Middle East, except SE Turkey. There is a record of C–T boundary within pelagics in western Taurides (SW Turkey) by Yurtsever et al., 2003; Bozcu et al., 2011; in Pontides by Yılmaz et al., (2010) well documented the C–T boundary with multiproxy records within pelagics. A hiatus at the Cenomanian–Turonian boundary has been reported from SE Turkey and the Middle East (Çelikdemir et al., 1991; Buchbinder et al., 2000), but its origin remains unclear. However, the latest Cenomanian–early Turonian hiatuses and extreme condensation are not local phenomena, but have been recorded from many Mediterranean platforms as a result of platform drowning (e.g., Philip and Airaud–Crumiere, 1991; Drzewiecki and Simo, 1997; Schlager, 1999). Thus, it cannot be excluded that a global control as a result of long term oceanographic changes linked

with the eustatic sea–level rise possibly also influenced the formation of the hiatus in SE Turkey. The present study aims at filling that gap. The present work in the Arabian Plate is part of a continued effort to investigate the relative sea–level changes recorded by depositional facies changes around the C–T boundary. Recent studies have shown that the bulk rock of shallow–water platform carbonates, despite their facies heterogeneity, is able to record unaltered $\delta^{13}C$ shifts (Bomou et al., 2013; Frijia et al., 2015, Mülayim et al 2019a and b). In addition to depicting how the CTBE is recorded on the carbonate platform of SE Turkey, the present study aims at integrating this in a regional synthesis from published data.

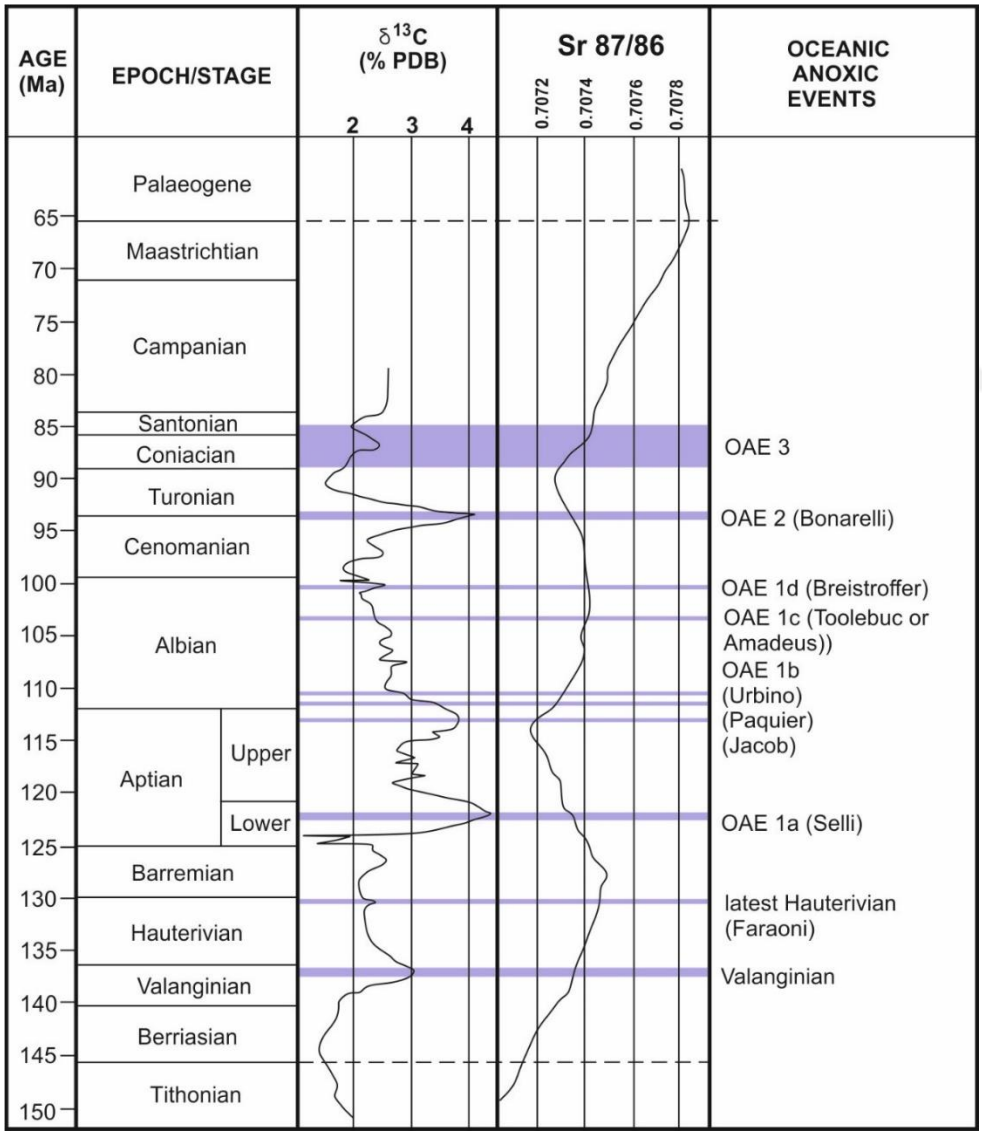


Figure 1.3. Cretaceous trends and excursions in carbon stable isotopes and 87Sr/86Sr and Oceanic Anoxic Events (OAE) (after Gradstein et al. 2004).

CHAPTER 2

GEOLOGICAL SETTING AND STRATIGRAPHY

The Upper Cretaceous stratigraphy of the SE Turkey has been focus of many studies since the early ’80s (Wagner and Pehlivanlı 1987; Duran and Aras 1990; Çelikdemir et al. 1991; Görür et al., 1991; Perinçek et al. 1991; Karabulut et al. 1992; Cater and Gillcrist, 1994; Coşkun 1996; Robertson et al. 2016; Mülayim et al. 2016; 2018; 2019a, 2019b, 2020; Özkan and Altıner, 2018; Simmons et al. 2020 in press). These studies have produced the number of formation names, controversial age assignments, and different facies models for the same deposit, devising the need for major refinement of the established stratigraphy. The stratigraphic units were defined by various researchers which are illustrated a correlated summary chart for SE Turkey. The main reason for the inconsistency among the stratigraphic columns is the fact that the important lateral variations in facies and age. Unfortunately, most workers underestimated the relationship between the lateral variation and spatiotemporal evolution. Such variations need to be assessed carefully and may provide useful clues to the temporal and spatial evolution. It is therefore indispensable to establish the mutual relationship between the evolution of the study area and resultant stratigraphic architecture. Although it is not the main focus of this dissertation to address all problems of the stratigraphic framework of SE Turkey, this study needs a working stratigraphic model to understand the evolution of the study area. Thus, it depends on, three measured stratigraphic sections, and borehole data (rock cuttings and gamma–ray logs) from around thirty exploration wells in order to refine the available stratigraphic models of the study area, particularly for the northwestern Arabian platform. Following this initial focus on the stratigraphy by this chapter, the

stratigraphic architecture will be related to the evolution of the study area in the following chapters. As a result, this chapter focuses only on the stratigraphic framework.

2.1 Cenomanian–Turonian Palaeogeography

The palaeogeography during the Cenomanian–Turonian time interval is remarkable because it includes one of the highest stands of sea–level (+260 m above present–day sea–level at the Cenomanian–Turonian stage boundary, 93.5 Ma; Haq, 2014). This highstand is bracketed by precipitous drops in sea–level during the mid–Cenomanian (down 80 m from highstand), and during the late Turonian (down 130 m from highstand). The highstand at 93.5 Ma is coincident with OAE 2, the "Bonarelli" Event. Due to high sea–levels, in is not suprising that the continents were flooded during the Cenomanian–Turonian. Approximately 33% of the continents were covered by shallow seaways. The most notable are the Mid– continental Seaway in North America, the Trans–Saharan Seaway in Africa, and the West Siberian–Caspian Seaway in Eurasia (Scotese, 2014) (Figure 2.1).

Stable platform conditions persisted over the region until the Mid–Cretaceous, resulting in predominately carbonate deposition over a large area. The principal controls on sedimentation were sea–level fluctuations and tectonic movements. Thick marine carbonates predominated in the Mid– and Late Cretaceous sedimentary sequences over most of the region (Sharland et al., 2001; Barrier and Vrielynck, 2009). The global sea–level was at a highstand in the late Cenomanian–early Turonian interval (Haq, 2014). The sedimentary succession in the SE Turkey and adjacent areas was greatly influenced by sea–level fluctuations and also tectonic movements. Shallow marine carbonates accumulated due to flooding over the platform during the initial period of sea–level rise (Barrier and Vrielynck, 2009). The Derdere carbonates formed during the highstand where the sediments were deposited on a passive margin of the Neo–Tethys Ocean (Figure 2.2). The lithofacies of the Derdere Formation changed during the cycle of relative sea–level (Mülayim et al. 2019a). Thickness variations of the Derdere Formation in the region are due to the effect of the basinal configuration and topography.

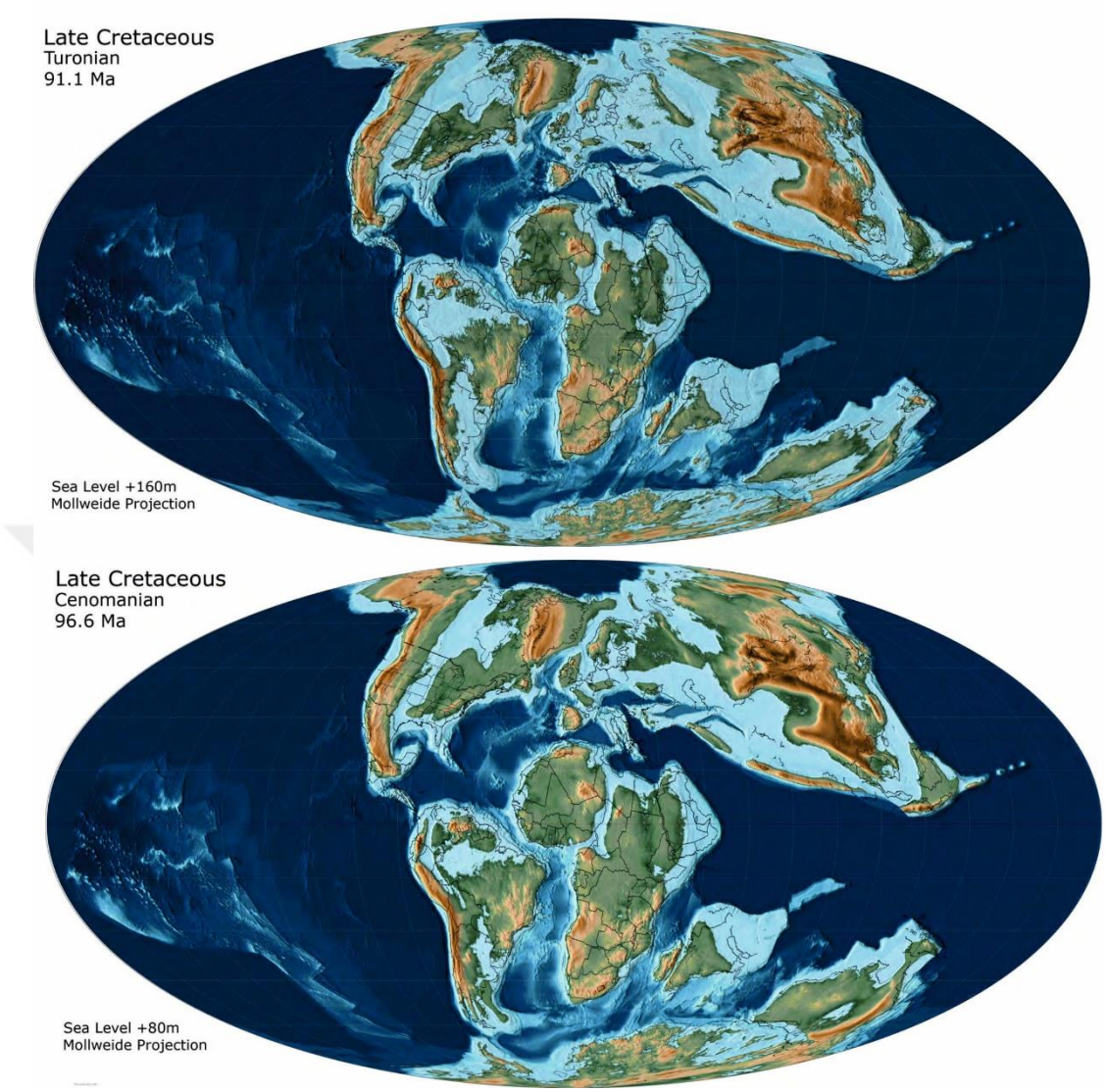


Figure 2.1. The palaeogeographic maps of the Cenomanian (96.6 Ma) and Turonian (91.1 Ma) (Scotese, 2014).

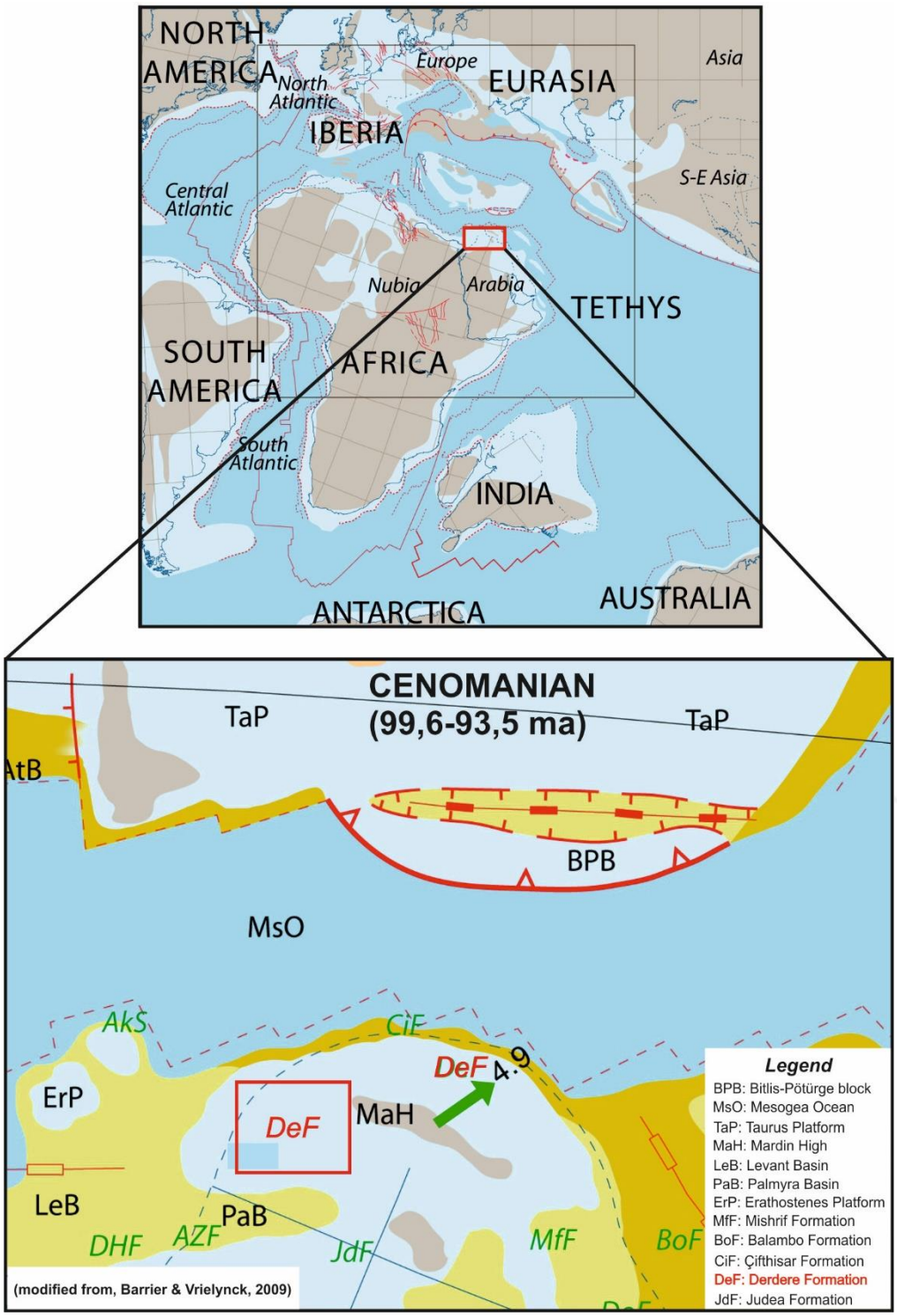


Figure 2.2. The palaeotectonic maps of the Middle East–northern margin of the Arabian Plate– Cenomanian (99.6–93.5 Ma) (Barrier and Vrielynck, 2009).

2.2 Regional Tectonic Setting

The most significant global tectonic events affected the region were the Hercynian Orogeny, the opening of Neo Tethys, Cimmerian Orogeny. The Hercynian Orogeny, which is the result of the collision of Gondwana and Laurussia in the Middle Carboniferous (Stocklin and Setudehnia 1972; Berberian and King, 1981). Ruban et al. (2007) stated that The Hercynian Orogeny created transpressional strike–slip faults and reverse faults along Gondwana (Figure 2.3) and caused laterally broad and extensive blocks (e.g., Mardin–Kahta paleo–highs in SE Anatolia) to uplift. The opening of the Neo–Tethys during the Mid Permian–Triassic period (Stampfli and Borel, 2002) and thus, progressive compression triggered the formation of a mid–ocean ridge in a semi–perpendicular direction to the collisional front between Gondwana and Laurussia (Figure 2.3). Therefore, beginning with the Mid–Permian, the northern margin of the Pangean–Gondwana turned into a subsiding passive margin over which some emerged lands are located (Figure 2.3). Pre–Cambrian and Paleozoic basement units were eroded whereas Triassic and Jurassic sequences were partly eroded or not deposited due to major orogenic events, glaciation periods, and/or sea–level falls particularly over the aforementioned emerged lands in the region. Uzunçimen et al. (2011) and Varol et al. (2011) stated that the rifting age of the Southern Tethyan Oceanic Basin in SE Anatolia is possibly earlier than the early Late Triassic (middle Carnian time). The Mardin–Kahta High, which is the most significant one of these reliefs, constitutes the structural basement of the study area of this research and shows tectonic activity contemporaneous with Hercynian, and Cimmerian orogenic phases.

In the Cimmerian Orogenic phase, the previously emerged lands (e.g., Mardin–Kahta high) had uplifted more and were subjected to further erosion until their peneplenization. After the end of the Cimmerian phase, the Arabian margin experienced an extensional regime accompanying the opening of the Neotethys Ocean, which caused an uneven bathymetry with structural highs and lows (Sungurlu, 1974; Ala and Moss, 1979). The direction of the extension was roughly in the N–S; whereas the direction of topographic highs and lows was roughly E–W (Yılmaz, 1993).

As a consequence of both tectonic depression and a long–term sea–level rise occurred in the Jurassic and Early Cretaceous periods (Haq, 2017). Especially, during the Aptian and Campanian, the passive Arabian margin was completely submerged and constituted the basement for the deposition of the Cretaceous carbonate ramp platform (Cros et al., 1999; Özkan and Altıner 2018; Mülayim et al., 2019; 2020)..

,

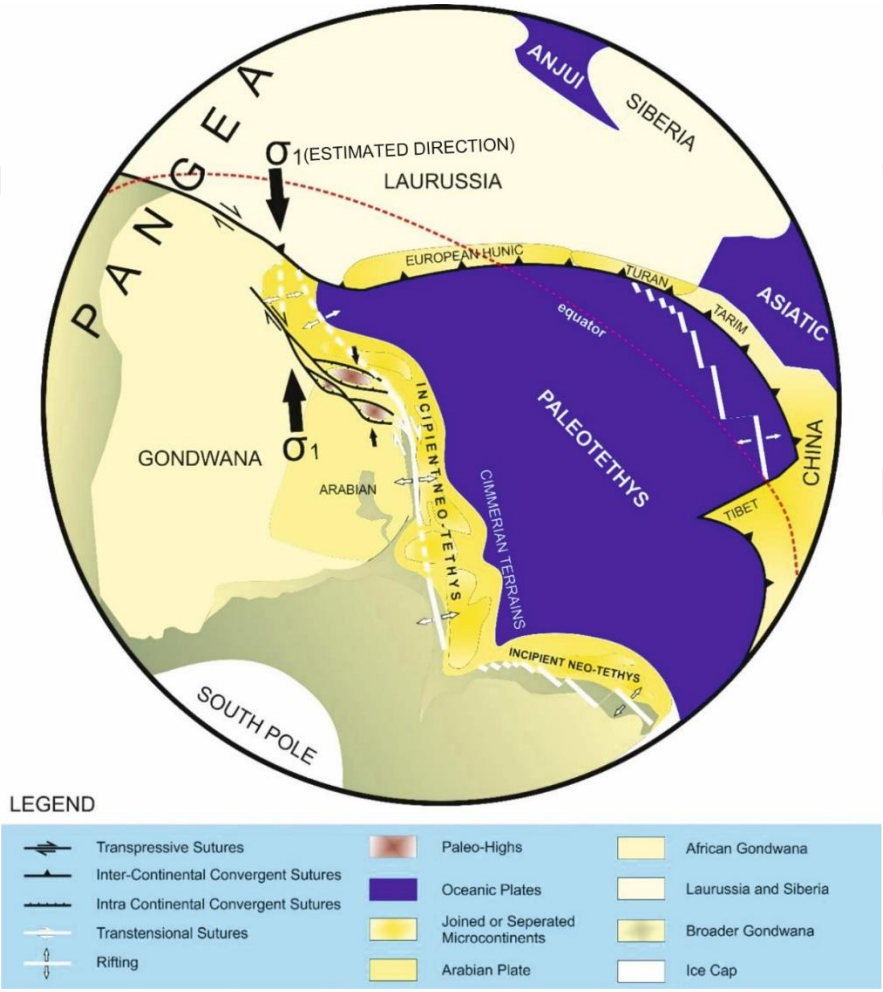


Figure 2.3. Late Early Permian palinspatic reconstruction map (after Stampfli and Borel, 2002). The modifications include the illustrations for the incipient faults of NeoTethys rifts as accommodative structures to lengthening related to progressive shortening caused by the collision between Gondwana and Laurussia and for *the formation of sporadic uplifts located at the Northern Arabian Plate.

The geologic evolution of Turkey during the Mesozoic and Cenozoic consisted of two main tectonic units, the Pontides, the Anatolides–Taurides, and the Arabian Platform respectively, which are separated today by suture zones (Okay and Tüysüz, 1999) (Figure 2.4). The Arabian Platform was separated from the Anatolide–Tauride Block by the Southern Branch of Neo–Tethys in the Mesozoic (Şengör and Yılmaz, 1981; Okay et al., 2006). The southeast Anatolia represents the northern part of the Arabian Platform (Şengör and Yılmaz, 1981; Harris et al. 1984; Flexer et al. 1986). The autochthonous sequence has been affected by two main tectonic phases.

The first episode of deformation occurred during Late Cretaceous (latest Campanian–mid–Maastrichtian) emplacement of ophiolites and accretionary melange onto an underfilled, flexural controlled foreland basin (Rigo de Righi and Cortesini, 1964; Horstnik, 1971; Parlak et al. 2009; Robertson et al. 2016). First, the ophiolite obduction onto the Arabian Platform occurred. SE Turkey is a key area to understand geological processes related to the closure of the Southern Neotethys. The Southern Neotethys is widely believed to have rifted during the Triassic and to have been bordered by passive margins during Jurassic to mid–Cretaceous time (Fontaine et al., 1989; Robertson et. al, 2015). The early Cretaceous was a period of maximum rifting of the Neo–Tethys Ocean, while the major phase of tectonics occurred in Late Cretaceous resulting in the closure of the Neo–Tethys ocean accompanied by major continental collision. Thus, the opening of Neo–Tethys probably ceased in mid–Cretaceous when the stable abrupt intensive reactivation of basement faults jostled the previously stable platform (Yılmaz, 1993; Cater and Gillcrist, 1994; Robertson, 1998). This activity led to uplifting and subsequent erosion. They were most active from the Turonian to the early Maastrichtian. (Yılmaz, 2011; Mülayim et al. 2016). These time periods correspond to major changes in basin configuration. Furthermore, isopach map patterns of facies distributions of Cretaceous sediments are more complex than for any other period (Koop and Stoneley, 1982).

The second episode of deformation occurred during early to mid–Miocene final closure of the Southern Neotethys. The northern, active continental margin, represented by the Tauride allochthon, was emplaced over the Arabian passive margin, resulting in flexural collapse and formation of the early Miocene foreland basin. The

foreland basin filled and was finally overridden by the Tauride allochthon. The emplacement is explained by the advanced collision of the Arabian and Anatolian plates. Post–collisional, non–marine clastic sediments accumulated during Mid–Late Miocene time associated with suture tightening (Yılmaz, 2011; Robertson et al., 2016).

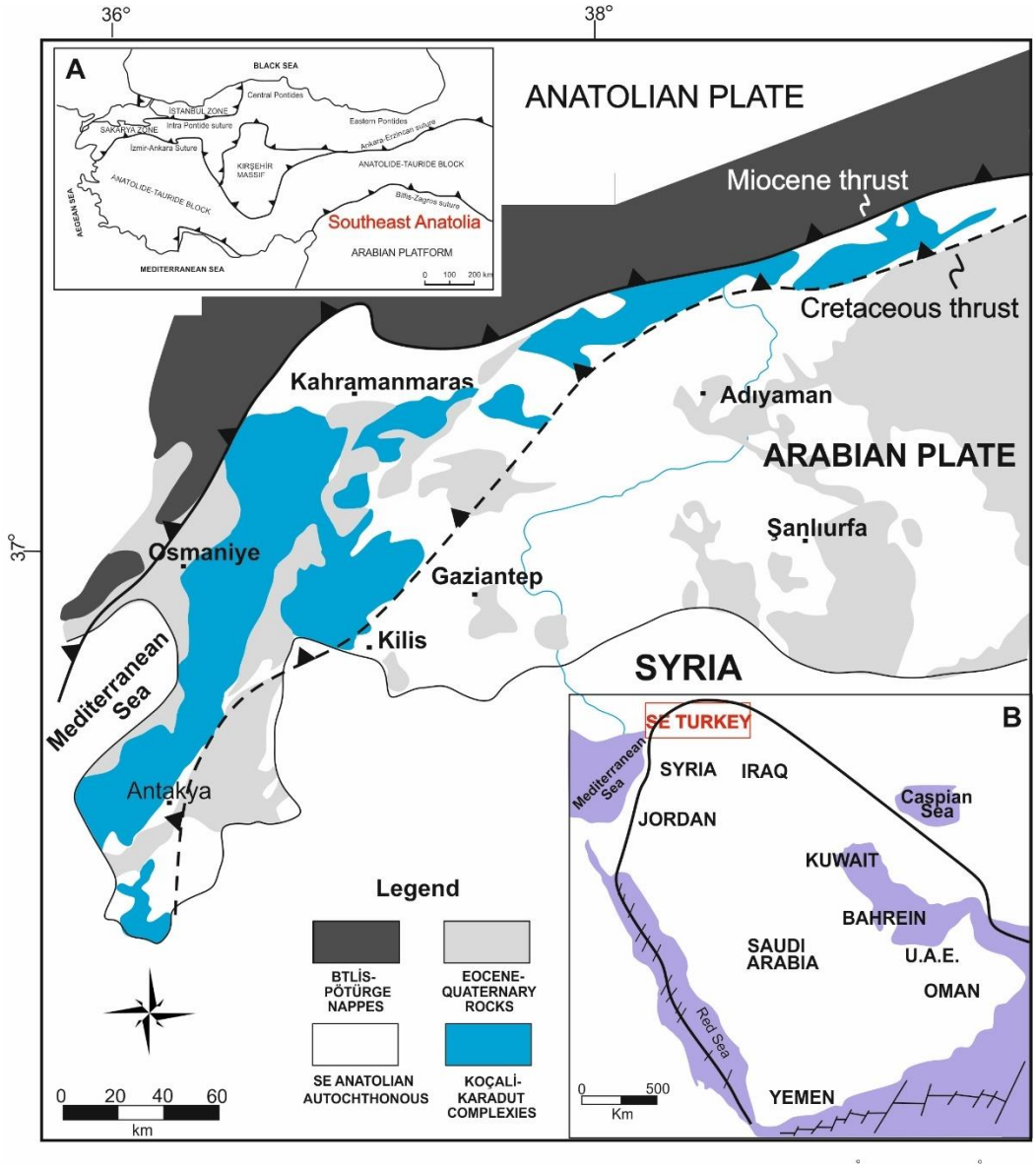


Figure 2.4. Simplified geological map of the northwestern part of Turkey (after Şenel, 2002 and Mülayim et al. 2019b). A. Tectonic map of Turkey showing the major sutures and continental blocks (after Okay and Tüysüz, 1999), B. The geographic location of SE Turkey in the northernmost part of the Arabian Platform (after, Sharland et al. 2001).

2.3. Regional Stratigraphy

Throughout southeast Turkey, pre–Cambrian to recent sedimentary successions are discontinuously preserved in the subsurface boreholes and outcrops (Figure 2.5). Post–Cambrian Paleozoic units along with Triassic, Jurassic, and the earliest Cretaceous units (pre–Aptian), which are described in this section are missing in the Adıyaman province including the field and subsurface survey sites of this research. Post–Cambrian pre–Aptian units are proven to have preserved somewhere else in southeast Turkey, such as around K.Maraş, Kilis, or Gaziantep provinces. Investigating how they become locally missing in the study area, however, may shed light on the tectonic and stratigraphic history of the region as a whole. The late Cambrian Sosink Formation and older units, which constitute the local basement, are overlain by the Aptian Areban Formation of the Mardin Group around the Adıyaman Province (Figure 2.5). The Derdere and Karababa formations (Cenomanian–Turonian) comprise organic–rich intervals whose presence is a prerequisite for the petroleum system in the study area Nevertheless, locally absent Silurian Dadaş Formation and Triassic–Jurassic Cudi Group's source rocks contribute to the petroleum system additionally to the Mardin Group source rocks elsewhere in southeast Turkey.

2.4 Stratigraphy of Cretaceous Rock Units

The Cretaceous rock units unconformably overlie the Paleozoic rock units at the Adıyaman region and Jurassic rocks of the K. Maraş and Kilis regions. Different lithological associations are described in three groups (Mardin, Adıyaman and Şırnak) and they display either lateral–vertical passages and/or display unconformable relationships (Figure 2.6). Cretaceous formations are described in basic characteristics of these units, based on personal field observations and available literature, which will be described in detail as below.

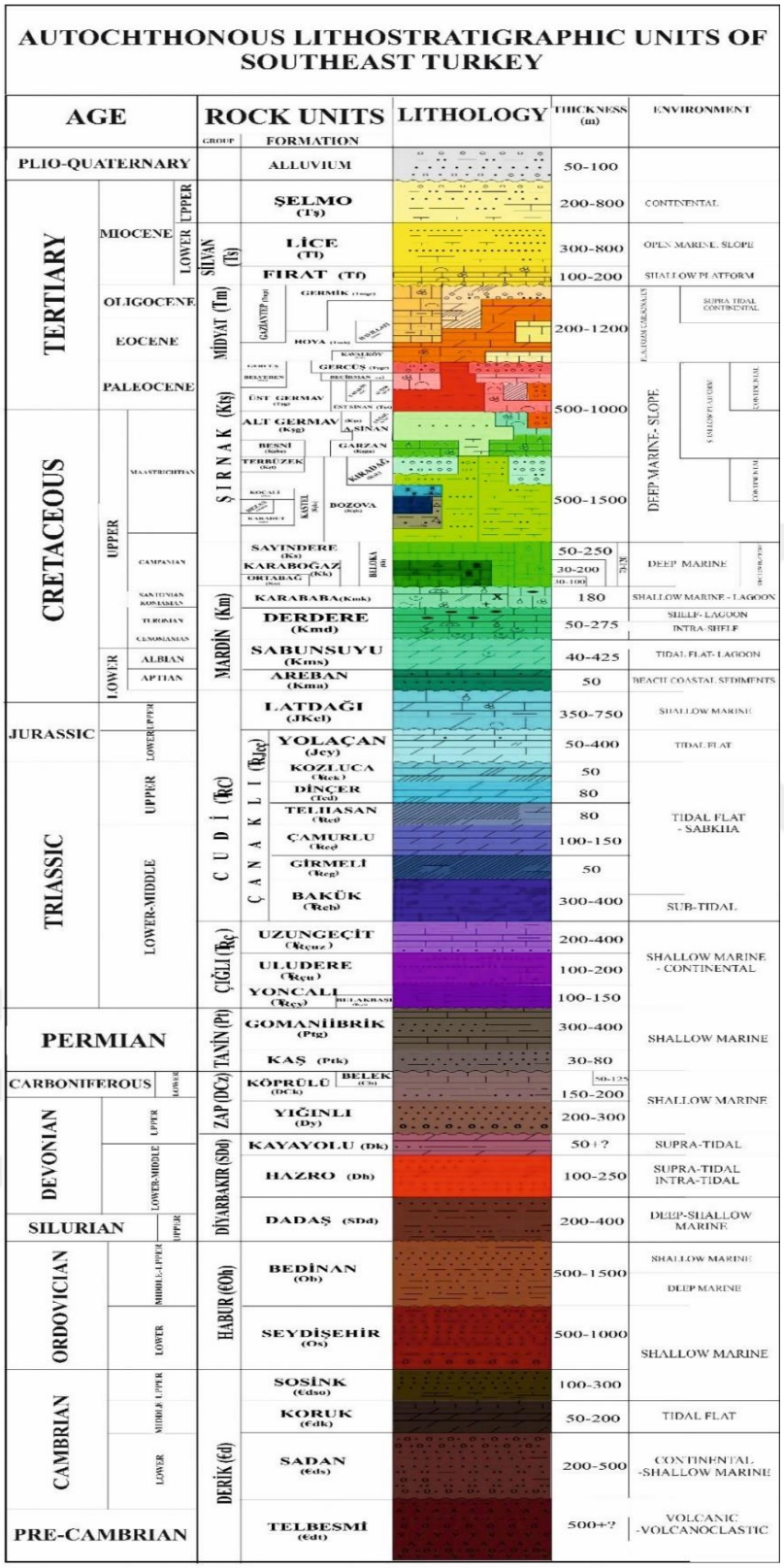


Figure 2.5. Generalized stratigraphic section of the southeast Turkey. (Güven et al. 1991).

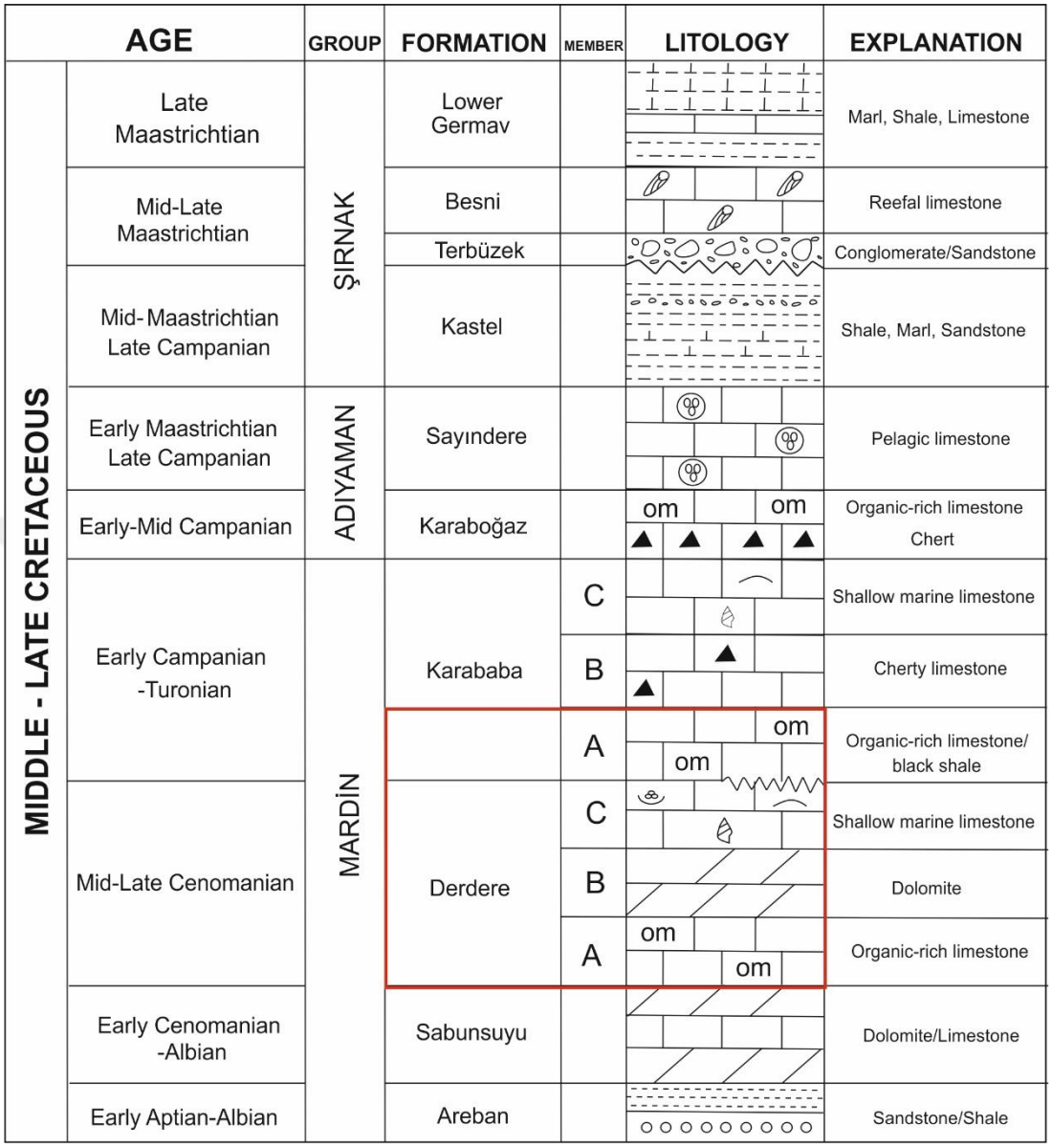


Figure 2.6. Generalized stratigraphic section of the study area and surroundings in SE Anatolia (after Mülayim et al. 2016)

2.4.1 The Mardin Group

The Mardin Group are exposed to outcrops and have been penetrated by wells in SE Turkey. These rocks are Aptian–early Campanian in age (Çoruh, et al 1997). They consist of limestones, dolomitic limestone, dolomites, and siliciclastic sediments. The Mardin Group represents deposition on a carbonate platform that developed on the passive, northern edge of the Arabian Plate prior to southerly–directed thrusting and

related folding (Görür et al., 1991; Cater and Gillcrist, 1994). The stratigraphic and sedimentological characteristics of the group have been described by Çelikdemir et al. (1991) and Coşkun (1992) four formations are recognized (to the top): the Areban, Sabunsuyu, Derdere and Karababa formations (Yılmaz and Duran, 1997) (Figure 2.6).

2.4.1.1 The Areban Formation

The Areban Formation at the base of the Mardin Group unconformably overlies the Paleozoic, Triassic, and Jurassic basement units in southeast Turkey. It composes of an alternation of sandstones, siltstones, claystones, sandy limestones (Çelikdemir et al., 1991) and fine–grained sandy dolomite and defined as deposits of shallow–marine (restricted lagoonal to tidal–flat), coastal (beach) or continental clastics environments. The age of the formation is assigned as Aptian (Sinanoğlu and Erkmen, 1980) and early Barremian?–Aptian (Özkan and Altıner, 2018).

2.4.1.2 The Sabunsuyu Formation

The Areban Formation is conformably overlain by the carbonates of the Sabunsuyu Formation. It is composed of shallow–marine carbonates (dolomites, dolomitic limestone–marl alternation and limestones) (Çelikdemir et al., 1991). This lithological association is ascribed to a restricted to semi–restricted shallow–marine and tidal–flat to subtidal carbonate platform deposit (Perinçek et al., 1991). The age of the formation is assigned as Albian–Cenomanian (Köylüoğlu, 1986); early Aptian to Albian (Özkan and Altıner, 2018).

2.4.1.3 The Derdere Formation

The Derdere formation unconformably overlies the underlying the Sabunsuyu Formation whereas the Karababa Formation is unconformable above. It composed of shallow marine limestones, dolomitic limestone dolomites, and organic–rich limestone (Çelikdemir et al., 1991; Mülayim et al., 2016) and defined as deposits of shelf marine environments (Çelikdemir et al., 1991; Mülayim et al., 2016). The age

of the formation is assigned as Cenomanian–Turonian (Robertson et al., 2016) and Albian–Turonian (Özkan and Altıner, 2018).

2.4.1.4 The Karababa Formation

The Karababa Formation overlies unconformably the Derdere Formation and is unconformably overlain by the Karaboğaz Formation. The Karababa Formation is subdivided into three members as Karababa A, B and C from its lowest to its upmost, respectively. The lowermost member Karababa–A is a very fine–grained, organic–rich pelagic lime mudstone; Karababa–B consists of cherty limestones; The uppermost member, the Karababa–C is represented by shallow–marine bioclastic limestones and partly dolomites (Çelikdemir et al., 1991; Mülayim et al., 2016). Karababa Formation is defined as deposits of intrashelf environments in the previous studies (Çelikdemir et al., 1991; Mülayim et al., 2016). The age of the formation is assigned as late Coniacian?– early Campanian (Yılmaz and Duran, 1997); late Turonian–Campanian (Robertson et al., 2016); middle Turonian–Santonian (Özkan and Altıner, 2018).

2.4.2 The Adıyaman Group

The Adıyaman Group is represented by a conformable sequence of four distinct formations; these are, from bottom to top, middle Campanian Karaboğaz Formation, middle Campanian Ortabağ Formation, upper Campanian Sayındere Formation and upper Campanian–upper Maastrichtian Beloka Formation (Figure 2.6). Among these formations, Karaboğaz and Sayındere formations are exposed in the study area. The unit displays conformable relationships with the underlying Karababa Formation of the Mardin Group and overlying Şırnak Group (Güven et al., 1991).

2.4.2.1 The Karaboğaz Formation

The Karaboğaz Formation unconformably overlies the underlying Karababa Formation likewise the Sayındere Formation is conformable above. It composes of organic–rich pelagic limestone with chert layers or nodular chertified limestone and

defined as deposits an anoxic deep–marine environment to platform shelf environment (Güven et al., 1991). The formation is also considered to have developed during a transgression (Cater and Gillcrist, 1994). The age of the formation is assigned as Middle Campanian (Güven et al., 1991).

2.4.2.2 The Sayındere Formation

The Sayındere Formation conformably overlies the underlying the Karaboğaz Formation likewise the Kastel Formation is conformable above. It composed of argillaceous limestone (Çelikdemir et al., 1991; Robertson et al., 2016). The Sayındere Formation was deposited over a block–faulted basement (Robertson et al., 2016) with undulated geometry which controls its thickness and local depositional facies. The Sayındere Formation is subdivided as lower, middle and upper members (Özkaya et al., 2019). The lower member of the Sayındere Formation comprises organic–rich carbonate mudstones and bioclastic limestones at basement lows. The middle member consists of clayey bioclastic limestone, and the upper member comprises pelagic biomicrites (Özkaya et al., 2019). The age of the formation is assigned as late Campanian (Güven et al., 1991).

2.4.3 The Şırnak Group

The Şırnak Group is represented by a sequence of several formations; these are, from bottom to top, Kastel, Bozova, Kıradağ, Terbüzek, Besni, Haydarlı, Garzan, Germav, Üçkiraz, Sinan, Antak, Kayaköy, Belveren and Becirman formations (Figure 2.6) (Güven et al., 1991; Perinçek et al., 1991). Among these formations, Kastel, Terbüzek, Besni, and Germav formations are exposed in the study area.

2.4.3.1 The Kastel Formation

The Kastel Formation conformably overlies the Sayındere Formation and commences with a progradational sequence. It shows gradational contact relationship with the underlying Sayındere and overlying Terbüzek formations. Allochthonous units

structurally overlie the formation (Güven et al.,1991). The Kastel Formation composes of marls, shale and sandstone alternation and is interpreted as deposit in a continental shelf to deep marine environment (Güven et al., 1991). The age of the formation is late Campanian–middle Maastrichtian (Güven et al., 1991).

2.4.3.2 The Terbüzek Formation

The Terbüzek Formation overlies unconformably the Kastel Formation with its cutting and filling downwardly scraping channels and unconformably overlain by the Besni Formation. Terbüzek Formation is composed of a fluvio–deltaic conglomerate, pebblestone, sandstone and mudstone alternation. The depositional environment is suggested as alluvial fan, fluvial and flood plain (Güven et al., 1991). Age of the formation is early–middle Maastrichtian (Güven et al., 1991).

2.4.3.3 The Besni Formation

The Besni Formation displays sharp conformable contact relationships with overlying the Germav Formation and gradational contact with the underlying the Terbüzek Formation. Where exposed, the formation unconformably overlies the Koçali and Karadut complexes. In places, it displays unconformable relationship with the Kastel Formation. It is composed of an altered sandstones and sandy–pebbly (ophiolitic clasts) limestones, continues with fossiliferous bioclastic limestones (Meriç et al., 1987; Güven et al., 1991; Özer, 1992). The depositional environment is suggested as shallow marine (Güven et al., 1991). Age of the formation is middle–late Maastrichtian (Güven et al., 1991).

2.4.3.4 The Germav Formation

The Germav Formation overlies the Besni Formation conformably and is unconformably overlain by the Belveren, Fırat and Becirman formations whereas it displays conformable contact relationships with the Midyat Group (Gercüş and Hoya formations) (Güven et al., 1991). The Germav Formation commences with alternation

of silty marl, siltstone, sandstone and marl with limestone beds, and shale with sandstone intercalations. The depositional environment is suggested as deeper sea and abyssal fan (Güven et al., 1991). Age of the formation is middle Maastrichtian–late Paleocene (Güven et al., 1991).

2.5 Lithostratigraphy

2.5.1 Revision of Cenomanian–Turonian Lithostratigraphic Depositional Units in the SE Turkey

The Cenomanian–Turonian successions are continuously preserved throughout the entire region of southeast Turkey. The Cenomanian Derdere Formation and Turonian Karababa–A Member within the Mardin Group, on the other hand, form essential source rocks of the regional petroleum system in the study area. As a consequence of both palaeotectonic activity and a long–term sea–level rise occurred in the Jurassic and Early Cretaceous periods (Haq, 2017), specifically during the Aptian and Campanian, the passive Arabian margin were completely submerged and constituted the basement for the deposition of the Cretaceous platform carbonates known as the Mardin Group (Görür et al., 1991). Derdere and Karababa formations comprise organic–rich intervals whose presence is a prerequisite for the petroleum system in the study area.

In the stratigraphic studies in and around the study area, it is clearly seen that there are still some problems related to stratigraphic nomenclature. One of the reasons for these inconsistent applications might be related to the palaeotectonic activity of the region and the rapid facies variations. In this study, a revision is realized for the formations and members of the Cenomanian–Turonian age exposed in the region.

2.5.2 Lithostratigraphic Nomenclature

The lithostratigraphic nomenclature in SE Turkey has changed considerably over more than a fifty years and is still changing as new techniques are implemented in the analysis of the basin, and new data are available. Most of the names assigned to the Cenomanian–Turonian units in SE Turkey (Perinçek, 1991; Çelikdemir, 1991; Çoruh et al., 1997; Mülayim et al., 2016; Robertson et al, 2016; Özkan and Altıner, 2019 and references therein) have been adopted (see Figures 2.7 and 2.8), producing misinterpretations in regional correlations and palaeogeographic reconstructions (Perinçek et al., 1991). Additionally, a number of unconformities present during the accumulation of these units make litho– and biostratigraphic correlations even more challenging. Considering the complex tectonic framework and lateral variation of facies within SE Turkey, using a single nomenclature system may not only be difficult but also counterproductive. In this study, the nomenclature proposed by Mülayim et al. (2019a; 2020) is adopted for SE Turkey. A new stratigraphic model has proposed for the Cenomanian–Turonian interval for SE Turkey. The revision of the stratigraphic nomenclature of the Derdere and Karababa formations is based on lithological descriptions and foraminiferal analyses from wells and outcrops located in three regions: İnişdere–Adıyaman; Sabunsuyu–Kilis and Türkoğlu–Kahramanmaraş respectively and boreholes sections. A detailed lithological and micropaleontological description of these outcrops and boreholes can be found in Mülayim et al., (2018, 2019a 2019b; 2020). Wells were selected based on their location, quality of the core recovered, intervals cored, and length of the sections recovered. It is worth noting that only a few cores cut the entire Derdere Formation and Karababa–A Member in SE Turkey. Therefore, the litho– and biostratigraphic information analyzed in this study was complemented with several well–log correlations performed in the study area (Figure 2.8).

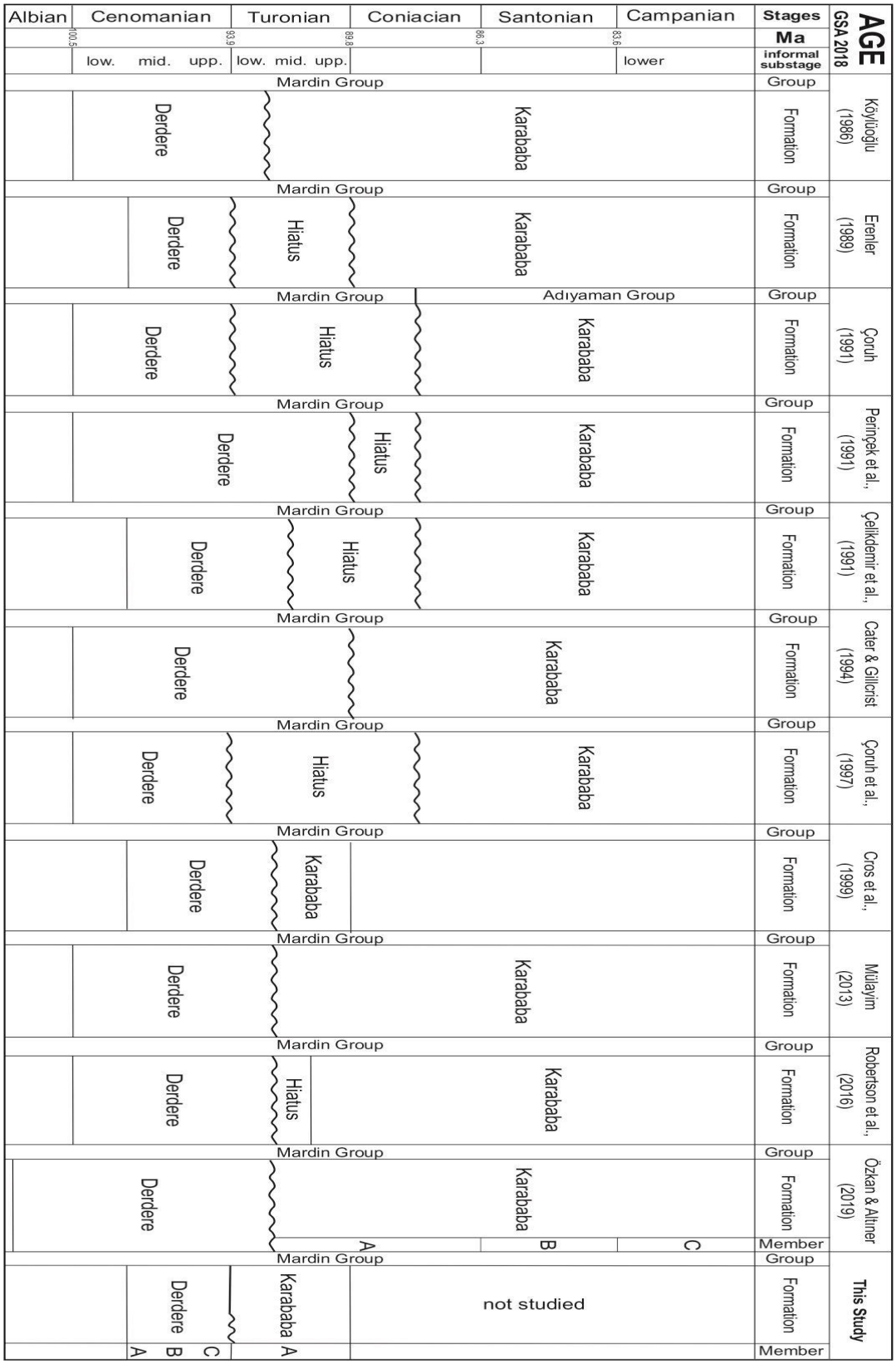


Figure 2.7. The correlation chart of the Cenomanian–Turonian formations in the SE Turkey

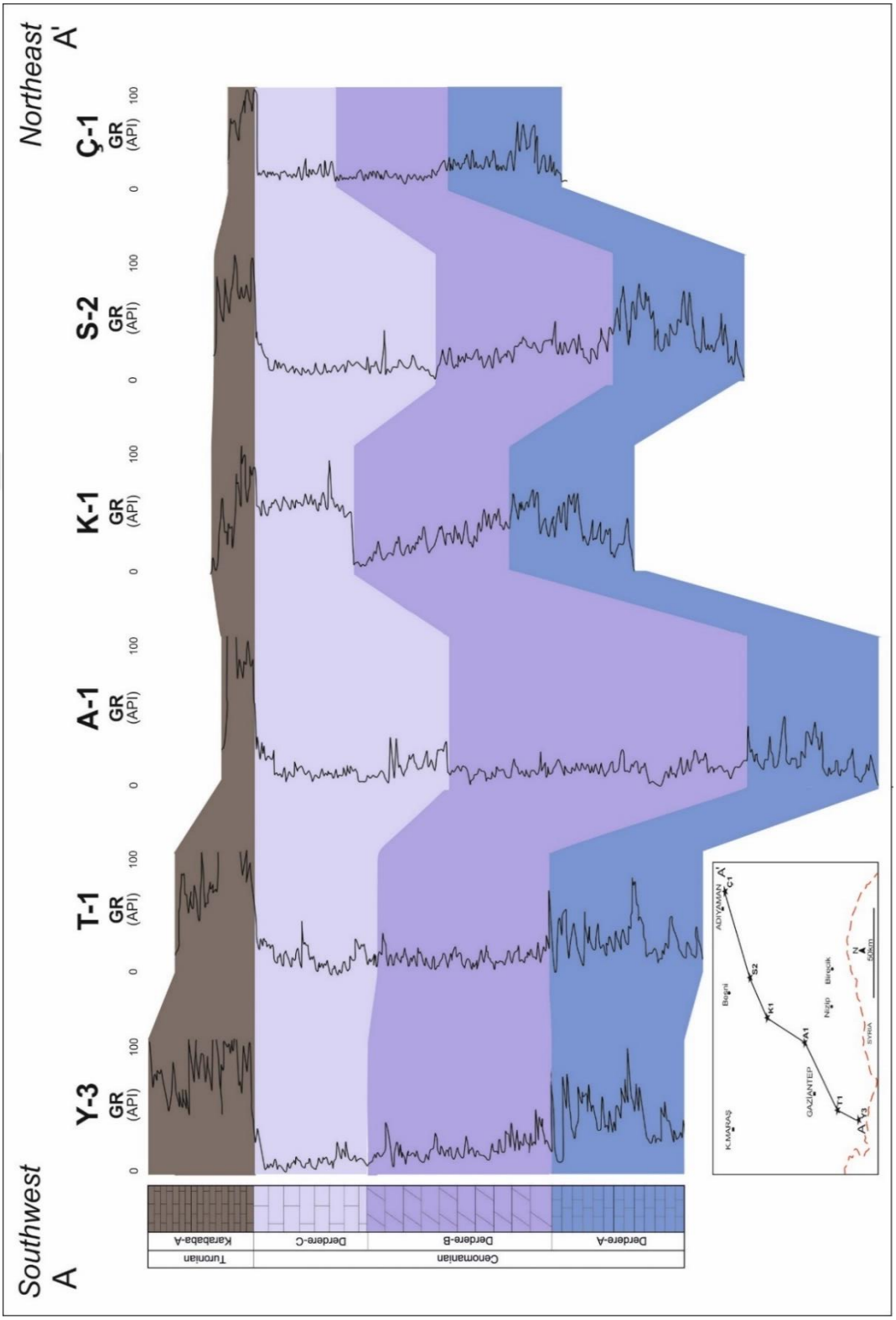


Figure 2.8. Generalised lithological log of the Boreholes with gamma–ray in Derdere Members A, B and C respectively and Karababa–A Member.

2.5.2.1 Derdere Formation

Derivation of name. Named for the village of Derdere located at the Cüngüş district of Diyarbakır. This formation was named first by Handfield et al. (1959).

Type section. The type section exposed in the Korudağ anticline (Handfield et al., 1959). Reference section for the upper part of the Derdere Formation is represented in İnişdere valley located 0.8 km north of Ünlüce Village in Adıyaman. The other reference section for the Derdere Formation is very well exposed along the Sabunsuyu stream on the 28 km northwest of Kilis. Antakya–Kilis main road is cut in the carbonate sequences up to the Sabunsuyu bridge. Additionally, in the K. Maraş region, the Türkoğlu stratigraphic section is located in the 25 km south of K. Maraş around the old quarry. It represents very well all sections of the Derdere Formation.

Underlying strata: Medium– to thick–bedded, sometimes dolomitic limestones and dolomites overlie thin–bedded and laminated, stromatolitic dolomites of the Sabunsuyu Formation.

Overlying strata: Last occurrence of dm– to cm–thin continuous organic–rich pelagic limestone, sometimes including glauconite and phosphate grains and fish bones of the Karababa–A Member.

Description: The Derdere Formation consists of often greyish limestones and especially within the upper part, beige limestones and dolomites, comprising (from base to top) macrofossil poor limestones, organic–rich pelagic limestones with interbedded marls and locally dolomites. In the middle part, above the limestones, there are dolomites. The upper third of the Derdere Formation contains macrofossil rich bioclastic limestones (e.g. Mülayim et al., 2020).

*Subdivisions. (from base to top):*Derdere–A Member, Derdere–B Member, Derdere–C Member.

Three sequential facies are represented in the Derdere Formation. They were designated as members by Mülayim et al., (2019) and based on type areas such as Adıyaman, K. Maraş, and Kilis and boreholes.

Derdere–A Member. The Derdere–A Member represents the lowermost part of the Derdere Formation. It mainly consists of dark grey blackish–grey colored, thin–bedded, organic–rich pelagic limestones with very thin yellowish shale beds and thin–bedded mud– and wackestones limestones. The basal strata are locally dolomitic (Mülayim et al., 2020) and overlie stromatolitic dolomites of the Sabunsuyu Formation. At some localities strata rich in roveacrinid and exogyras occur near the base of the Derdere–A Member. They often represent the lowermost part of the Derdere–A Member, but similar lithology may occur in the lower part as unpublished boreholes data. The lowermost microfossil–rich stratum of the Derdere–A Member is often rich in pithonellids and planktonic foraminifera. These pithonellids and foraminiferas are usually dolomitized. The gamma–ray logs in the Derdere–A Member is characterized by a positive peak (Figure 2.8). While the Derdere–B Member and the Derdere–C Member are characterized by decreasing clay content (Figure 2.7). Also, It is a good seal for the underlying Sabunsuyu Formation and a good source rock for the entire petroleum system of the region.

Derdere–B Member. The Derdere–B Member represents the middle part of the Derdere Formation which occurs grey colored thin–bedded to massive dolostone and interbedded with dolomitic limestones (Figure 2.7). Especially the middle part of the Derdere Formation is often dolomitized. In some regions the dolomitized Derdere–B Member locally contains chert nodules (e.g. Mülayim et al.,2020). Macrofossils are rare. The middle of the Derdere–B Member is defined by a change from (dolomitic) limestone with single dolomitic strata to both laterally continuous and pure dolomite. Due to the diagenetic nature of the upper boundary of the Derdere–B Member, the level of the boundary varies within the Derdere Formation. It is, therefore, possible that the normally overlying Derdere–C Member directly rests on the Derdere–B Member, if dolomitization is used as classification criterion and if dolomitization affected the uppermost strata rich in Derdere–C Member. In that case, the Derdere–C Member is not developed as such in Diyarbakır, Şanlıurfa and Siirt areas. The fossils are mostly dolomitized (Mülayim et al., 2020) and, therefore, lost their internal structure. If the dolomitization also concerns the matrix, the fossil shapes often can be recognized under the microscope only. The lower boundary is defined by the change from (dolomitic) limestone with single dolomitic strata to a laterally continuous and

several m–thick pure dolomites. In this member, dolomite content has to exceed 90 percent. Macroscopically the dolomite varies considerably. The lower part often cannot be separated sharply from the underlying limestones of the Derdere–B Member visually. Due to the diagenetic nature of the lower boundary of the Derdere–B Member, the level of the boundary varies within the Derdere Formation. It is, therefore, possible that the Derdere–B Member directly rests on the Derdere–C Member if dolomitization reached down to the uppermost strata rich in bioclastic level. The dolomites of the Derdere–B Member nowadays have a mudstone appearance, but they mostly seem to have been mud– and wackestones prior to dolomitization. Locally bivalve and gastropod strata occur within the dolomites (Mülayim et al., 2020).

Derdere–C Member. It represents the uppermost part of the Derdere Formation (Figure 2.7). It is mainly composed of beige, dirty white–colored, thin to medium–bedded limestone which is containing debris of bivalve (rudist) shells or layers with gastropod/roveacrinid shells which are prominent in the upper part of the formation in some levels. They typically form fining–upward cycles. Some marl may be interbedded. Some roveacrinid debris may occur in overlying strata, but mostly they are limited to the top of the strata, whereas the strata themselves are built up mainly by bivalve shells. The top of the Derdere–C Member is defined by the first occurrence of successional rudist shell–rich float– to rudstones above bioturbated wackestones and packstones.

Occurrence: Southeastern Turkey (Anatolia)

Thickness. The type section measures 74 m in thickness. A general decrease in thickness towards the northern can be detected. Local maxima and minima seem to be associated with the preexistent palaeotectonic activity of the region.

Contact relationships. Derdere Formation is conformably underlain and unconformably overlain by Sabunsuyu and Karababa formations, respectively. In outcrop evidence analogous to a drowning unconformity, was observed between Derdere and Karababa formations.

Fossils. The Derdere Formation comprises predominantly benthic foraminifera assemblages including Miliolidae, Textulariidae, Gavelinellidae, Discorbidae, Lenticulinidae, Nubeculariidae, *Meandrospira* sp. *Cuneolina pavonia, Nezzazatinella picardi, Sellialveolina viallii, Nezzazata simplex, Biplanata peneropliformis, Dicyclina schlumbergeri, Dicyclina* sp. *Thaumatoporella parvovesiculifera, Spiroloculina cretacea, Ovalveolina maccagnoae, Meandrospira* sp.. A higher biostratigraphic resolution on the basis of the distribution of benthic foraminifera does not seem possible. The rudist fauna of the Derdere Formation is characterized by *Sauvagesia* sp., *Durania* sp., *Biradiolites* sp., *Durania acuticostata, Sauvagesia sharpei* and *Bournonia?* sp., *Caprinula* sp. (*C.* cf. *sharpei*), *Radiolites* sp., *Ichthyosarcolites triangularis, Ichthyosarcolites monocarinatus* and *Neithea fleuriausiana*. The Derdere Formation comprises poor planktonic foraminifera assemblages such as *Asterohedbergella asterospinosa, Muricohedbergella planispira*. In addition, Cenomanian algae *Marinella lugeoni* and *Permocalculus* sp. and pithonellids; *Pithonella sphaerica, Pithonella ovalis, Pithonella lamelleta, Bonetocardiella conoidea* species, as well as roveacrinids; *Roveacrinus communis, Roveacrinus* cf.*alatus, Roveacrinus spinosus, Roveacrinus* sp. Roveacrinidae indet. *Applinocrinus* sp. Saccocomidae indet. and annelida are also present in this interval. No Cenomanian nannofossil taxa could be found in Derdere Formation.

Chronostratigraphic age: middle–late Cenomanian according to Mülayim et al., 2020; and Simmons et al., 2020 in press.

Depositional environment. The Derdere Formation was deposited in deeper to shallow carbonate ramp environments (Cros et al., 1999; Robertson et al., 2016, Özkan and Altıner, 2019, Mülayim et al., 2018; 2019a; 2019b; 2020).

2.5.2.2 Karababa–A Member

Derivation of name. Named for Karababa Mountain located in the Adıyaman–Şanlıurfa road boundary. First, this formation was named by Gossage (1956).

Type section. The type locality is 32 km of Adıyaman province, the northern side of the Euphrates valley in the south of Karababa Mountain.

Underlying strata: Thin– to medium–bedded shallow marine limestones, sometimes dolomitic limestones and dolomites of the Derdere Formation. It is a good seal for the underlying Derdere Formation and a good source rock for the entire petroleum system of the region.

Overlying strata: Thin–to medium hemipelagic limestone with chert nodules, sometimes including glauconite and phosphate grains of the Karababa–B Member. It is described by a gradual grain size coarsening with respect to the Karababa–A.

Description: The Karababa–A Member consists of dark brownish blackish–grey colored, thin–bedded, very fine–grained, organic–rich pelagic lime mudstone (Figure 2.7). It is slightly recrystallized into microspar, and has few microfossils such as planktonic foraminifera, thin filament fragments, pithonellids, roveacrinids and, in addition, phosphatized grains (fish bones) cemented by abundant micrite. Planktonic fossils gradually decrease upwards in abundance (Mülayim et al., 2019a; 2019b).

Occurrence: Southeastern Turkey (Anatolia)

Thickness. The type section measures 106,5 m in thickness. A general decrease in thickness towards the north can be detected. Local maxima and minima seem to be associated with the preexistent palaeotectonic activity of the region.

Contact relationships. Karababa–A Member, is unconformably underlain and conformably overlain by Derdere Formation and Karababa–B Member, respectively. In outcrop evidence analogous to a drowning unconformity, was observed between Derdere and Karababa formations.

Fossils. The unit is dominantly represented by planktonic foraminifera assemblages. These assemblages are mainly dominated by whiteinellids, which are associated with

dicarinellids, marginotruncanids and rare helvetoglobotruncanids. Taxa identification is hampered by widespread recrystallization. The age data are obtained based on the presence of four distinctive planktonic foraminiferal assemblages. *H. praehelvetica* is rare at the base and observed only at a single level in the upper part of the member. Whiteinellids (i.e. *Whiteinella baltica, W. archaeocretacea, W. aprica* and *W. brittonensis),* marginotruncanids (i.e. *Marginotruncana tarfayaensis, Marginotruncana* sp. cf. *M. sigali, M. schneegansi, Marginotruncana* sp. cf. *M. paraconcavata, Marginotruncana* sp. cf. *M. pseudolinneiana* and *M. renz*i) and rare dicarinellids (i.e. *Dicarinella* sp. cf. *D. marionasi* and *Dicarinella* sp. cf. *D. primitiva*). In addition, some pithonellids species are characterized in the unit; *Pithonella sphaerica, Pithonella ovalis, Pithonella lamellata, Bonetocardiella conoidea.* Also, the few calcareous nannofossil markers present include *Eiffellithus eximius, Lucianorhabdus maleformis,* and *Quadrum gartneri* from around borehole data.

Chronostratigraphic age: Early–late Turonian (Mülayim et.al., 2019a; 2019b).

Depositional environment. The Karababa–A was deposited in deeper outer ramp environments (Cros et al., 1999; Robertson et al., 2016, Özkan and Altıner, 2019, Mülayim et al., 2019a; 2019b).

2.5.3 Isopach Maps

An isopach maps of the Derdere Formation and Karababa–A Member (Figures 2.9 and 2.10) were constructed using the data of 100/322 boreholes respectively and two outcrops. Wherever well path deviation data were available, they were considered to identify the true thickness. In SE Turkey, many borehole data were available from the TPAO archive. Locally they show a highly variable thickness of the Derdere Formation and Karababa–A Member. This variation is interpreted to result from drilling differently inclined strata that were shown the paleotopographic conditions with a tectonic effect. Therefore inaccurate outliers were not considered. The unpublished/published data from TPAO were used for constructing the isopach maps.

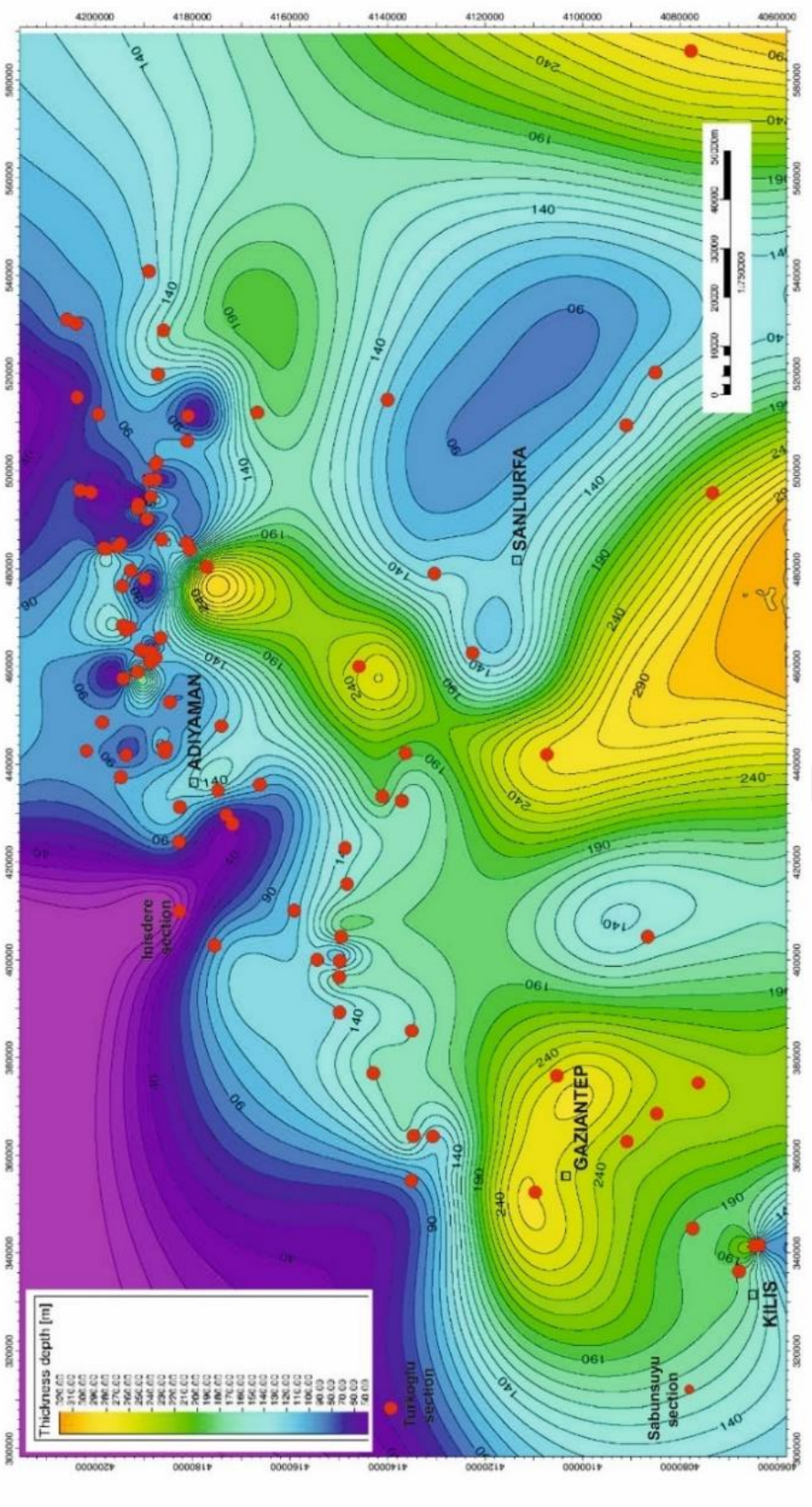


Figure 2.9. Isopach map of the Derdere Formation in SE Turkey.

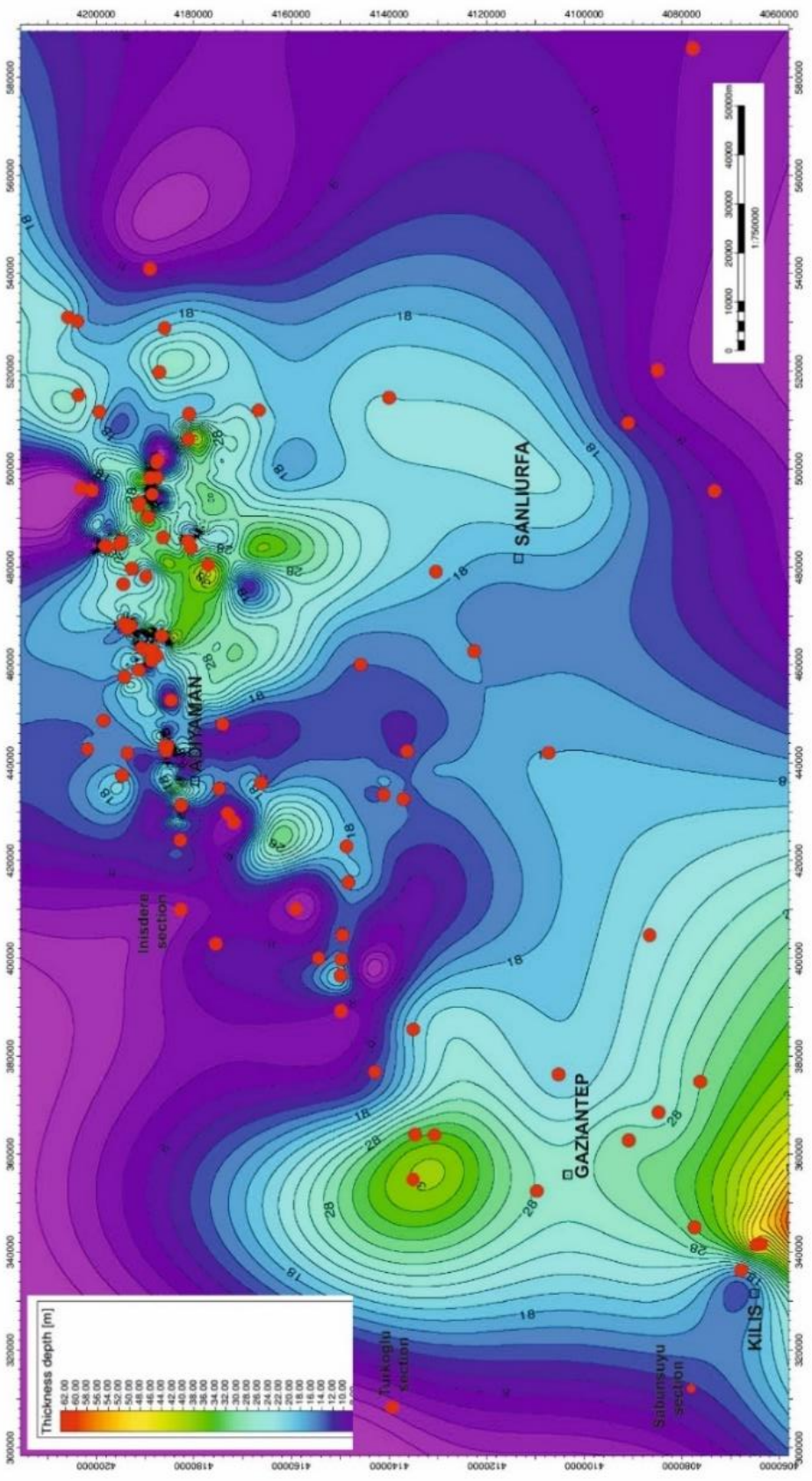


Figure 2.10. Isopach map of the Karababa–A Member in SE Turkey.

2.6 Lithostratigraphy of the Stratigraphic Sections

Three of the studied stratigraphic sections are Sabunsuyu–Kilis, Sabunsuyu Stratigraphic Section (SSS); İnişdere–Adıyaman, İnişdere Stratigraphic Section (ISS) and Türkoğlu–Kahramanmaraş, Türkoğlu Stratigraphic Section (TSS). The exact coordinates for the sections are given in Table 1.1.

2.6.1 Sabunsuyu Stratigraphic Section

The Sabunsuyu stratigraphic section is located to the northwest of the city of Kilis and represents an excellent outcrop that allowed us to understand the stratigraphy of the Derdere and Karababa formations. 68.20 m–thick strata were measured in stratigraphic section (Figures 2.11 and 2.12). As a result of the new observations through the stratigraphic section, nine different stratigraphic levels (seven from the Derdere Formation and two from the Karababa–A Member) are identified which are described from base.

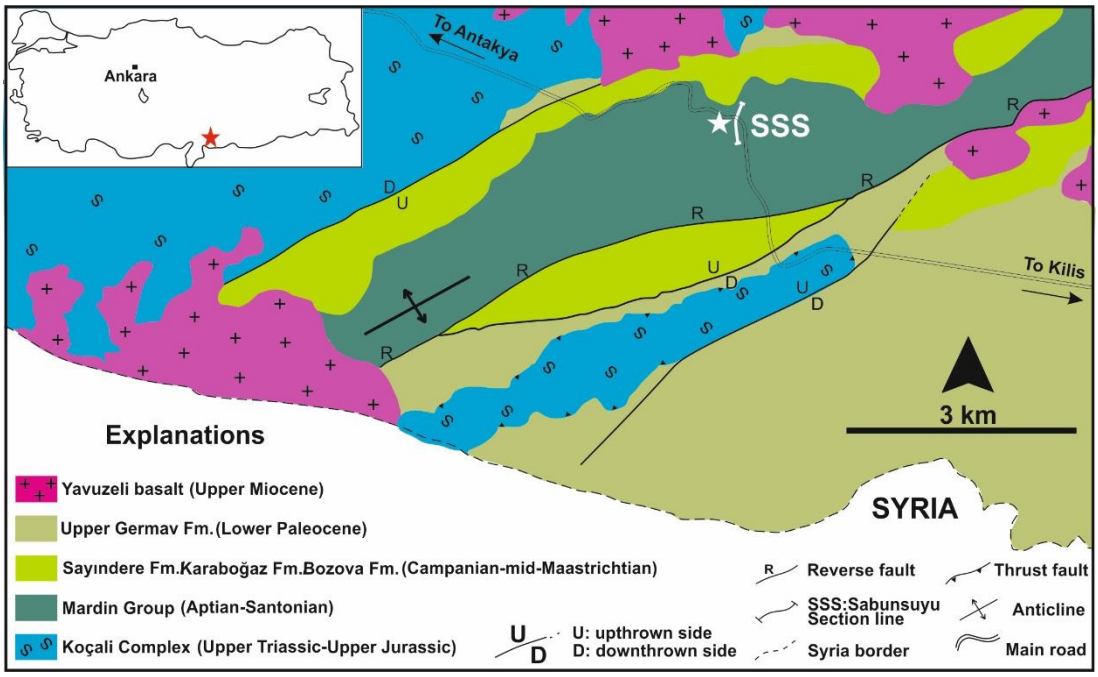


Figure 2.11. Geological map of the study area including the position of the Sabunsuyu stratigraphic section (after Şenel, 2002).


A
Karababa Fm.
Derdere Fm
B
base of Karababa
top of Derdere
C
D
E
F

Figure 2.12. (A) General field view of the Sabunsuyu strtatigraphic succession (B) Field view of the contact between the Derdere and Karababa formations (C) Pre–drowning rudist–rich limestone beds belong to the top of the Derdere Formation. (D) The Derdere–C Member where host carbonate facies are mainly mud– to wackestone, including many bivalve clasts. (E) Bioclastic limestones in the upper part of the Derdere Formation. (F) Chert nodules in middle part of the Derdere Formation.

Level–1) 4 m thin–bedded, beige, dark brownish, dolomitic limestone and limestone with shales interbedded in the lowermost part of Derdere Formation (Derdere–A Member); these exhibit also limonitisation (Figures 2.13 and 2.14). Exogyrine oysters are abundant in (wavy and parallel) shale layers with calcite veinlets. Abundant small planktonic foraminifera, pithonellids, rare roveacrinids and benthic foraminifera are also present in dolomitic thin limestone beds. Dolomitization are common in microfossils. Minor silica precipitation partially replaces some of the calcitic planktonic foraminifera. The silica was probably provided by the dissolution of the sponge spicules, common in the this interval. Sedimentary structures such as predominantly parallel lamination, locally wavy and cross lamination and grading are frequent.

Level–2) 19.32 m thick, thin–bedded intercalation of dark grey, massive dolomitic limestones/dolostones and grey, cherty limestones (nodular and band) with fine lamination, cross–stratification and calcite veinlets in texture (Derdere–B Member). (Figure 2.14). Chert bands are parallel to the strike of the limestones. Calcite–filled fractures are also common. Bioturbations are rarely observed. Dolomitization phenomena are diffused in the lower part of the orders (I–II) and can lead to near–complete obliteration of original textures. More frequently, very thin to thin layers are recognizable with different dolomitization intensity. Many of the bed boundaries correspond to sharp surfaces. These latter are in some cases represented by dolomitized thin layers that may laterally thicken. The cherty limestones comprise well–preserved planktonic foraminifera.

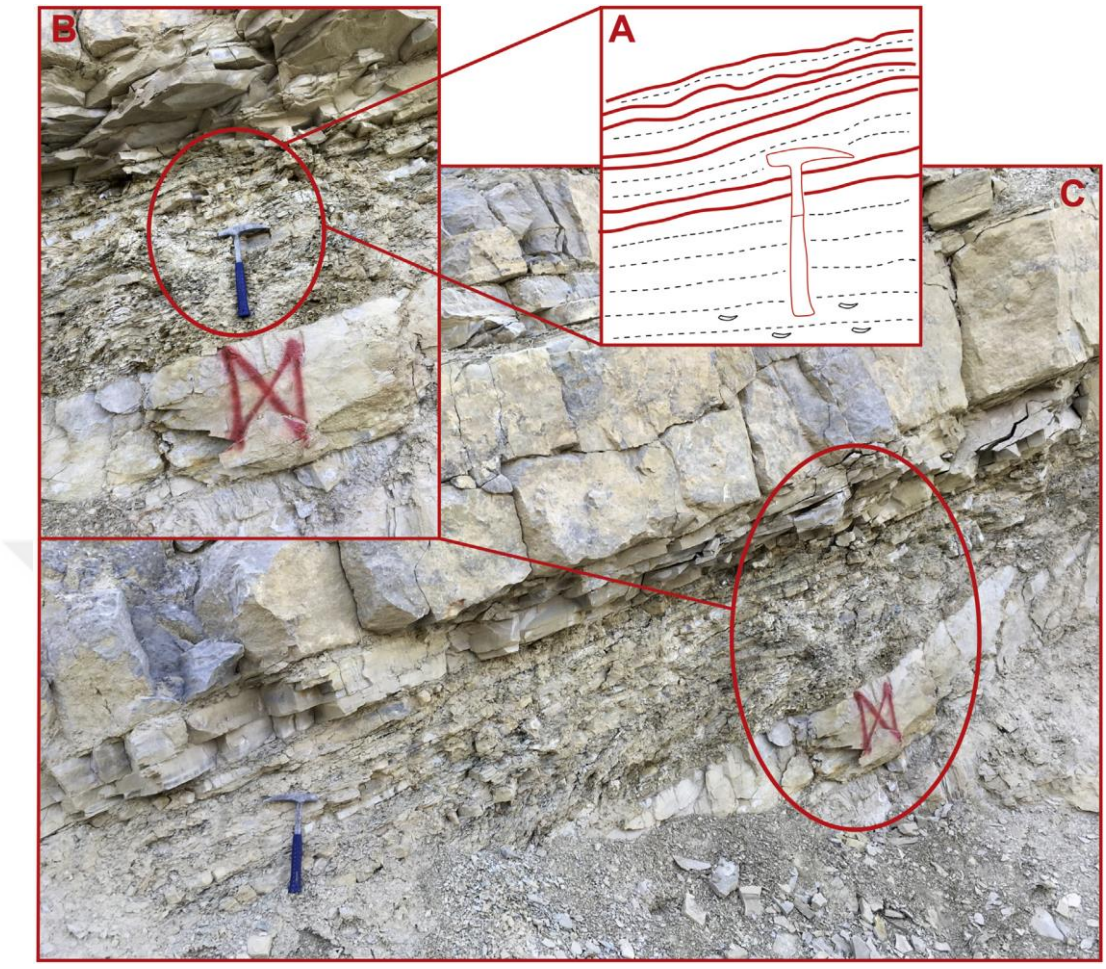


Figure 2.13. Outcrop evidence of intercalation of dolomitic limestone and shale beds at the base of the Derdere Formation. Exogyrine oysters are observed in shale layers, which are indicated in the area (red square, A), just below the hammer.

Level–3) 14.93 m very thick–bedded intercalation of grey, dolomitic limestones/dolostones and dark grey, unfossiliferous massive limestones (Derdere–B Member) (Figure 2.14). These dolomitic limestones do not yield any index microfossils. Dolomitization is a common characteristic of this part of the succession; it may characterize beds or alternating millimetre to centimetre–scale layers. In some cases, it may completely obliterate preceding structures. Dolomitized layers show undulating contacts, locally indented with non–dolomitized lithologies. These phenomena attenuate upwards in the interval.

Level–4) 10.55 m medium–to very thick–bedded, grey, rudist–bearing limestones, bioclastic limestones and limestone intercalations (Derdere–C Member) (Figure 2.14).

Two rudist–bearing limestones are distinguished from base to top in this part of the section. The lower one is very thick and consists mainly of radiolitid fragments, of which large quantities are of angular/subangular and poorly sorted nature. Some echinoids with spines are also present. The upper rudist–bearing limestones alternate with limestones and are around 3 m thick. Roveacrinid skeletons are locally dissociated and found scattered within mud–supported matrix. These rudist–bearing limestones do not yield foraminifera. Bioturbation is occasionally observed in this part of the section. Calcite veinlets are also common in this interval. Pithonellids and occasional planktonic foraminifera are associated with the previous species upwards into the succession.

Level–5) 1 m thick, medium–bedded limestone and very thin–bedded limestone, interbedded with chert bands (Derdere–C Member). Planktonic foraminifera and pithonellids are present see Figure 2.14).

Level–6) 6.5 m thick upper part, (Derdere–C Member) composed of grey, fossiliferous, very thick– to medium–bedded limestones and bioclastic limestones in alternation (Figure 2.14). The upper part is characterised by grey, massive, very thick rudist–bearing limestones containing mainly rudist shell fragments. Indeterminate radiolitid fragments are abundant; *Sauvagesia* and *Radiolites* have been noted. Bivalves, gastropods, echinoid fragments and roveacrinids are abundant in these limestones, but poor preservation precludes specific identification. Peloids are abundant throughout the succession. No large–scale sedimentary structures (cross bedding, graded bedding) can be identified. These limestones can present enriched foraminiferal levels as well as *Asterohedbergella asterospinosa* and *Globigerinelloides* sp. Planktonic foraminifera appear with a higher frequency upwards and are found in alternations of wackestone with benthic foraminifera.

Level–7) 5.4 m thick, very thick–bedded limestone containing two rudist–bearing limestones characterized mainly by abundant ichthyosarcolitids (Derdere–C Member) (Figure 2.14). This facies is very easy to identify in the field, due to the presence of recognizable, large macrofaunas. Often the matrix is neomorphically altered to

microspar, or dolomitized to fine–grained dolomite. No large–scale sedimentary structures have been identified in this facies. The first rudist–bearing level is very thick and consists usually of small ichthyosarcolitids. Indeterminate bivalves have also been observed. There are ichthyosarcolitid fragments in the rudist–bearing limestones, but they are accumulated in their original environment and are not reworked and transported. Peloids are abundant throughout the succession. A hardground–type surface is seen at the top of this interval.

Level–8) 3 m thick part of the succession consists of dark grey, thin–bedded silty limestones (Karababa–A Member) (Figure 2.14). Macrofossils are uncommon. Thin–section analysis identifies a microfaunas which are not identifiable at hand specimen scale. The pithonellids are especially common, scattered throughout beds.

Level–9) 3.5 m thick, grey, thick–bedded limestone consisting of two rudist–bearing limestone levels (Figure 2.14). Dolomitization and bioturbation are usually observed. Upwards in the section, intercalations of grey limestones and bioclastic limestones with rudists are seen. The thickness of the rudist–bearing limestones is laterally variable from thick to very thick. Other bivalves are represented by abundant, but unidentifiable specimens. Fossils are disarticulated, abraded, deposited concordant to bedding, and include bivalves and unidentifiable fossil debris. Bioclastic material is present and abraded in specific intervals but fossil identification is difficult. Rudists are usually in life position; however, intense fragmentation and accumulation of rudists and bivalves can be observed. In other cases, they are associated with very thin bioclastic laminae which locally show thin accumulations of rudist shells, both pristinely preserved and highly abraded. The bioclastic matrix (packstone) is composed almost exclusively of bioeroded rudist–shell fragments, associated with rare benthic foraminifera. Mollusc, echinoid fragments and roveacrinids are also present. Peloids are rare throughout the succession. Fragmentation of rudists is rarer than in the lower rudist–bearing level.

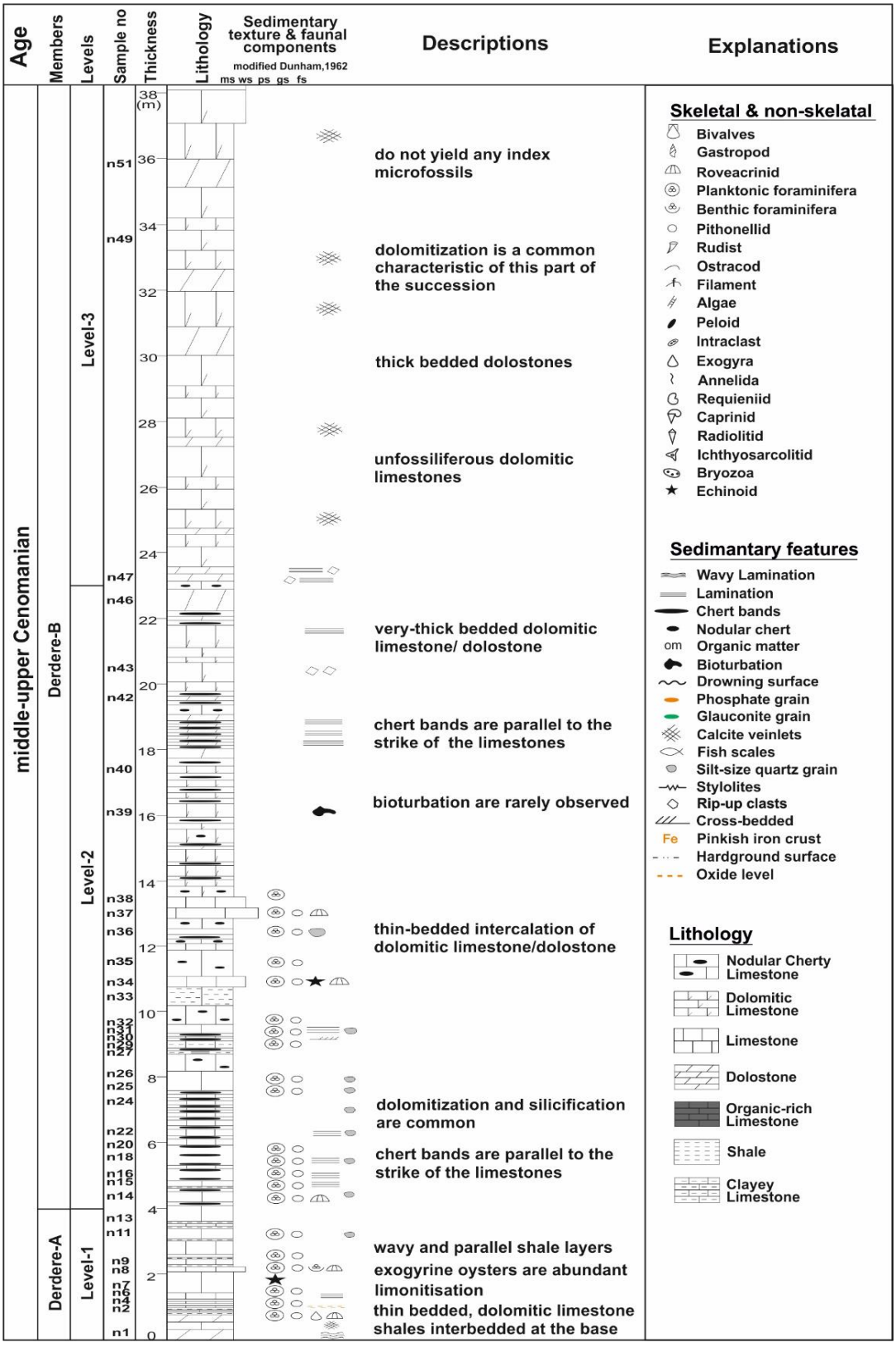


Figure 2.14. Log of the Sabunsuyu stratigraphic section and sampling levels. Showing the distribution of fossils and lithological changes in composition (after Mülayim et al., 2020).

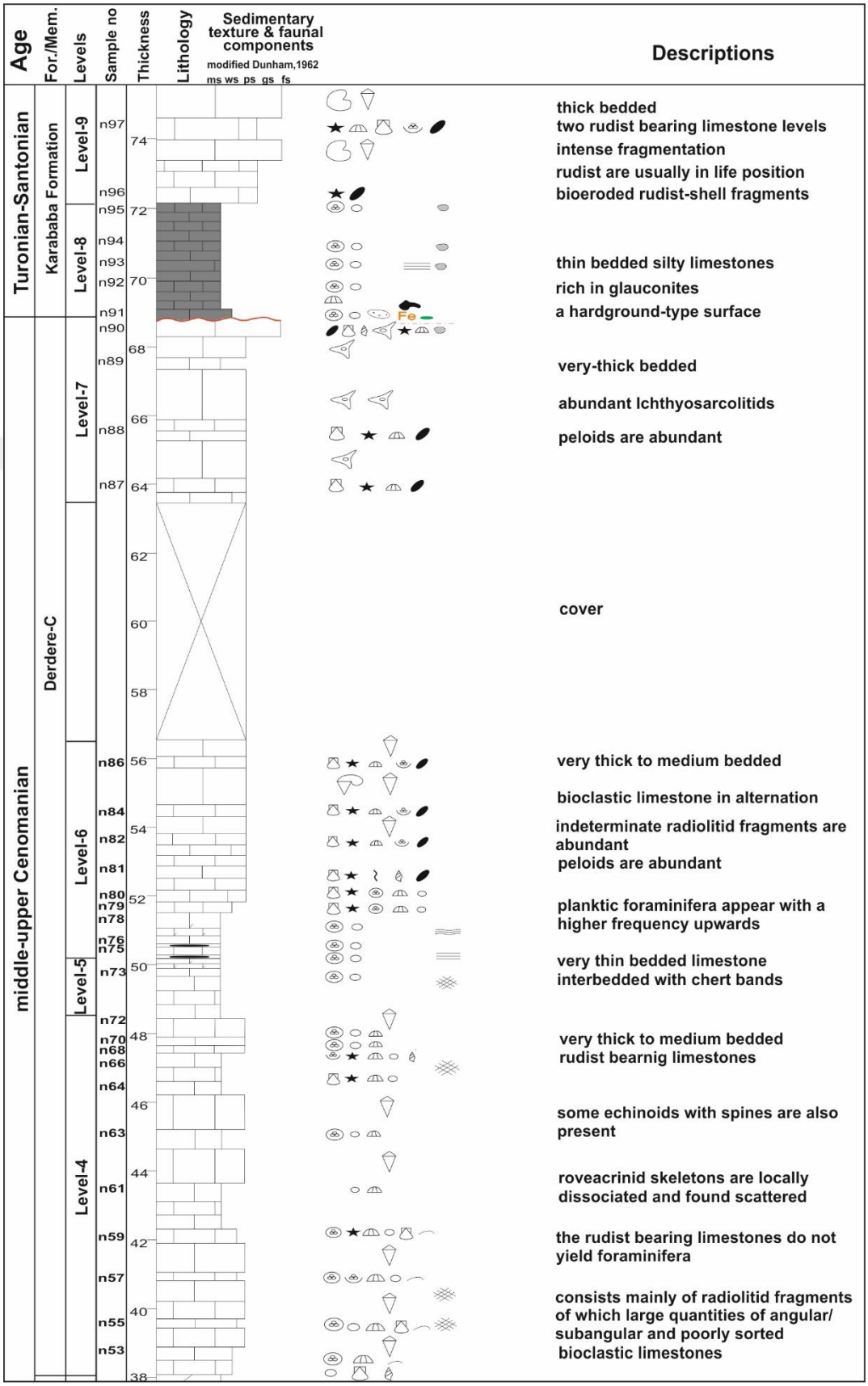


Figure 2.14 (continued)

2.6.2 İnişdere Stratigraphic Section

The İnişdere stratigraphic section (ISS) is situated about 1 km north to the Ünlüce Village. The İnişdere valley cuts across carbonate sequences around the Ünlüce village and represents an excellent outcrop that allowed us to understand the stratigraphy of the Derdere and Karababa formations. 10.23 m–thick limestone succession is measured in stratigraphic section (Figures 2.15 and 2.16). Based on the new observations through the stratigraphic section, five different stratigraphic levels are identified belonging to Derdere Formation and Karababa–A Member, which are described from base to top below;

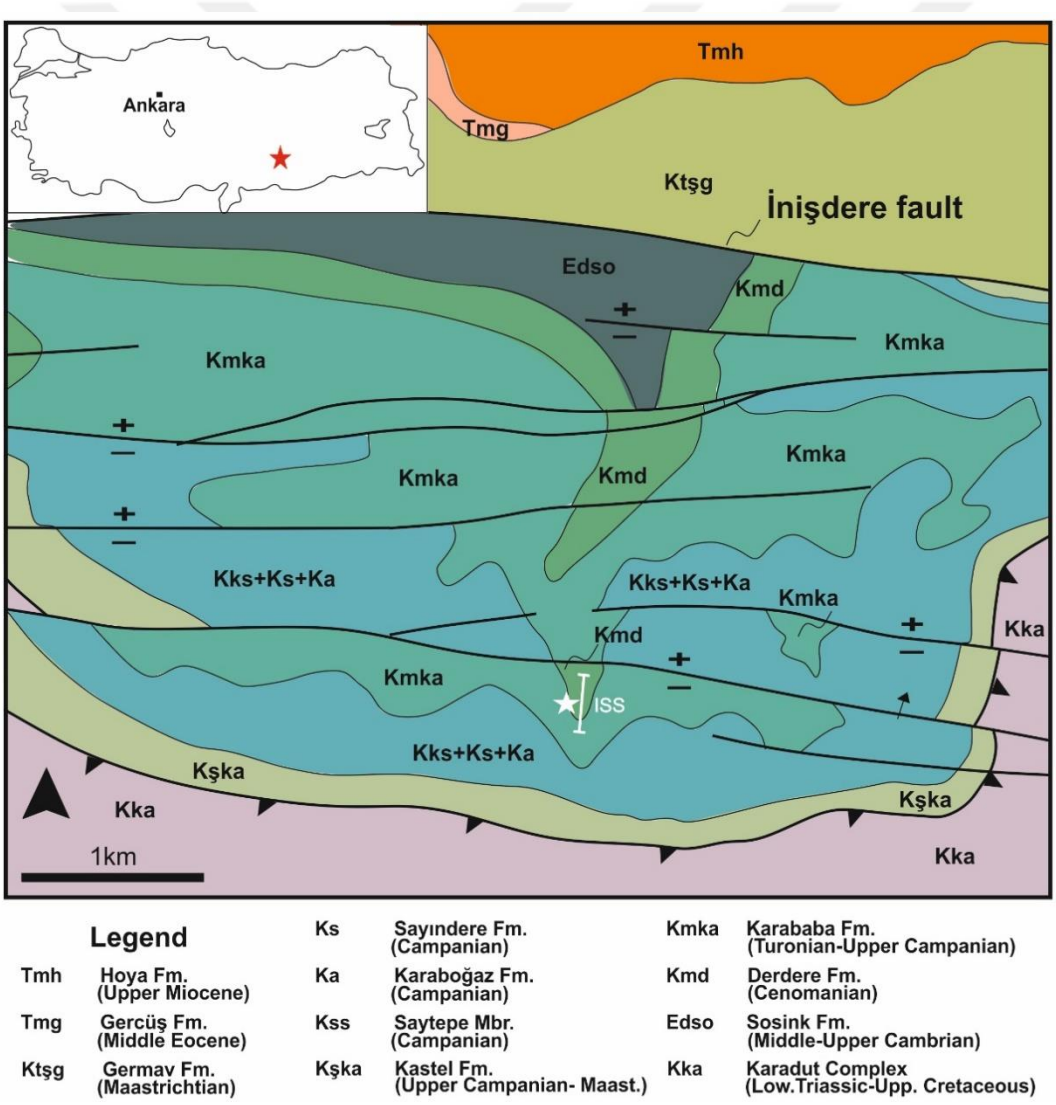


Figure 2.15. Geological map of the study area including the position of the İnişdere stratigraphic section. (after Sungurlu, 1974).



Figure 2.16. (A) Field view of the contact between the Derdere and the Karababa formations. (B) The Karababa–B Member includes irregular chert nodules and horizons where host muddy carbonate facies are mainly lime mudstone and fine–bioclastic wackestone. (C) Pre–drowning well–bedded (light grey), limestone beds belonging to the Derdere Formation, and post–drowning thinly bedded pelagic condensed carbonates (dark grey) belonging to the Karababa–A Member which lie parallel to the drowning surface. (D) The upper unit where host carbonate facies are mainly mud– to wackestone, including many bivalve clasts. (E) Well–bedded Derdere Formation limestone includes thin–bedded dolomitic beds.

Level–1) 3,74 m thick, grey colored, medium–bedded, dolomitic limestone and limestone at the base of the upper part of the Derdere Formation (Derdere–C Member) is represented by some thin beds with wavy joints and dolomitic bioclastic limestones (Figure 2.17). They become the grains, first fine, become coarser upward and rich in shells fragments of rudist; laying parallel to the bedding plane. They seem to have been reworked with their lithified internal filling sediment. These elements have been affected by early dissolution also filled up with internal dark–grey sediment, which forms the matrix of the breccia. These reworked elements indicate in some parts of the rudist–bearing platform. Some lens of polymictic breccias, in thick, contain different types of reworked elements: rudist–bearing, bioclastic limestones with coarse perforate grains, carbonate intraclasts and a minor extraclast component consisting of silt–sized quartz coming from various areas of the platform bottom. Among the fine debris, we may note microbioclasts of bivalves, mainly rudists, ostracods, pithonellids, echinoderms, roveacrinids, and small benthic foraminifera. These fine bioclastic facies alternate with micritized packstones (miliolids, and rudists fragments). These data indicate an external ramp platform environment influenced by an active synsedimentary submarine diagenetic process.

Level–2) 0,41 m thick yellowish–white thin dolostone bed and calcite veinlets in texture. No fossils observed (Figure 2.17).

Level–3) 1,88 m thick grey colored, medium–bedded limestone dominated by rounded, to elongate peloids, exhibiting varying degrees of compaction. Primary pore space is infilled with sparite, although some micritic matrix is locally present. The biota includes poorly–preserved benthic foraminifera (including miliolids), fragmentary shell material (thick–shelled forms and fragmentary thinner–shelled forms) of filaments and bivalves (Figure 2.17). These limestones are related to transgression; as the bioclastic component is mainly benthic foraminifera and bivalvia fragments reworking increase in the upper part of the Derdere Formation (Derdere–C Member).

Level–4) 4 m thick dark grey black colored, very thin to thin bedded organic–rich pelagic limestones rich in planktonic foraminifera (Figure 2.17) (whiteinellids, and marginotruncanids) and occasional fragmented filaments and fish remains. Bed contacts are sharp. Additional features include platy structure and overall blackish tint. The micritic matrix exhibits traces of lamination. This anoxic pelagic horizon is thicker than those of the horizons in the Sabunsuyu stratigraphic section; it constitutes a good marker on a regional scale.

Level–5) 0,20 m thick brownish grey colored, medium–bedded pelagic limestones. It consist of poorly sorted, rounded, elongate, to spherical clasts of glauconite and phosphate (< 0.5–1 mm in size) (Figure 2.17), which in one case contains a small benthic foraminifer indicating a sedimentary origin. The colourless clasts exhibit variable ornamentation suggesting an origin as bones and fish scales. Minor alteration to calcite is seen in some clasts. The host sediments are foraminiferal wackestone (10% bioclastic material), with benthic and planktonic foraminifera and a minor (< 10%), terrigenous component of silt–sized quartzose grains. The micrite matrix has undergone partial recrystallization to microspar and dolomite. Macrofossils are, on the whole, poorly represented in this facies; however, rare bivalves are within some parts.

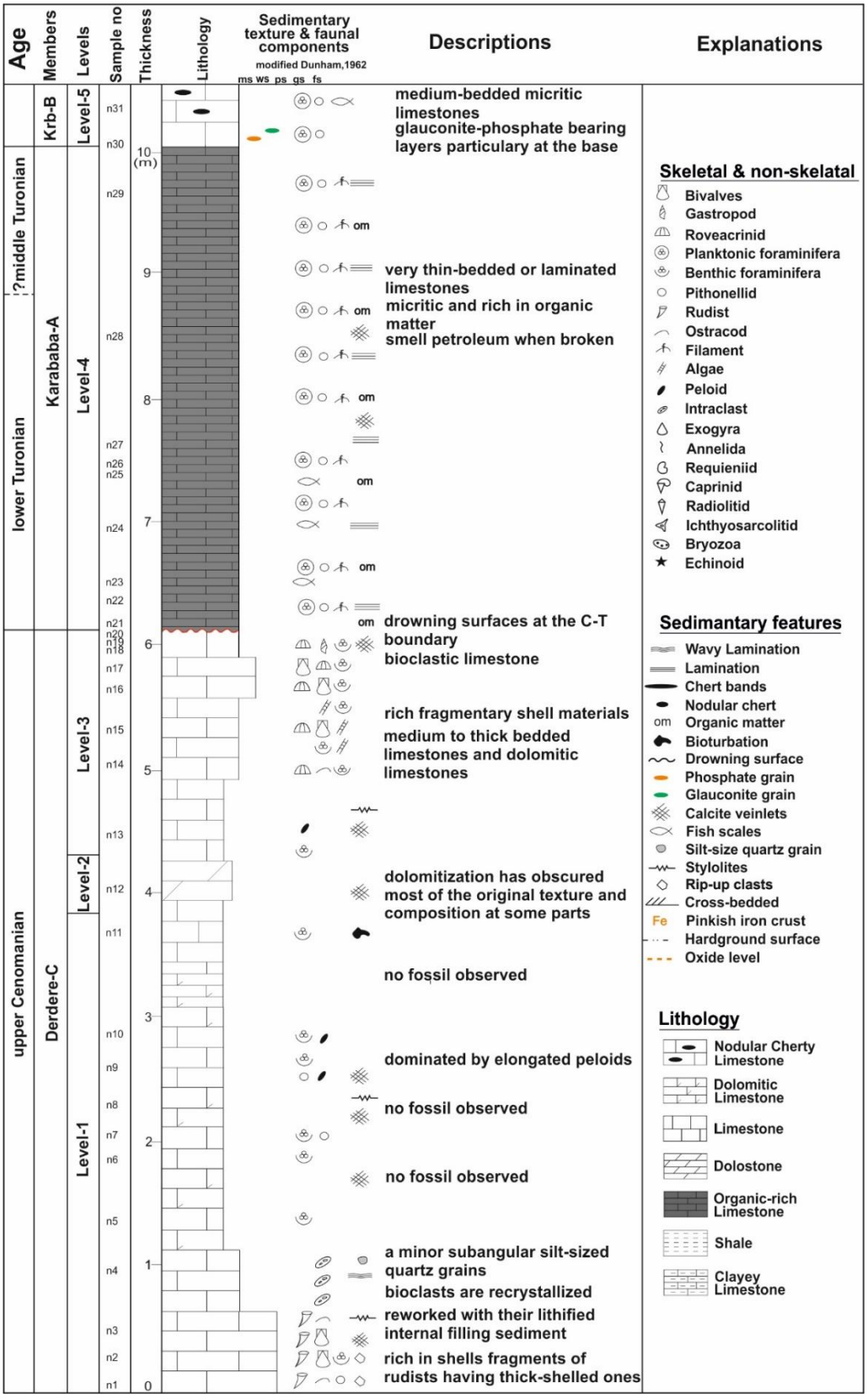


Figure 2.17. Log of the İnişdere stratigraphic section and sampling levels. Showing the distribution of fossils and lithological changes in composition.

2.6.3 Türkoğlu Stratigraphic Section

The Türkoğlu Stratigraphic Section is located, to the 25 km south in Kahramannaraş around the old quarry. In Türkoğlu location crops out a section of Upper Cretaceous series that allowed us to understand the stratigraphy of the Derdere and Karababa formations. 56.70 thick succession was (Figure 2.18). Based on the new observations through the stratigraphic section, four different stratigraphic levels are identified belonging to Derdere Formation and Karababa–A Member, which are described from base to top below;

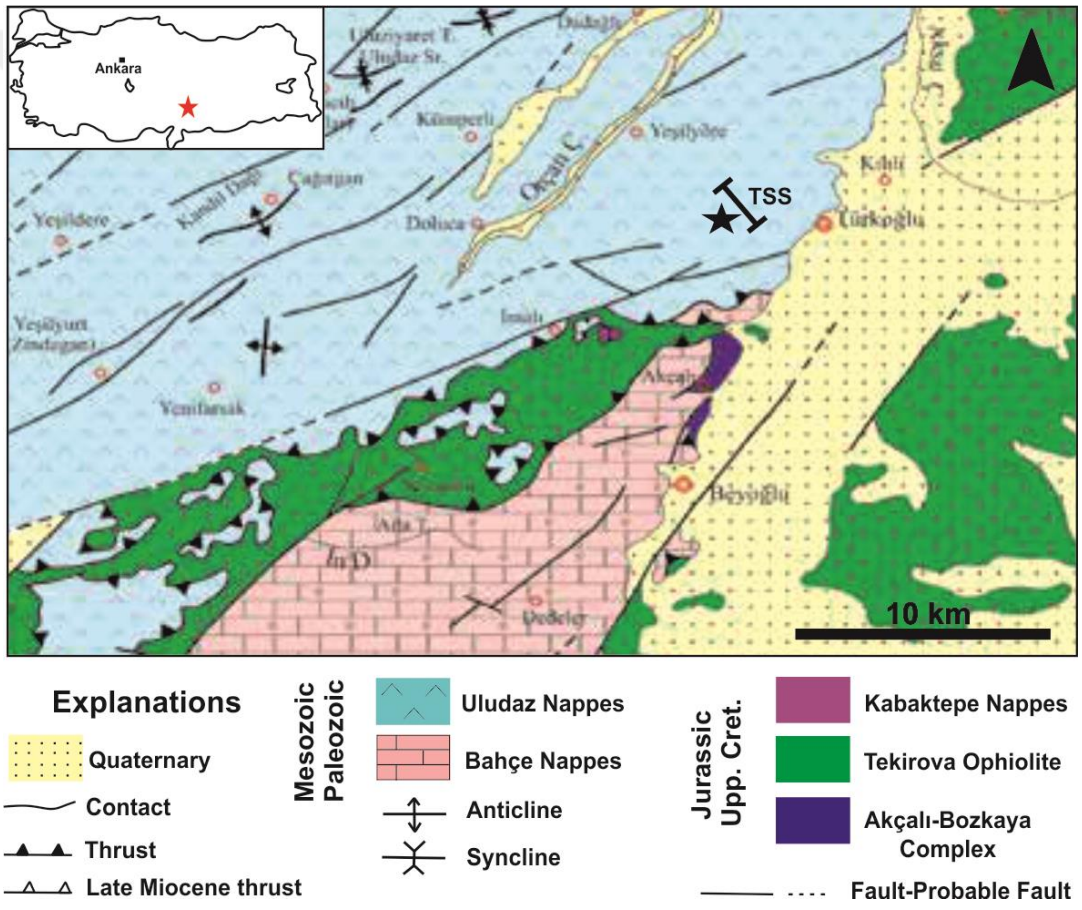


Figure 2.18. Geological map of the study area including the position of the Türkoğlu stratigraphic section. (after Usta et al. 2015).

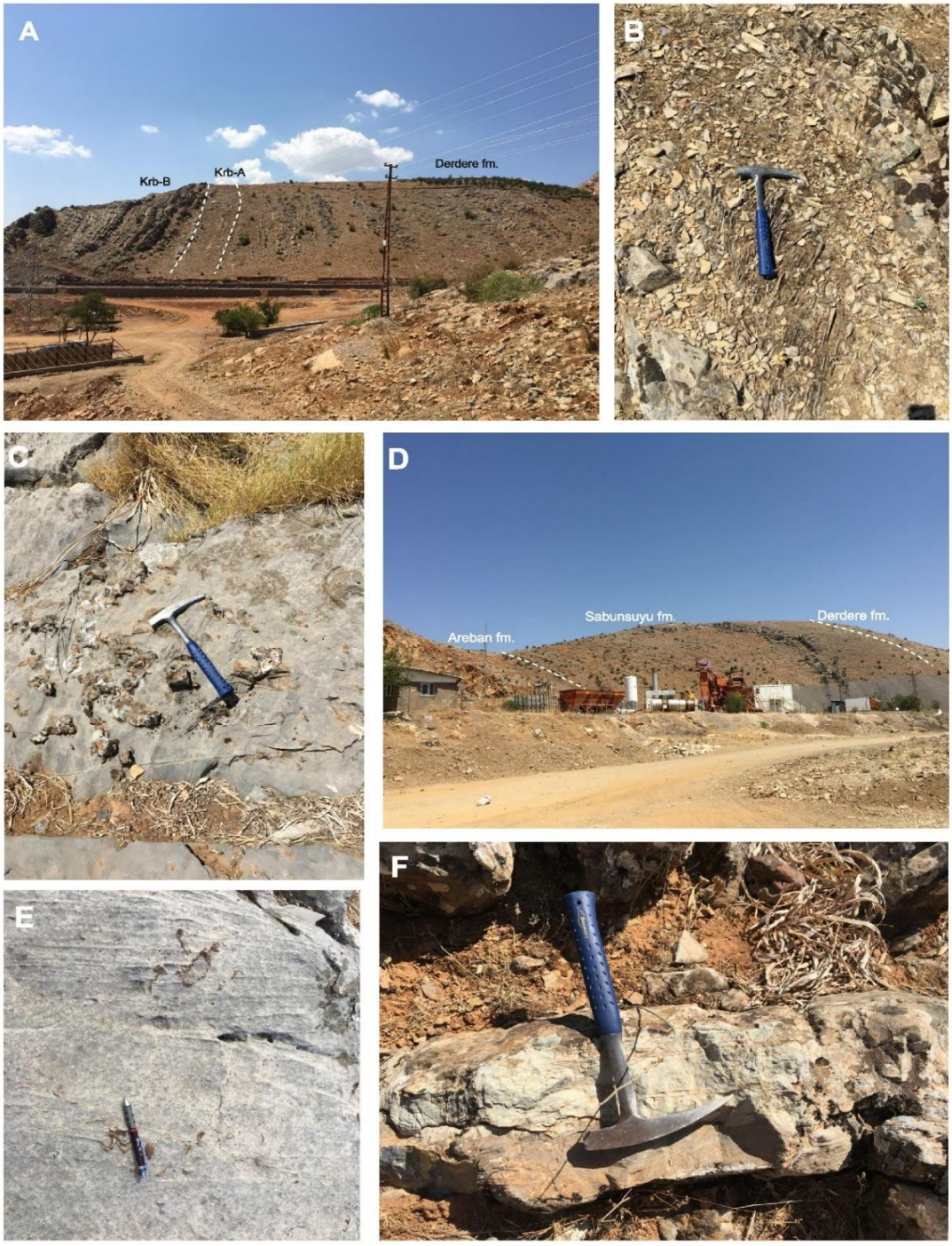


Figure 2.19. A. Field view of the contact between Derdere Formation, and Karababa–A Member. B. The Derdere–A Member includes organic–rich thin– bedded limestone. C. Nodular cherty limestone in the Karababa–B Member. D. General view of the contact between the Areban–Sabunsuyu and Derdere formations. E. Rudist remains in the Derdere–C Member. F. Laminated dolomudstone in the Derdere–B Member.

Level–1) 8,54 m thick, thin bedded, brownish colored, organic rich limestone in the lowermost part of the Derdere Formation (Derdere–A Member). Abundant small planktonic foraminifera, and pithonellids are also present but, taxa identification is hampered by widespread recrystallization. Dolomitization and silicification are common in microfossils. Some sedimentary structures are great such as predominantly parallel lamination and oil seams were observed. Lamination is quite distinct in the uppermost levels, so that laminae may be easily broken up into 1–2 mm thick plates (Figure 2.20.

Level–2) 38,83 m thick the middle part of the Derdere Formation (Derdere–B Member) are extensively dolomitized and are light gray to gray colored, medium to thick–bedded dolostone and dolomitic limestone therefore, they are easily discernible from the lower and upper members of the formation (Figure 2.20). They are always unfossiliferous, and often laminated with some laminae being contorted. Bioturbation sometimes disturbs lamination. Dissolution seams and stylolites are among the most common chemical compaction features in most of the members within the Derdere succession. The calcite veinlets are common in texture. Different sets of fractures with variable orientations occur in the this interval, but two sets of them are more common; vertical fractures and sub–horizontal fractures are also great. Vertical fractures, which appear to have a wider opening (more than 2 mm in some cases) comparing to second set and are partially or completely sealed with calcite cement (Figure 2.20). The second set of fractures which is approximately horizontal, cross–cuts the earlier set and the calcite cement filling the ealier set and also stylolites and dissolution seams. Laminations and alterations of dark, clay–rich beds with pure micritic beds and with clay–rich dolomitic beds are predominantly caused by intensive pressure solution and the formation of abundant stylolites with low amplitudes. Apertures do not exceed few micrometers and are devoid of cement. The origins of these small–scale fractures is not completely understood. They could be related to minor tectonic events in the area. Dolomitization and silicification are common features. These facies are commonly found in the all SE Turkey, and characterized by dolomitic limestone and dolostone of peloidal–miliolid mudstone to wackestone. Other grains include fragments of molluscs. Early cementation of these facies reduces dolomitization effects; however,

selective dolomitization is frequently recognized and lagoonal dolomudstone can be found alternating with the limestone.

Level–3) 7,17 m thick the uppermost part of the Derdere Formation (Derdere–C Member) is represented by dark/gray colored, medium–thick bedded limestone layers with bioturbation structures and rudists (Figure 2.20). Limestone layers are composed of peloid and benthic foraminifera–bearing wackestone and mudstone lithofacies, and their fauna content is similar to that of the upper level of Sabunsuyu and İnişdere stratigraphic sections. The bedding is usually planar and laterally persistent, with sharp bases. A rich faunal assemblage of benthic foraminifera, bivalves and peloids are present. Many of the bioclasts are broken and disarticulated. Unidentifiable shell hash is a common constituent in the matrix phase. The matrix is mainly micritic in nature, although a mix of spar and matrix is not uncommon. Sedimentary structures are common in this facies. Graded bedding is especially common, where accumulations of bioclasts at the base of a bed grade into a relatively bioclast–free facies. Bioclasts are often in a hydraulically stable position and/or concentrated in discontinuous lenses. Cross bedding or lamination is sometimes identified. Calcite–filled fractures are common and dominantly perpendicular to bedding. Limestone layers, except for intraclast–bearing wackestone at the base, consist of algae and benthic foraminifera–bearing wackestone–mudstone lithofacies. Limestone layers appearing at the upper part of the formation are represented by mudstone–skeletal wackestone and peloidal wackestone lithofacies and have similar fauna content as the lower and middle levels. However, their types are different and the abundance of benthic foraminifera and algae are higher than those of the biota of lower and middle levels.

Level–4) 2,16 m thick dark grey blackish colored, very thin to thin bedded organic–rich recrystallized pelagic limestones with rich planktonic foraminifera. The micritic matrix exhibits traces of lamination (Figure 2.20).

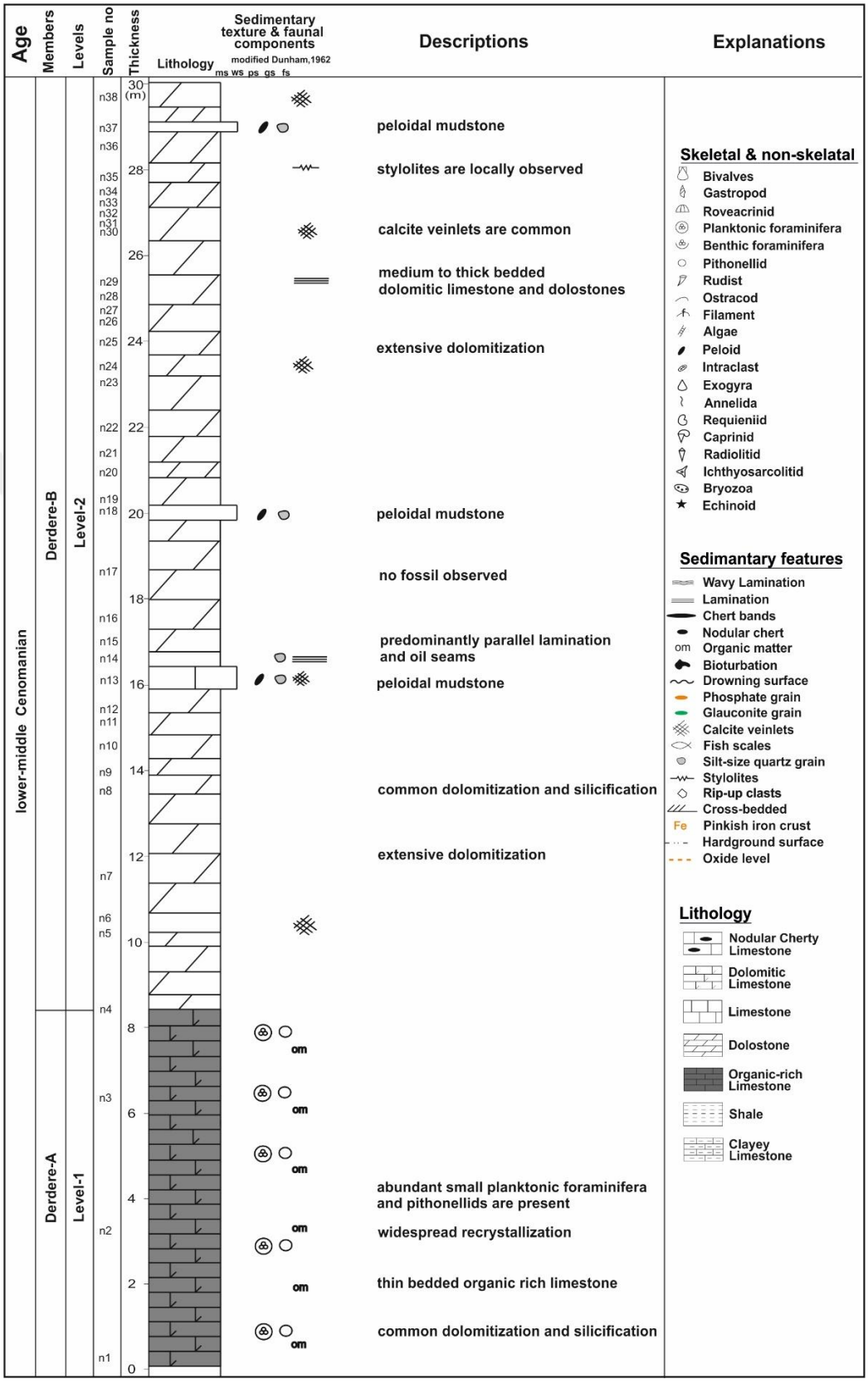


Figure 2.20. Log of the Türkoğlu stratigraphic section and sampling levels. Showing the distribution of fossils and lithological changes in composition.

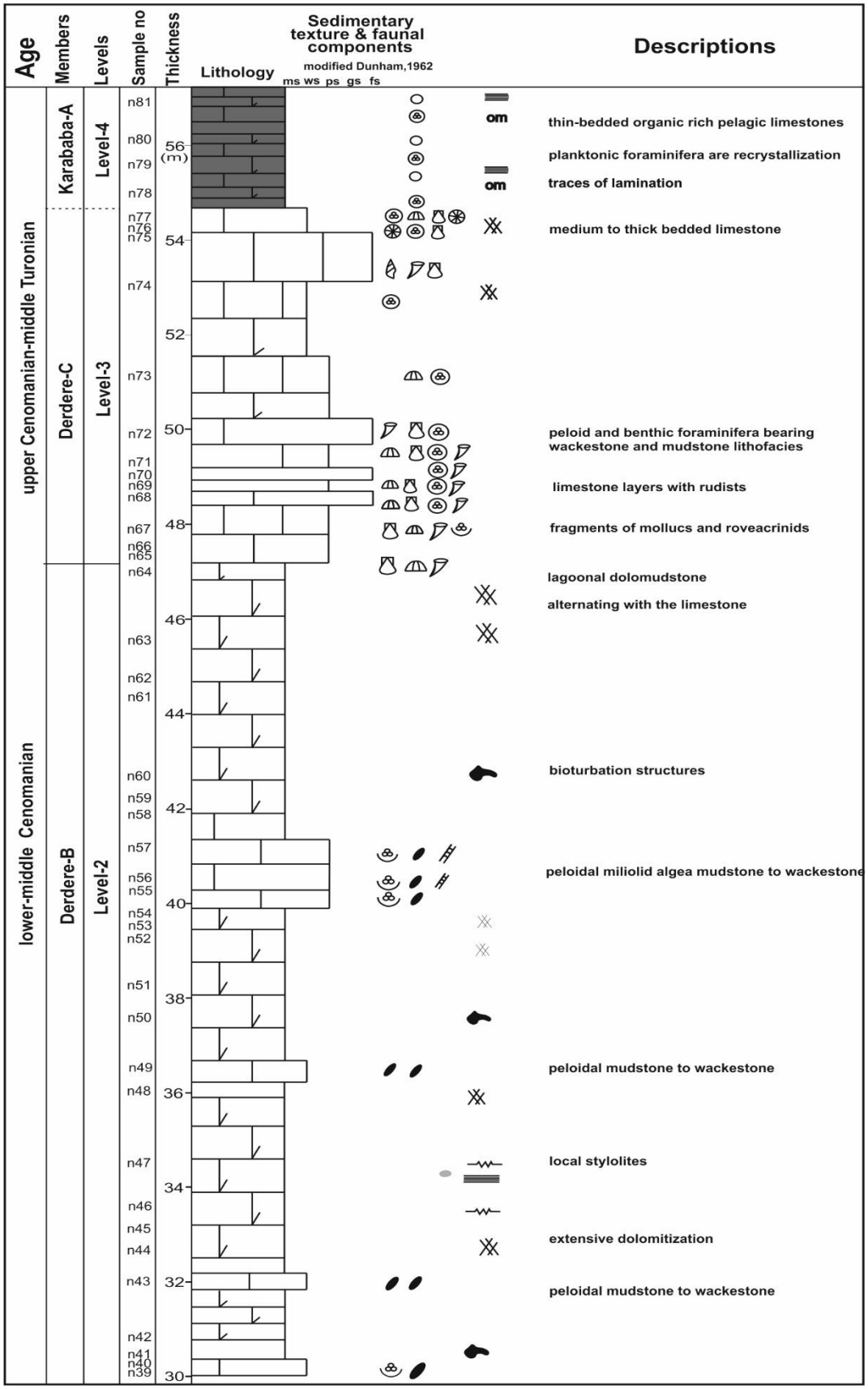


Figure 2.20 (continued)

CHAPTER 3

BIOSTRATIGRAPHY

3.1 Macro– and Microfossil Assemblages

A substantial change in the marine macro– and microfossil assemblages was recorded around the Cenomanian–Turonian boundary in the study area. The biotic changes around the Cenomanian–Turonian boundary particularly affected planktonic and benthic foraminifera, rudist, roveacrinid, calcareous nannofossil and pithonellid. However, biostratigrapic interpretation of shallow–water sequences is inherently more challenging because of the generally low species diversity, the sporadic microfossil occurrences and the low diversity and endemism in macrofossils. These difficulties are also apparent in the İnişdere, Sabunsuyu, Türkoğlu and boreholes sections. However, sufficient age control can be obtained for the Cenomanian–Turonian transition by integrated macro– and microfossil biostratigraphy. Roveacrinids have been identified by Prof. Dr. B. Ferre (France); calcareous nannofossils have been determined by Prof. Dr. M. Wagreich (Austria); pithonellids have been determined by Prof. Dr. J. Wendler (Germany); planktonic foraminifera have been determined by Prof. Dr. B. Sarı (Turkey), benthic foraminifera have been determined by Dr. Prof. K. Taslı (Turkey); rudist have been determined by Prof. Dr. S. Özer (Turkey). Additionally, biostratigraphic assesment of the each fossil group has been carried out by the related researcher.

3.1.1 Roveacrinids

Borehole Sections

In the northwestern part of the Arabian Platform, the Adıyaman district (SE Turkey) displays some lower–middle Cenomanian deep–marine sediments of the Derdere Formation. These sediments yielded abundant echinodermal remains, among which some thecal and brachial plates are assignable to roveacrinids. Routine microfacies analysis of the lower–middle Cenomanian part of the Derdere Formation revealed unexpected lower–middle Cenomanian assemblages of roveacrinoidal ossicles, comparable with those formerly reported further south in the Cenomanian–Turonian of the Arabian Platform. For the first time, genuine and undisputable Roveacrinidae are illustrated for SE Turkey. Seven borehole sections were scrutinized in search of microcrinoidal sections, most especially within carbonate microfacies. Within the scope of better constraining the position of the lower–middle Cenomanian, we had been compiling the successive occurrence of respective identified roveacrinid remains. These roveacrinidal assemblages are consisting in: *Roveacrinus communis* (Douglas) (= *R. derdereensis* Farinacci and Manni); *Roveacrinus* cf. *alatus* (Douglas); *Roveacrinus spinosus* (Peck); *Roveacrinus* sp.; Roveacrinidae indet.; *Applinocrinus* sp.; and Saccocomidae indet. These specimens provide significant clues to constrain the palaeogeographic reconstruction of Tethyan seaways, and represent potential fossil index candidates for the lower–middle Cenomanian stratigraphy of the Adıyaman district.

The roveacrinoidal contribution to the Cretaceous limestones was reported in detail by Ferré and Berthou (1993, 1994). The roveacrinoidal sections were only a few mentioned in the previous literature, most of the time gross identified as “Saccocoma limestones” [by comparison to seminal works on Jurassic rocks of Lombard (1937, 1945), and Verniory (1954, 1955, 1956, 1960, 1961, 1962) or simply turned down by petroleum industry owing to the ignorance of their true nature and potentials. From this rather limited number of papers, it appears that the crinoidal component of carbonate rocks consists mostly of blooming populations of opportunistic roveacrinids; their mass occurrence and post–mortem accumulation are largely responsible for these very special microfacies scattering the Cretaceous carbonate

series worldwide (e.g., Scott et al. 1977). The first formal evidence of roveacrinoid contribution to the Cretaceous carbonate factory in Turkey were brought by Ferré et al. (1997) and Cros et al. (1999). However, the first sections of genuine roveacrinidal affinity in SE Turkey were first illustrated by Farinacci and Manni (2003) with the erection of a new species: *Roveacrinus derdereense* Farinacci and Manni, now and here regarded as a junior synonym of *R. communis* Douglas. Purported at first for roveacrinids (Ferré and Berthou 1993, 1994), the section orientation scheme was extended to saccocomids by Ferré and Dias–Brito (1999) for extended typological comparison to Jurassic saccocomid sections, see Benzaggagh et al. (2018, for details and literature within). Meanwhile, Ferré and Granier (1997a, b, 2001) defined in length the orientation and taxonomic use of roveacrinid sections. Following that, the systematic assignment of the Cretaceous roveacrinidal sections has been fully argumented for both the roveacrinids and the saccocomids (Ferré 1997; Ferré et al. 1999). This scheme was adopted in the following (Figure 3.1). Since these minute discarded or accumulated roveacrinid remains are not easily spotted in the field and require to be studied under a petrographic microscope and/or scanning electron microscopy (SEM), they are usually mentioned as microcrinoids or often misinterpreted as planktonic crinoids (instead of pelagic). The thecal size does not exceed a few millimeters; a complete specimen is about 5 cm wide. Roveacrinids are small articulate crinoids with five dichotomous arms, each displaying many brachial plates (up to three dozen in complete specimens) (Figure 3.1). Their minute theca is devoid of any stem or anchoring device, and is built of two sets of plates, basal and dorsal, sometimes showing a prominent centrodorsal bulge. When exceptionally preserved, it displays an inner plate ring defining a double body cavity (Schneider 1987, 1989). Each roveacrinid species displays a distinctive architecture and bears a wide array of ornamental elements, such as a spine–like aboral element, simple bowls with or without processes, flanged or winged brachials, lateral processes, and flanges or spines (e.g., Schneider, 1987, 1989; Jagt, 1999; Hess, 2015; Gale, 2016) (see. Figures 3.1; 3.2; 3.3; 3.4; 3.5).

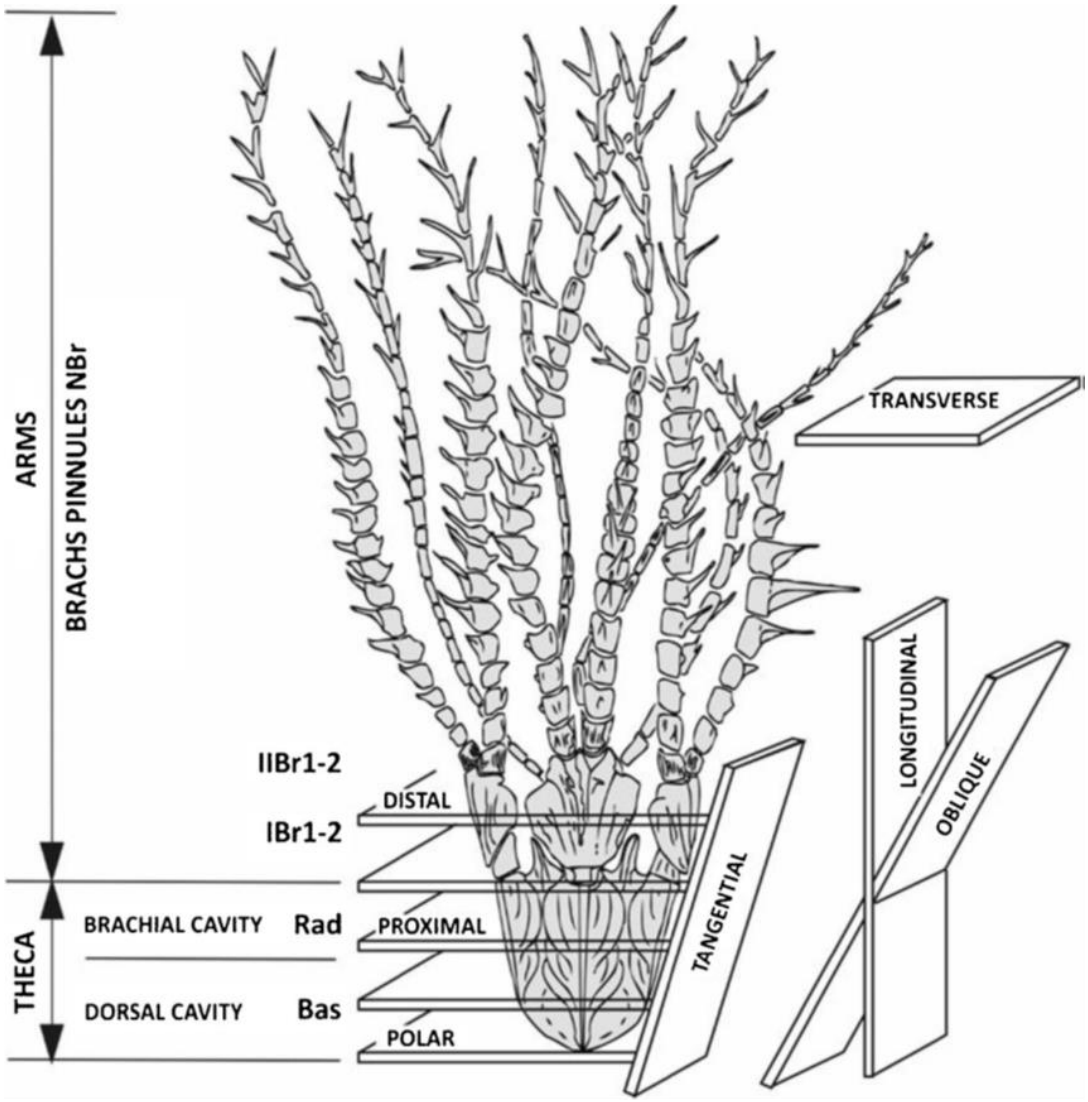


Figure 3.1. Morphological reconstitution of a complete roveacrinid individual with orientation of possible section planes (after Ferré and Berthou, 1993, 1994; Ferré and Granier, 1997a, b, 2001; Mülayim et al. 2018).

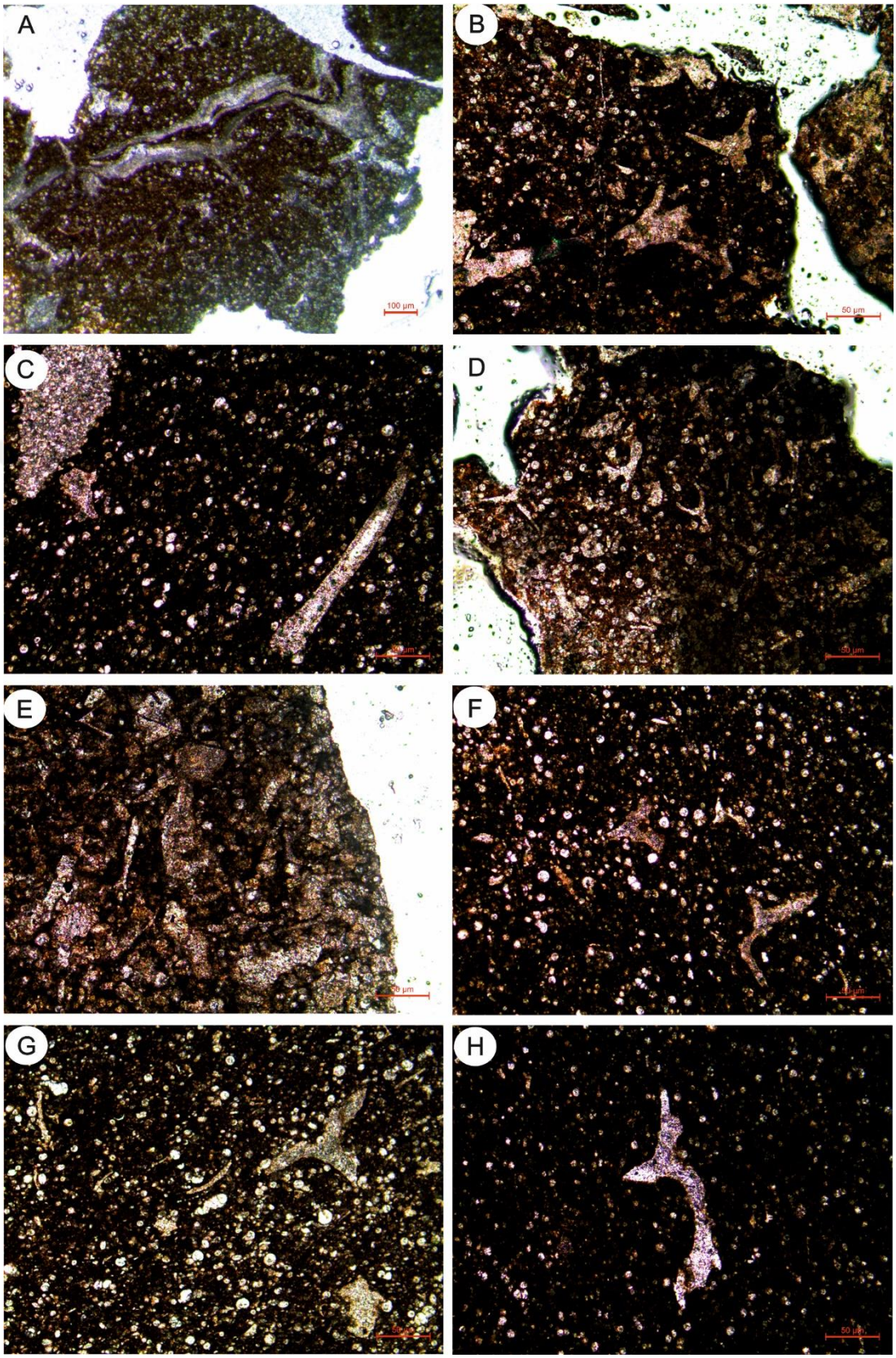
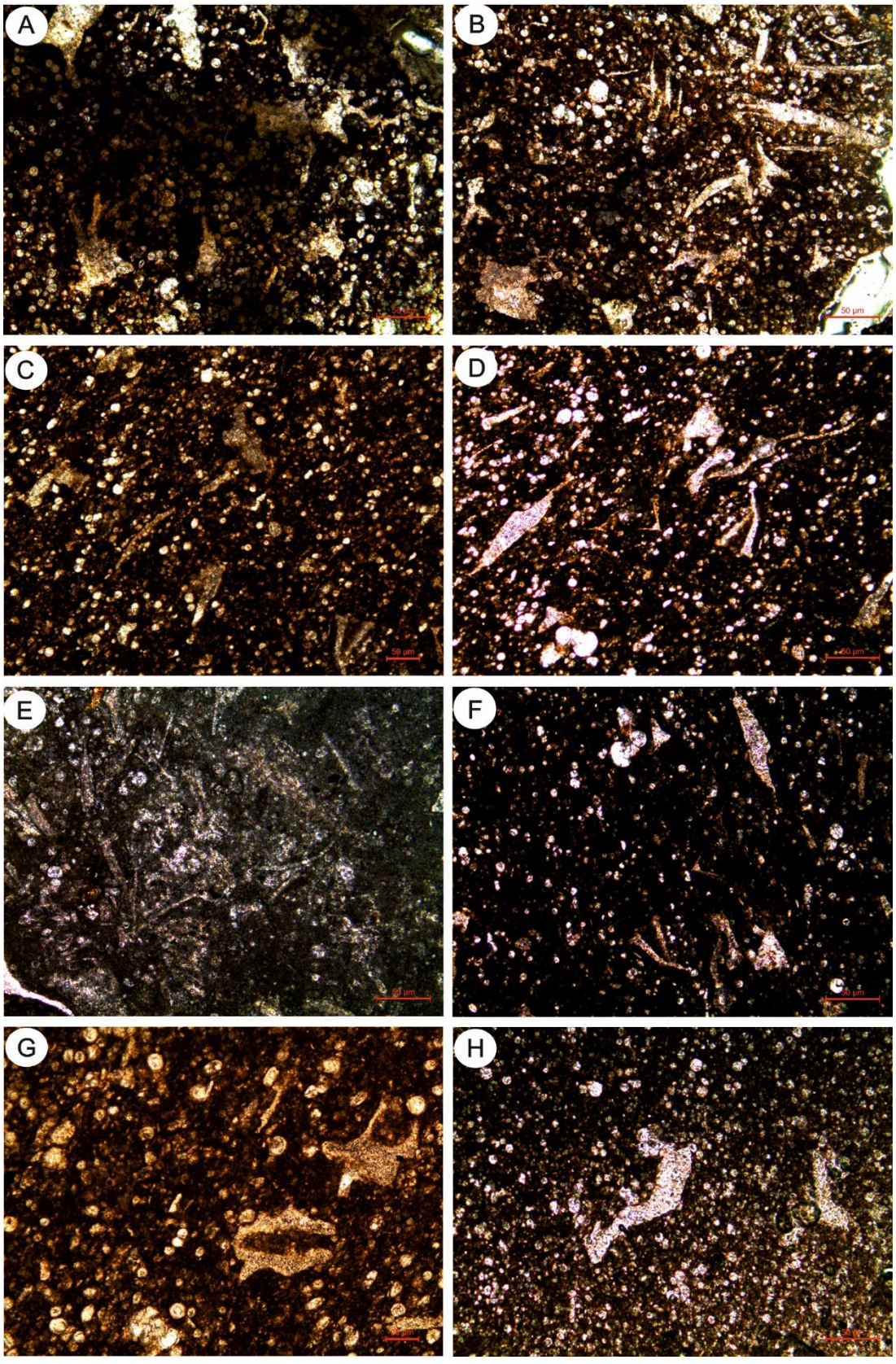

A
100 µm
B
50 µm
C
D
E
F
G
H

Figure 3.2. The thin–section photographs of roveacrinid ossicles, lower–middle Cenomanian, Adıyaman area, SE Turkey. A. *Roveacrinus communis* Douglas *(= R. derdereensis* Manni, in Farinacci and Manni), Obl/sub–TS–Rad and OblS–NBrn, core sample B–1–1484.1; B. *Roveacrinus communis* Douglas TS–Rad, Tg/LgS–Rad, and Lg/TgSRad, core sample S–2–2204.1; C. *Roveacrinus* cf. *alatus* Douglas OblS–Rad, core sample Bz–1–4–8; D. *Roveacrinus* cf. *alatus* Douglas, (TS–Rad) and Roveacrinidae indet. (TS–NBrn), core sample S–2–2202.3; E. accumulation of roveacrinoidal brachial plates (*Roveacrinus* cf. *alatus*), core sample D–1–2552.2; F. *Roveacrinus* sp., TS–Rad and Obl/TS–IBr2, core sample Bz–1–4–7.1; G. *Roveacrinus* sp., TS–Theca and OblS–I/IIBrn, core sample Bz–1–4–9.1; H. *Roveacrinus* sp., OblS–Theca, core sample Bz–1–4–10.1 (after Mülayim et al. 2018).

Figure 3.3. The thin–section photographs of roveacrinid ossicles, lower middle Cenomanian, Adıyaman area, SE Turkey. A. *Roveacrinus spinosus* Peck, Lg/TgS–IBr1 and OblS–NBrn, core sample S–2–2202.4; B. *Roveacrinus spinosus* Peck bearing typical spinose ornamentation (Lg/TgS–NBrn), and Roveacrinidae indet. (TgS–IBr1), core sample S–2–2202.5; C. *Applinocrinus* sp. (Lg/TS–Rad) and Saccocomidae indet. (TgSIBr2; OblS–NBrn), core sample Bz–1–4–7.3 (ex Bz–1–4.7); D. Saccocomidae indet., indeterminable plates, core sample Bz–1–4–7; E. Saccocomidae indet., Obl/TSN/ IIBrn/Rad, core sample B–1–1508.1; F. Roveacrinidae indet., TgS–IBr2, core sample Bz–1–4–7.2; G. Roveacrinidae indet., TgSIBr1 and TgS–IBr2, core sample Bz–1–4–9.2 (ex Bz–1–4.9.10x); H. Roveacrinidae indet., brachial plates, core sample Bz–1–4–10 (after Mülayim et al. 2018).


A
B
C
D
E
F
G
H

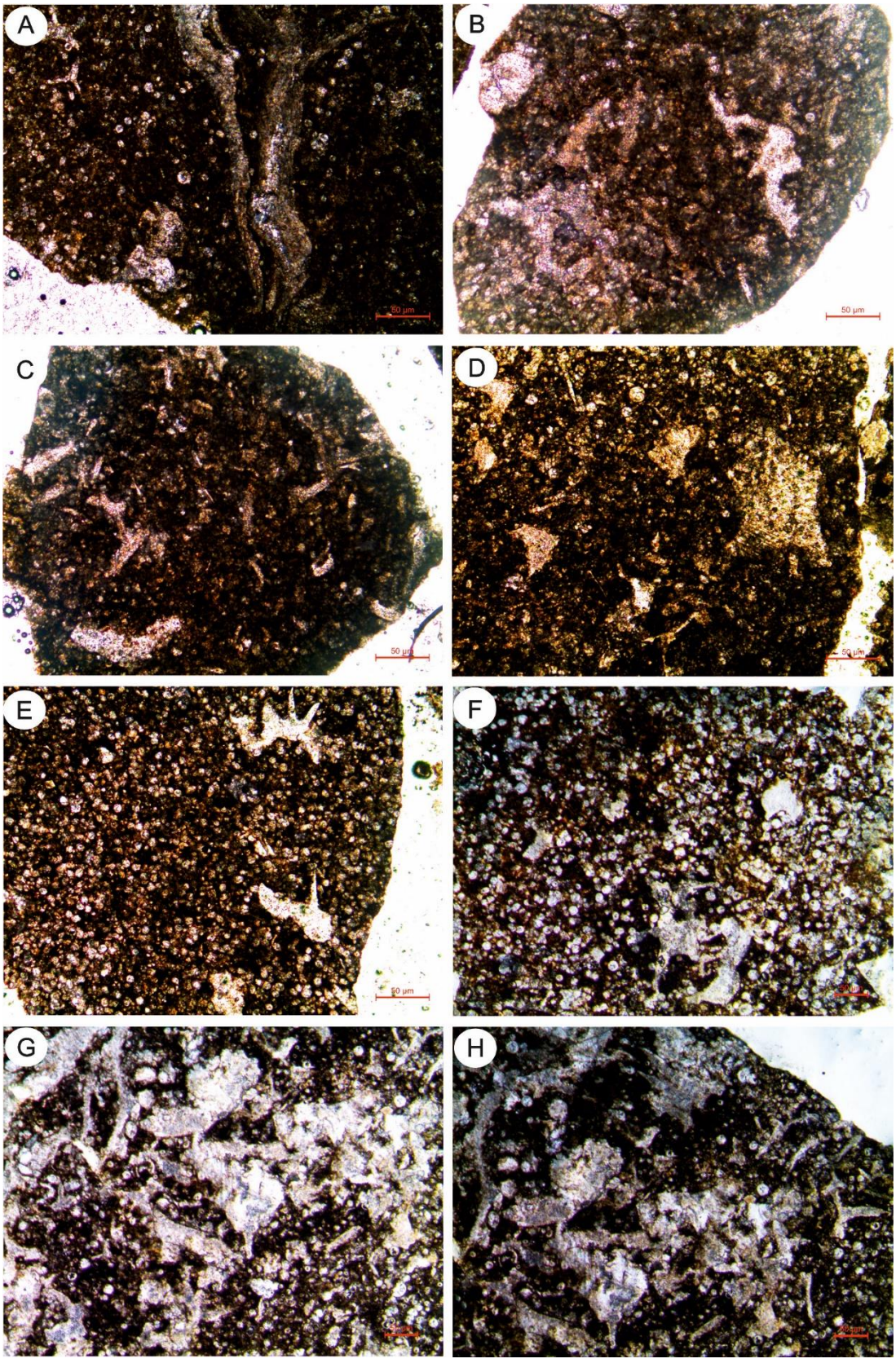
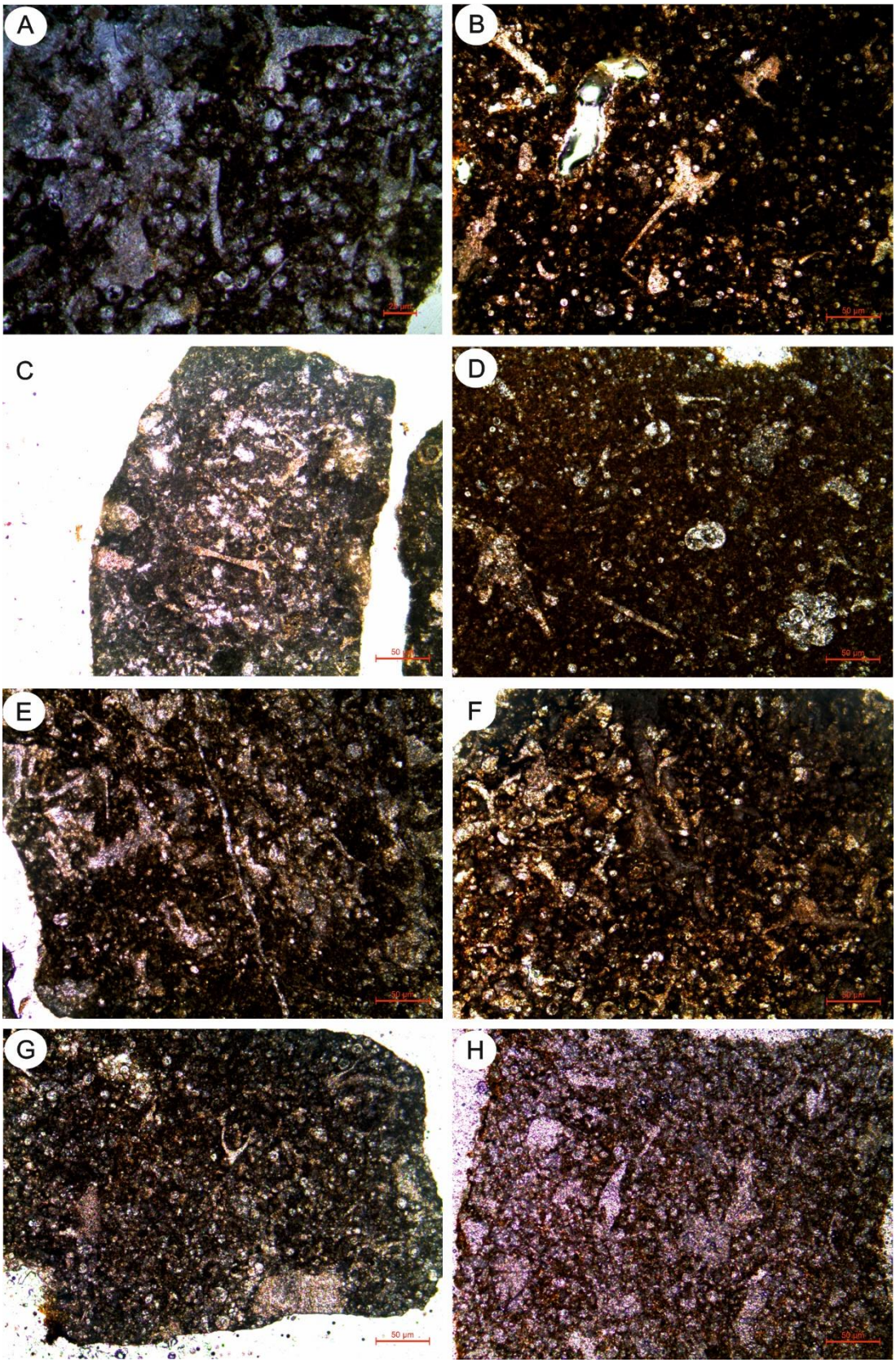

A
B
C
D
E
F
G
H

Figure 3.4. The thin–section photographs of roveacrinid ossicles, lower–middle Cenomanian, Adıyaman area, SE Turkey. A. Roveacrinidae indet., TS–NBrn and TgS–IBr1, core sample B–1–1484.1; B. Roveacrinidae indet., TS–NBrn, core sample D–1–2488.1; C. Roveacrinidae indet., accumulation of broken brachial plates (NBrn), core sample D–1–2488.2; D. Roveacrinidae indet., TS–Theca and Lg/TgS–NBrn, core sample G–1–2980; E Roveacrinidae indet., OblS–IBr2, core sample G–1–2992; F. Roveacrinidae indet.,TgS–IBr1, OblS–NBrn and TgSIBr2, core sample S–2–2202–5x; G. Roveacrinidae indet. (sturdy morphology), OblS–NBrn, core sample S–2_2206; H. Roveacrinidae indet. (sturdy morphology), OblS–NBrn, core sample S–2–2206–5x (after Mülayim et al. 2018).

Figure 3.5. The thin–section photographs of roveacrinid ossicles, lower–middle Cenomanian, Adıyaman area, SE Turkey. A. Roveacrinidae indet. (sturdy morphology), OblS–NBrn, core sample S–2–2206–10x; B. Roveacrinidae indet., TS–NBrn, core sample S–2–2202.1; C. Indeterminable roveacrinoidal sections, core sample S–2–2274.1; D. Roveacrinidae indet., IBr2 and NBrn, core sample B–1–1484.2; E. Roveacrinidae indet., accumulation of brachial plates (OblSNBrn), core sample Bk–1–1962.4; F. Roveacrinidae indet., accumulation of brachial plates NBrn, core sample D–1–2552; G. Roveacrinidae indet., TS–NBrn and TgS–IBr2, core sample D–1–2492; H. Roveacrinidae indet., TgS–IBr2, core sample K–1–1630 (after Mülayim et al. 2018).


A
B
C
D
E
F
G
H

3.1.2 Rudists

Sabunsuyu Stratigraphic Section

Rudists are dominant components throughout the Sabunsuyu stratigraphic section (Figure 3.6) The study of rudist facies in southeast Turkey carbonate ramps and their comparison with those of Arabian Plate allow a better determination of the age of the Derdere and Karababa formations. These biostratigraphical data indicate a middle–late Cenomanian and Coniacian–Santonian age for Derdere and Karababa formations, respectively. According to recent studies, Cenomanian–Santonian carbonate sedimentary rocks rich in rudists are widespread throughout southeastern Turkey. Rudist beds are widely exposed in Cenomanian to Maastrichtian (Upper Cretaceous) time intervals of the northern part of the Arabian Platform (Steuber, 2002; Özer and Ahmad, 2015, 2016; Khazaei et al., 2010; Özer and El–Sorogy, 2017, Özer et al. 2013; 2019a). Although previous studies have hinted at the presence of rudist fragments in the Upper Cretaceous the Derdere and Karababa formations in southeast Turkey, the rudist fauna has never been described in detail. Recent studies have shown that the Cenomanian–Santonian formations (Derdere and Karababa) yield well–identifiable rudists that are of biostratigraphical importance in the Sabunsuyu stratigraphic section of the Kilis area. Although few rudist fragments have also been reported from these formations along the eastern side of the road, and upstream, in the area of the western Kilis by Cros et al. (1999). The rudist–rich facies are represented mainly in the Derdere and Karababa formations. Rudists indicate middle–late Cenomanian and Santonian ages for the Derdere and Karababa formations, respectively. The sedimentology and taphonomic signature of the rudist shell beds have been described in order to obtain a better understanding of the depositional environment and the physical processes that controlled Cenomanian–Santonian sedimentation. Monospecific tabular beds characterize mainly the upper part of the series (topmost part of the Derdere and Karababa formations); more complex rudist concentrations, characterized by moderate species diversity, increase upsection.

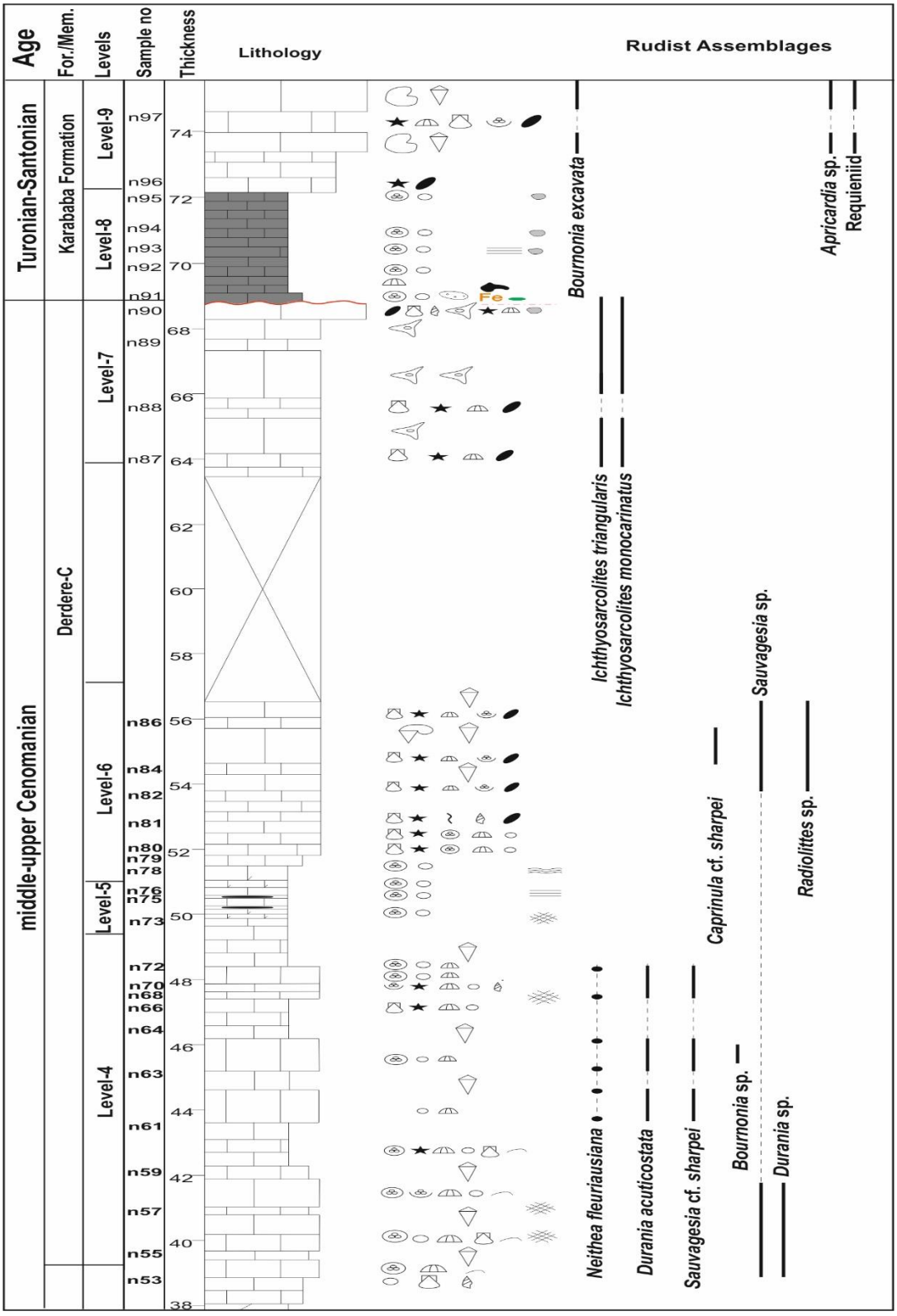


Figure 3.6. Distribution of rudists and some bivalvia in the Sabunsuyu stratigraphic section (after Mülayim et al. 2020).

In these rudists have been described from the Derdere and Karababa formations (Figures 3.6–3.12). Radiolitid fragments are present in the middle part of the Derdere Formation. Some subsquare right valve sections with more and less developed ribs and circular to semi–circular sections might belong to *Biradiolites* sp. and *Durania* sp., respectively (Figures 3.7B,D; 3.8A,B). However, some radiolitids of biostratigraphical importance in the upper Cenomanian, such *as Durania acuticostata* Caffau and Pleničar and *Sauvagesia* cf. *sharpei* Bayle are found around the middle part of the formation. Many transverse sections of right valves of *D. acuticostata* Caffau and Pleničar show characteristic features such as a thin outer shell layer, strong and acute ribs delimited by wider sinuses, wide and flat ventral and slightly concave posterior radial bands separated by a concave interband (Figure 3.8F,H). This species is well known from the upper Cenomanian of Friuli, Italy (Caffau et al., 1996) and Trieste, Italy (Pons et al., 2011). Some conical right valves in growth position and transverse sections of *S. sharpei* Bayle present finely ribbed ornamentation, the flat and slightly protruding radial structures separated by a concave interband and a very small, triangular ligamental ridge (Figures 3.8J, 3.10A, B). The age of *S. sharpei* Bayle is late Cenomanian at its type locality (Alcantara, Portugal); the species is well–known from the upper Cenomanian or undefine Cenomanian of the northern and southern sides of the Mediterranean Tethys (Steuber, 2002; Chikhi–Aouimeur, 2010; Pons et al., 2011). It has recently been described for the Arabian Platform from the upper Cenomanian of northern Jordan by Özer and Ahmad (2015, 2016). *Neithea fleuriausiana* Orbigny co–occurs (Figure 3.8I, J). Although this species ranges from the Cenomanian to the Turonian in Tethyan rudist limestone (Dhondt, 1973), it was found together *D. acuticostata* Caffau and Pleničar and *S. sharpei* Bayle in upper Cenomanian limestones of Friuli, Italy (Caffau et al., 1996). Thus, faunal content shows clear similarities to those of the fauna from these localities.

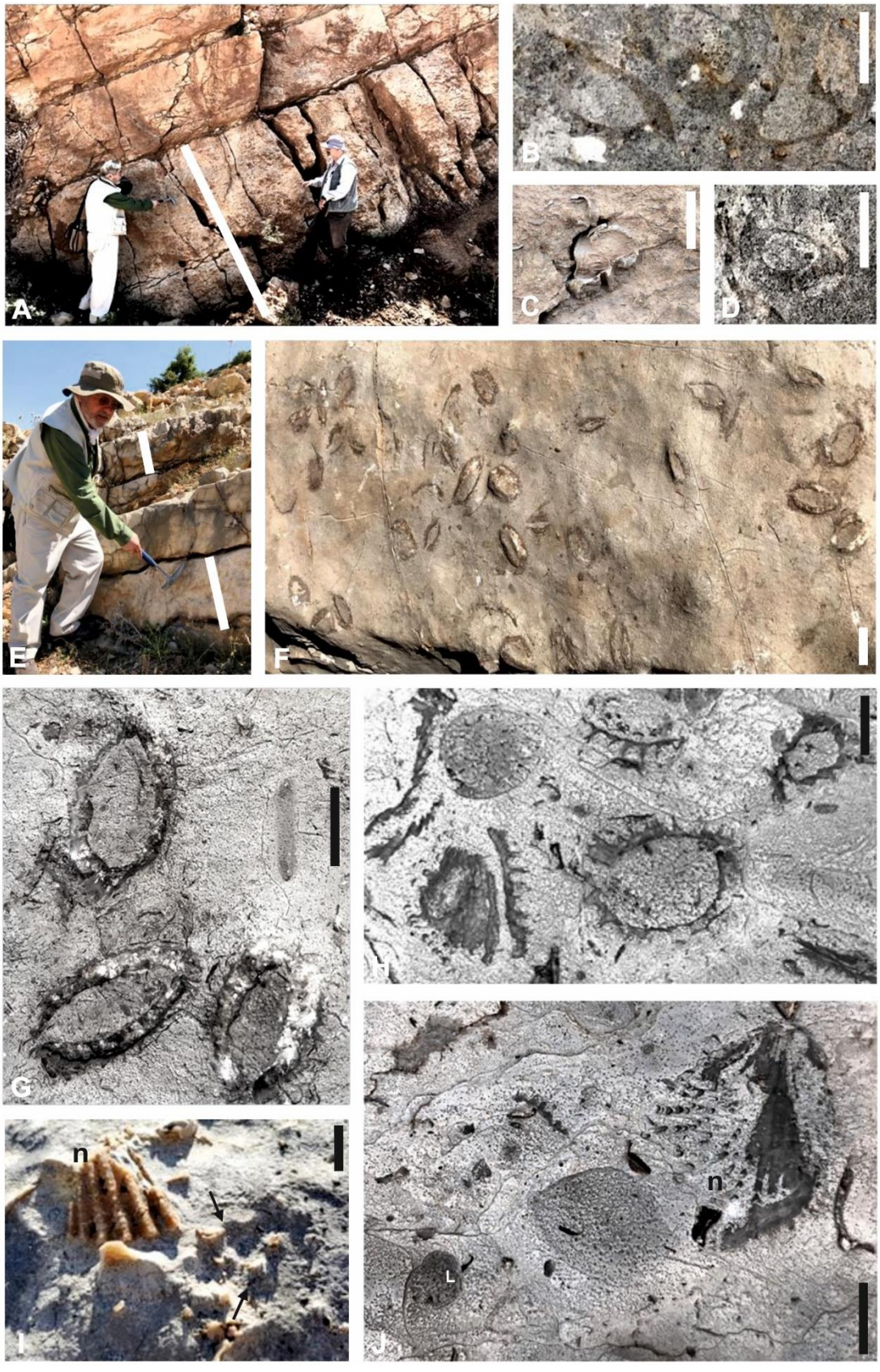

A
B
C
D
E
F
G
n
I
n
L
J

Figure 3.7. Rudist–bearing limestones of the Derdere Formation in the Sabunsuyu stratigraphic section. A. Field view showing thickness (white bar equals 2.90 m) of lower rudist–bearing limestones of unit IV. B, D. Close up of previous photograph showing transverse and oblique sections of rudist fragments (BeC. *Biradiolites* sp.; *D. Durania* sp.), scale bar equals 10 mm. E, J. Field views of upper rudist bearing limestones of unit IV. E. Rudist–bearing limestones alternating with limestones (white bar equals 40–50 cm, indicating rudist–bearing limestones. F, H. Close up of previous photograph showing transverse sections of monospecific *Durania acuticostata* Caffau. Note thin outer shell layer and strong and acute ribs limited by wider sinuses (scale bar equals 10 mm). I. *Neithea fleuriausiana* d'Orbigny (n) and small radiolitidis (thin black arrows) in life position (scale bar equals 10 mm). J. Transverse sections of right valves of *Sauvagesia sharpei* Bayle (thin black arrows). Note thick outer shell layer, small, triangular ligamental ridge (L) and presence of *Neithea fleuriausiana* d'Orbigny (n) (scale bar equals 10 mm) (after Mülayim et al. 2020).

Some small oval sections of radiolitids seem to show the radial structures of *Bournonia* in these levels of the middle part of the section (Figures 3.8D; 3.9C; 3.10B, C). These may be correlated even with those of *B. africana* Douvillé as demonstrated by Steuber (1999, text–Figure 29 F). However, to date this genus has not been recorded from the Cenomanian, which listed it here with a query. The bioclastic limestones of the uppermost middle part of the section contain poorly preserved canaliculate rudist fragments. Some of the transverse sections of the right valve are suboval, showing only a very thin internal shell layer consisting of one or two rows of small rounded pallial canals in the posterior part (Figure 3.9F). The poor canaliculation is characteristic of *Caprinula sharpei* Choffat, differing from other species of the genus, as demonstrated by Douvillé (1888) and Özer and Ahmad (2016). *Caprinula sharpei* Choffat is suggestive of a Cenomanian age in the central part of the northern side of the Mediterranean Tethys (Steuber, 2002). The species is known from the Arabian Platform from the upper Cenomanian strata of northern Jordan (Özer and Ahmad, 2016) and has recently been noted from the central Taurides (Turkey), in the lower–middle Cenomanian strata by Özer and Kahrıman (2019). The radiolitid

sections belong to *Biradiolites* sp. and may be *Radiolites* is also found in these bioclastic limestones (Figure 3.9G).

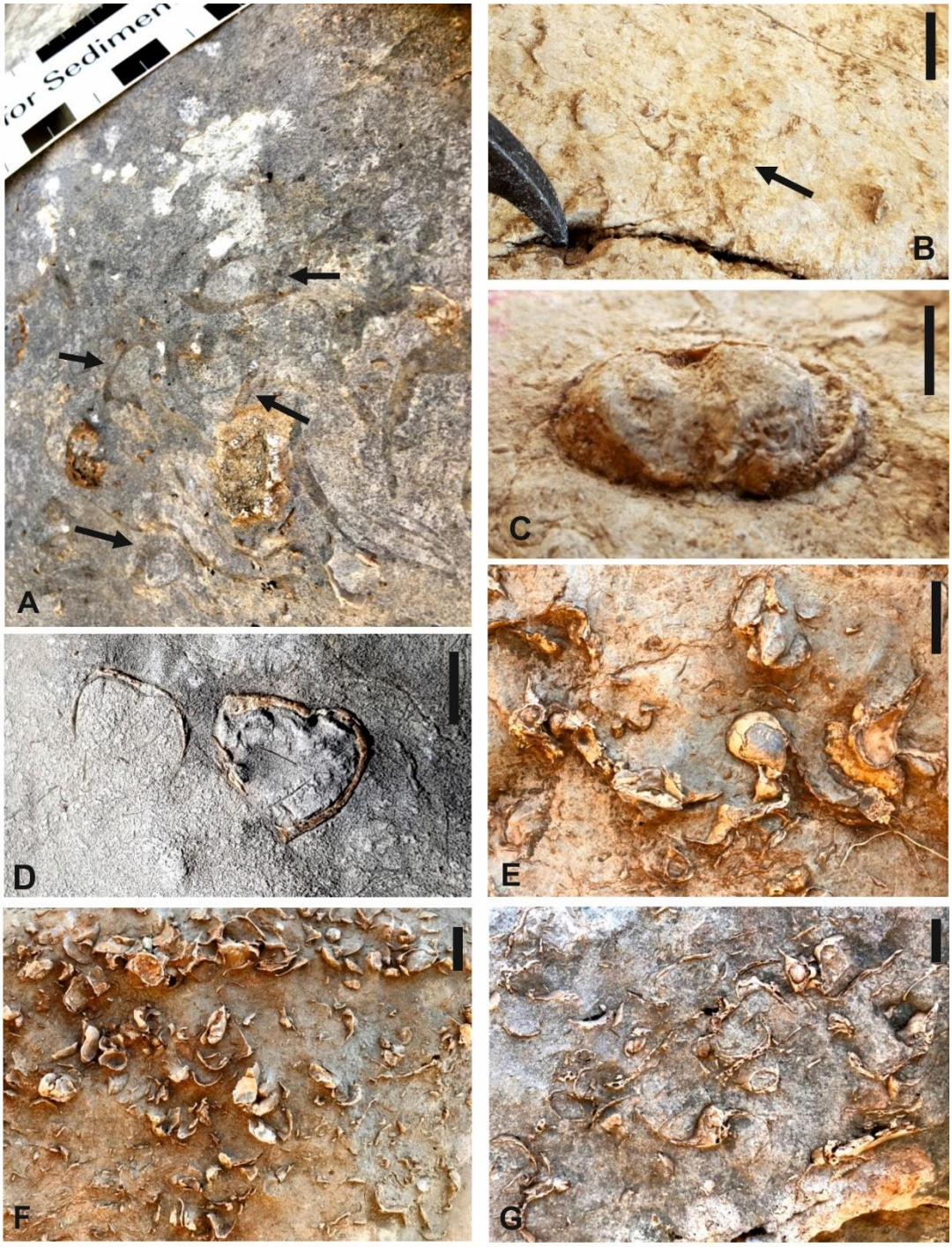


Figure 3.8. A, C. Radiolitid valve fragment lithosome in the Sabunsuyu stratigraphic section. A, B. This lithosome consist mainly of the radiolitid fragments, however some radiolitid transverse and oblique sections (probably *Durania/Sauvagesia*,

Biradiolites) are rarely observed (arrows). C. Some echinid moulds preserving the spicules are also present. D. *Bournonia* sp. transverse sections. E,G. Ichthyosarcolitid–Bivalvia lithosome. Small Ichthyosarcolitid undetermines Bivalvias. Scale bar indicates 10 mm (after Mülayim et al. 2020).



Figure 3.9. Rudist–bearing limestones of the Derdere Formation, outcrop photographs in the Sabunsuyu stratigraphic section. A. *Sauvagesia sharpei* Bayle, two right valves in growth position. B. *Sauvagesia sharpei* Bayle, transverse section of right valve showing thick outer shell layer, short triangular ligamental ridge (L), flat and slightly protruding radial structures separated by a concave interband (Ib). Cellular structure seems to be partially preserved (thin black arrows). C. *Bournonia?* sp., transverse section of right valve; radial structures showing some similarities to those of the genus. D. Stalk elements of crinoids. E. Field views of rudist–bearing limestones of unit VI (scale bar equals 2 m). F, G. Close up of previous photograph. F. Poorly preserved transverse section of right valve of a canaliculated rudist fragment showing very thin internal shell layer with one or two rows of small rounded pallial canals in posterior part (white arrows), as in *Caprinula sharpei*. G. *Biradiolites* sp., transverse section of right valve showing acute ribs (scale bar equals 10 mm in all photographs, except E (after Müülayim et al. 2020).



Figure 3.10. A. Field view showing rudist–bearing limestones of Derdere (unit VII) and Karababa (units VIII and IX) formations in the Sabunsuyu stratigraphic section. BeI. Rudists of the Derdere Formation, outcrop photographs (scale bar equals 10 mm). B,F. *Ichthyosarcolites monocarinatus* Slišković. B,E. Transverse sections of right

valve with single flange on anteroeventral side (black arrow), internal shell layer consisting of dense, ovaloid and round pallial canals, a single very thin tabula (yellow arrow) and elongated teeth sockets of left valve. F. Curved left valve (umbo to right) showing pallial canals in eroded part, some parts may be belong to right valve (black arrow). G,I. *Ichthyosarcolites triangularis* Desmarest, triangular transverse sections of right valve with single projecting flange on dorsal side (white arrow). Teeth sockets of left valve may be present in part. Concave tabulae observed in internal moulds of body cavity (yellow arrow, in G). J. Field view showing thickness of lower (a) and upper (b) rudist–bearing limestones of unit IX (hammer for scale). K,O. Rudists of the Karababa Formation, outcrop photographs (scale bar equals 10 mm). K–M. *Bournonia excavata*, transverse sections of small right valves showing subrounded dorsal side, ventral radial band (black and white arrows) better developed than posterior one and concave interband. N,O. *Apricardia* sp., small valves, strongly coiled left valve and conical, slightly capuloid right valve (after Mülayim et al. 2020).

The upper part of the Derdere Formation comprises mainly monospecific ichthyosarcolitids, *Ichthyosarcolites monocarinatus* Slišković and *Ichthyosarcolites. Triangularis* Desmarest (Figures 3.10A,I; 3.11A,E). The former species presents abundant right valve sections showing typical characteristics of the species such as a slightly elliptical transverse section of the right valve and a single flange on the antero–ventral side (Figures 3.10B,F; 3.11A,E). The external shell layer is partially observed, the internal shell layer consists of dense, ovaloid and round pallial canals, a single very thin tabula; elongated teeth sockets of the left valve are observed. Some curved left valves are present. These sections present close similarities to descriptions of Slišković (1966), Polšak (1967), Cestari et al. (1998), Pleničar and Jurkovšek (2000), Troya Garcia (2015), Rineau and Villier (2018) and Özer and Kahrıman (2019). *Ichthyosarcolites triangularis* Desmarest has a triangular shell shape with a single projecting flange on the dorsal side of the right valve, a thick internal shell layer with dense, small, round to ovoid pallial canal sections and many concave tabulae in the internal moulds of the body cavity (Figure 3.10G,I), which are characteristics of the species (Desmarest, 1817; d'Orbigny, 1847, 1850; Troya Garcia, 2015; Rineau

and Villier, 2018; Özer and Kahrıman, 2019). Ichthyosarcolitids suggest a Cenomanian date, having been described from lower, middle–upper and upper Cenomanian formations in the periphery of the Mediterranean Tethys (Steuber, 2002). They have recently been described from the Central Taurides (Turkey) from the lower–middle Cenomanian by Özer and Kahrıman (2019). The find of this species in the uppermost part of the formation suggests a late Cenomanian age.



Figure 3.11. A,E. *Ichthyosarcolites triangularis* lithosome in the Sabunsuyu stratigraphic section A) Field view of the lithosome showing. the bed thickness of the Derdere and Karababa A contact, (white bar is approximately 310 cm). B. *Ichthyosarcolites triangularis* Desmarest, transverse section of the right valve. C,E.

general view of the monospecific lithosome and transverse section of the right valve of *Ichthyosarcolites triangularis* Desmarest. Scale bar indicates 10 mm. (after Mülayim et al. 2020).

The rudist fauna of the Karababa Formation is characterised by an abundance of *Bournonia excavata*, but *Apricardia* sp. and indeterminate requieniids are also present (Figure 3.12A,E). *Bournonia excavata* d'Orbigny represents small, cylindro–conical right valves, with subrounded dorsal side, the ventral radial band being more developed than the posterior one and the concave interband separating the radial bands (Figure 3.12A,E). *Apricardia* sp. shows a small, strongly coiled left valve and a conical, slightly capuloid right valve (Figure 3.12A,E). The age of *B. excavata* is early Santonian at its type locality (d'Orbigny, 1850; Toucas, 1907; Macé–Bordy, 2007). However, it has been recorded from Coniacian levels in Germany and Spain and Santonian strata in Italy, France, Spain and Romania (Steuber, 2002; Cestari, 2008; Lucena Santiago, 2014). In previous studies (covering Italy, Bosnia–Herzegovina, Croatia, Cuba, Afghanistan and Somalia), also a Campanian–Maastrichtian date has been attributed to *B. excavata*, but the majority of these lack figure(s) and descriptions from (for references, see Steuber, 2002). Some studies present merely figure(s) and/or descriptions of this species from the Campanian–Maastrichtian or Maastrichtian of Montenegro, Italy, Guatemala and Iran (see Steuber, 2002; Khazaei et al., 2010). Thus, a Campanian–Maastrichtian date for *B. excavata* d'Orbigny is questionable (Steuber, 2002; Lucena Santiago, 2014), but the discussion continues. In the present study, favouring dating *B. excavata* as Coniacian–Santonian, with respect to its stratigraphical distribution in Tethyan areas and the age of the Karababa Formation.

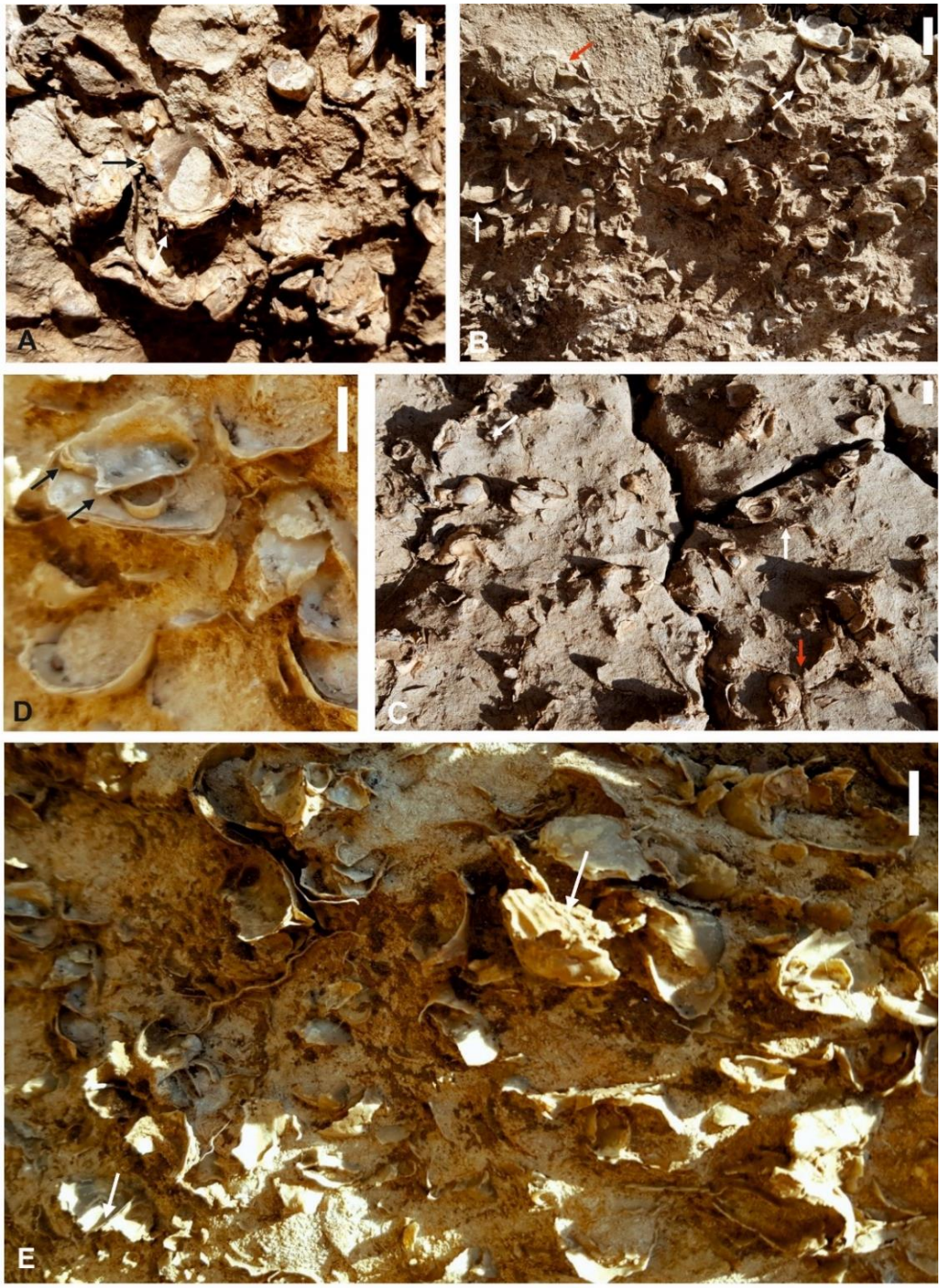


Figure 3.12. A,E *Bournonia excavata* lithosome in the Sabunsuyu stratigraphic section. A,D Note radial bands (arrows) and in growth position of the valves. B,C Rare, small *Bournonia excavata* (thick white arrows), *Apricardia* sp. (thick red arrows) and undeterninable bivalvia are present. E. general view of the lithosome showing the transverse sections and moulds of the species and also radial bands on the surface of the right valve (arrows). Scale bar is 10 mm (after Mülayim et al. 2020).

3.1.3 Planktonic Foraminifera

İnişdere Stratigraphic Section

These assemblages are mainly dominated by whiteinellids, which are associated with dicarinellids, marginotruncanids and rare helvetoglobotruncanids. Taxa identification is hampered by widespread recrystallization. For this reason, precise biostratigraphy based on the first and last occurrences cannot be presented in the İnişdere stratigraphic section; instead, the age data are obtained based on the presence of four distinctive planktonic foraminiferal assemblages. Fifteen species were recognized in the approximately 4 m–thick pelagic facies interval (Figures 3.13 and 3.14). *H. praehelvetica* Trujillo (Figures 3.13 and 3.14) is rare at the base and observed only at a single level in the upper part of the member (Figures 3.13 and 3.14). Whiteinellids (i.e. *Whiteinella baltica* Douglas and Rankin, *W. archaeocretacea* Pessagno *W. aprica* Loeblich and Tappan, and *W. brittonensis*, Loeblich and Tappan) dominate the planktonic foraminifera assemblages and are associated with some marginotruncanids (i.e. *Marginotruncana tarfayaensis* Lehmann, *Marginotruncana* sp. cf. *M. sigali* Reichel, *M. schneegansi* Sigali, *M. paraconcavata* Porthault, *M. pseudolinneiana* Pessagno, and *M. renzi Gandolfi*) and rare dicarinellids (i.e. *Dicarinella* sp. cf. *D. marionasi* Douglas and *Dicarinella* sp. cf. *D. primitiva* Dalbiez) in the İnişdere stratigraphic section (Figures 3.13 and 3.14).

More or less similar assemblages were documented from many low– to mid–latitude lower to middle Turonian successions (Robaszynski et al. 1990; Premoli Silva and Sliter, 1995; Petrizzo, 2000; 2001; 2003; Caron et al. 2006; Hart, 2008; Huber and Petrizzo, 2014; Coccioni and Premoli Silva 2015; Falzoni et al. 2016; 2018; Huber et al. 2017; Özkan and Altıner, 2019). A specimen in sample IND–22 is defined as a transitional form between *H. helvetica* and its ancestor *H. praehelvetica* (Figures 3.13 and 3.14). The extinction of *H. praehelvetica* is slightly younger (Robaszynski and Caron, 1979; Sliter, 1989) or older (Caron, 1985; Premoli Silva and Verga, 2004) than the extinction of the zonal marker *H. helvetica*. Although the *H. helvetica* Zone is placed to the early Turonian by Anthonissen and Ogg (2012), the first and last occurrences of the nominate taxon and its ancestor *H. praehelvetica* have long been

discussed (e.g. Carter and Hart, 1977; Hart and Weaver, 1977; Caron et al. 2006; Desmares et al. 2007; Hart, 2008; Huber and Petrizzo, 2014; Huber et al. 2017) owing to the diachroneity of the datum levels in different successions. Despite prevailing arguments, several recent studies have shown that the last occurrence of *H.praehelvetica* was within the middle Turonian (Huber and Petrizzo, 2014; Coccioni and Premoli Silva, 2015; Huber et al. 2017). Marginotruncanids became more diverse in the late Turonian (Robaszynski and Caron, 1979; Caron, 1985; Premoli Silva and Sliter, 1999), but the timing and rate of this speciation event have not been well documented so far (Huber et al. 2017). Marginotruncanid diversification began in the earliest Turonian according to Falzoni et al. (2016). Several studies have shown that many large marginotruncanid and dicarinellid species (mostly known from upper Turonian successions), such as *D. marionasi, D. primitiva, M. marginata, M. paraconcavata, M. sigali* and *M. tarfayaensis*, make their first occurrences within the *H. helvetica* Zone and therefore co–occur with *H. praehelvetica* in several Tethyan and higher–latitude successions (Robaszynski et al. 1990; Premoli Silva and Sliter, 1995; Petrizzo, 2000; Nishi et al. 2003; Caron et al. 2006; Gebhardt et al. 2010; Bomou et al. 2013; Coccioni and Premoli Silva, 2015; Falzoni et al. 2016; Huber et al. 2017; Lowery and Leckie, 2017; Özkan and Altıner, 2019). The data above show that the age of the lower part of Karababa–A Member in the İnişdere succession is early to middle Turonian, partly coeval to the *H. helvetica* Zone. Özkan and Altıner (2019) suggested a late middle Turonian age for the lower part of the member. Although *D. concavata* generally appeared after the dissaperance of *H. Praehelvetica* (e.g. Premoli Silva and Verga, 2004), Özkan and Altıner, (2019) reported co–occurrence of the two taxa in the middle part of the member and suggested a late Turonian–Coniacian age for the middle and upper parts of the member. The abundance of whiteinellids (non–keeled, r–selected taxa) suggests unstable conditions (i.e. a weakly stratified upper water column in a mesotrophic environment) for planktonic foraminifera (Hart and Bailey, 1979; Caron and Homewood, 1983; Robaszynski and Caron, 1995; Hart, 1999; Premoli Silva and Sliter, 1999; Petrizzo, 2002) during deposition of the Karababa–A Member. Bornemann and Norris, (2007) and Norris and Wilson, (1998) suggested that the genus *Marginotruncana,* which is known as a k–strategist taxa

(Petrizzo, 2002) grew primarily in surface waters along with globular, non–keeled species such as *Whiteinella*.

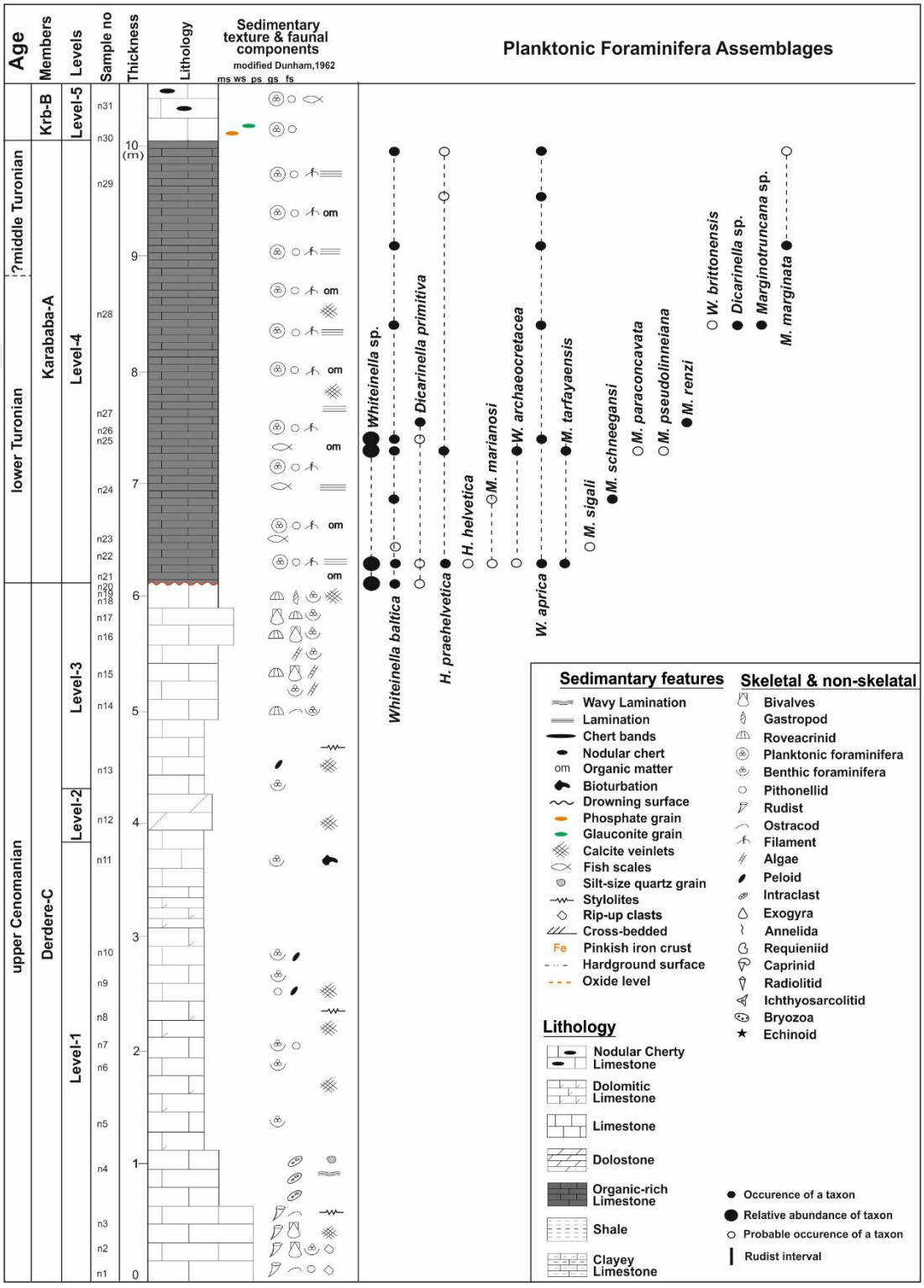


Figure 3.13. Distribution of planktonic foraminifera in the İnişdere stratigraphic section (after Mülayim et al. 2019a).

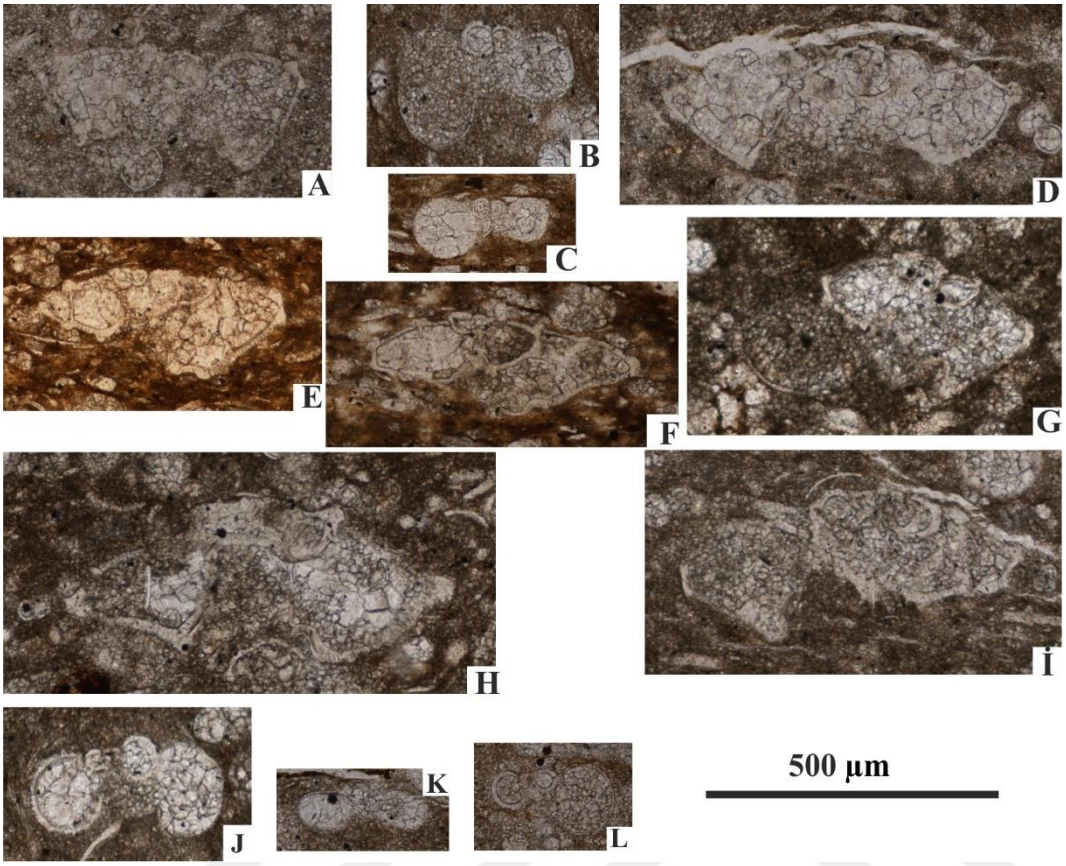


Figure 3.14. Thin–section images of the planktonic foraminifera observed in the Karababa–A Member. (A–L) İnişdere stratigraphic section; A. *Dicarinella* cf. *primitiva* (Dalbiez), sample IND–22; B. transitional from *H. praehelvetica* to *H. helvetica*, sample IND–22; C. *Helvetoglobotruncana praehelvetica* (Trujillo), sample IND–25; D. *Dicarinella* cf. *marianosi* (Douglas), sample IND–22; E. *Marginotruncana* cf. *paraconcavata* Porthault, sample IND–25; F. *Marginotruncana renzi* (Gandolfi), sample IND–27; G. *Marginotruncana schneegansi* (Sigal), sample IND–24; H. *Marginotruncana* cf. *sigali* (Reichel), sample IND–23; İ. *Marginotruncana tarfayaensis* (Lehmann), sample IND–22; J. *Whiteinella aprica* (Loeblich and Tappan), sample IND–22; K. *Whiteinella* cf. *archaeocretacea* Pessagno, sample IND–22; L. *Whiteinella baltica* Douglas and Rankin, sample IND–24. (after Mülayim et al. 2019a).

Sabunsuyu Stratigrahic Section

Planktonic foraminifera are also rare throughout the succession These poor assemblages are represented by reselected taxa, dominated by Hedbergellidae, (*Muricohedbergella planispira* Tappan*)* which are described from the base and the middle/upper part of the Derdere Formation. *Asterohedbergella asterospinosa* Hamaoui, characterised by a tubulospinate extension in the last chamber(s) of the final whorl, has been rarely documented so far, with records from middle to upper Cenomanian strata in Israel (Hamaoui, 1965; Loeblich and Tappan, 1988; BouDagher–Fadel, 2012). These biostratigraphical data indicate a middle–late Cenomanian for Derdere Formation (Figure 3.15 and 3.16).

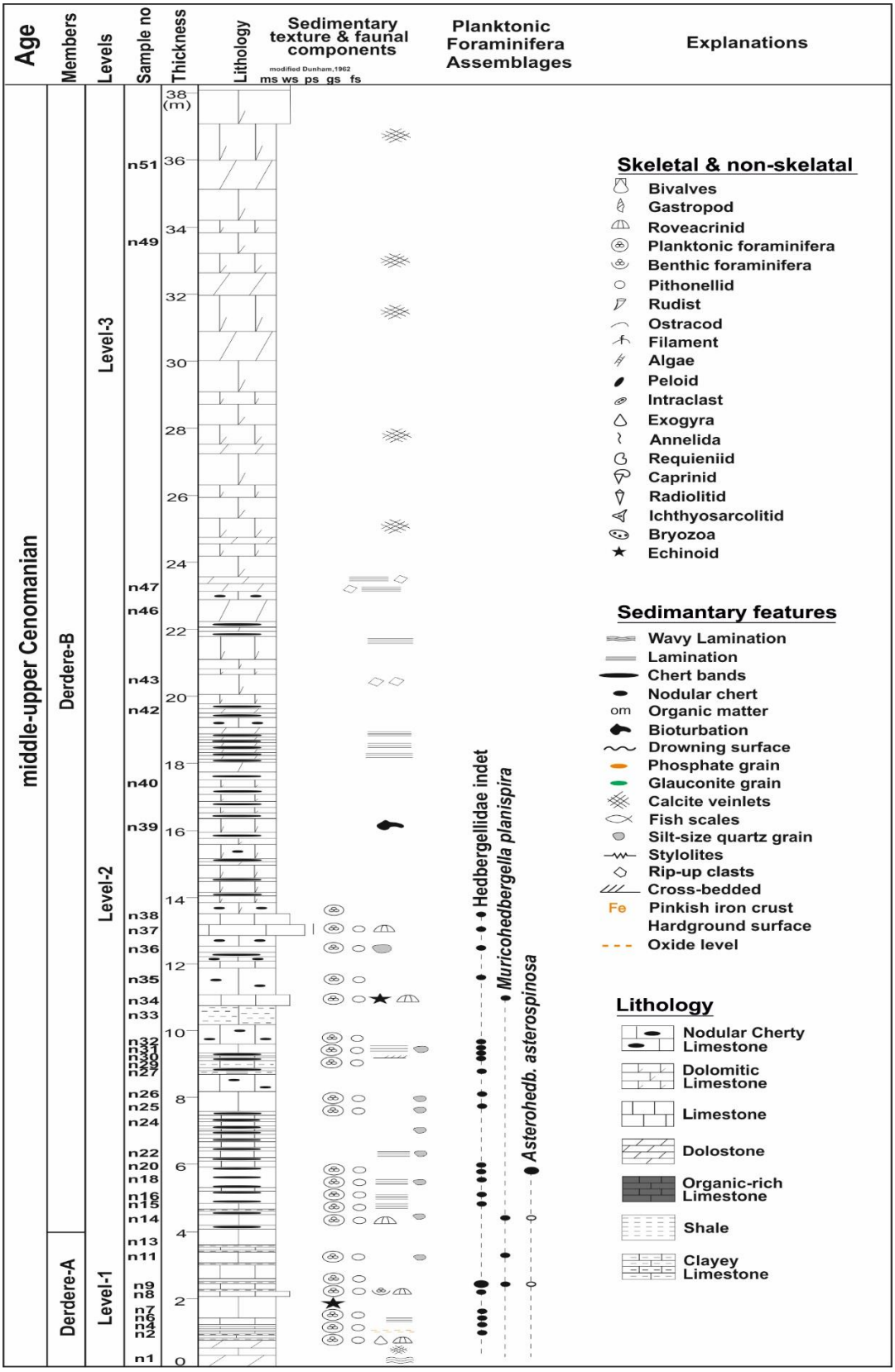


Figure 3.15. Distribution of planktonic foraminifera in the Sabunsuyu stratigraphic section (after Mülayim et al. 2020).

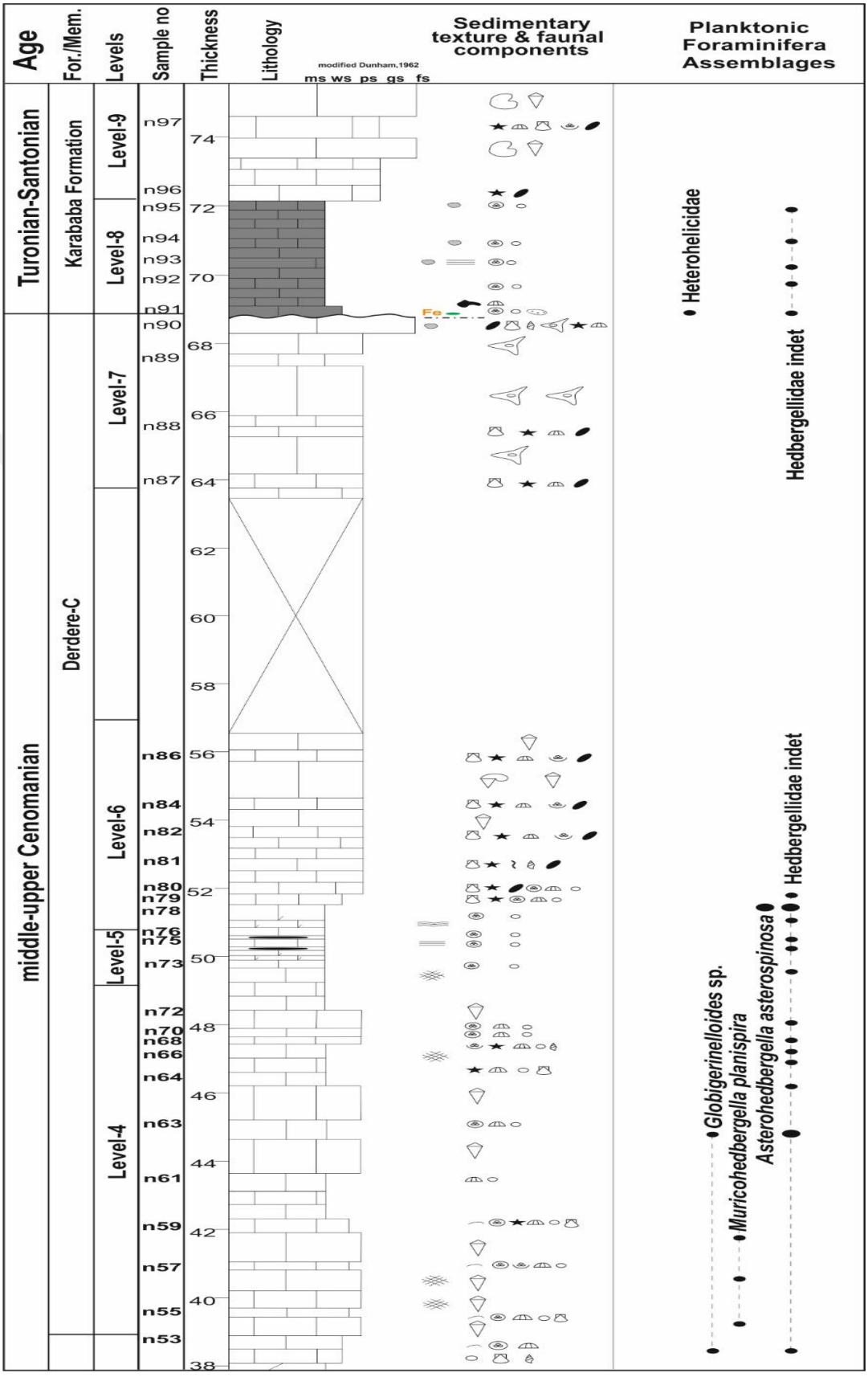


Figure 3.15. (continued)

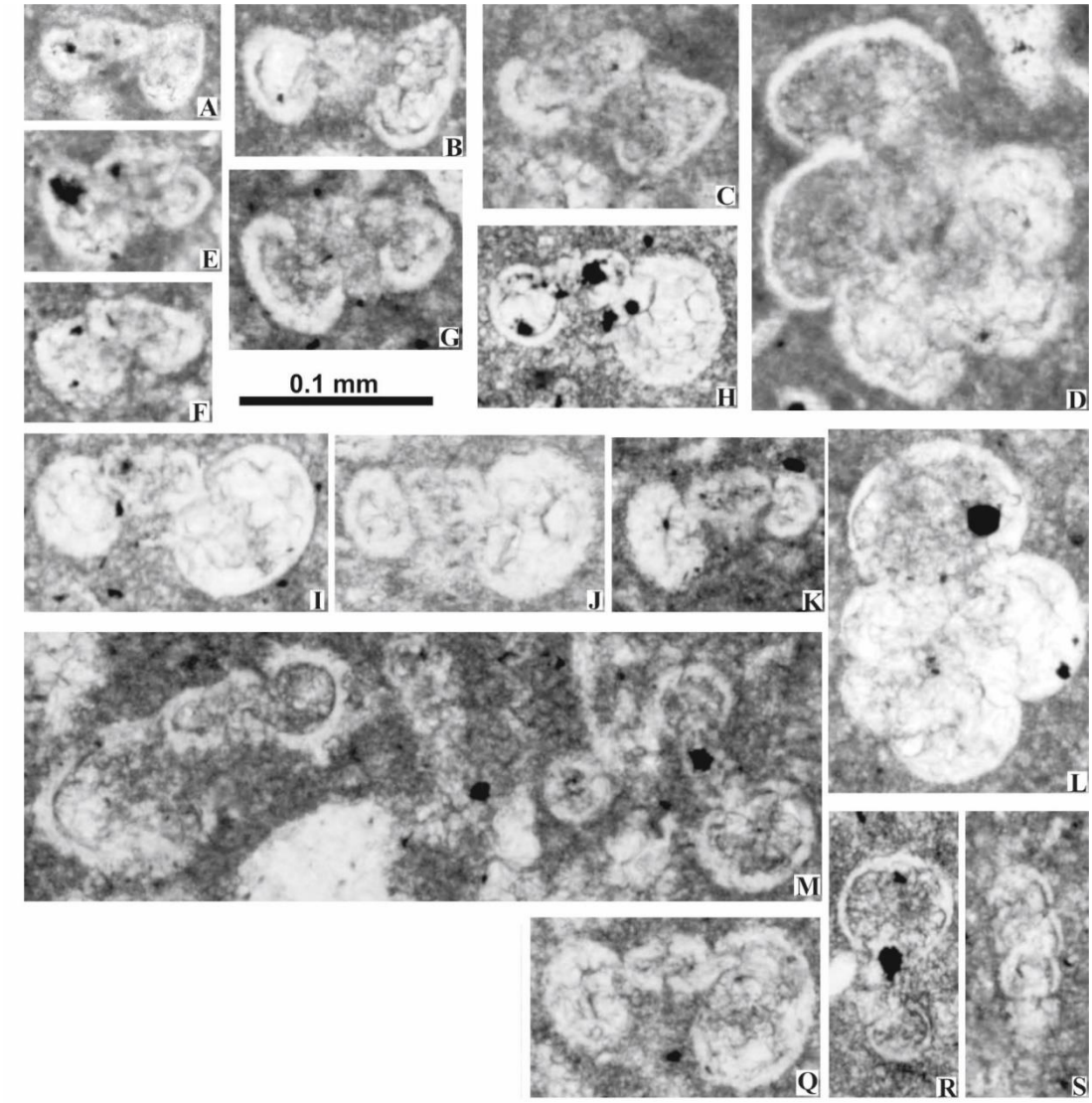


Figure 3.16. Thin–section images of the planktonic foraminifera taxa observed in the Sabunsuyu stratigraphic section. A,C. *Asterohedbergella asterospinosa* Hamaoui ,MU, samples 19, 79 and 79, respectively; DeL. Hedbergellidae indet., MU, samples 79, 1D, 1A, 1D, 19, 19, 79, 63 and 63, respectively; M. Hedbergellidae indet. (left) and *Globigerinelloides* sp. (right), MU, sample 86; Q. Hedbergellidae indet., MU, sample 80; R. *Globigerinelloides* sp., MU, sample 63; S. Heterohelicidae indet., MU, sample 1A (after Mülayim et al. 2019a).

Türkoğlu Strtatigraphic Section

The upper part of the Derdere Formation comprises poor planktonic foraminiferal assemblages including *Whiteinella aprica* Loeblich and Tappan, *Whiteinella baltica* Douglas and Rankin, *Whiteinella* sp. *Dicarinella* sp. *Marginatruncana.* sp. and *H*. cf. *praehelvetica. Whiteinella baltica* and *Whiteinella aprica* long ranging late Cenomanian–Coniacian taxa (Anthonissen and Ogg, 2012). *H*. cf. *praehelvetica* Trujillo, occurring in two samples at the top of the unit is known as a late Cenomanian–middle Turonian species in many low to mid–latitude successions (Figure 3.17).

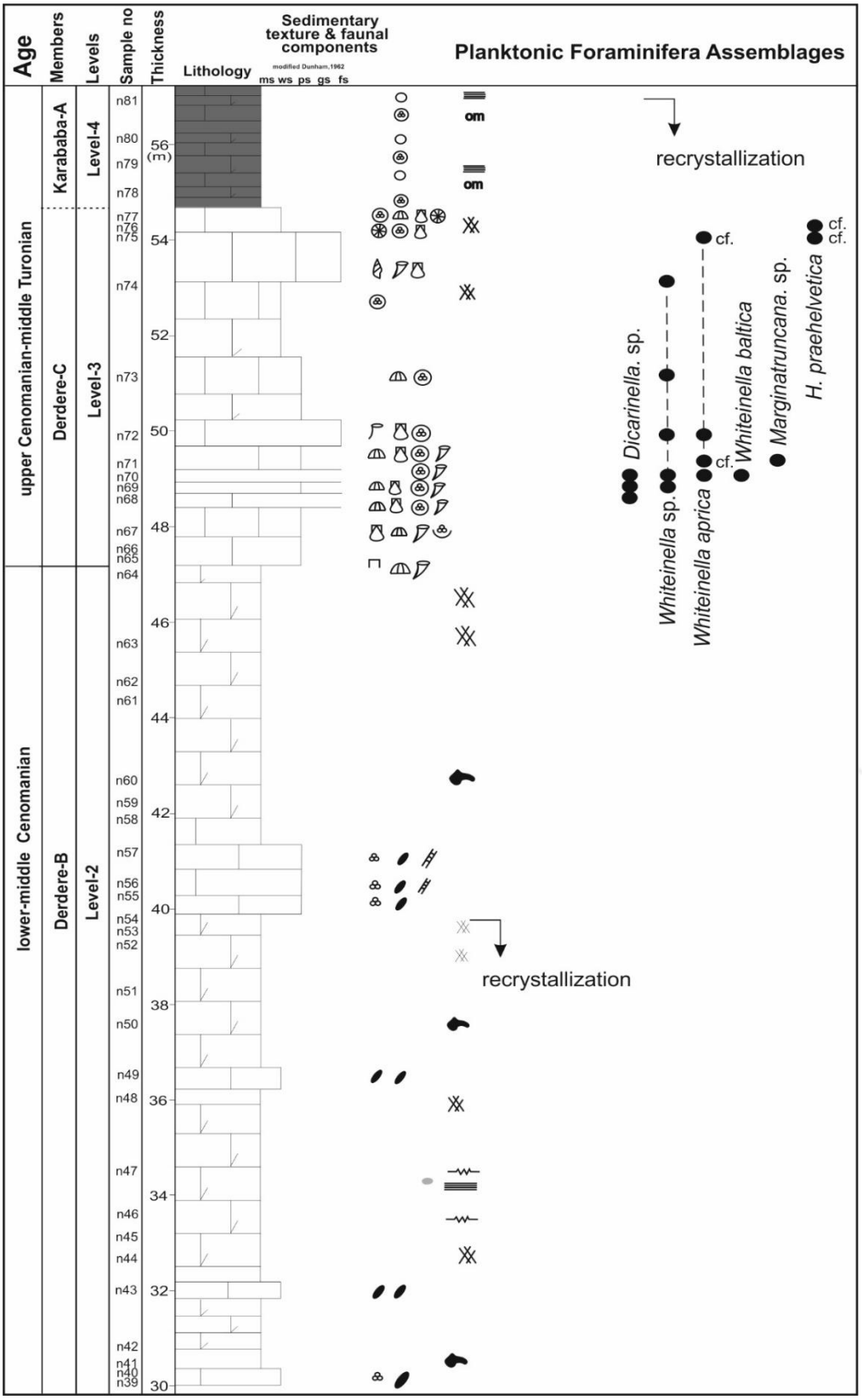


Figure 3.17. Distribution of planktonic foraminifera in the upper part of the Türkoğlu stratigraphic section (after Mülayim et al. 2019b).

Borehole sections

The planktonic foraminifera assemblages of the 18 m–thick A–1 borehole succession are dominated by whiteinellids (e.g. *Whiteinella aprica*, *W.* cf. *archaeocretacea*, *W. baltica*, *W. brittonensis*, *W. inornata*, *W.* cf. *paradubia*), which are associated with some dicarinellids (e.g. *Dicarinella hagni*, *D. primitiva*, *D. canaliculata*, *D. concavata*), marginotruncanids (e.g. *Marginotruncana marginata*, *M.* cf. *schneegansi*, *M. renzi*, *M. tarfayaensis*, *M.* cf. *pseudolinneiana*, *M. sigali*, *M.* cf. *paraconcavata*), rare praeglobotruncanids (e.g. *Praeglobotruncana algeriana*) and helvetoglobotruncanids (e.g. *Helvetoglobotruncana helvetica* and *H. praehelvetica*) (Figures 3.18 and 3.22). Planktonic foraminifera are very rare particularly at the base of the succession and in some certain levels. The nominate taxon of the *H. helvetica* Zone *H. helvetica* makes its LO and HO in the 11–m–thick interval between samples 13/4 and 11/6 respectively and occurs rarely. Although the *H. helvetica* Zone is placed to the early Turonian by Anthonissen and Ogg (2012) and Coccioni and Premoli Silva (2015), the LO and HO of the nominate taxon and its ancestor *H. praehelvetica* is still being discussed (e.g. Caron et al., 2006; Desmares et al., 2007; Hart, 2008; Huber and Petrizzo, 2014; Huber et al., 2017) owing to the diachroneity of the datum levels in various Tethyan and Boreal successions. Following the recent data of Huber and Petrizzo (2014) and Huber et al. (2017), which suggest that the HO of *H. helvetica* is within the middle Turonian. A single occurrence of *D. concavata* in sample 11/3 indicates that the age of the uppermost part of Karababa–A member in the A–1 succession is the latest Turonian. *D. concavata* is the nominate taxon of the *D. concavata* Zone, of which lower limit ranges down to the latest Turonian according to the recent studies (Anthonissen and Ogg, 2012). However, the lower boundary of the zone is not fixed chronologically. A relatively thin stratum (around 1,7 m.) between the HO of *H. helvetica* and the LO of *D. concavata* may indicate that the first appearance of *D. concavata* is earlier than it has been known if the succession is not condensed (Figure 3.18).

Appearance and diversification of marginotruncanids was established within the Turonian and the evolution of the group is important for Turonian biostratigraphy. Marginotruncanids appeared within the *H. helvetica* Zone during the restoration of k–

selected taxa, after the *W. archaeocretacea* Zone of r–selected groups such as whiteinellids (Caron et al., 2006). Although marginotruncanids became more diverse in the late Turonian (Robaszynski and Caron 1979; Caron, 1985; Premoli Silva and Sliter, 1999), Huber et al. (2017) show that the timing and rate of this speciation event have not been well documented. Diversification began in the earliest Turonian according to Falzoni et al. (2016). Several studies have shown that many large marginotruncanid species (mostly known from upper Turonian successions) such as, *M. marginata*, *M. paraconcavata*, *M. sigali* and *M. tarfayaensis*, make their LOs within the *H. helvetica* Zone in several Tethyan and higher–latitude successions (Robaszynski et al., 1990; Premoli Silva and Sliter, 1995; Petrizzo, 2000; Nishi et al., 2003; Caron et al., 2006; Gebhardt et al., 2010; Bomou et al., 2013; Coccioni and Premoli Silva, 2015; Falzoni et al., 2016; Huber et al., 2017; Lowery and Leckie, 2017; Özkan and Altıner, 2019; Mülayim et al., 2019a). The first marginotruncanids in the A–1 succession appear in the 6th meter of the succession (Figure 3.18). The data above show that the age of the lower part of Karababa–A Member in the A–1 borehole section is early to middle Turonian as in the İnişdere succession in the neighbouring area to NE. Because of the absence of any index taxa in the 4–m–thick lowermost part of the succession, a ?latest Cenomanian–earliest Turonian age could be suggested based on the planktonic foraminiferal assemblages.

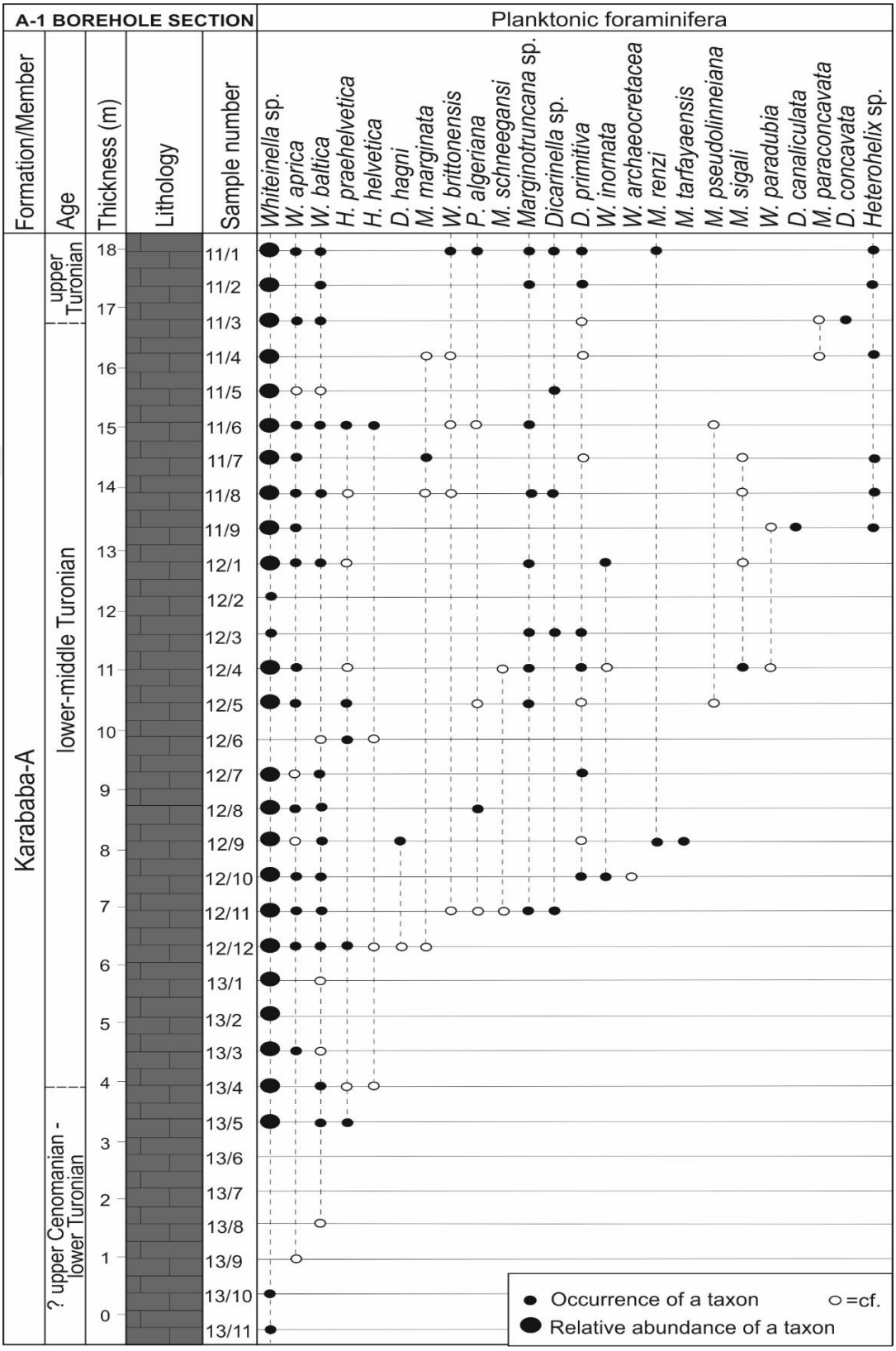


Figure 3.18. Stratigraphic distribution of planktonic foraminifera in the A–1 borehole section. (after, Mülayim et al. 2020b).

The planktonic foraminifera assemblages of the 4 m–thick BS–1 borehole succession are dominated by whiteinellids. The LO and HO of *H.* aff. *helvetica* and *H.* cf. *helvetica* in samples 1.2 and 1.5 respectively suggest that the age of this part of the succession is early–middle Turonian. The presence of *D.* cf. *concavata* in sample 1.6 shows that the age of the uppermost part of the succession is the latest Turonian. The thickness of the limestones between the HO of *H.* cf. *helvetica* (sample 1.5) and the LO of *D.* cf. *concavata* (sample 1.6) is about 0,5 m. (Figures 3.19 and 3.22).

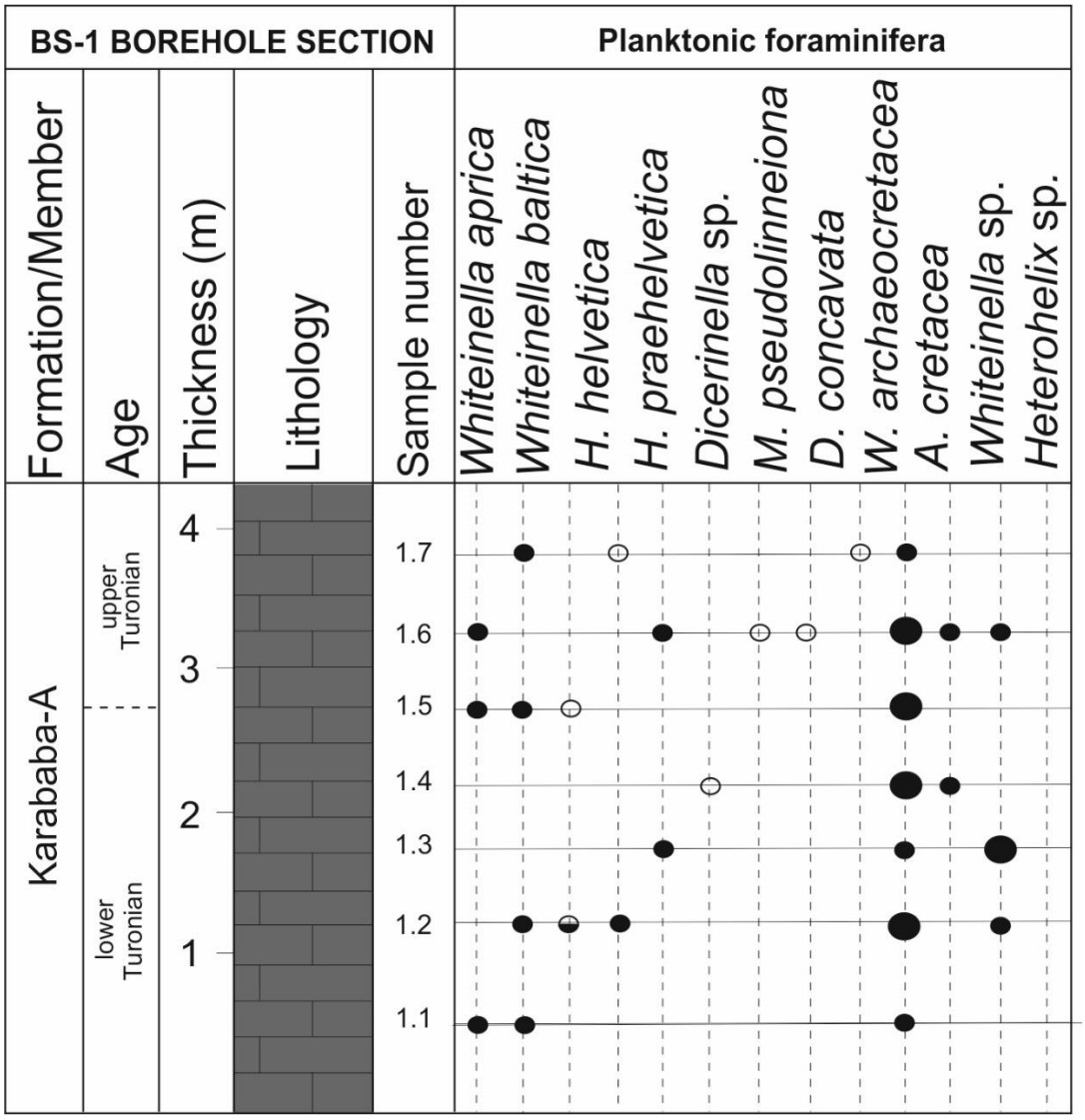


Figure 3.19. Stratigraphic distribution of planktonic foraminifera in the BS–1 borehole section. (after Mülayim et al. 2019a).

Whiteinellids dominate the planktonic foraminifera assemblages in the approximately 9 m–thick KM–1 succession as in the other three borehole successions. The presence of *H.* cf. *helvetica* in samples 1.9 and 1.10 at the base of the succession suggests that the age of the succession can not be older than Turonian. *H. praehelvetica* occurs throughout the section and shows that the succession can not be younger than the Turonian (Figures 3.20 and 3.22).

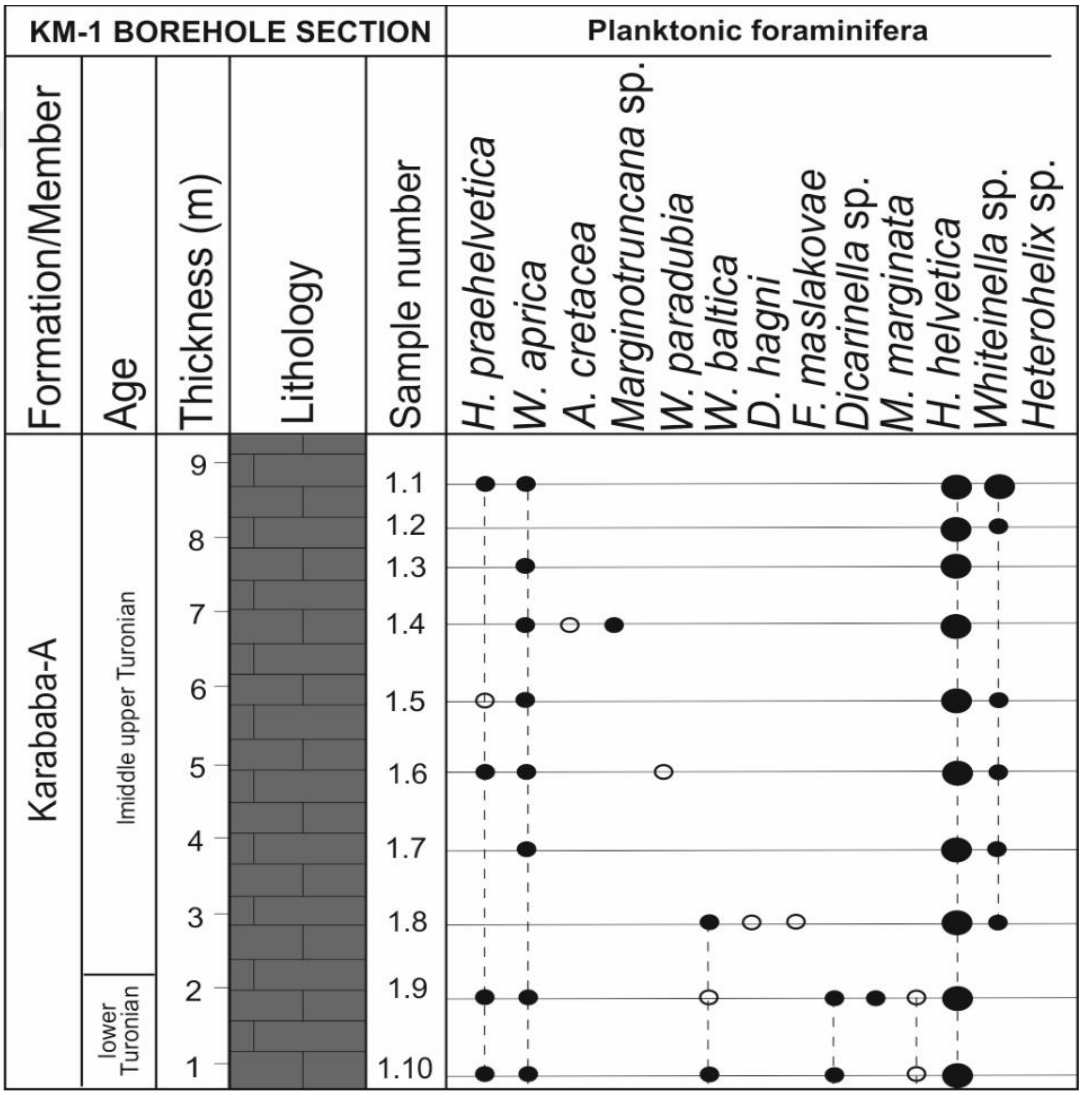


Figure 3.20. Stratigraphic distribution of planktonic foraminifera in the KM–1 borehole section. (after Mülayim et al. 2019a).

The 8 m–thick CM–14 succession is represented by poor planktonic foraminiferal assemblages. The presence of *M.* cf. *coronata* and *P. algeriana* in samples 14.4 and 14.7 respectively may indicate a middle Turonian age (Figures 3.21, 3.22, and 3.23).

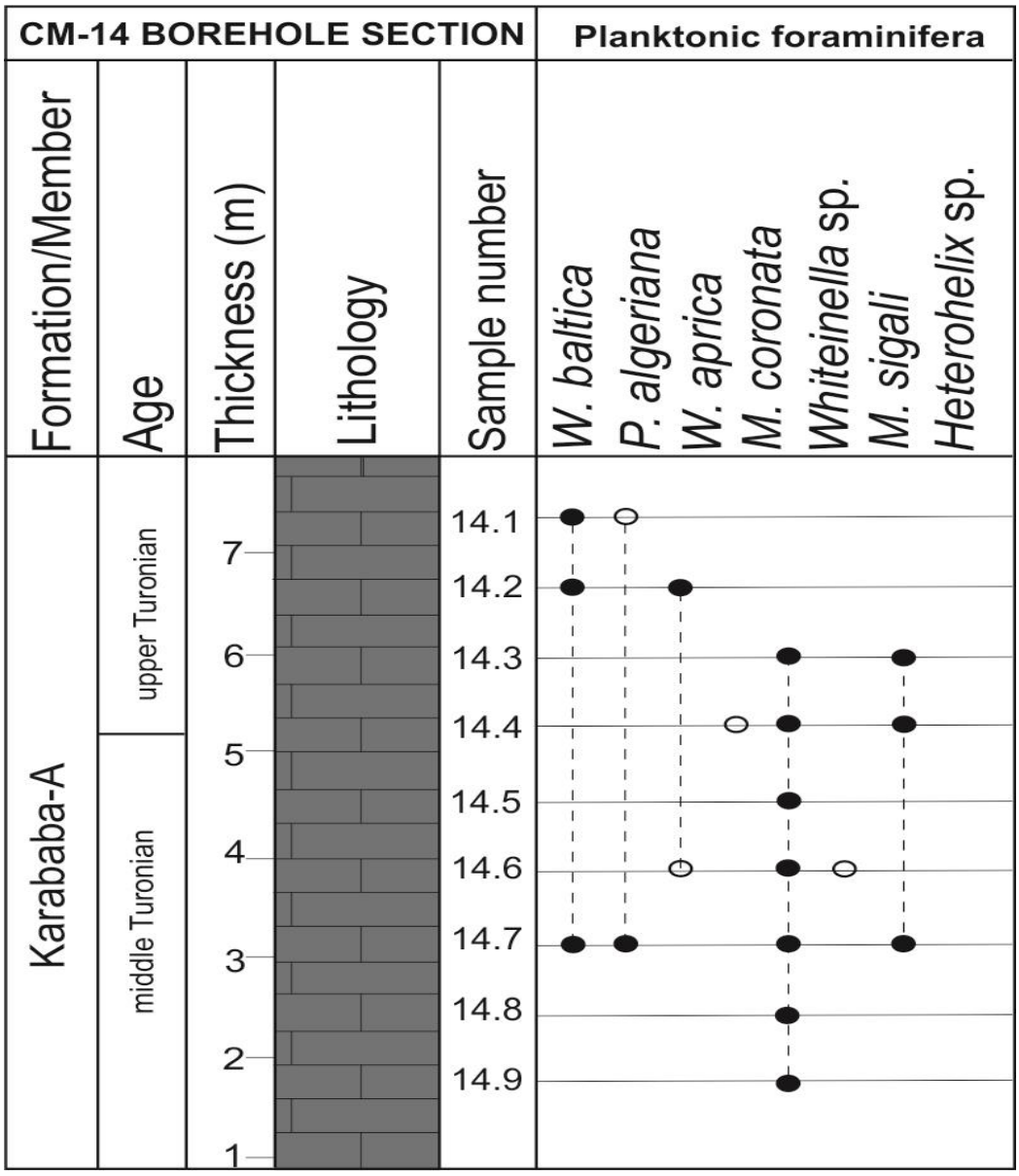


Figure 3.21. Stratigraphic distribution of planktonic foraminifera in the CM–14 borehole section. (after Mülayim et al. 2019a).

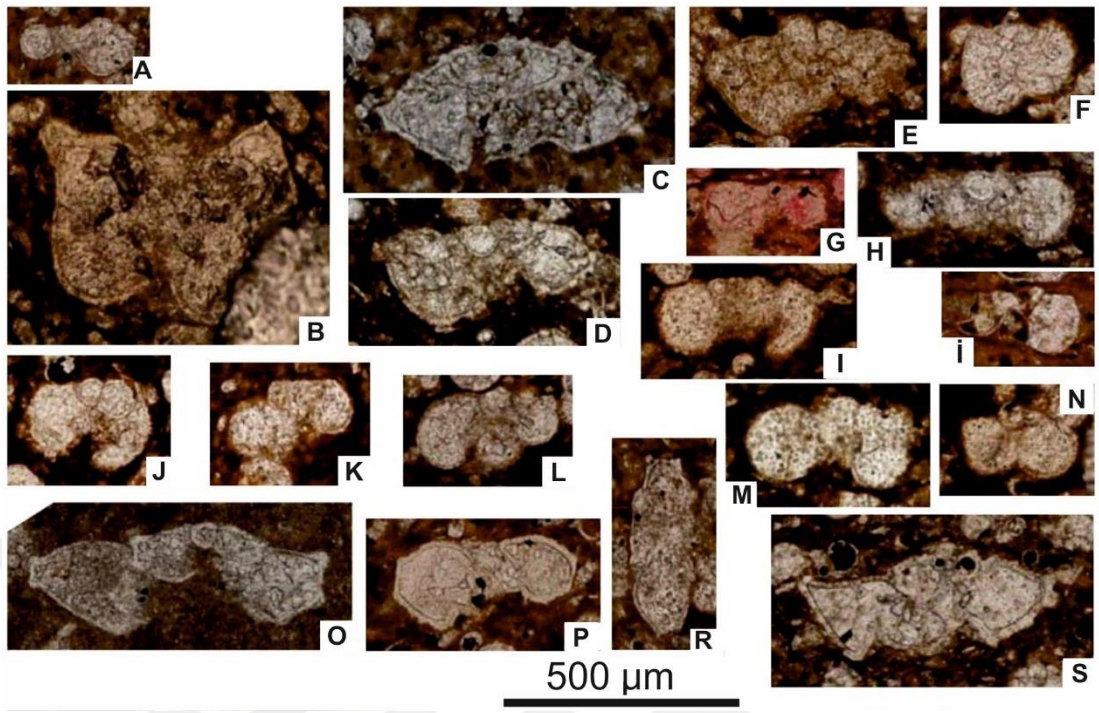


Figure 3.22. Thin–section images of the planktonic foraminifera taxa observed in the four borehole sections. A. *Archaeoglobigerina* cf. *cretacea*, Sample BS 1–7, BS–1 section; B. *Dicarinella concavata*, Sample K– 11/3–1, A–1 section; C. *Dicarinella* cf. *hagni* Sample KM 1– 8, KM–1 section; D. *Dicarinella primitiva*, Sample K–12/4–1, A–1 section; E. *Dicarinella primitiva*, Sample K–12/4–1, A–1 section; F. *Helvetoglobotruncana* aff. *helvetica*, Sample BS 1–2, BS–1 section; G. *Helvetoglobotruncana helvetica*, Sample K–11/6–1, A–1 section; H. *Helvetoglobotruncana* cf. *helvetica*, Sample K–12/12, A–1 section; I. *Helvetoglobotruncana* cf. *helvetica*, Sample K–11/6–2, A–1 section; İ. *Helvetoglobotruncana* cf. *helvetica*, Sample K–13/4–1, A–1 section; J. *Helvetoglobotruncana* cf. *helvetica*, Sample KM 1–10, KM–1 section; K. *Helvetoglobotruncana* cf. *praehelvetica*, Sample BS 1–2, BS–1 section; L. *Helvetoglobotruncana praehelvetica*, Sample BS 1–2, BS–1 section; M. *Helvetoglobotruncana praehelvetica*, Sample K–12/5–1, A–1 section; N. *Helvetoglobotruncana praehelvetica*, Sample KM 1–1, KM–1 section; O. *Marginotruncana* cf. *coronata*, Sample 14–4, CM–14 section; P. *Marginotruncana marginata*, Sample KM 1–9, KM–1 section; R. *Marginotruncana* cf. *pseudolinneiana*, Sample BS 1–4, BS–1 section; S. *Marginotruncana renzi*, Sample K– 12/9, A–1 section.

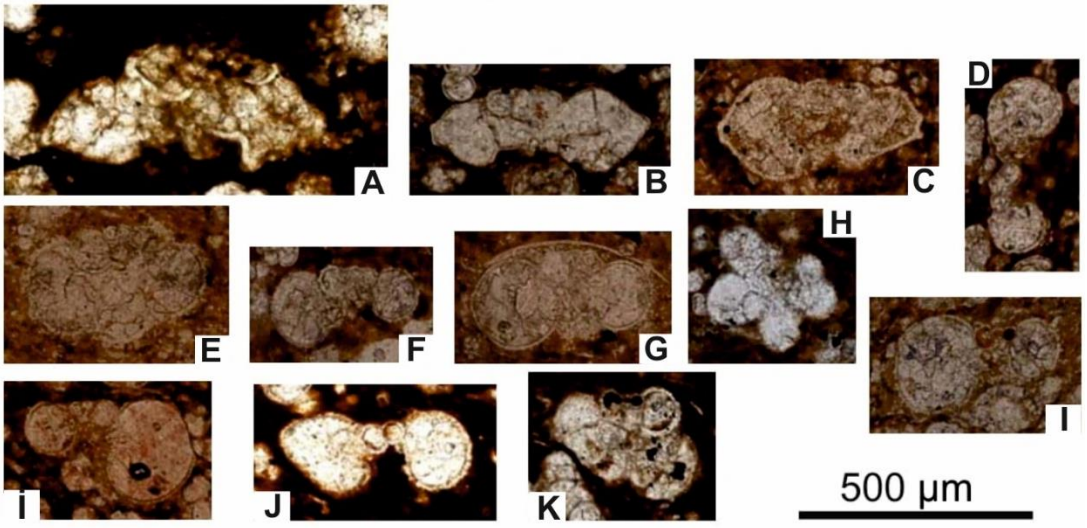


Figure 3.23. Thin–section images of the planktonic foraminifera taxa observed in the four borehole sections. A.*Marginotruncana* cf. *sigali*, Sample K–12/4–1, A–1 section; B. *Praeglobotruncana algeriana*, Sample K–11/1–1, A–1 section; C. *Praeglobotruncana algeriana*, Sample 14–7, CM–14 section; D. *Whiteinella aprica*, Sample BS 1–2, BS–1 section E. *Whiteinella aprica*, Sample K–12/11, A–1 section;; F. *Whiteinella aprica*, Sample KM 1–7, KM–1 section; G. *Whiteinella aprica*, Sample 14–2, CM–14 section; H. *Whiteinella* cf. *archaeocretacea*, Sample BS 1–6, BS–1 section; I. *Whiteinella baltica*, Sample K– 12/8, A–1 section; İ. *Whiteinella baltica*, Sample K– 11/3–1, A–1 section; J. *Whiteinella inornata*, Sample K–12/1–2, A–1; K. *Whiteinella* cf. *paradubia*, Sample K–12/4–1, A–1 section (after Mülayim et al. 2019a).

3.1.4 Benthic Foraminifera

İnişdere Stratigraphic Section

The biostratigraphic analysis revealed the following upper Cenomanian foraminifera association in the İnişdere succession. (Figures 3.24 and 3.25). The upper part of the Derdere Formation comprises poor benthic foraminiferal assemblages including Miliolidae, Discorbidae, *Cuneolina pavonia* d'Orbigny and *Nezzazatinella picardi* Henson. The species are long–ranging taxa, specifically the lowermost Cenomanian in the peri–Mediterranean platforms (Velić, 2007). A higher biostratigraphic

resolution on the basis of the distribution of benthic foraminifera does not seem possible.

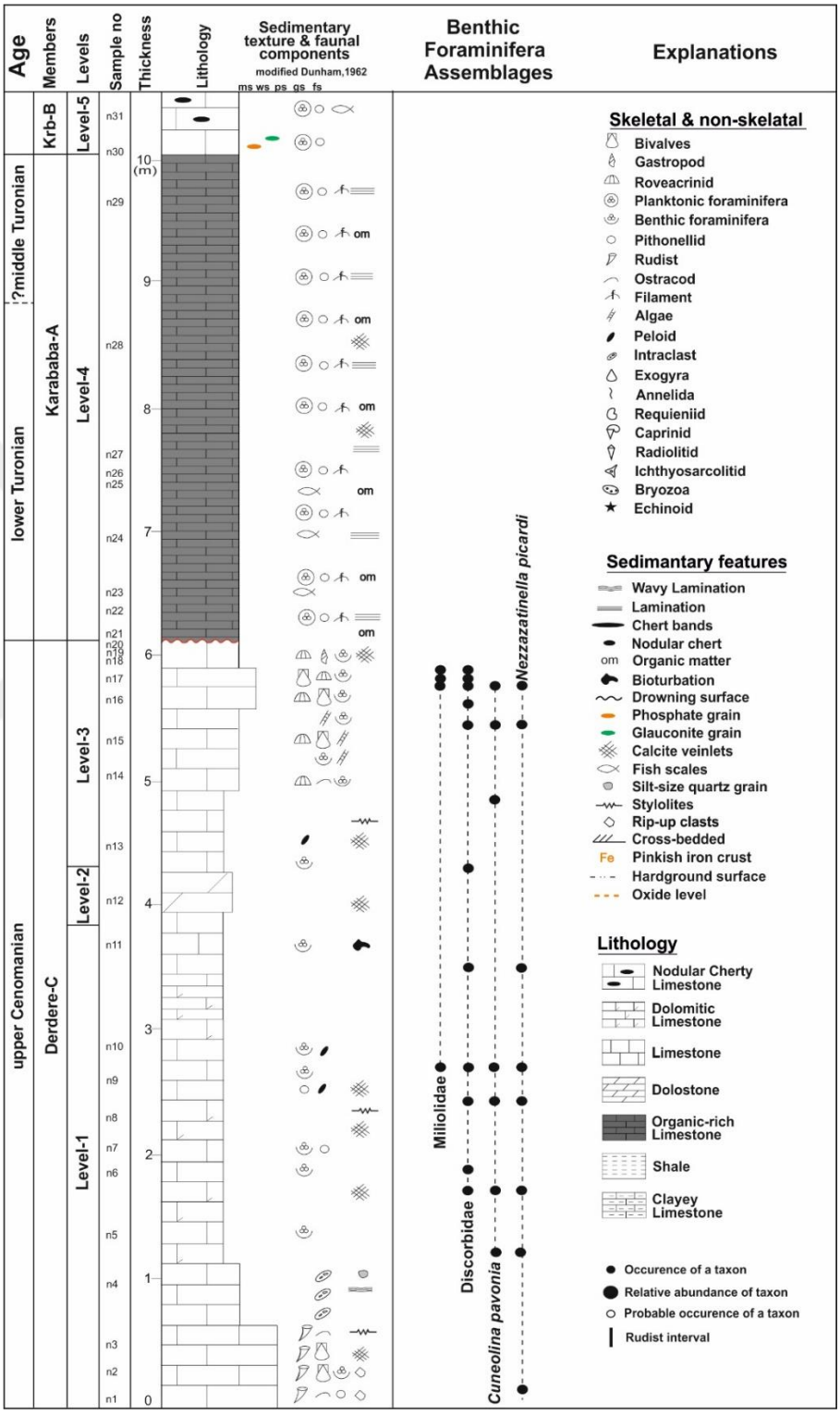


Figure 3.24. Stratigraphic distribution of benthic foraminifera in the İnişdere stratigraphic section. (after Mülayim et al. 2019a).

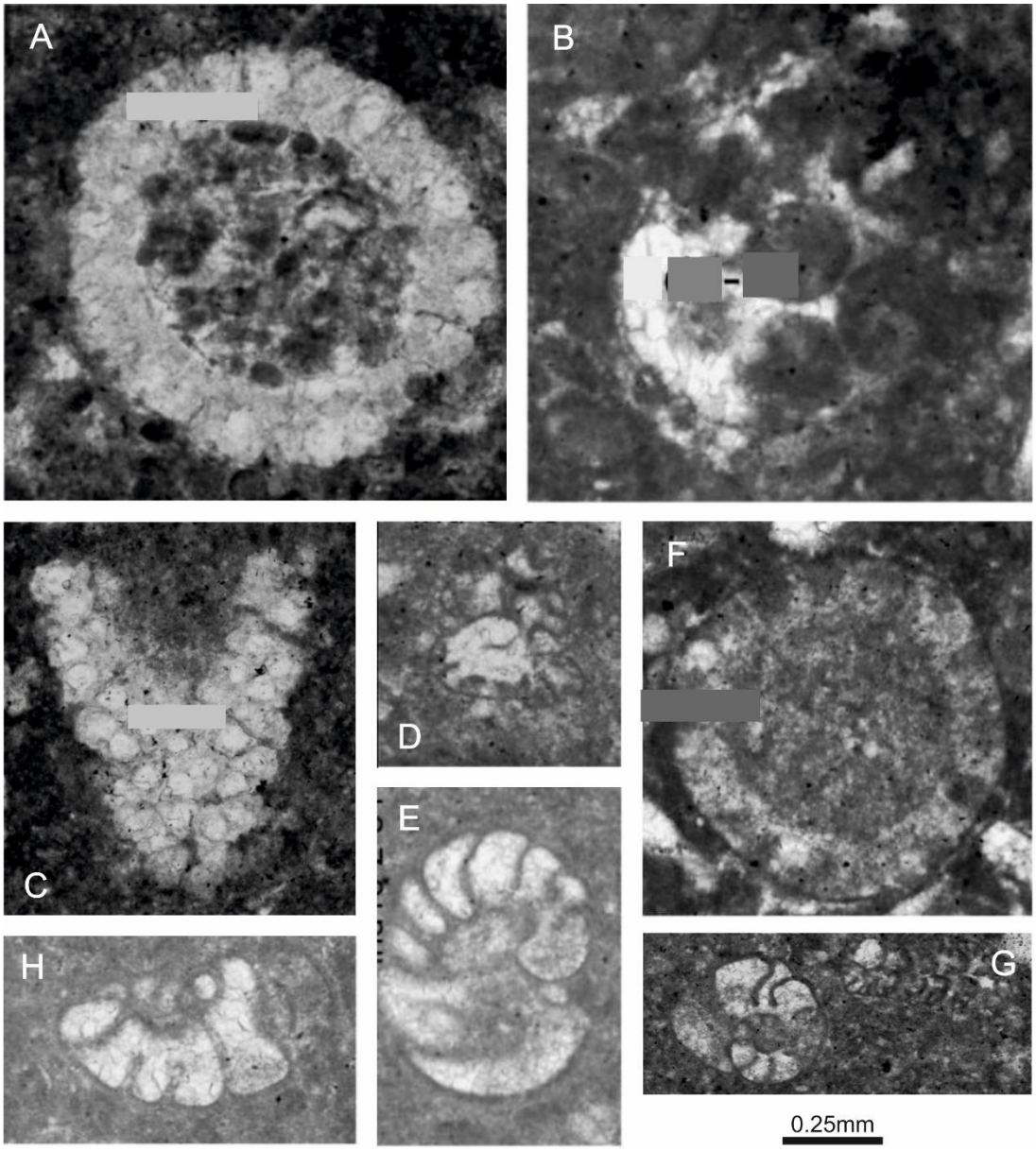


Figure 3.25. Thin–section images of the benthic foraminifera and dasycladalean algae observed in the Derdere Formation in the İnişdere stratigraphic section; (A, B) (C, F) dasycladalean algae, samples IND–5.33; IND–5,89. (D) *Cuneolina pavonia*, d'Orbigny, sample IND–5.33 (E, H, G) *Nezzazatinella picardi,* Henson samples IND–2.84; IND–5.33.

Sabunsuyu Stratigraphic Section

Rare benthic foraminifera, such as *Meandrospira* sp., *Dorothia* sp., Gavelinellidae and Lenticulinidae are uncommonly associated with pithonellids and planktonic foraminifera. Despite the presence of these bio–fragments and benthic foraminifera throughout the section, they do not help unravel the chronostratigraphy of the succession (Figure. 3.26).

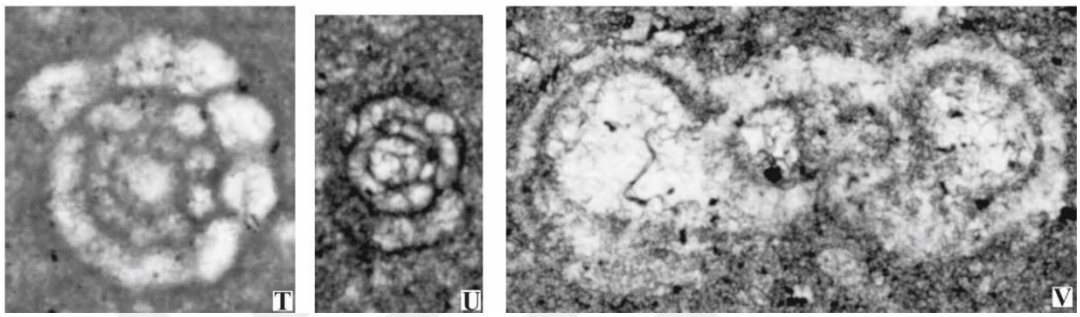


Figure 3.26. Thin–section images of the benthic foraminifera observed in the Derdere Formation. (A, G) Sabunsuyu stratigraphic section; benthic foraminifera: T, U. *Meandrospira* sp., MU, samples 53 and 84, respectively; V. Gavelinellidae, MU, sample 8.

Türkoğlu Stratigraphic Section

The biostratigraphic analysis revealed the following lower Cenomanian–middle Turonian foraminiferal association in the Türkoğlu succession. The lower part of the Derdere Formation comprises poor benthic foraminiferal assemblages including *Spiroloculina cretacea* Reuss, *Ovalveolina maccagnoae* De Castro, *Cuneolina pavonia* d'Orbigny, *Nezzazata simplex* Omara, *Thaumatoporella parvovesiculifera*, Raineri, Textulariidae, and Miliolidae (Figures 3.27 and 3.28). The species are long–ranging taxa except for *Ovalveolina maccagnoae* which is characteristic for the lower Cenomanian, specifically the lowermost Cenomanian in the peri–Mediterranean platforms (Velić, 2007). In addition, Cenomanian algae *Marinella lugeoni* Pfender, and *Permocalculus* sp. as well as roveacrinidae and rudists are also present in this interval.

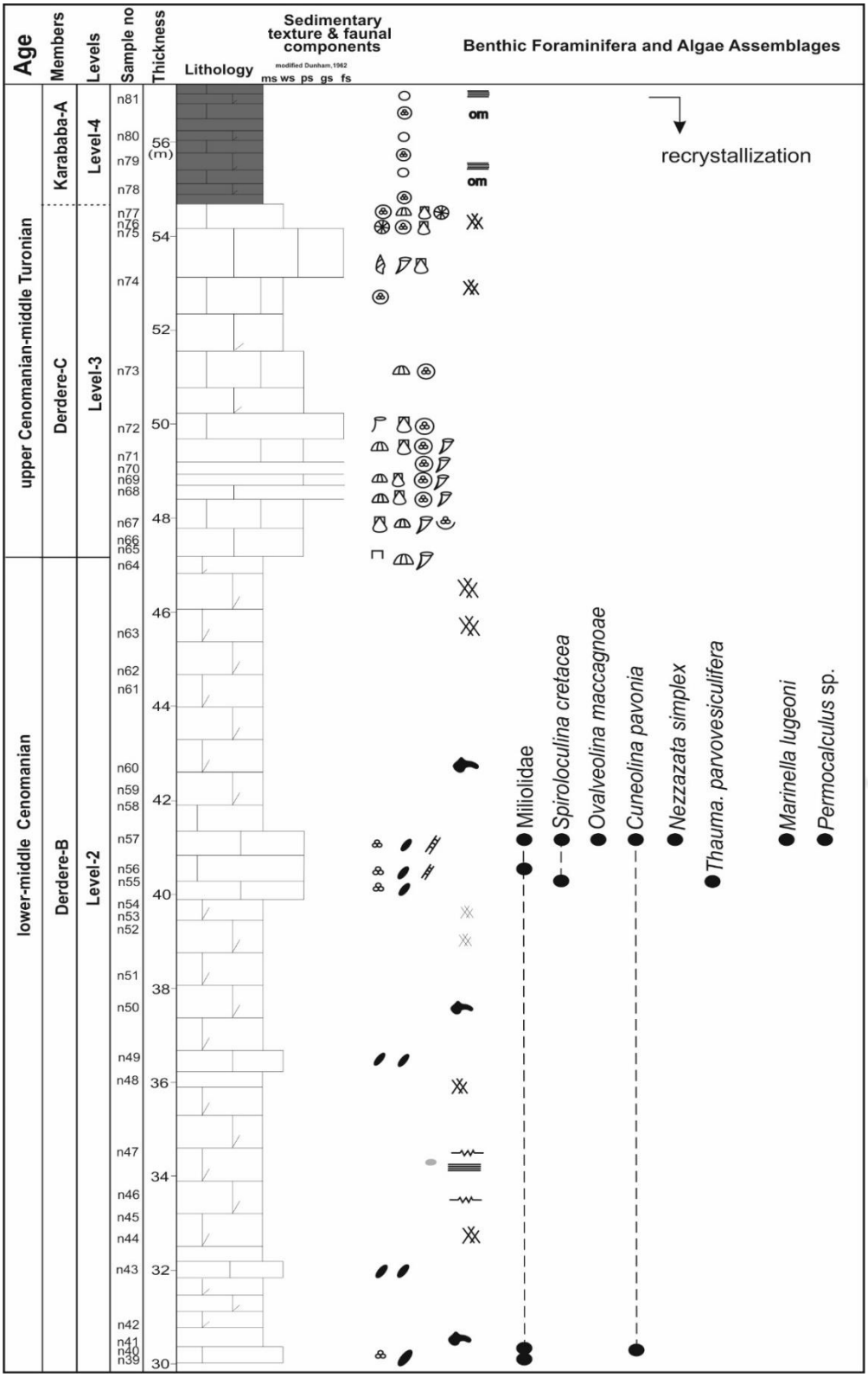


Figure 3.27. Stratigraphic distribution of benthic foraminifera and dasycladalean algae in the upper part of the Türkoğlu stratigraphic section. (after Mülayim et al. 2019b).

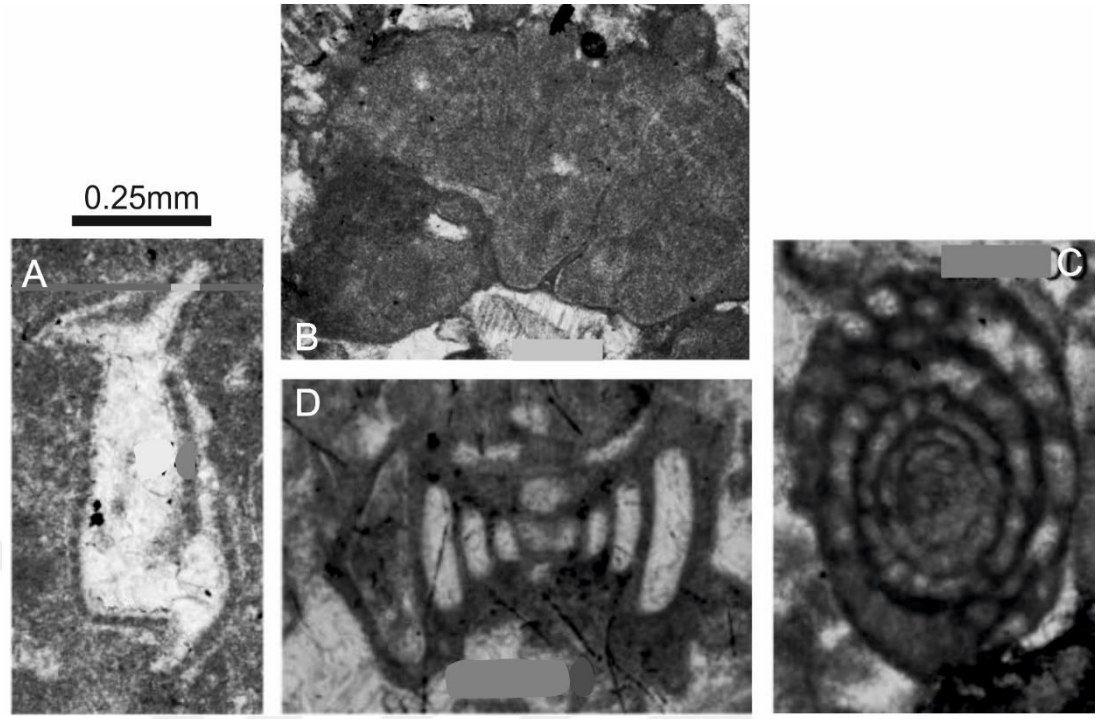


Figure 3.28. Thin–section images of the benthic foraminifera and dasycladalean algae observed in the Derdere Formation of the Türkoğlu section; A. *Thaumatoporella parvovesiculifera*, Raineri, sample TRK–40,37, B. *Marinella lugeoni*, Pfender sample TRK–41,00, C. *Spiroloculina cretacea*, Reuss, sample TRK–41,00, D. *Ovalveolina maccagnoae*, De Castro, sample TRK–41,00.

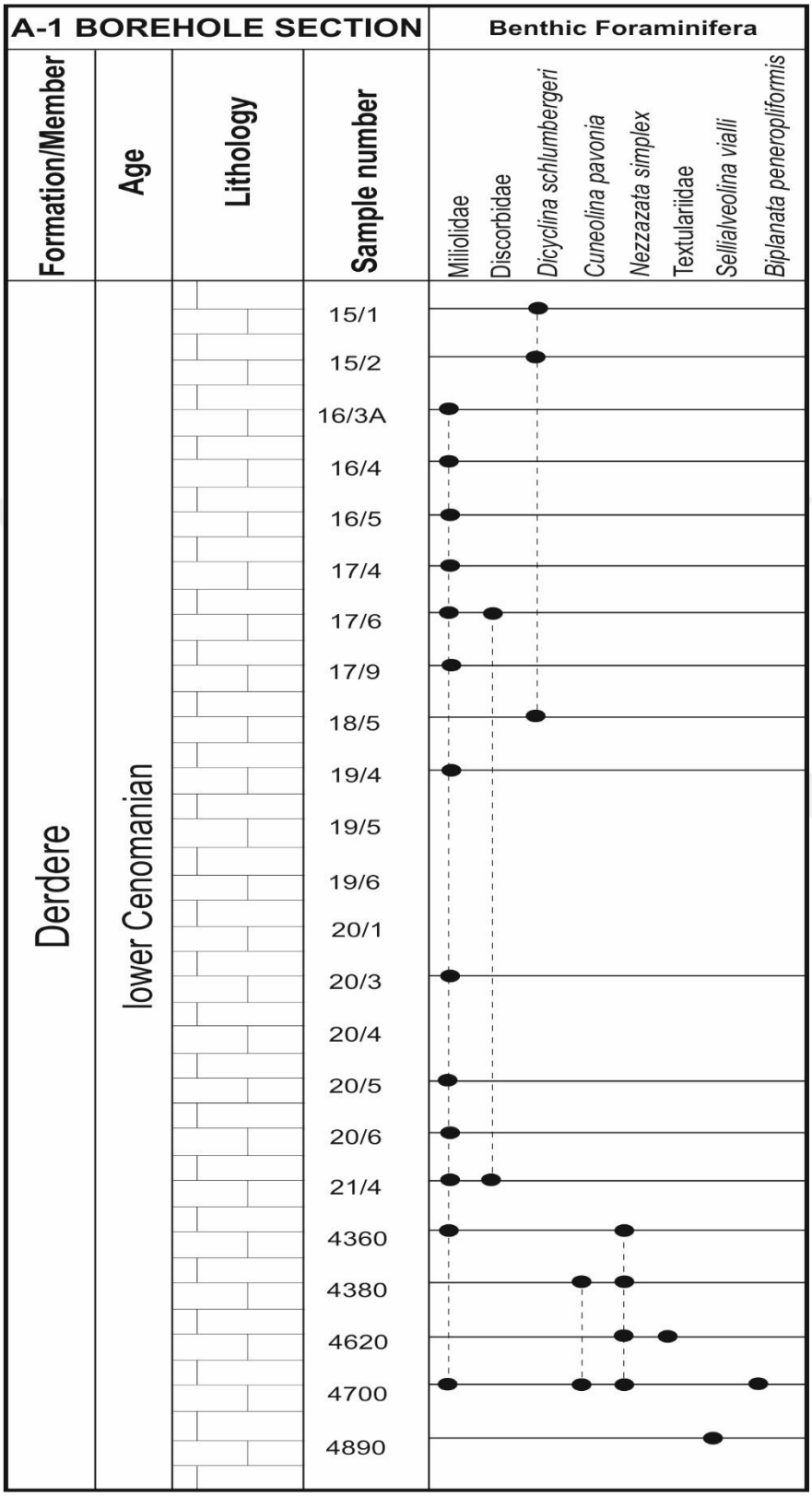


Figure 3.29. Stratigraphic distribution of benthic foraminifera in the A–1 borehole section.

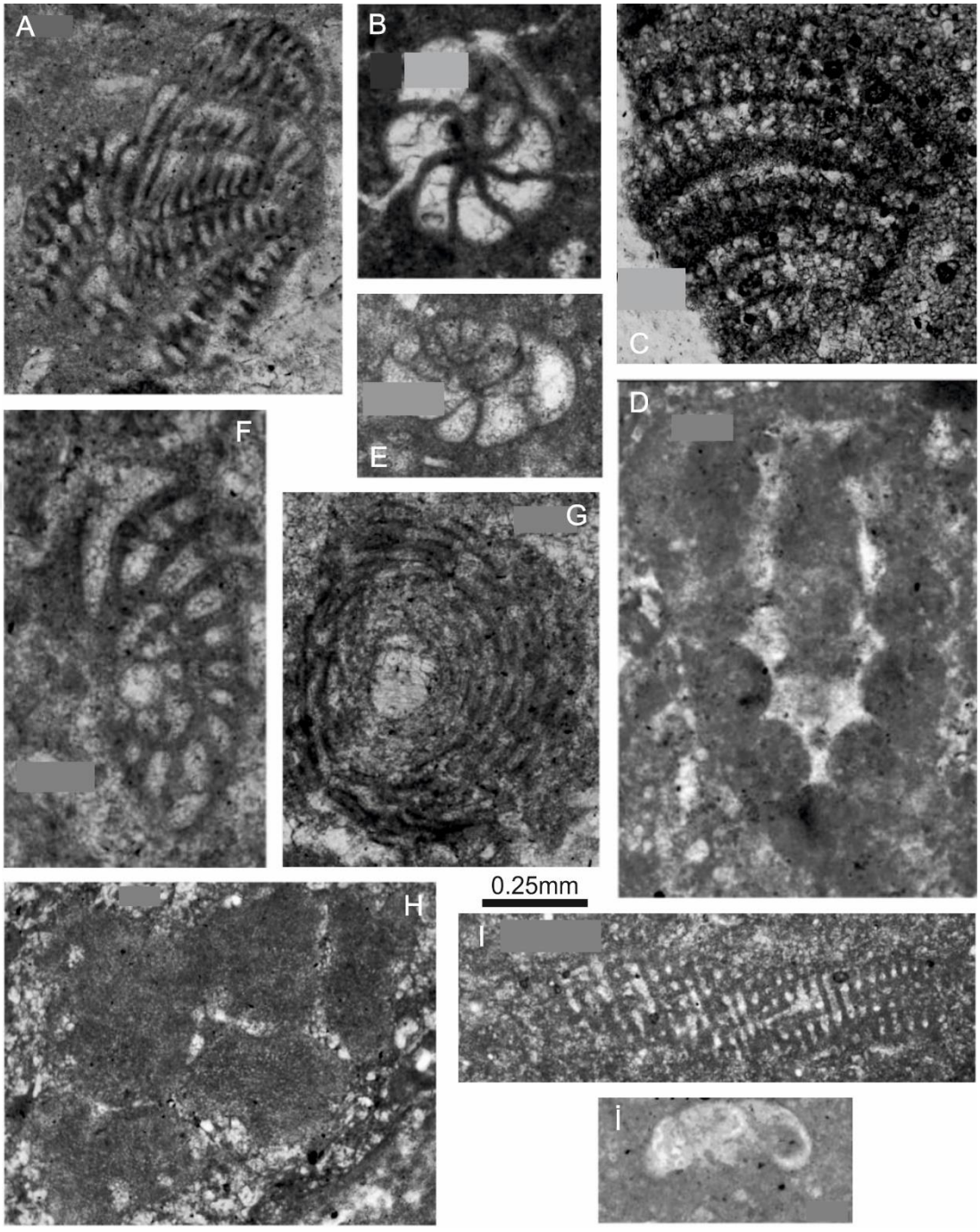


Figure 3.30. Thin–section images of the benthic foraminifera and dasycladalean algae observed in the Derdere Formation of the A–1 borehole section; A,G *Sellialveolina viallii*, Colalongo, sample 4890, B, E *Nezzazata simplex*, Omara, samples 4380 and 4620, C. *Cuneolina pavonia*, d'Orbigny, sample 4380, D. dasycladalean algae, sample 16/5, F. *Biplanata peneropliformis*, Hamaoui & Saint–Marc, sample 4700, B. *Marinella lugeoni*, Pfender, sample 15/1, I. *Dicyclina schlumbergeri*, Munier–Chalmas, sample 15/2, İ. Discorbidae, sample 17/6.

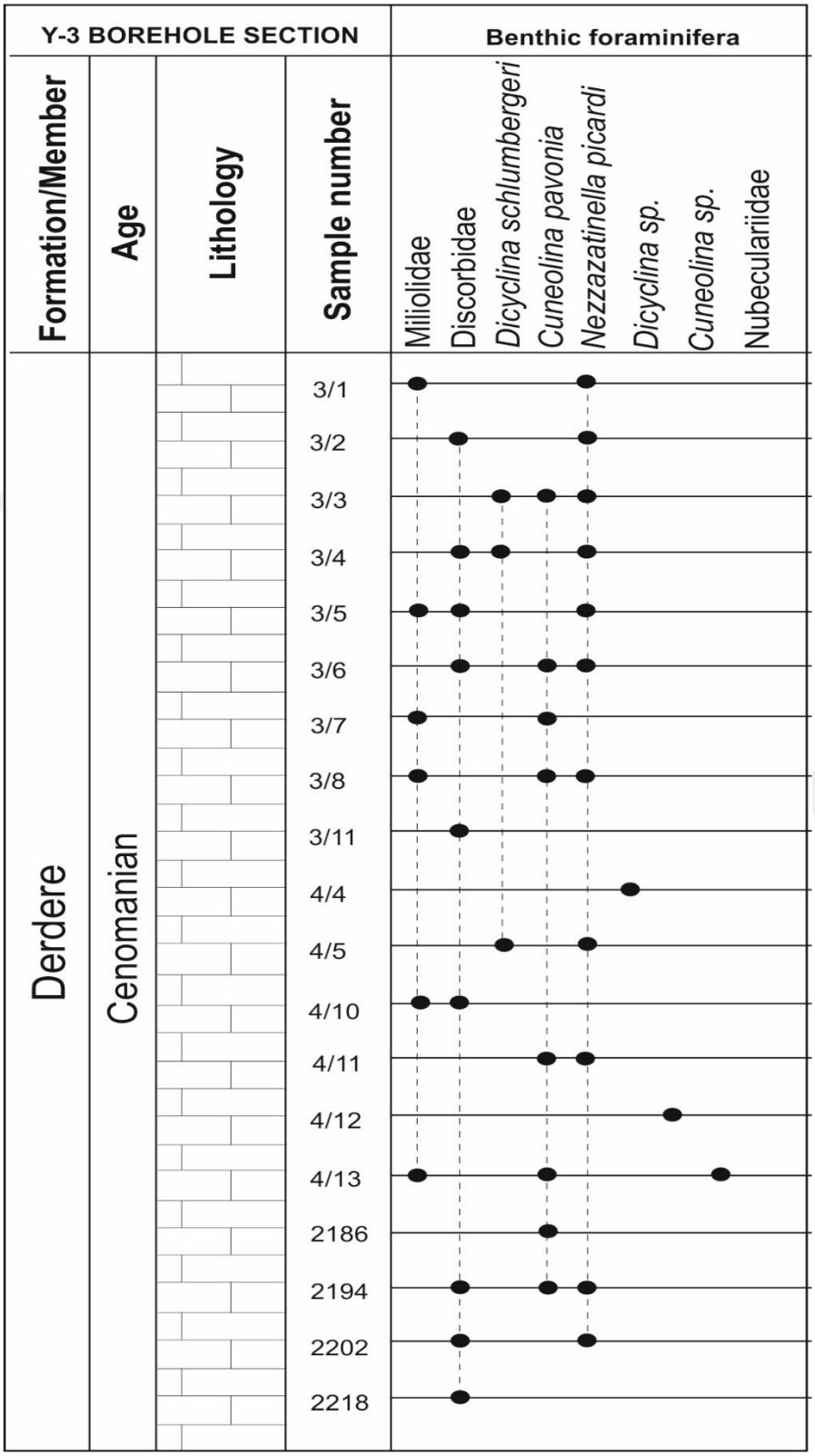


Figure 3.31. Stratigraphic distribution of benthic foraminifera in the Y–3 borehole section.

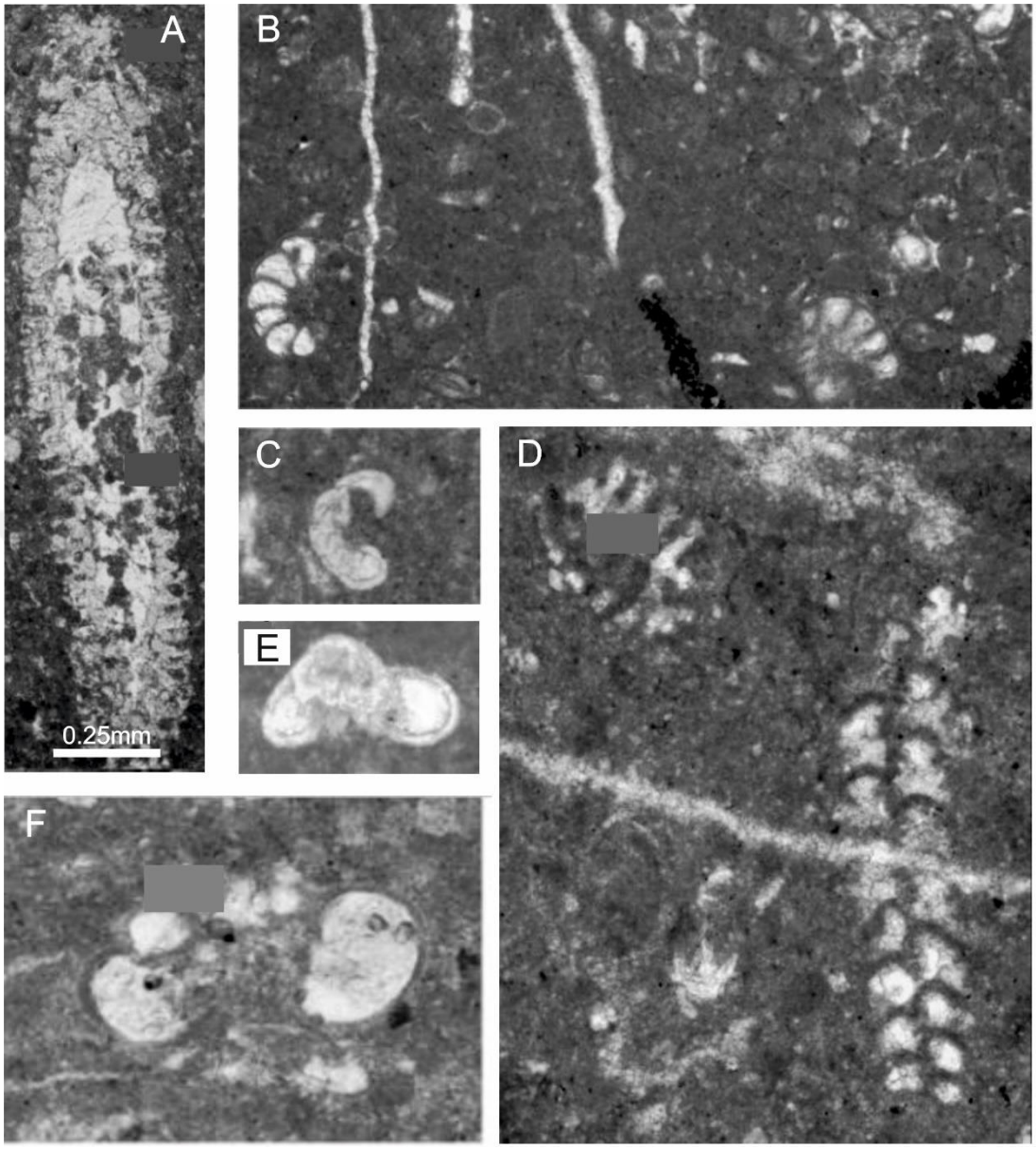


Figure 3.32. Thin–section images of the benthic foraminifera and dasycladalean algae observed in the Derdere Formation of the Y–3 borehole section; A. dasycladalean algae, samples 3/3, C, E Discorbidae, samples 3/1 and 3/2 B, F *Nezzazatinella picardi*, Henson, samples 3/1 and 3/2, D *Cuneolina pavonia*, d'Orbigny, sample 3/6.

3.1.5 Calcareous Nannofossils

As for calcareous nannofossils, there is a wider extinction interval with the last appearances of several taxa like *Lithraphidites acutus, Corollithion kennedyi, Cretarhabdus striatus, Helenea chiastica, Cylindralithus biarcus* and *Axopodorhabdus albianus* (e.g. Burnett 1998) and subsequent fast evolution in the Quadrum group in the latest Cenomanian to earliest Turonian. Calcareous nannofossils are generally scarce (fewer than one specimen per field–of–view under the light microscope), poorly preserved in the Cenomanian–Turonian succession in the İnişdere section and limited to distinct lithostratigraphic units. The total number of observed species is only 25. Diversity and frequencies increase in the Turonian strata whereas the dark limestones around the CTBE yield only very poor nannofossil results owing to strong dissolution and overgrowth. Index taxa are present only in the Turonian part of the section. However, some discrepancies in the chronostratigraphic assignments of the bio–events are obvious in the study area and adjacent regions (e.g. Sinai, Marzouk and Lüning 1998; Egypt, Andrawis et al. 1986; Tunisia, Robaszynski et al. 1990; Nederbragt and Fiorentino 1999). The few nannofossil markers present include *Eiffellithus eximius* Stover (in sample BS–1.4; a marker for middle Turonian), *Lucianorhabdus maleformis* Reinhardt (in samples BS–1.7, CM–14–1.4, CM–14–1.2; a marker for late Turonian) and *Quadrum gartneri* Prins and Perch–Nielsen (in samples BS–1.7 and KM–1.8; a marker for early Turonian) from around borehole data (Figure 3.33). This suggests a Turonian age for most of the section of the Karababa–A Member that yielded calcareous nannofossils. No Cenomanian taxa could be found.

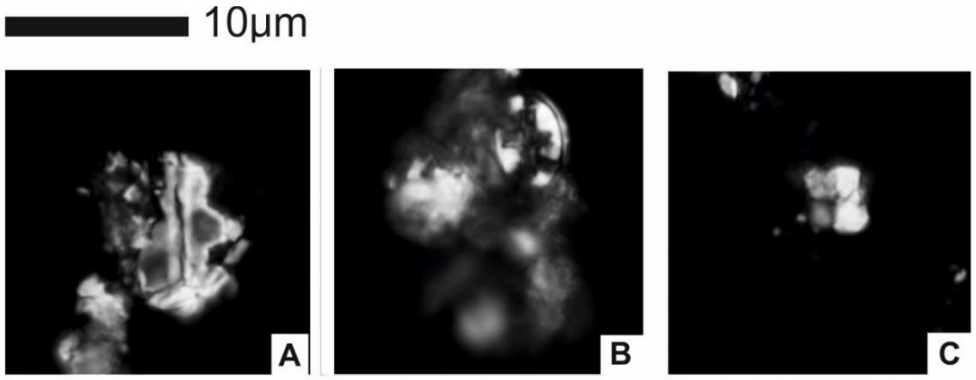


Figure 3.33. Light microscope photographs of calcareous nannofossil species from the Karababa–A Member in the CM–14 and BS–1. All figures were taken under cross–polarized light. A. *Lucianorhabdus maleformis* Reinhardt, sample CM–14–2; B. *Eiffellithus eximius* Stover, sample BS–1–4; C. *Quadrum gartneri* Prins and Perch–Nielsen, sample BS–1–7 (after Mülayim et al. 2019a).

3.1.6 Pithonellids

Upper Cretaceous deposits characteristically contain a high abundance of spherical calcareous microfossils commonly called ‘‘calcispheres’’. Their walls consist of evenly inclined crystal aggregates (pithonelloid wall–type according to Janofske and Keupp, 1992; Young et al., 1997). The pithonellids are most probably calcareous dinoflagellate cysts. However, they are taxonomically very problematic and evidence is needed to evaluate their affinity with the dinoflagellates. Wendler et al. (2002b) summarized the arguments on this aspect and gave evidence to support the dinoflagellate affinity of species of *Pithonella.* Keupp (1987) established the subfamily Pithonelloideae including all pithonelloid wall–type genera. This term is used here to comprise all genera discussed; however, it is not valid in taxonomy as the pithonelloid wall–type is probably present in calcareous remains of various families. In order to make accurate palaeoecological interpretations of these microfossils, it is crucial to understand their taxonomic affinities. Various morphological observations strongly suggest an affinity of some pithonelloid wall–type species with the dinoflagellates (Wendler et al.,2004). The lower part of the Derdere formation (early–middle Cenomanian) are composed of pithonellids (e.g. *Bonetocardiella conoidea*

Bonet, *Pithonella ovalis* Kaufmann, *P. sphaerica* Kaufmann, *P. lamellata* Keupp*)* (Figures 3.34, 3.35, and 3.36).

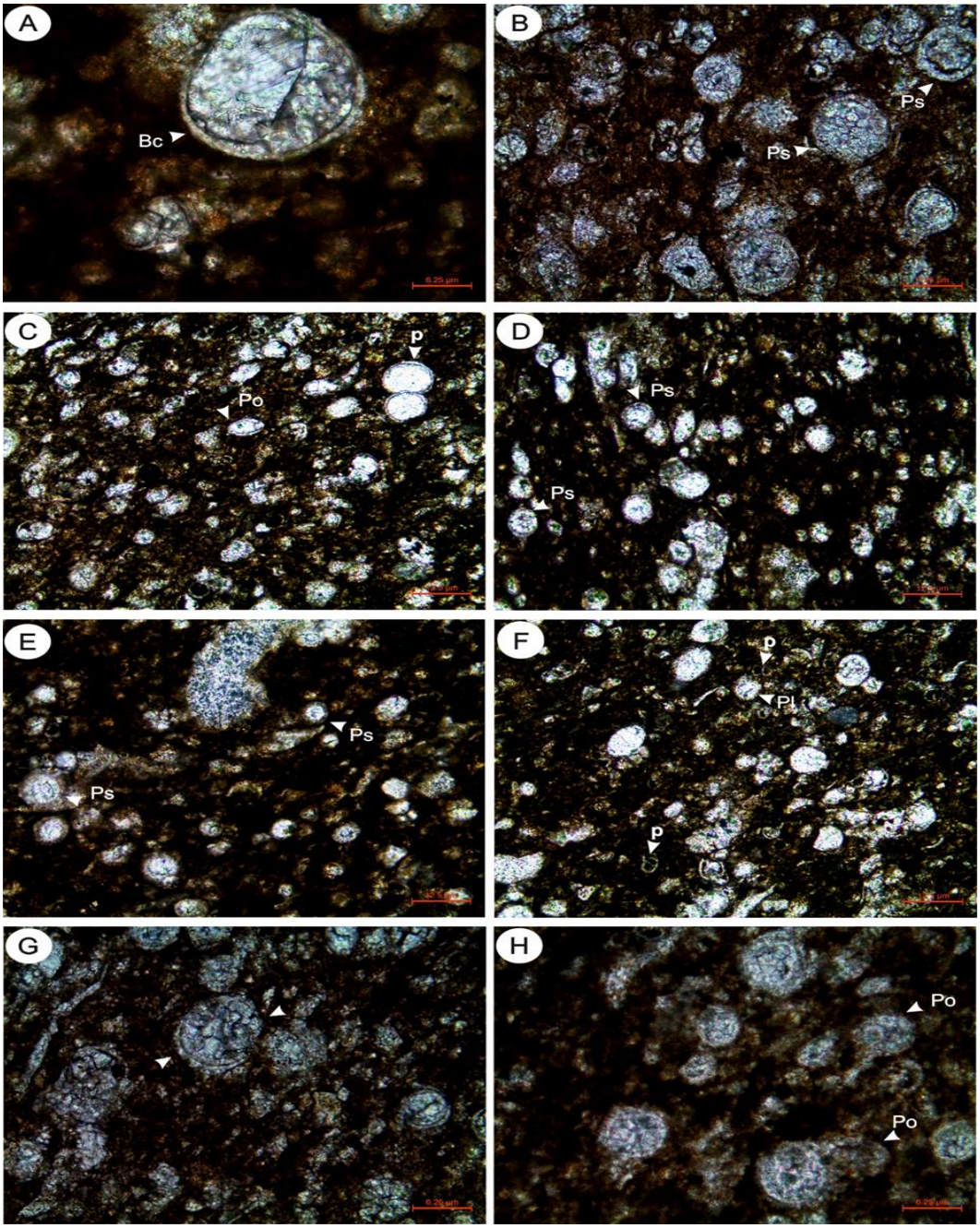


Figure 3.34. Thin–section photographs of pithonellids in BZ–1 borehole section, lower–middle Cenomanian, Adıyaman area, SE Turkey. A. a cone–shaped form, *Bonetocardiella conoidea*, Bonet, Bc, core sample 370039. B. thick–walled spherical form with typical pithonelloid crystal–orientation–*Pithonella sphaerica*, Kaufmann,

Ps; right middle and upper corner: organic walls are preserved, core sample 370034. C. center–*Pithonella ovalis*, Kaufmann, Po, core sample 370025. D. left (10 o'clock above center) and others on the left: *Pithonella sphaerica*, Kaufmann, Ps, core sample 370030. E. left = very clear *Pithonella sphaerica* Kaufmann, with crystal orientation nicely seen core sample 370022. F. a multi–layered form, possibly from the *Pithonella lamellata* Keupp, form spectrum, core sample 370021. G. the multi–layered type, core sample 370019. H. *Pithonella ovalis*, Kaufmann, core sample 370005.

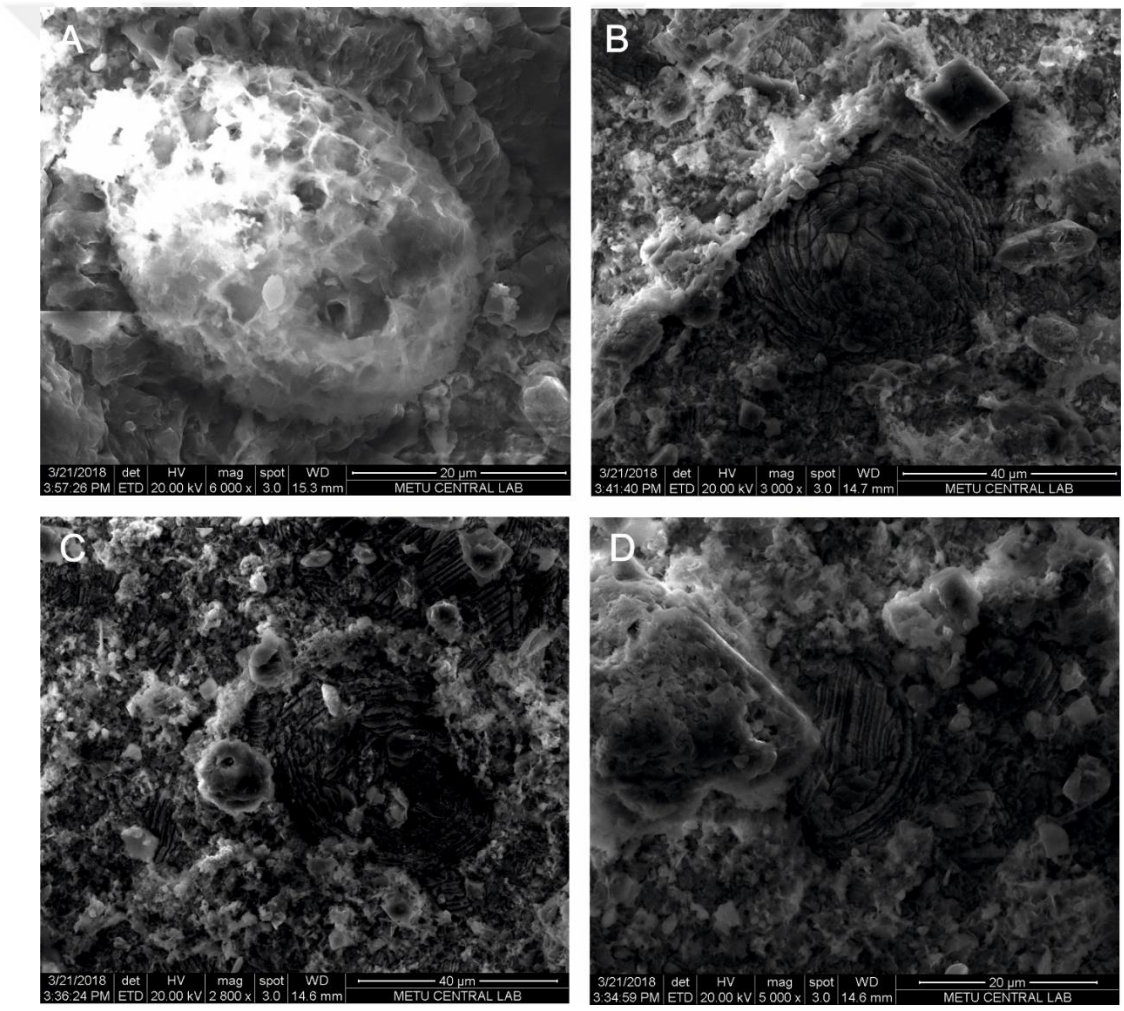


Figure 3.35. SEM photographs of the pithonellids in the BZ–1 borehole section, lower–middle, Cenomanian, Adıyaman area, SE Turkey. A. The typical pithonellid wall type. One sees on the left and the right side of the sphere that the crystals are uniformely inclined towards a point of the sphere at around 11 o'clock, sample 2023.

2003. B: *Pithonella sphaerica* Kaufmann, with a spiral crystal arrangement, sample 2011. C and D. *Pithonella sphaerica* Kaufmann, with blocky cement infillings (the parallel lines are cleavage lamellae) samples, 2002.

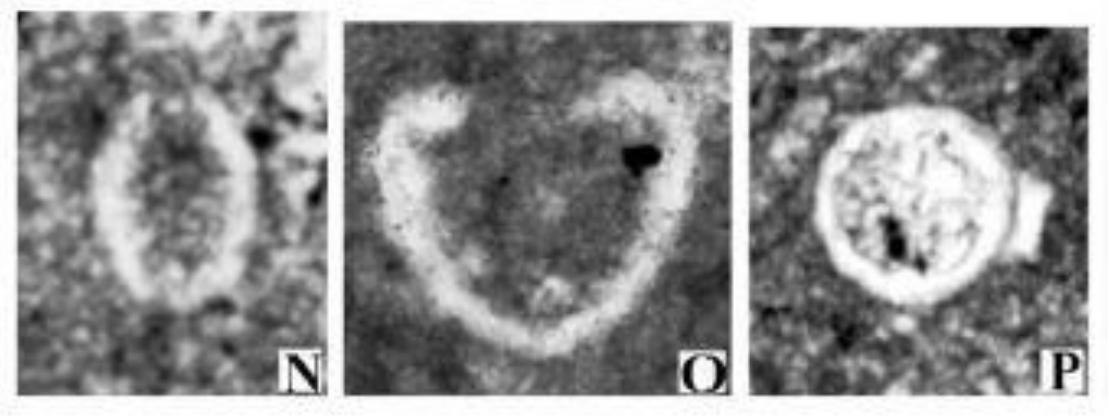


Figure 3.36. Thin–section images of the pithonellids observed in the Derdere Formation. (N, P) Sabunsuyu stratigraphic section: N. *Pithonella ovalis*, Kaufmann MU, sample SAB–7; O. *Bonetocardiella conoidea*, Bonet, MU, sample SAB–53; P: *Pithonella sphaerica*, Kaufmann, MU, sample SAB–19.

CHAPTER 4

MICROFACIES ANALYSES AND SEDIMENTOLOGY

Today, microfacies is regarded as the total of all sedimentological and paleontological data which can be described and classified from thin–sections, peels, polished slabs and rock samples (Tucker and Wright, 1990; Flügel, 2004). Grain types, matrix/cement types, depositional fabrics, fossils and depositional texture types should be considered in the determination of the microfacies types (Flügel, 2004). The microfacies study in this work aims to understand the depositional history of the area by examining the sedimentological and paleontological characteristics of the samples. Microfacies analyses have been performed by examining the main components, textures, macro–, and microfossil associations of the samples. Lithological variations observed in the outcrop have also been considered. In addition, most frequently used facies models have been examined (Tucker and Wright, 1990; Flügel, 2004) and the depositional environments of the rocks have been determined.

4. 1 Results of Point–Counting and Measurements

In order to determine the percentage constituents of microfacies, the point–counting method has been carried out and results of point counting were used to categorize changes in the composition of the microfacies. Through the petrographic studies, peloids, ooids, bioclasts, intraclast, extraclast, cement, and matrix have been recognized and counted per thin–section as quantitatively (Flügel, 2004). The point counting quantitative measurement percentage data is presented in Tables 4.1 and 4.2. The grain size of some microfacies were measured (Table 4.3). The grain size is used to indicate the depositional environment and a major factor that affects porosity and permeability values. Micritic ooids are characterized by reduced sedimentation rates and random growth in the marine environment. The presence of radial ooids illustrates low–moderate energy condition for the deposition. The graphic interpretation of intraclast measurements indicates that the formation is deposited at shallow marine. The peloids and intraclast peaks in Figure 4.3 illustrate that environment is shallow but few high peaks of the lime matrix indicate lagoonal to shoal.

Table 4.1. Petrographic and point counted data of the outcrop and borehole samples.

Sample	Section	Peloids	Ooids	Bioclasts	Intraclast	Extraclast	Cement	Matrix	Other	Total
S–0.05	IND	17	0	259	3	0	220	421	0	920
S–1,04	IND	48	0	0	176	54	55	799	5	1137
S–1,96	IND	37	0	137	0	0	7	800	0	981
S–2.37	IND	192	0	2	8	0	51	595	2	850
S–5.33	IND	26	0	53	0	0	6	726	3	814
S–6.00	IND	6	0	149	0	0	19	1180	4	1358
S–0.17	IND	2	0	287	1	0	237	425	0	951
S–0.48	IND	12	0	272	0	0	264	426	0	974
S–1.41	IND	40	0	127	0	9	6	801	8	995

Table 4.1. (continued)

S–2.04	IND	34	0	133	19	0	11	773	17	987
S–2.76	IND	38	0	121	5	0	25	807	0	996
S–2.84	IND	43	0	108	0	0	23	814	0	988
S–3.74	IND	47	0	138	11	0	11	762	5	974
S–4.55	IND	30	0	54	8	10	7	773	5	887
S–5.08	IND	37	0	78	6	13	5	750	3	892
S–5.84	IND	436	0	57	0	4	28	873	4	1402
S–5.97	IND	351	0	17	4	3	44	963	2	1384
S–6.02	IND	413	0	53	2	3	57	866	0	1396
S–6.03	IND	450	0	60	8	10	41	852	0	1421
S–4.4	BRH	0	0	250	0	0	0	1145	0	1395
S–4.5	BRH	0	0	247	0	0	0	971	0	1218
S–4.6	BRH	0	0	280	0	0	0	953	0	1233
S–4.9	BRH	294	0	0	0	0	0	960	0	1254
S–4.10	BRH	623	0	142	5	8	0	376	125	1279
S–4.11	BRH	578	0	145	4	5	0	550	0	1275
S–4.12	BRH	1052	12	24	18	19	26	109	0	1260
S–4.13	BRH	854	2	3	6	8	22	377	0	1268
S–4.14	BRH	934	3	5	8	10	46	248	0	1254
S–3.1	BRH	695	0	80	38	0	75	97	0	985
S–3.2	BRH	44	0	44	0	0	15	872	0	975
S–3.3	BRH	85	0	66	0	0	4	810	0	965
S–3.4	BRH	88	0	65	0	0	5	754	0	912
S–3.5	BRH	41	0	39	0	0	1	861	0	942
S–3.6	BRH	36	0	38	0	0	5	888	0	967
S–3.7	BRH	782	0	31	0	0	91	84	0	988
S–3.8	BRH	51	0	39	0	0	42	858	0	990
S–3.9	BRH	48	0	27	0	0	8	916	0	999

Table 4.1. (continued)

S–3.10	BRH	46	0	30	0	0	16	856	0	948
S–3.11	BRH	60	0	50	0	0	0	862	0	972
S–16.16	TRK	753	0	3	0	0	79	317	0	1152
S–40.37	TRK	576	0	65	0	0	91	515	0	1247
S–40.42	TRK	492	0	30	0	0	62	605	0	1189
S–41.00	TRK	677	0	175	0	0	111	190	0	1153
S–47.37	TRK	0	0	521	0	0	0	744	0	1265
S–47.49	TRK	4	0	674	0	0	0	609	0	1287
S–48.57	TRK	3	0	440	0	0	0	801	0	1244
S–48.97	TRK	3	0	509	0	0	0	724	0	1236
S–49.92	TRK	5	0	483	0	0	0	810	0	1298
S–714	BRH	580	0	43	53	0	33	478	0	1187
S–1095	BRH	884	0	105	98	0.	47	43	0	1176
S–18/5	BRH	471	0	57	45	0	0	596	0	1181

Table 4.2. Percentage data of the quantitative analysis using point count data fort he measured outcrop and borehole sections.

Sample	**Section**	**Peloids%**	**Ooids%**	**Bioclasts%**	**Intraclast%**	**Extraclast%**	**Cement%**	**Matrix%**	**Other%**	**Total**
S–0.05	IND	1.9	0	28.2	0.1	0	24.0	45.8	0	100

Table 4.2. (continued)

S–1,04	IND	4.3	0	0	15.5	4.8	4.9	70.3	0.2	100
S–1,96	IND	3,8	0	13.9	0	0	0.7	81.6	0	100
S–2.37	IND	22.6	0	0.2	0.9	0	6.0	70.1	0.2	100
S–5.33	IND	3.2	0	6.6	0	0	0.6	89.3	0.3	100
S–6.00	IND	0.4	0	11.0	0	0	1.4	86.9	0.3	100
S–0.17	IND	1.7	0	30.2	0.2	0	25.0	44.7	0	100
S–0.48	IND	1.5	0	28.0	0	0	27.2	43.8	0	100
S–1.41	IND	4.1	0	12.8	0	1.0	0.7	80.6	0.8	100
S–2.04	IND	3.5	0	13.5	2.0	0	1.2	78.4	1.4	100
S–2.76	IND	3.9	0	12.2	0.2	0	2.6	81.1	0	100
S–2.84	IND	4.4	0	11.0	0	0	2.2	82,4	0	100
S–3.74	IND	4.8	0	14.2	0.5	0	0.9	78.3	0.3	100
S–4.55	IND	3.4	0	6.1	1.0	1.0	0.8	87.2	0.5	100
S–5.08	IND	4.2	0	8.8	0.7	1.5	0.5	84.1	0.2	100
S–5.84	IND	31.1	0	4,1	0	0.3	2.0	62.3	0.2	100
S–5.97	IND	25.4	0	1.2	0.3	0.2	3.2	69.6	0.1	100
S–6.02	IND	29,6	0	3.8	0.1	0.3	4.1	62.1	0	100
S–6.03	IND	31.7	0	4.2	0.6	0.7	2.8	60.0	0	100
S–4.4	BRH	0	0	17.9	0	0	0	82.1	0	100
S–4.5	BRH	0	0	20.3	0	0	0	79.7	0	100
S–4.6	BRH	0	0	22.7	0	0	0	77.3	0	100
S–4.9	BRH	23.5	0	0	0	0	0	76.5	0	100
S–4.10	BRH	48.7	0	11.1	0.4	0.6	0	29.4	9.8	100
S–4.11	BRH	45.4	0	11.4	0.4	0.5	0	43.2	0	100
S–4.12	BRH	83.5	0.9	1.9	1.4	1.5	2.1	8.7	0	100
S–4.13	BRH	67.4	0.1	0.2	0.5	0.6	1.8	29.4	0	100
S–4.14	BRH	74.5	0.2	0.4	0.6	0.8	3.7	19,8	0	100
S–3.1	BRH	70.6	0	8.1	3.9	0	7.6	9.8	0	100

Table 4.2. (continued)

S–3.2	BRH	4.5	0	4.5	0	0	1,5	89.5	0	100
S–3.3	BRH	8.8	0	6.8	0	0	0.4	84.0	0	100
S–3.4	BRH	9.6	0	7.1	0	0	0.6	82.7	0	100
S–3.5	BRH	4.4	0	4.1	0	0	0.1	91.4	0	100
S–3.6	BRH	3.8	0	3.9	0	0	0.5	91.8	0	100
S–3.7	BRH	79.2	0	3.1	0	0	9.2	8.5	0	100
S–3.8	BRH	5.2	0	3.9	0	0	4.2	86.7	0	100
S–3.9	BRH	4.8	0	2.7	0	0	0.8	91.7	0	100
S–3.10	BRH	4.9	0	3.2	0	0	1.7	90.4	0	100
S–3.11	BRH	6.2	0	5.1	0	0	0	88.7	0	100
S–16.16	TRK	65.3	0	0.2	0	0	6.8	27.5	0	100
S–40.37	TRK	46.2	0	5.2	0	0	7.1	41.3	0	100
S–40.42	TRK	41.4	0	2.5	0	0	5.2	50.3	0	100
S–41.00	TRK	58.7	0	15.2	0	0	9.6	7.2	0	100
S–47.37	TRK	0	0	48.2	0	0	0	59.6	0	100
S–47.49	TRK	0.3	0	52.4	0	0	0	47.3	0	100
S–48.57	TRK	0.2	0	35.4	0	0	0	64.4	0	100
S–48.97	TRK	0.2	0	41.2	0	0	0	58.6	0	100
S–49.92	TRK	0.4	0	37.2	0	0	0	62.4	0	100
S–714	BRH	48.9	0	3.6	4.4	0	2.8	40.3	0	100
S–1095	BRH	75.2	0	8.9	8.3	0.	4.0	3.6	0	100
S–18/5	BRH	39.9	0	4.8	3.8	0	0	51.5	0	100

Table 4.3. Grain size measurement of some samples of the outcrop and borehole sections.

Sample No.	Intraclasts			Sample No.		Peloids			Sample No.		Peloids		
	X	Y	Shape		Content	X	Y	Shape		Content	X	Y	Shape
S-4-12	653,58	724,87	S A	S-4-12	M	177,16	289,71	R	S-4-16	M	63,46	66,55	SR
S-4-12	867,4	655,14	S A	S-4-12	M	325,72	459,08	R	S-4-16	M	133,64	83,08	SR
S-4-12	313,57	107,28	S A	S-4-12	M	302,21	528,3	R	S-4-16	M	41,88	46,65	SR
S-4-12	579,28	1256,66	SR	S-4-12	M	83,84	122,17	R/RO	S-4-16	M	42	68,71	SR
S-4-12	487,71	704,95	SR	S-4-12	M	87,71	167,18	R	S-4-16	M	122,45	83,45	SR
S-4-12	539,71	777,38	SR	S-4-12	M	105,22	167,53	SR	S-4-16	M	46,73	107,49	SR
S-4-12	518,44	672,12	SR	S-4-12	M	82,29	109,8	R	S-4-16	M	53,97	51,82	SR
S-21-2	710,42	1007,04	SA	S-4-12	M	144,43	209,97	R	S-4-16	M	70,73	53,28	SR
S-21-2	560,04	370,85	SA	S-4-12	M	78,79	135,33	R	S-4-16	M	78,47	80,14	SR
S-21-2	638,6	410,06	SA	S-41.00	M	104	112	R	S-4-16	M	66,76	182,49	SR
S-21-2	1338,48	510,4	SA	S-41.00	M	66,24	71,28	R	S-4-16	M	65,27	67,16	SR
S-21-2	463,13	417,82	SR	S-41.00	M	156,15	108,99	R	S-4-16	M	68,48	85,21	SR
S-21-2	741,33	612,51	SA	S-41.00	M	109,22	140,84	R	S-4-16	M	98,84	74,45	SR
S-21-2	548,53	261,17	SR	S-41.00	M	71,05	139,71	R	S-4-16	M	99,79	126,73	SR
S-21-2	975,19	722,64	SR	S-41.00	M	114,05	74,98	R	S-4-16	M	45,08	78,79	SR
S-21-2	295,01	231,21	SR	S-41.00	M	59,39	117,89	R	S-17-6	M	158,17	144,89	R/SR
S-21-2	519,74	564,53	SR	S-41.00	M	126,9	91,98	R	S-17-6	M	185,41	266,17	R/SR
				S-41.00	M	116,81	61,55	R	S-17-6	M	128,73	236,02	R/SR
				S-41.00	M	138,93	74,45	R	S-17-6	M	68,35	95,69	R/SR
				S-41.00	M	104,88	140,15	R	S-17-6	M	146,44	185,6	R/SR
				S-41.00	M	96,27	94,77	R	S-17-6	M	148,8	257,64	SA
				S-41.00	M	187,91	91,7	R	S-17-6	M	68,22	110,21	SR
				S-41.00	M	94,52	97,61	R	S-17-6	M	208	258,49	SR
				S-41.00	M	198,43	76,01	R	S-17-6	M	78,07	165,32	SR
				S-41.00	M	72,87	53,4	R	S-17-6	M	117,06	176,09	SR
				S-41.00	M	74,03	102,61	R	S-17-6	M	190,64	306,68	SR
				S-41.00	M	88,35	52,09	R	S-17-6	M	127,41	244,39	SR
				S-41.00	M	74,13	127,81	R	S-17-6	M	105,48	125,59	SR
				S-41.00	M	83,58	80,14	R	S-17-6	M	92,77	131,32	SR
				S-41.00	M	122,37	71,55	R	S-17-6	M	109,8	251,52	SR
				S-2.37	M	75,32	57,69	R	S-4-12	M	181,17	358,72	R
				S-2.37	P	30,19	85,52	SR	S-4-12	M	198,21	219,11	R
				S-2.37	M	75,4	53,64	R	S-4-12	M	138,77	270,01	R
				S-2.37	M	60,23	60,82	SR	S-4-12	M	218,36	345,25	R
				S-2.37	M	53,26	84,21	R	S-4-12	M	190,83	353,45	R
				S-2.37	M	51,82	71,05	SR	S-4-12	M	245,55	249,1	R
				S-2.37	M	100,24	93,76	SR	S-21-2	M	524,67	568,49	R
				S-2.37	M	35,2	75,22	R	S-21-2	M	242,38	244,54	R
				S-2.37	M	96,27	69,54	R	S-21-2	M	495,77	480,69	R
				S-40.42	M	400,96	194,65	SR	S-21-2	M	88,06	116,35	SR
				S-40.42	M	186,59	197,68	SR	S-21-2	M	103,75	124,53	SR
				S-40.42	M	212,75	237,77	R	S-21-2	M	319,34	178,81	SR
				S-40.42	M	177,72	209,47	R	S-21-2	M	279,24	461,39	SR
				S-40.42	M	215,83	306,95	SR	S-21-2	M	154,01	198,02	SR
				S-40.42	M	192,8	308,45	SA	S-21-2	M	154,64	152,44	SR
				S-40.42	M	79,97	102,36	R	S-21-2	M	161,15	260,98	SR
				S-40.42	M	96,97	93,46	R	S-21-2	M	184,44	151,73	SR
				S-40.42	M	84,21	144,97	R	S-21-2	M	130,55	101,92	SR
				S-4-12	M	543,07	680,21	R	S-4-12	M	181,65	406,33	R
				S-4-12	M	322,97	471,23	R	S-4-12	M	423,74	549,72	R
				S-4-12	M	246,64	469,89	R	S-4-12	M	365,76	468,92	R
				S-4-12	M	324,34	500,83	R	S-4-12	M	391,04	572,2	R
				S-4-12	M	227,9	144,89	R	S-4-12	M	265,09	341,94	SR
				S-4-12	M	293,81	613,6	R	S-4-12	M	334,55	486,79	R
				S-4-12	M	228,89	166,4	R	S-4-12	M	359,59	504,25	R

4.2 The Determination of Ramp Microfacies Types (RMF Types)

Flügel (2004) described 30 microfacies types for carbonate ramps as ramp microfacies types (RMF) (Figure 4.1).

The Derdere and Karababa carbonates of SE Turkey have been studied with respect to microfacies characteristics covering shelf facies by many authors previously (i.e. Mülayim, 2013, Mülayim et al., 2016; Robertson et al., 2016). Although individually, the microfacies schemes offered by these authors, it is important in this thesis that a complete ramp microfacies scheme is used covering ramp facies present. Therefore, Chapter 4 aims to synthesize the observations made in the field and borehole areas and presents a composite microfacies scheme for palaeogeographic situations. Carbonate deposition was initiated in a homoclinal ramp setting, where a slight slope existed with no true barrier.

This chapter presents a detailed microfacies scheme for the ramp setting. It was important to set up a ramp microfacies scheme since platform geometries, together with many other factors, dictated which depositional environments were present. As the ramp facies were the primary objective of the study for this thesis, they are described in detail. The sampling and thin–section techniques used in this study are discussed in detail in Chapter 1. Appendix 1 presents the thin–section information obtained during this study. Microfacies analysis is the microscopic evaluation of the total of all the paleontological and sedimentological criteria of carbonate rocks using thin–sections and cuttings. The analysis was conducted based on petrographic studies of 1588 thin–sections selected from core and cutting samples from 28 wells and 3 outcrop sections (İnişdere, Türkoğlu, and Sabunsuyu) for the examined interval. Comparisons are made with the "Standard Microfacies Types" by Flügel (2004). The microfacies (MF) analyses based on texture, sedimentary structures, and fossils identified in thin–sections have led to the determination of MF types within the carbonates of the Derdere Formation and Karababa–A Member.

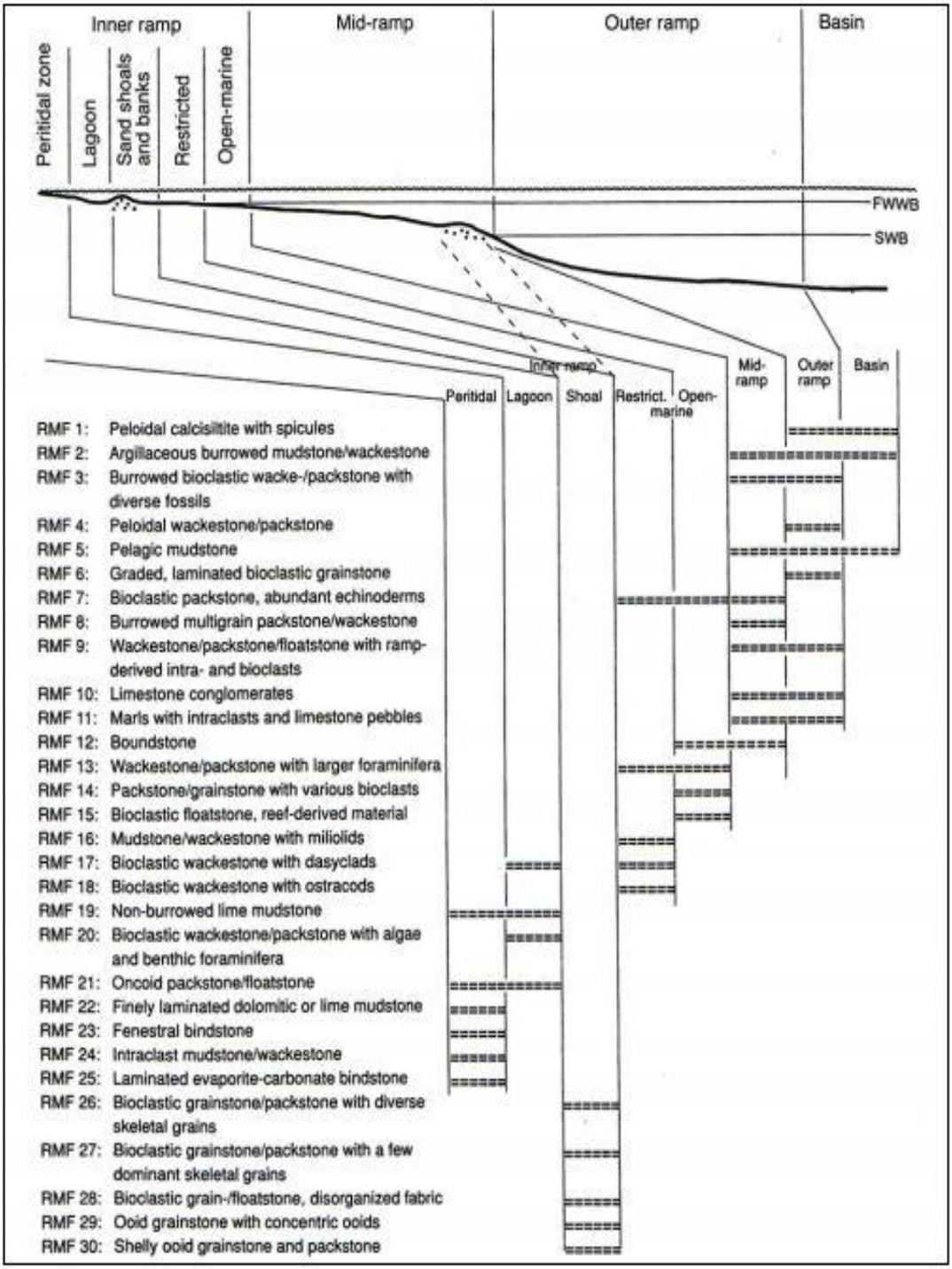


Figure 4.1. Generalized distribution of microfacies types in different parts of a homoclinal carbonate ramp (Flügel, 2004).

4.1.1 Microfacies of the Derdere–A Member (Derdere Formation)

The microfacies documents a mudstone to packstone texture with dominantly pithonellids, planktonic foraminifera and roveacrinids. Based on petrographic analysis of the Derdere–A Member, four microfacies are interpreted to represent mid– to outer–ramp environments.

4.1.1.1 Mf–1: Non–Laminated, Silt–Bearing Pelagic Lime Mudstone

This microfacies consists of finely textured, dense, dark brown microcrystalline calcite and contains rich–small pithonellids and planktonic foraminifera floating in a mud–supported fabric and scattered silt or fine sand–sized quartz grains in places (Figure 4.2). Pithonellids are the predominant skeletal grains in this microfacies, ranging from 90 to 95 percent in abundance and show a concentric wall structure. Planktonic foraminifera range from 5 to 10 percent and roveacrinids range from 1 to 2 percent in present. Fine bioclastic grains are evenly distributed in a micritic matrix. Subordinate grains predominantly are roveacrinid bioclasts. Also, the mud shows a slight degree of recrystallization into xenotropic microspar and is dolomitized in parts. Dolomitization and silicification are common in microfossils that are poorly preserved. Chambers of some planktonic foraminifera are almost completely replaced by dolomite in places. Dolomite occurs as rhombic crystals or patches which replace the chambers partially or completely in a matrix. Mf–1 belongs to outer ramp settings and corresponds to RMF 5 of Flügel (2004).

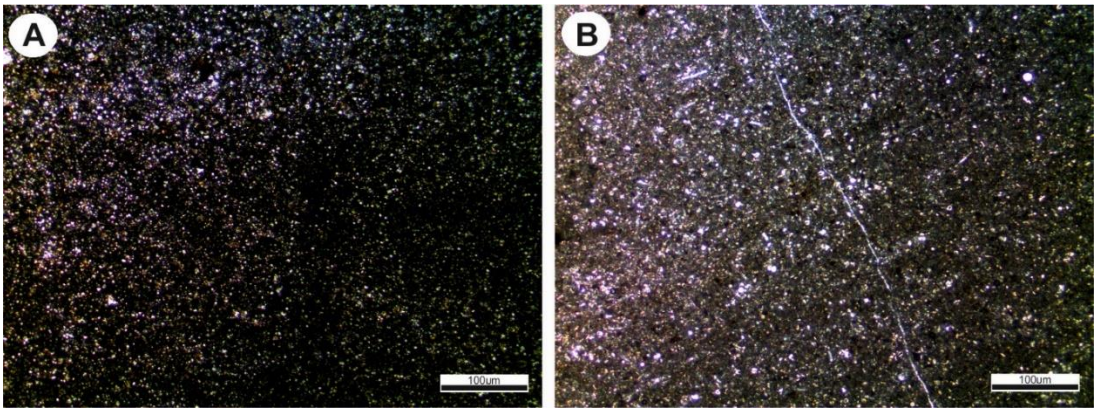


Figure 4.2. Photomicrographs of microfacies types. Mf–1: Non–laminated silt–bearing lime mudstone, A. sample 1.1, SSS and B. sample 7.1. SSS.

4.1.1.2 Mf–2: Pithonellid–Planktonic Foraminifera Wackestone–Packstone

Pithonellids are the dominant skeletal grains in this microfacies (Figures 4.3 and 4.4), ranging from 90 to 95 % in abundance. First pithonellids are the major components (i.e *Bonetocardiella conoidea* Bonet, *Pithonella ovalis* Kaufmann, *Pithonella sphaerica* Kaufmann, *Pithonella lamellata* Keupp) (Figure 4.4). Pithonellids generally range in size from 0.05 to 0.1mm in diameter in size, containing common planktonic foraminifera such as (Heterohelicidae and Hedbergellidae). They are generally widely distributed on fine–grained, dark brown micritic matrix with no specific orientation and highly affected by neomorphism and replacement. Chambers of planktonic foraminifera and pithonellids are completely replaced by dolomite at places. The dolomites occur as rhombic crystals or patches which replace the chambers partially. This microfacies are interpreted to represent outer ramp settings and corresponds to RMF 5 of Flügel (2004).

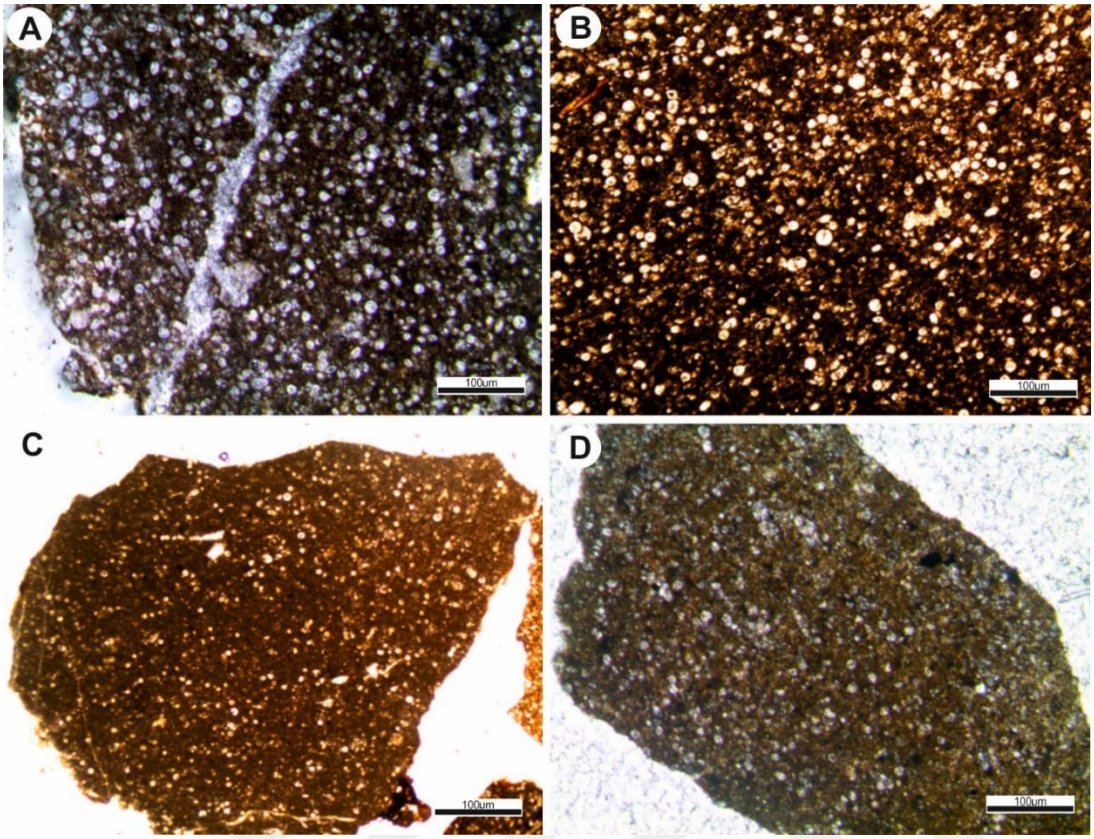


Figure 4.3. Photomicrographs of microfacies types. Mf–2: Pithonellid–planktonic foraminifera wackestone–packstone A. sample–2270, S–2 borehole section B. sample–4.9, B–1 borehole section C. sample–1700, K–1 borehole section, D. sample–2570, G–1 borehole section.

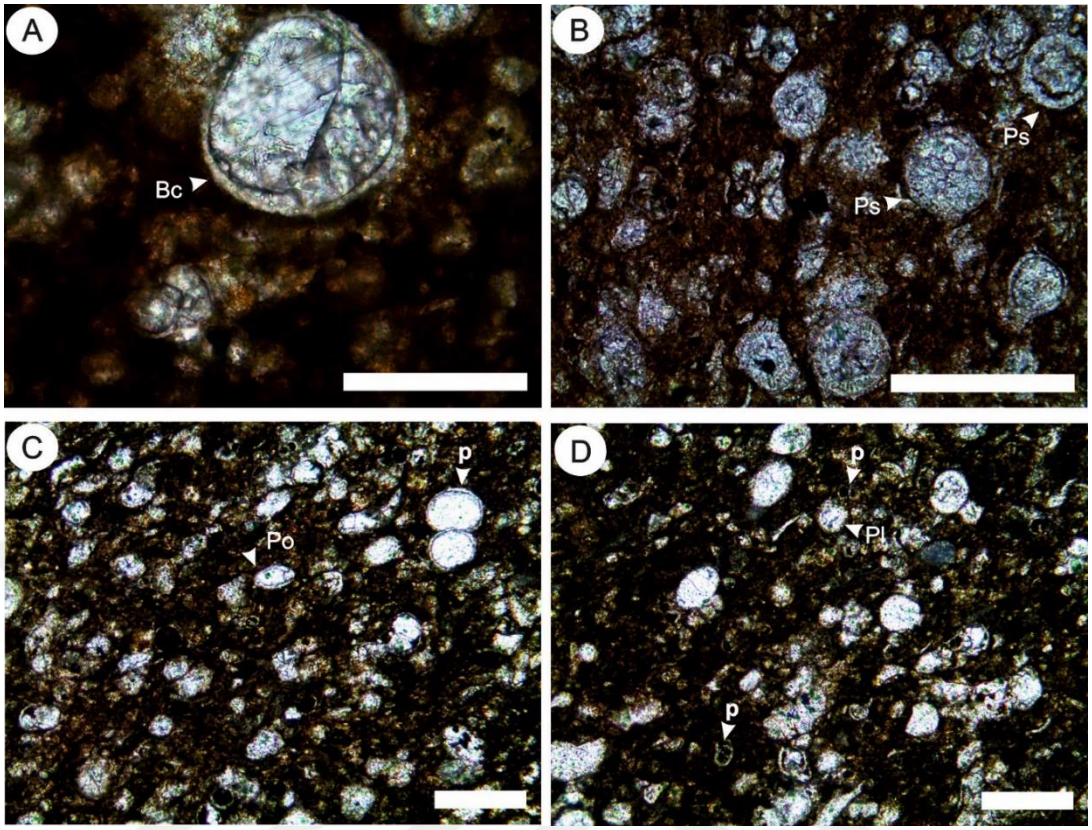


Figure 4.4. Thin–section photographs of pithonellids in the BZ–1 borehole section, lower?–middle, Cenomanian, Adıyaman area, SE Turkey. A: a cone–shaped form, *Bonetocardiella conoidea,* Bonet Bc, core sample 370039. B: thick–walled spherical form with typical pithonelloid crystal–orientation–*Pithonella sphaerica*, Kaufmann Ps; right middle and upper corner: organic walls are preserved, core sample 370034 C: center–*Pithonella ovalis*, Kaufmann Po, core sample 370025. D: left = very clear *Pithonella sphaerica* with crystal orientation nicely seen core sample 370022. Bc: *Bonetocardiella conoidea,* Po: *Pithonella ovalis*, Ps: *Pithonella sphaerica*. (Scale bar: 100μm and 200μm).

4.1.1.3 Mf–3: Pithonellid–Roveacrinid Wackestone–Packstone

The main constituents of this microfacies are pithonellids and roveacrinids, as well as planktonic foraminifera. Roveacrinids range from 5 to 30 % in abundance (Roveacrinidae indet.) The microfacies documents a wackestone–packstone texture with pithonellids, roveacrinids, and planktonic foraminifera. Planktonic foraminifera are 0.10 to 0.15 mm in size and poorly preserved (Figure 4.5). Chambers of some planktonic foraminifera are completely filled in with dolomite at places. Dolomite occurs as rhombic crystals or patches which replace the chambers partially or completely. Chambers are generally filled with sparite. Skeletal grains are evenly distributed in a micritic matrix of wackestone textures. Other subordinate grains are roveacrinid bioclasts. The matrix is generally composed of earthy to dark–brown micrite. The abundance of pithonellids along with roveacrinids, fine bioclasts, and mud–supported fabric all indicate a low–energy and relatively deep–water environment. This microfacies are interpreted to represent mid– to outer–ramp settings and corresponds to RMF 7 of Flügel (2004).

4.1.1.4 Mf–4: Bioclastic Roveacrinoidal Wackestone

This microfacies contain various bioclasts including dominantly roveacrinids (brachial and thecal plates of roveacrinoids, lateral plates of ophiuroids, and echinoid spines), bivalves, as well as planktonic and some benthonic foraminifera and fine peloids (Figure 4.6). No organic matter is preserved. The presence of a micrite matrix evidences a low–energy environment. Disarticulation of bioclasts is due to bioturbation or storm activity. The combination of abundant and fragmented marine fauna, a micritic matrix, and texture suggests that the bioclastic wackestone facies was deposited in an open marine environment, probably below the wave base. This microfacies are interpreted to represent mid– to outer–ramp settings and corresponds to RMF 7 of Flügel (2004).

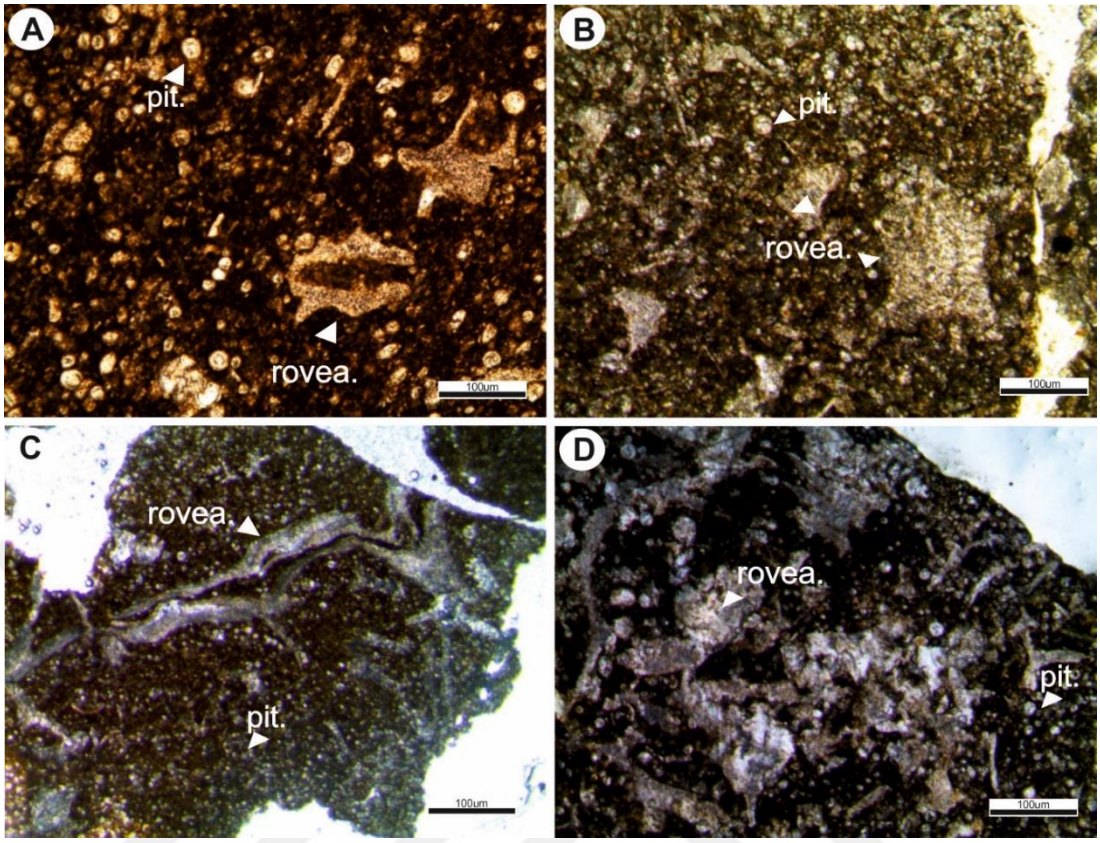


Figure 4.5. Photomicrographs of microfacies types. Mf–3: Pithonellid–**r**oveacrinid wackestone–packstone. A. sample–4.9, BO–1 borehole section; sample–2900, G.K–1 borehole section, sample–1404.1, BA–1 borehole section,, sample–2206, S–2 borehole section. Rovea. Roveacrinid, pit. Pithonellid.

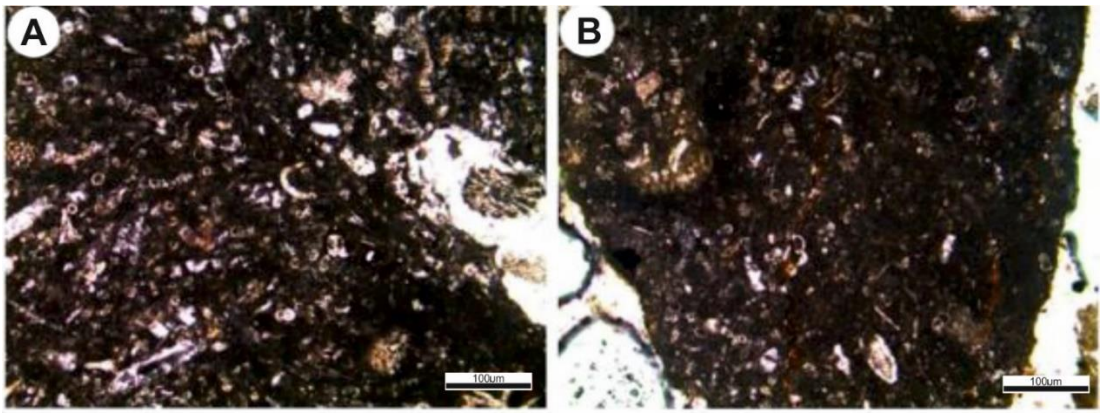


Figure 4.6. Photomicrographs of microfacies types. Mf–4: Bioclastic roveacrinoidal wackestone, calcareous benthic foraminifera (*Lenticulina* sp.) with bioclasts in the S–2 borehole section, sample 2274.2, and a transverse section of an echinoid spine in the S–2 borehole section, sample 2274, respectively.

4.1.2 Microfacies of the Derdere–B Member (Derdere Formation)

In the study area, Derdere–B Member varies from dolomitic limestone to dolomite. Three major types of dolomite are identified on the basis of petrography and distribution: (1) fine crystalline planar–s dolomite mosaic (2) medium crystalline planar–e–s dolomite mosaic and (3) coarse crystalline planar–e–s dolomite mosaic. Dolomitization selectively affects the matrix or both matrix and grains simultaneously. In dolomitic limestone, bioclastic dolowackestone, peloidal dolowackestone–dolopackstone, and benthic foraminiferal dolowackestone usually occurs in discrete beds within dolomudstone, although in a few places they grade into one another. Based on the petrographic analysis of the Derdere–B Member, seven microfacies are interpreted to represent as in below.

4.1.2.1 Mf–5: Bioclastic Dolowackestone

Bioclastic dolowackestone is characterized by bivalve fragments which are the only skeletal constituents (%10) in medium crystalline dolomite (%90) (Figure 4.7). Dolomite is characterized by either medium crystalline (20–100 μm), planar–e to planar–s type, or by fine crystalline mosaic especially when it is associated with bioclasts of a quiet environment. Dolomitization selectively affects matrix, or both matrix and grains simultaneously. Porosity is intercrystalline in dolomitic parts, and in the non–dolomitized parts consists of intraskeletal pore types. Also, fracture porosity is the common porosity type. Dolowackestone usually occurs in discrete beds within dolomudstone, although in a few places they grade one into the other.

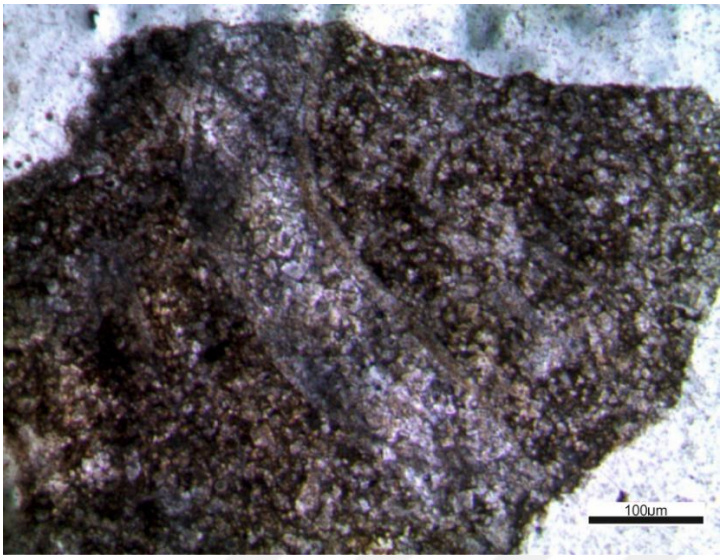


Figure 4.7. Photomicrographs of microfacies type. Mf–5: Bioclastic dolowackestone with medium crystalline dolomite mosaic, sample 2194, S–2 borehole section.

4.1.2.2 Mf–6: Peloidal Dolowackestone–Dolopackstone

Peloids are the dominant grain types with partially to completely dolomitized matrix (%80–90). Benthic foraminifera, green algae, and mollusc fragments are locally concentrated (%20–10). Preservation of fossil fragments are generally indicating a relatively quiet environment and early stabilization/cementation. Dolomite occurs either as selectively replacing a matrix by finely crystalline mosaic texture, or as isolated, euhedral, and planar–p, dolomite rhombs. Porosity commonly occurs as leached intergranular spaces (Figure 4.8).

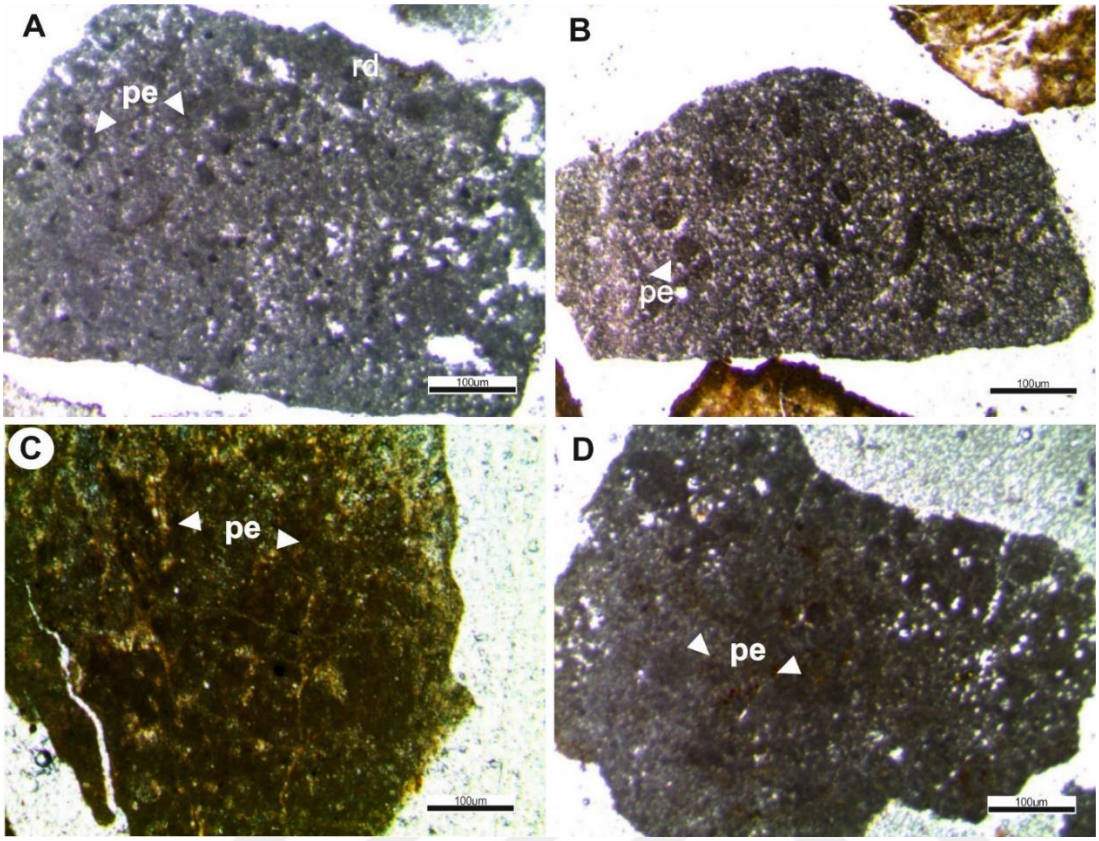


Figure 4.8. Photomicrographs of microfacies types. Mf–6: Peloidal dolowackestone, A. sample 970, AK–1, borehole section. B. sample 2145 El–1 borehole section. C. sample 2472, D–1 borehole section, D. sample 1372, Al–1 borehole section sample Pe: Pellet.

4.1.2.3 Mf–7: Benthic Foraminiferal Dolowackestone

Benthic foraminifera is the characteristic skeletal grains of this microfacies. Grains are usually embedded in a micritic matrix (%10) (Figure 4.9). Other skeletal grains include fine bioclasts of foraminifera and other shallow–marine fauna. Lamination can be recognized in thin–sections. Coarse bioclasts are sporadically concentrated and leached yielding a mouldic porosity. Dolomite is represented by floating rhombs of medium crystalline mosaic (%90).

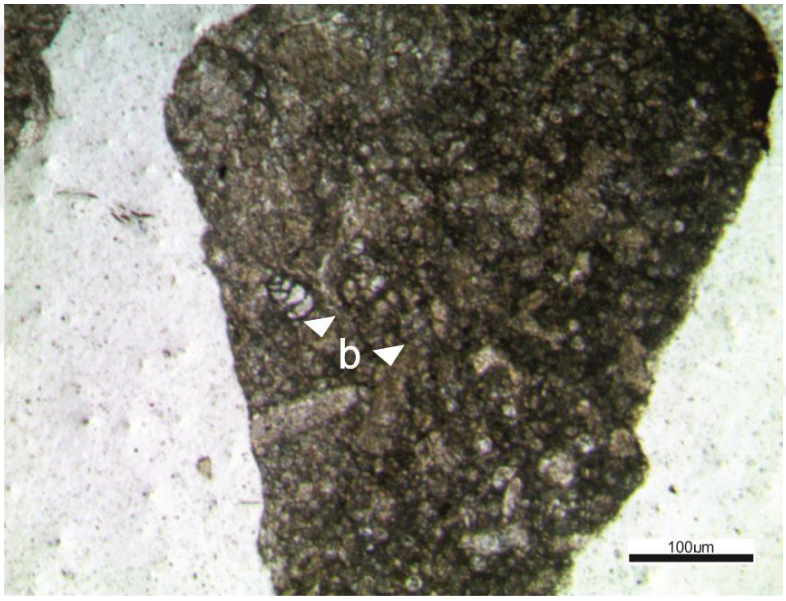


Figure 4.9. Photomicrographs of microfacies type. Mf–7: Benthic foraminiferal dolowackestone, sample 2518, G–1 borehole section. .b: Benthic foraminifera.

4.1.2.4 Mf–8: Dolomudstone

Dolomudstone is a massive, current laminated or mottled (bioturbated) fine–crystalline carbonate rocks composed principally of 10–20 pm dolomite crystals (%100) and is generally stained brown (Figure 4.10). The dolomite is mostly fabric–retentive. Crystals are very fine–grained, commonly less than 0.05mm in diameter and have both xenotopic and idiotopic mosaics. Anhedral and euhedral crystals are both common. Sometimes filled with patches of sparry calcite cement. Grains are rare bioclasts and peloids. The pore types could be distinguished into micro intercrystalline pore spaces, microvugs, and fractures. This facies was probably originally micritic in nature since it has been dolomitized to a fine–grained mosaic and primary sedimentary structures have been preserved. The planar and wavy mm thick lamination and stylolites (horse tails) is the prominent sedimentary textures. The facies appears unfossiliferous, which suggests that environmental conditions were not suitable to support faunas. However, since these rocks have been dolomitized it is possible that microfossils may have been present and later dolomitized with little fabric–retention.

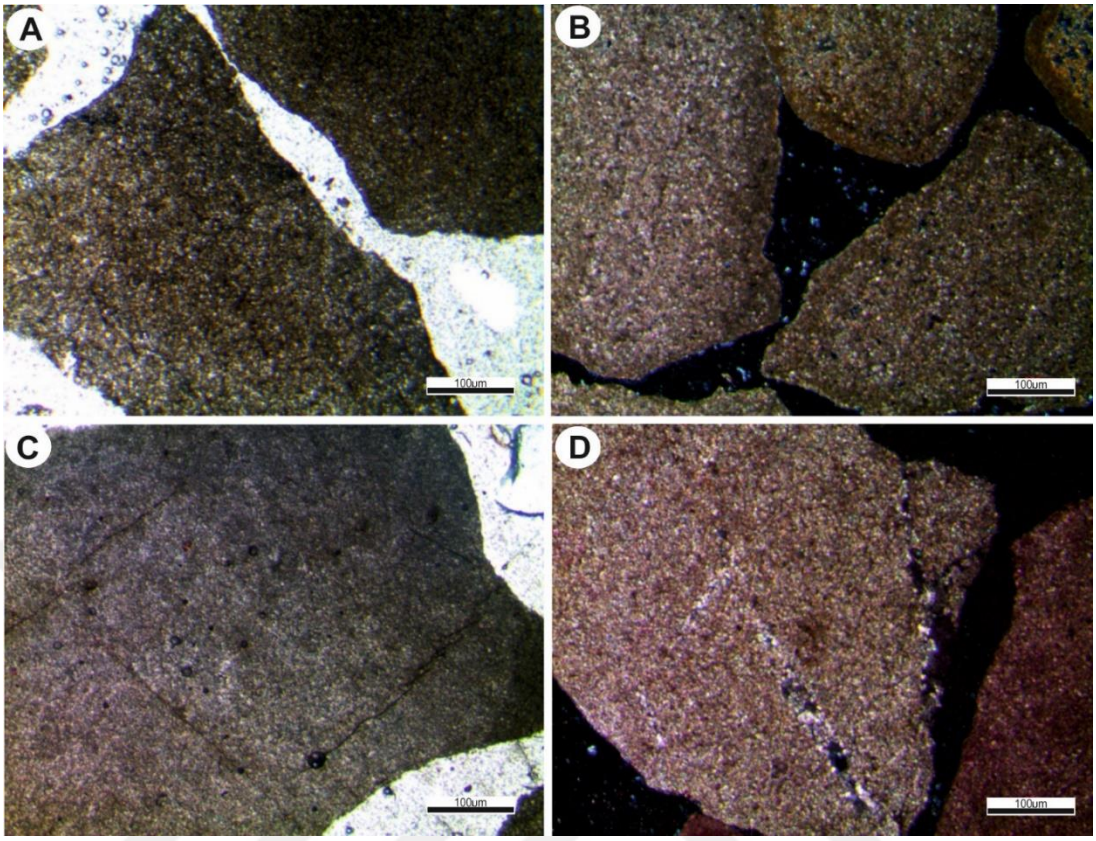


Figure 4.10. Photomicrographs of microfacies types. Mf–8: Dolomudstone. A. sample 2822, Gö–1 borehole section, B. sample 1122, Ya–1 borehole section, C. sample 752, Be–1 borehole section D. sample 6860 Ka–1 borehole section.

4.1.2.5 Mf–9: Fine Crystalline Planar–s Dolomite Mosaic

The dolomite of this microfacies is characterized by finely crystalline (10–20 μm) of planar–s type (Figure 4.11). It commonly forms a homogenous ground mass with dark sporadic clouds, and occasionally ghosts of fine shell bioclastic fragments. Dolomite crystals are anhedral in shape especially when finely crystalline (> 10 μm) with no relics of the original fabric. Another special form of dolomite in this microfacies is coarser crystalline (10–20 μm), euhedral dolomite mosaics showing considerable amounts of microvugular porosity. Other textures are characterized by a finely crystalline planar–s type of dolomite, which incompletely replaces the original limestone matrix. Pores in this microfacies are mostly intercrystalline.

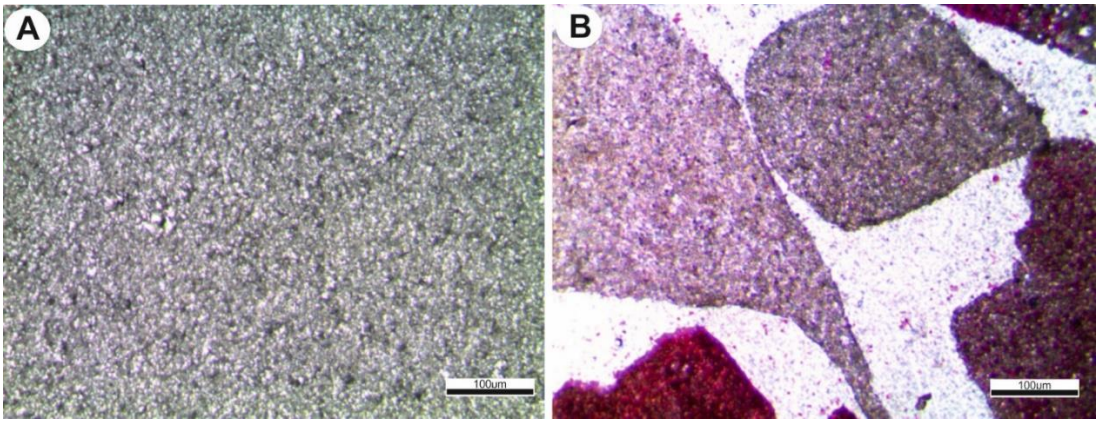


Figure 4.11. Photomicrographs of microfacies types. Mf–9: Fine crystalline planar–s dolomite mosaic. A. sample 1886, GB–1 borehole section. B. sample 6870, Ka–1 borehole section.

4.1.2.6 Mf–10: Medium Crystalline Planar–e–s Dolomite Mosaic

This dolostone is characterized by medium crystalline (20–50 μm) and locally even coarsely crystalline planar–e to planar–e to planar–s mosaic (Figure 4.12). In some cases, the texture is cloudy non–planar–a mosaic with relics of original micritic matrix mosaic. In other cases, relics of the original micrite developed as a peloidal fabric. Ghosts of skeletal grains such as benthic forams and skeletal debris are also present. The most common type of porosity is intercrystalline. In the more coarsely crystalline fabric, inter–crystalline porosity becomes larger and coalesces to isolated microvugs. Additional porosity comes from unhealed fractures. This facies represents the best reservoir facies based on its excellent petrophysical properties.

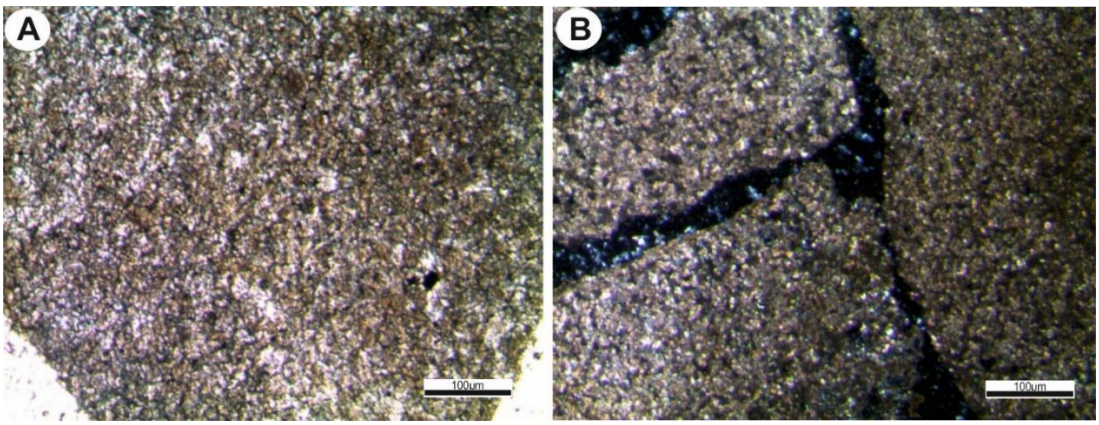


Figure 4.12. Photomicrographs of microfacies types. Mf–10: Medium crystalline planar–e–s dolomite mosaic. A. sample 2972, G.K–1 borehole section, B. sample, 6940 Ka–1 borehole section.

4.1.2.7 Mf–11: Coarse Crystalline Planar–e–s Dolomite Mosaic

This type of dolomite is characterized by coarse (> 100 μm), euhedral to subhedral dolomite crystals of planar–e to planar–s type with low intercrystalline but high vuggy porosity (Figure 4.13). Crystals sometimes occur as nonplanar–a with cloudy centers which show noticeable low porosity. Dolomite crystals in some cases are very coarse and show progressive dissolution. Undolomitized bioclasts can be occasionally recognized.

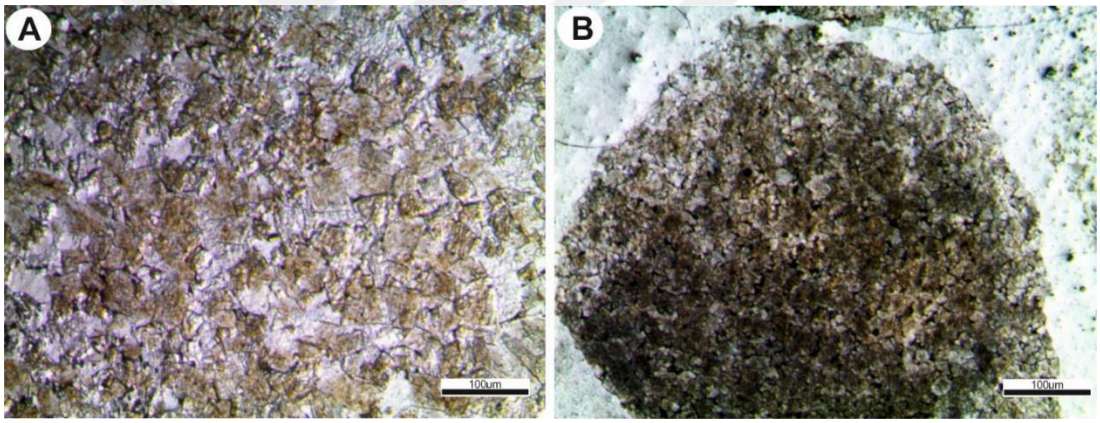


Figure 4.13. Photomicrographs of microfacies types. Mf–11: Coarse crystalline planar–e–s dolomite mosaic. A. sample 2032, G.B–1 borehole section, B. sample 2508, B–1 borehole section.

4.1.3 Microfacies of the Derdere–C Member (Derdere Formation)

The microfacies document a mudstone–rudstone texture with predominantly rudists, pithonellids, planktonic and benthic foraminifera, echinoids, ostracods, gastrapods, bivalves, algae and roveacrinids skeletal constituents. Based on petrographic analysis of the Derdere–C Member eleven microfacies are here interpreted to represent inner to mid–ramp settings.

4.1.3.1 Mf–12: Bioturbated Wackestone

These microfacies are composed of mainly benthic foraminifera, small ostracods, and rare dasycladalean algae. Peloids are also uncommon. Bivalves are usually very thin–shelled and have both crenulated and smooth shells. They are often very well–preserved, being less than 0.5 mm in length with valves still articulated. Bivalves were originally aragonitic and therefore are now recrystallized to calcite spar. They are often disarticulated. The matrix is micritic, and often dolomitized or recrystallized to calcite microspar.

Bioturbation is very common (Figure 4.14). It occurs in discrete patches and the matrix is thoroughly bioturbated and is picked out by dolomitization. Often the matrix is clay–rich. Rarely bioclasts are aligned, or bivalve shells are in a hydraulically stable position. The micritic matrix and well–preserved bioturbation structures indicate deposition well below the normal wave base. Storms occasionally impinged into this environment, therefore it is just below the storm wave base. MF–12 could be ascribed to characterize mid–ramp settings and correspond to RMF–8 of Flügel (2004).

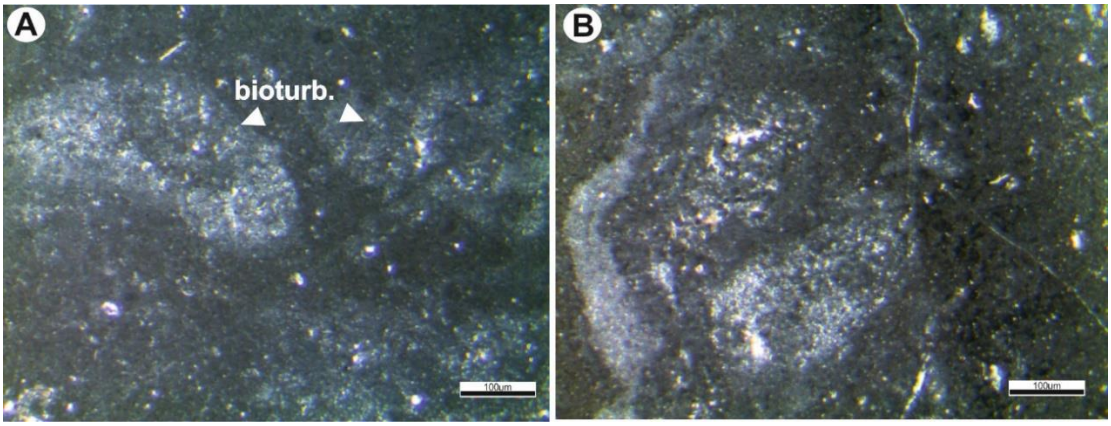


Figure 4.14. Photomicrographs of microfacies types. Mf–12: Bioturbated wackestone, A, B 17–1; 17–4.2 sample, A–1 borehole section. bioturb. Bioturbated.

4.1.3.2 Mf–13: Rudist Floatstone–Rudstone

This microfacies is composed of large rudists. The rudist fragments up to >2mm–sized and constitute almost 50% of the rock embedded in a micritic matrix with a large proportion derived from bioerosion of rudist shells (Figure 4.15). The silty matrix is composed of fine packstone to wackestone with abundant peloids, skeletal fragments of bivalves, echinoids, gastropods and small benthic foraminifera with a large proportion derived from bioerosion of rudist shells and broken down to silt–sized grains. Finely dispersed dolomite rhombs occur in the matrix locally. Non–skeletal grains are rare and consist of small intraclasts (1%). The rudist shells of the MF–13 could be ascribed to characterize mid–ramp settings and correspond to RMF–9 of Flügel (2004).

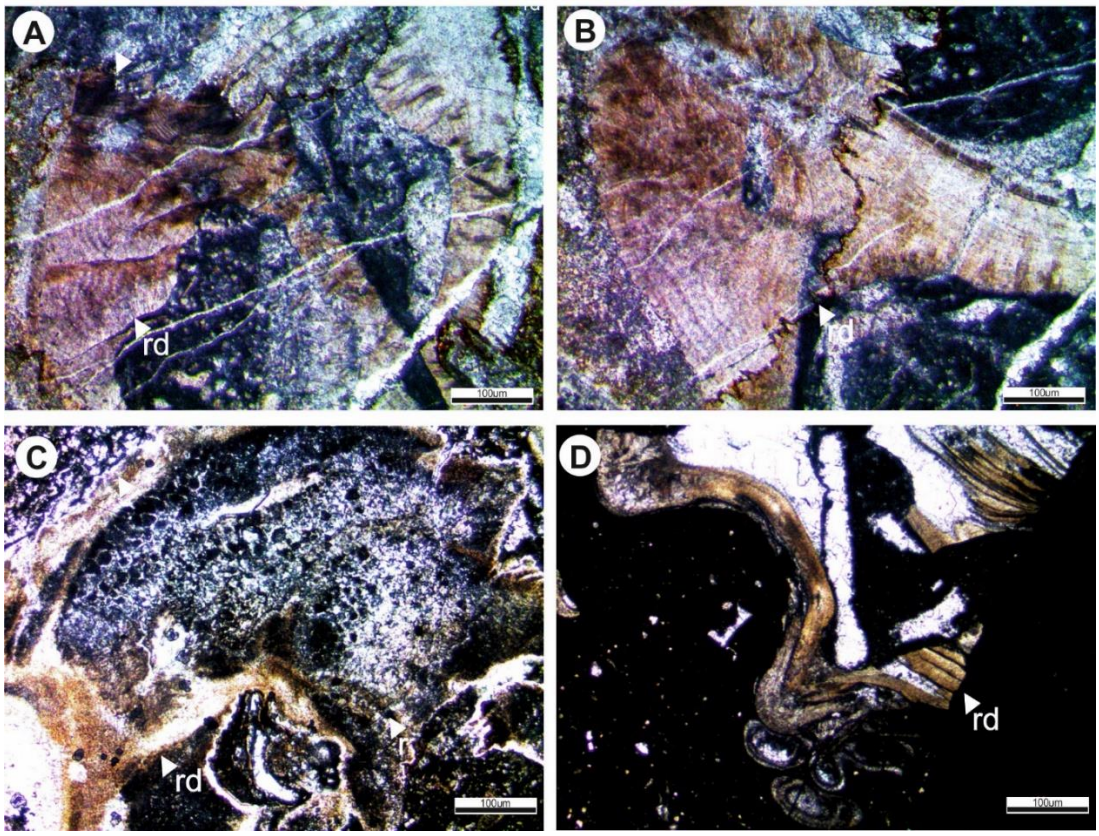


Figure 4.15. Photomicrographs of microfacies types. Mf–13: Rudist floatstone/rudstone, A,B, samples IND–0.17.1–3, İSS, C,D, samples SAB–70.2–3, SSS. Rd: Rudist.

4.1.3.3 Mf–14: Intraformational Breccia

This microfacies is characterised by intraformational breccia deposits. The breccia is mainly clast–supported and poorly–sorted. Clasts are angular to subangular in shape and range in size from less than 1 cm to 5 cm diameter (Figure 4.16; Table 4.1 4.2, and 4.3). However, broken limestone clasts and poor fossil–bearing micritic clasts are also abundant. Coarse–grained, poorly–sorted rudstone consists large rounded extraclasts and smaller mud peloids. Larger black grains are aggregate grains, smaller grains are peloids. Many grains were locally eroded by storm events, transported over short distances, and redeposited. Grains are peloids, micritic extraclasts, some shells and echinoderm fragments embedded within a heterogenous microspar matrix (Figure 4.16). Most clasts show an alignment parallel to bedding. (Figure 4.16). No imbrication and preferred transport direction can be seen. There is not any evidence of subaerial exposure. Cros et al. (1999) and Robertson et al. (2016) stated that the similar characteristics observed in the Derdere formation in the İnişdere stratigraphic section. Since many of the clasts are angular or subangular, a short transport distance is envisaged. They have been ripped–up from the underlying beds, therefore it is likely to be an intraformational breccia. MF–14 could be ascribed to characterize mid–ramp settings and correspond to RMF–10 of Flügel (2004).

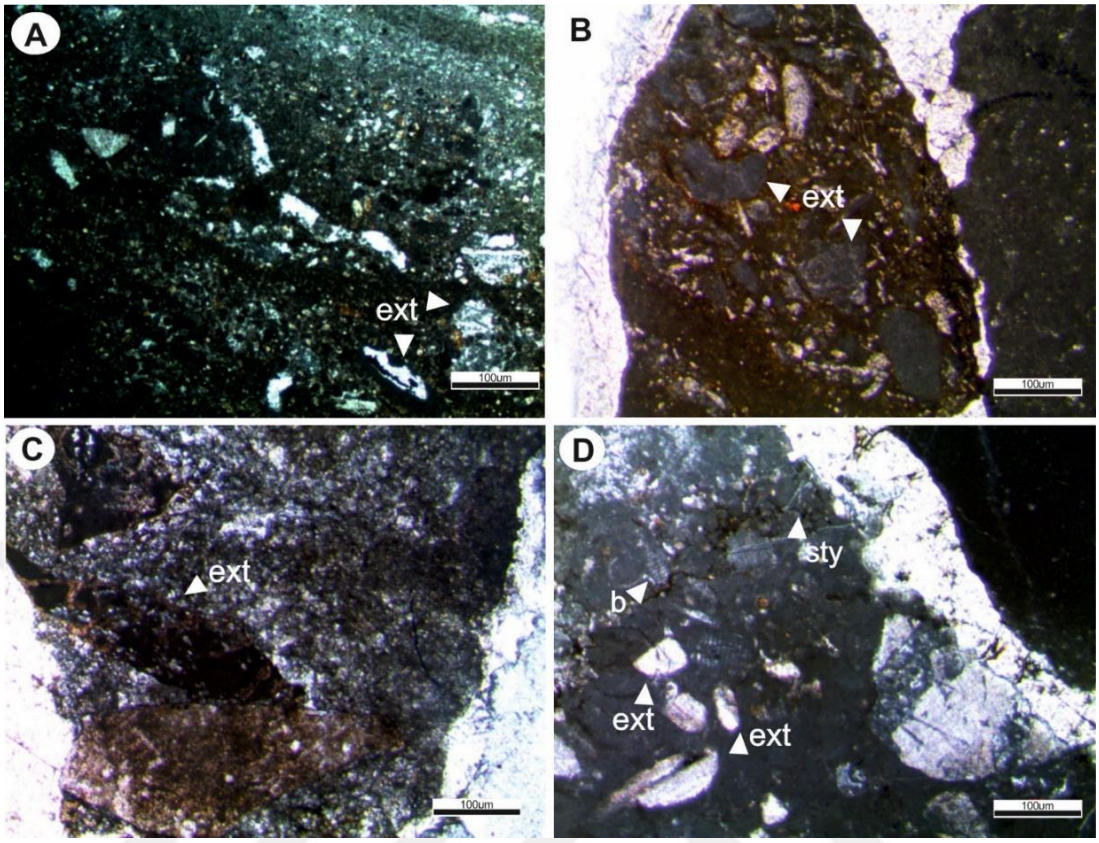


Figure 4.16. Photomicrographs of microfacies types.. Mf–14: Intraformational breccias, A. sample IND–1,04, İSS. B. sample 880,4, Ak–1 borehole section, C–D. sample 728.3–732, Be–1 borehole section. Ext: Extraclast, sty: Stylolites.

4.1.3.4 Mf–15: Poorly Sorted Intraclastic Peloidal Packstone–Grainstone

Intraclasts are the main component of this microfacies. Intraclasts are generally polymodal in size, ranging from 0,2 to 0,5 mm. Most of the intraclast are subangular to angular consist in low proportions of echinoderms, and bivalve bioclasts (total 5%) (Figure 4.17; Table 4.1, 4.2 and 4.3). Some intraclasts are internally homogeneous and consist of micrites, while others display internal compositions such as peloids and fossils. Granular and blocky sparry calcite fills the interstices between grains. Intraclastic pack– to grainstones of facies may represent the highest–energy shallow environments. These deposits likely formed due to storm wave erosion and reworking of various shallow marine sediments (Flügel 2004). This microfacies Mf–15 could be ascribed to open inner–ramp settings and corresponds to RMF–14 of Flügel (2004).

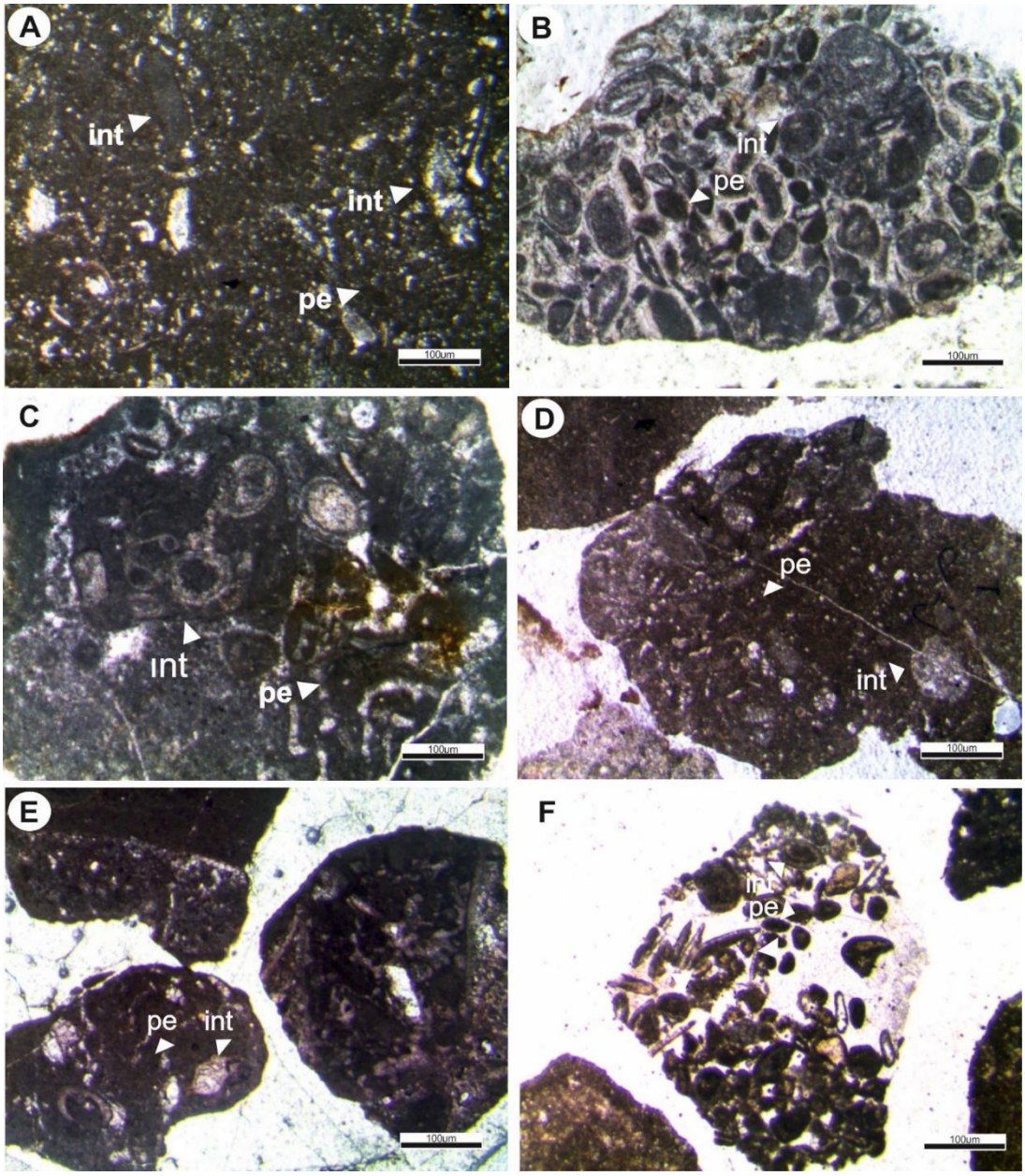


Figure 4.17. Photomicrographs of microfacies types. Mf–15: Poorly sorted intraclastic peloidal packstone–grainstone. A. sample 16.4, A–1 borehole section, B, C samples 2964 and 2976, respectively, G.K–1 borehole section, D sample 2194, Y–3 borehole section, E. sample 3410, Y–1 borehole section , F sample 896, E–1 borehole section .pe: Pellet, int: Intraclast.

4.1.3.5 Mf–16: Bivalve–Roveacrinid Floatstone

This microfacies is characterised by an accumulation of up to >2mm–sized bivalves and roveacrinids (Figure 18; Table 4.1 and 4.2) embedded in a micritic matrix which is mostly randomly or less commonly concordantly oriented. They are well preserved, positioned obliquely or parallel to bedding and do not show any micritisation. Sparitic shelters and geopetal textures are present. Microcrystalline spar is observed at the top of some valves. Planktonic foraminifera and pithonellids are minor grains. The bivalve shells of the MF–16 could be ascribed to characterize open inner–ramp environment and correspond to RMF–15 of Flügel (2004).

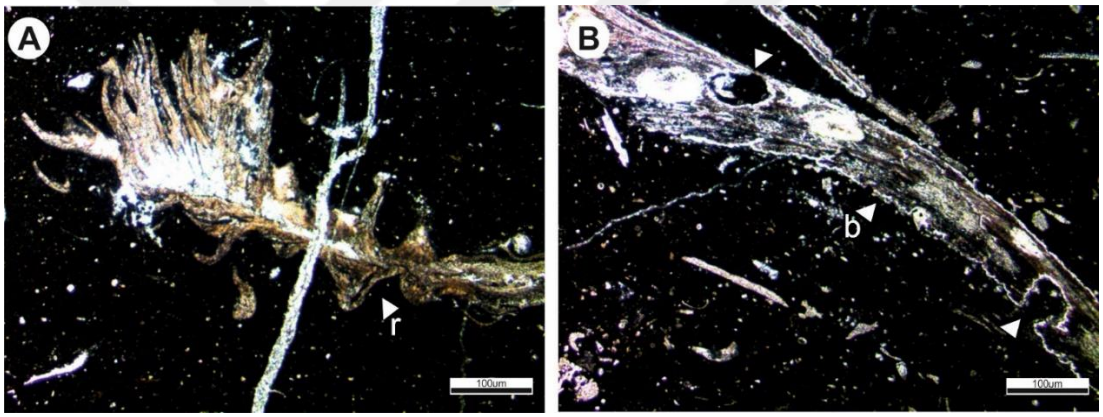


Figure 4.18. Photomicrographs of microfacies types. Mf–16: Bivalve and roveacrinid floatstone, samples, A,B samples,72.3 and 72.4 respectively, SSS. b. Bivalve, r. Roveacrinids.

4.1.3.6 Mf–17: Benthic Foraminifera Bioclastic Silty Wackestone–Packstone

This grained dominated facies contains benthic foraminifera (e.g Valvulinidae, Miliolidae and Nezzazatidae) and some other bioclasts (e.g. algae, bivalve) as main allochems. Benthic foraminifera are often micritized and commonly intraskeletal pores are filled with calcite cement. Peloids are present as subordinate grains (Figure 4.19; Table 4.1 and 4.2). It has wackestone to packstone texture. No sedimentary structures are observed. Micritization and marine cementation are two notable early

diagenesis features. The micritization of some benthic foraminifera makes the recognition of skeletal grains difficult at some parts in this microfacies. Recrystallization has critical a role in modifying the internal structure in some of the benthic foraminifera. This facies is commonly associated to other grains– to mud dominated facies which is ascribed to the semi–restricted lagoonal environment on the basis of these characteristics (Flügel, 2004). Considering its texture and fossil content, MF–17 belongs to a lagoonal environment and inner–ramp settings and corresponds to RMF–16 of Flügel (2004).

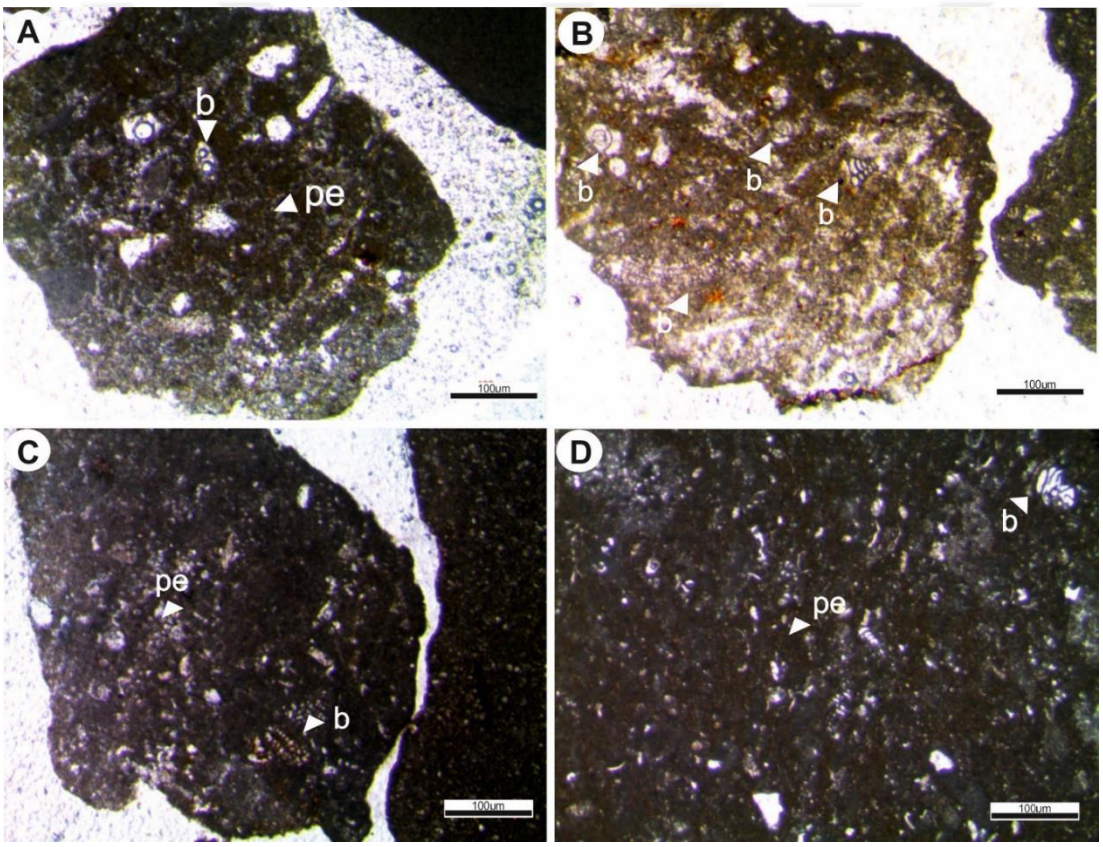


Figure 4.19. Photomicrographs of microfacies types. Mf–16: Benthic foraminifera bioclastic silty wackestone–packstone,, A sample 858.3, A–1 borehole section, B. sample 1028.2, E–1 borehole section, C–D samples 2186.3 and 3.4,2 respectively. Y–3 borehole section..pe: Pellet, b: Benthic foraminifera.

4.1.3.7 Mf–18: Peloidal Packstone

This is a medium–grained peloidal packstone dominated by peloids (90 vol% of allochems), bioclasts (3%) and intraclasts (5%) (Figure 4.20; Table 4.1 and 4.2). Peloids are rounded to subrounded and up to 0.5 mm in size. The some peloids are irregular in shape and contain microstructures, suggesting that they are either small intraclasts or micritized bioclasts rather than primary pellets. Most peloids are micritized grains, discernible by the elongate shape. Where they have a long axis, alignment is apparent. These grains are variably micritized. They do not exhibit regular stripes or internal patterns. Some of them have still a bioclastic center. Small some micritic lithoclasts and ooids are rare components of these microfacies.

Some mollusc valves have a coating of micrite on the convex side. Many valves preserve their internal microstructure; however, some show recrystallization and are recognized by their micrite envelopes. Bioclasts include calcitic and transformed aragonite bivalves. Fractures within larger intraclasts are probably formed by physical deformation owing to differential compaction prior to final cementation. Intraclasts are up to 5 mm in size and consist of micrite, peloidal grainstone and peloidal packstone. Borings in some intraclasts are filled with sparry cement. Larger intraclasts have fractures infilled with sparry calcite. Grain–support and the low biotic diversity of MF–18 indicate that these sediments were deposited in protected, restricted, well–oxygenated, low–energy environments and inner–ramp settings (Flügel, 2004). This MF–18 could be ascribed to characterize shoal inner–ramp environment and correspond to RMF–17 of Flügel (2004).

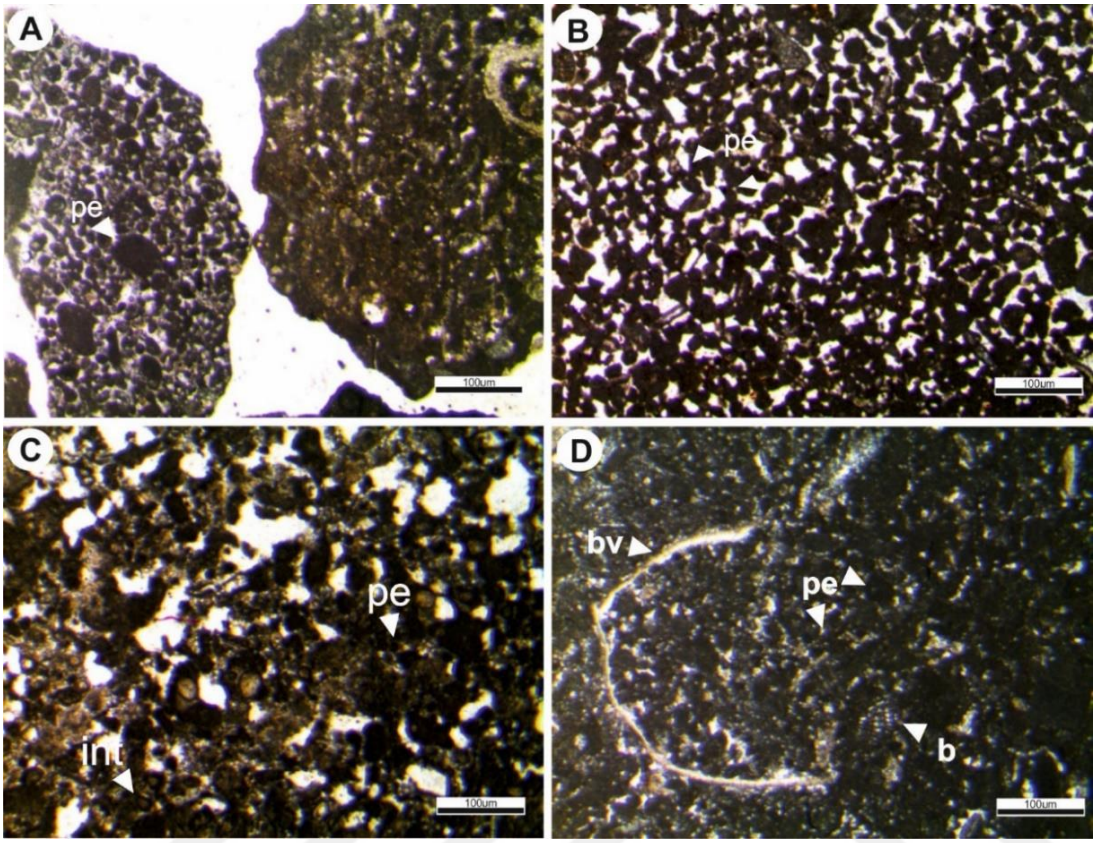


Figure 4.20. Photomicrographs of microfacies types. Mf–18: Peloidal packstone A, sample 882, E–1 borehole section. B. sample 3.7, Y–3 borehole section, C,D samples 16–3 and 16–4 respectively. A–1. borehole section pe: Pellet, bv: Bivalve.

4.1.3.8 Mf–19: Bioclastic Wackestone–Packstone

The main characteristics of this MF are poorly sorted bioclasts of various sizes (Figure 4.21). All bioclasts (bivalves, echinoderms, and gastropod) are very fragmented. The most prevalent bioclasts are bivalves. Bivalves are often aligned parallel to each other and in a hydraulically stable position. Bivalves are also broken into around 1–3mm long bioclasts and articulated and sometimes have a micrite envelope. Echinoderms and gastropod are commonly broken into around 1mm bioclasts. Micrite envelopes are rare. The matrix consists of bioturbated micrite. The matrix is mostly micritic, yet in many samples recrystallization to calcite microspar or dolomitization is mostly common. Preserved bioturbation structures are rare. The fabric, textural characteristics

and fossil content of this facies suggest turbulent conditions considering the variations in size and type of bioclasts, textural inversion, an admixture of the planktonic and benthic foraminifera assemblages and turbulent fabric. The varied assemblages present in these microfacies suggest an open–marine depositional environment. Most of the bioclasts are broken up and were probably intensively winnowed. The sparitic matrix indicates moderate to high energy environments. The remaining lime mud/micrite would have been washed out. Disarticulation of bioclasts was due to storm or wave activity. Thus, MF–16 could be ascribed to deposition in protected and low–energy inner ramp environments and corresponds to RMF–17 of Flügel (2004).

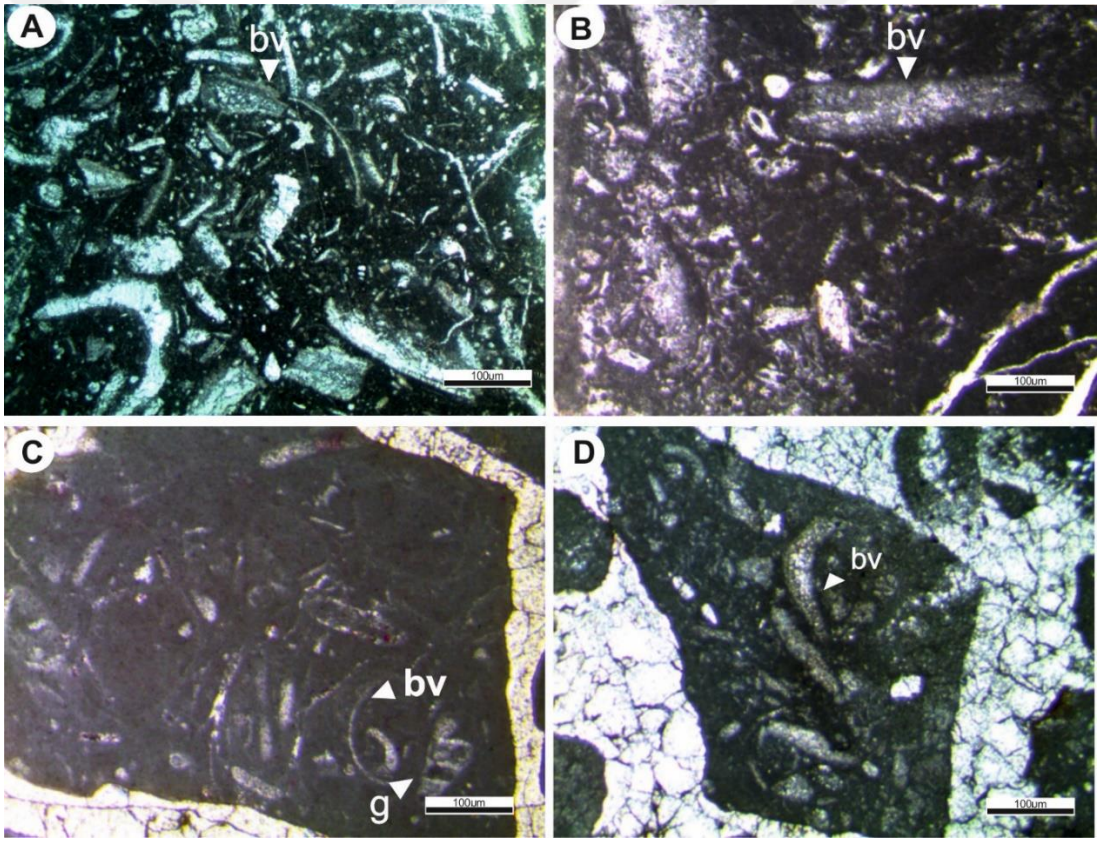


Figure 4.21. Photomicrographs of microfacies types. Mf–19: Bioclastic wackestone–packstone, A,B samples, TRK–48.82 TSS, B. sample 880, Ak–1 borehole section. D, sample 3320, Y–1 borehole section .bv. Bivalve, g. Gastropod.

4.1.3.9 Mf–20: Peloid Bioclastic Silty Packstone

Peloidal grains are common constitutes in the packstone texture (Figure 4.22; Table 4.1 and 4.2). The size of peloids ranges between 0.1 and 0.5 mm. Peloids are spherical, ellipsoidal and rarely angular but are mostly well rounded and show weak to moderate sorting. Peloids often merge into a pseudo–micritic matrix, causing a clotted texture. Sparry calcite partly replaces the micritic matrix. The characteristic of this microfacies is the poorly sorting of microbioclasts of various sizes which comprise fine rudist fragment, bivalves, roveacrinids, echinoids, as well as planktonic and benthic foraminifera, subordinate ostracods, gastropods, bryozoans and annelids. These are distributed in a mud–supported matrix or/and replaced partially to completely by sparry calcite or dolomite. Intraskeletal pores are commonly filled with sparry calcite. Peloids of the MF–20 could be ascribed to have developed in partly protected and mixed high–to–low–energy inner ramp environments and correspond to RMF–18 of Flügel (2004).

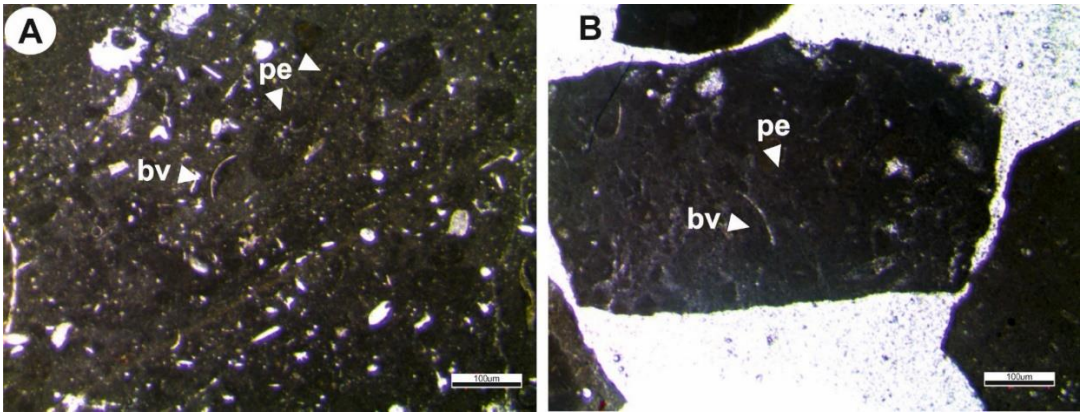


Figure 4.22. Photomicrographs of microfacies types Mf–20: Peloid bioclastic silty packstone A,B samples 1–12 and 1410 respectively. Ba–1 borehole section, bv. Bivalve, pe. Pellet.

4.1.3.10 Mf–21: Ooidal Grainstone

This is a medium–grained ooidal grainstone dominated by ooids (95 vol% of allochems), peloids (3%), and minor bioclasts. Ooids are 0.1mm to 0.5mm in diameter. Ooids range in shape from spherical to elongate (Figure 4.23; Table 4.1, 4.2, and 4.3). The laminae are mainly isopachous (~0.05 mm thick); however, some ooids display lamina with asymmetric thicknesses. Both radial and concentric textures are well developed in the laminae. Some ooids have two or three identifiable laminae.Concentric radial ooids are also abundant. The nucleus of the ooids is commonly a peloid, or a small broken–up bioclasts. The shape of the ooid is often determined by the morphology of the nucleus. Peloids are especially common and bioclasts often possess a micrite envelope. The oolitic grainstones do not display any cross–bedding. However, grains with long axes are rarely aligned and no lamination or graded bedding has been identified. This MF–21 could be ascribed to characterize shoal inner–ramp environment and correspond to RMF–29 of Flügel (2004)

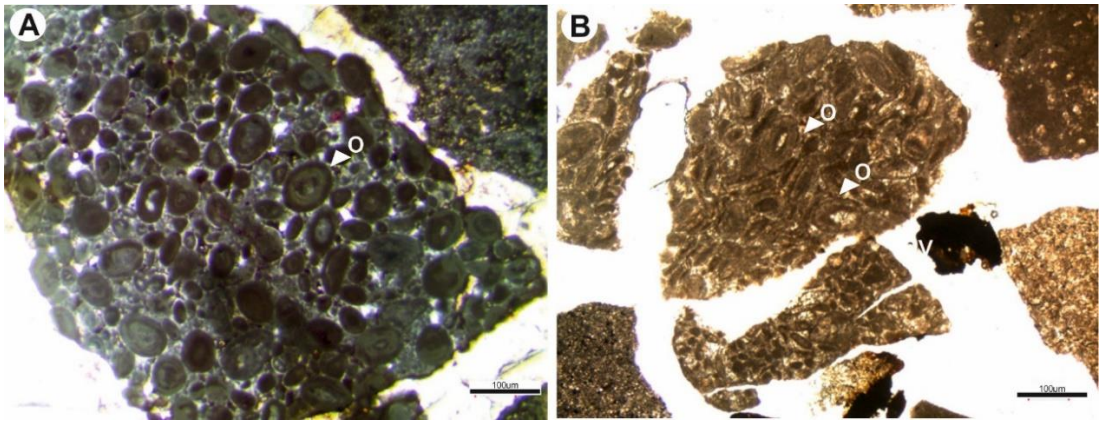


Figure 4.23. Photomicrographs of microfacies types. Mf–21: Ooid grainstone. A. sample 3300, Y–1 borehole section, B, sample 2610, K–9 borehole section, .o. Oolite.

4.1.3.11 Mf–22: Non–Borrowed Lime Mudstone

The pure, homogeneous mudstone without any bioturbation phenomena and only traces of bioclasts is also missing even slight laminations. The lime mudstones are composed of dense micrite (98%) with rare bioclast fragments such as ostracods, roveacrinids, bivalves (1–2%), scattered silt and/or fine sand–sized quartz grains in places (Figure 4.24). This facies was probably deposited below the normal wave base in very low–energy, calm–water, shallow conditions and low sedimentation rate is inferred. Mf–22 belongs to an inner ramp settings and corresponds to RMF–19 of Flügel (2004).

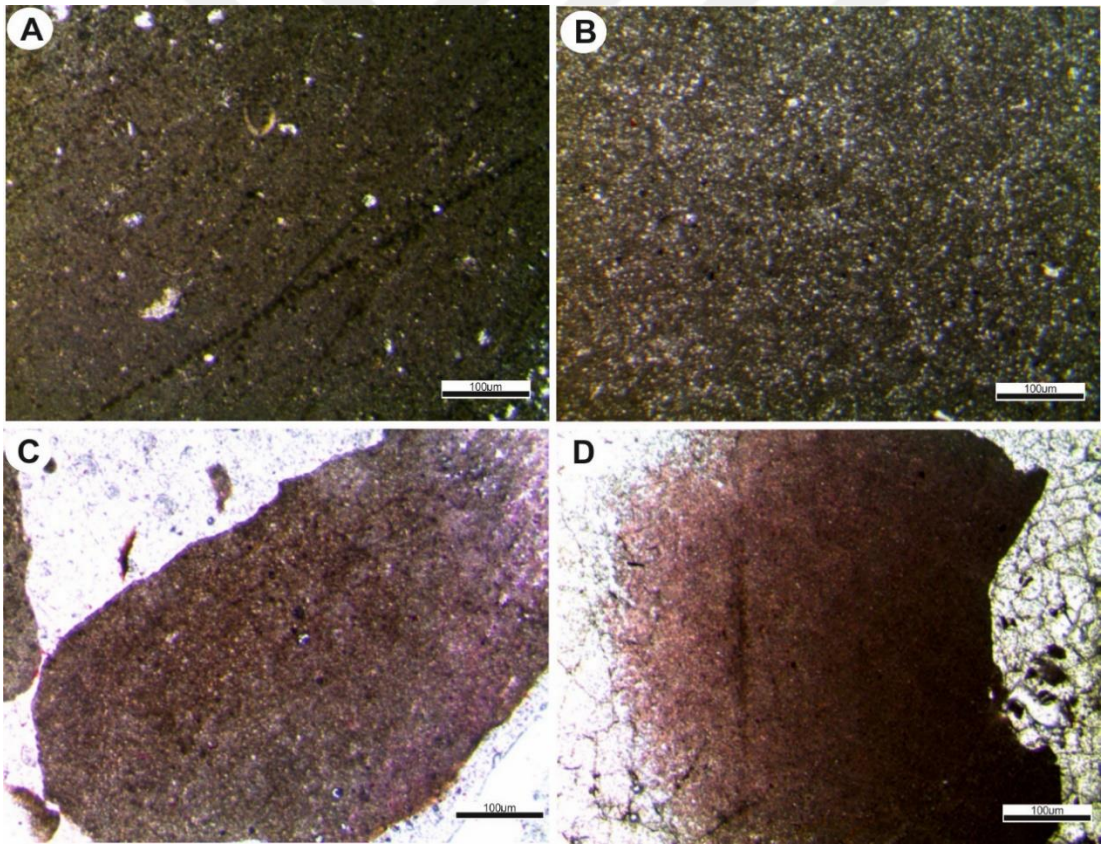


Figure 4.24. Photomicrographs of microfacies types. Mf–22: Non–borrowed, lime mudstone A sample 13.1, Ba–1 borehole section , B. sample 16–1, A–1 borehole section, C, sample 6770, K–1 borehole section, D, sample 1064, Ç–1 borehole section.

4.1.4 Microfacies –Karababa–A Member

The MF analyses based on texture, sedimentary structures and fossils identified in thin–sections have led to the determination of three MF types from the Karababa–A Member carbonates.

4.1.4.1 Mf–23: Finely Laminated, Silt–Bearing Pelagic Lime Mudstone

This microfacies consists of finely textured, dense, dark grey microcrystalline calcite and contains planktonic foraminifera and pithonellids floating in a mud–supported fabric. Some parts are thinly laminated in poorly sorted silt–sized quartz (Figure 4.25). Pithonellids are the predominant skeletal grains in this microfacies, ranging from 80 to 90 percent in abundance and show a concentric wall structure. Roveacrinids range from 1 to 3 percent in abundance. Fine bioclastic grains are evenly distributed in a micritic matrix. Subordinate grains predominantly are roveacrinid bioclasts. Also, the mud shows a slight degree of recrystallisation into xenotopic microspar and is dolomitized in parts. Dolomitization and silicification are common in microfossils that are poorly preserved. Chambers of some planktonic foraminifera are almost completely replaced by dolomite in places. Dolomite occurs as rhombic crystals or patches which replace the chambers partially or completely in a matrix. Mf–23 belongs to outer ramp settings and corresponds to RMF 5 of Flügel (2004).

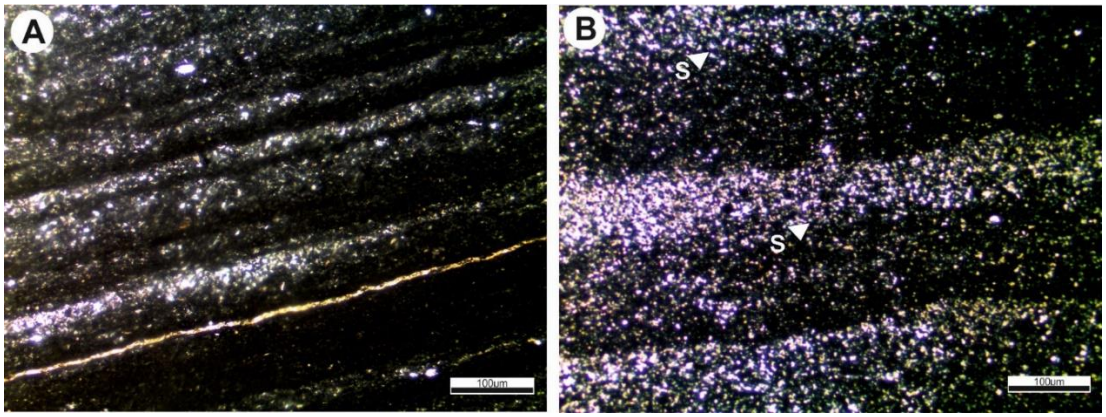


Figure 4.25. Photomicrographs of microfacies types. Mf–23: Finely laminated, silt–bearing lime pelagic mudstone A,B sample 3a, SSS.

4.1.4.2 Mf–24: Planktonic Foraminifera Bearing Wackestone/Packstone

This microfacies consists mainly of dark brown micrite containing organic–rich material. It is slightly recrystallized into microspar. It has some microfossils such as planktonic foraminifera, thin pelagic bivalves (filaments), pithonellids, roveacrinids. In addition, phosphatized grains (fish bones) cemented by abundant micrite. Planktonic foraminifera are infilled with fine sparry calcite cement. Microscale vertical size grading occurs. This MF is dominated by planktonic foraminifera, including the genera *Dicarinella, Marginotruncana* and *Helvetoglobotruncana*, which occur in the homogeneous microcrystalline calcite (Figure 4.26). This microfacies could be ascribed to outer–ramp settings and to RMF–5 of Flügel (2004).

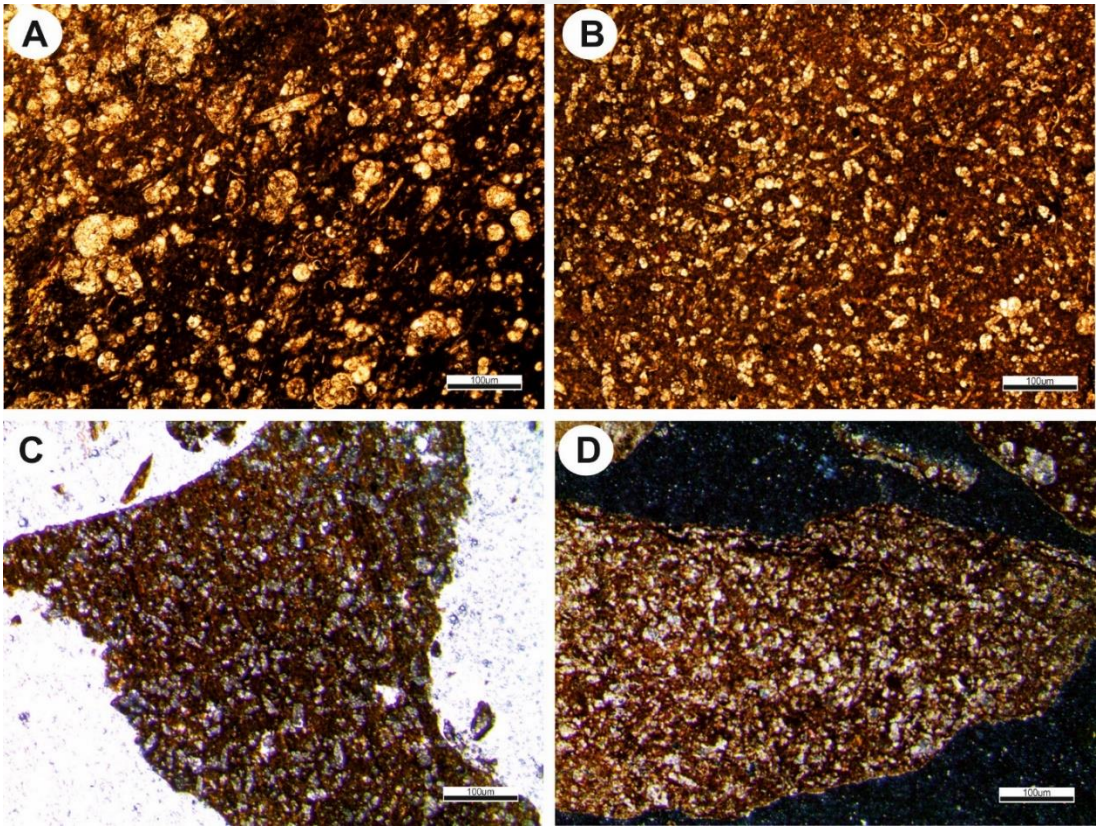


Figure 4.26. Photomicrographs of microfacies types. Mf–24: Planktonic foraminifera bearing wackestone/packstone, samples, A sample 11.8, A–1 borehole section, B, sample k1, K–1 borehole section, C sample 1874, G.B.–1 borehole section, D sample 6740, Ka–1 borehole section.

4.2. Diagenesis

Diagenetic processes are defined as all the physical and chemical changes that occur in sediments before and after the burial process (Flügel, 2004). Carbonate rocks are one of the most affected rocks of diagenesis processes, so the impact of diagenetic processes is huge in the formation. The Derdere Formation has been subjected to extensive and variable diagenetic modifications after its deposition in a shallow marine environment and subsequent burial (late diagenesis). Major diagenetic processes affecting the Derdere carbonates include micritization, dissolution, cementation, neomorphism, dolomitization, stylolites and dissolution seams. The following is a short summary of these processes (Figure 4.27).

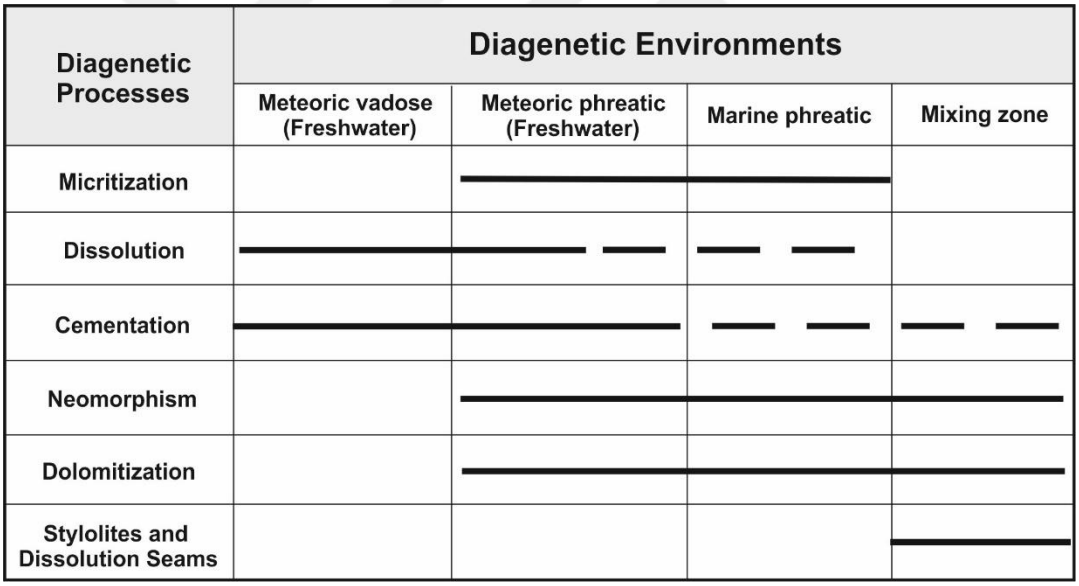


Figure 4.27. Diagenetic modifications in the carbonate succession of the Derdere Formation and Karababa–A Member in the studied sections.

4.2.1 Micritization

Micritization is the first diagenetic phase, and it takes place in the marine diagenesis environment of limestone. This is a process whereby bioclastic grains are altered on the seafloor or just below by bacteria, fungi, and algae in quieter–water areas, leading to the formation of micritic envelops around bioclasts (Tucker and Wright, 1990). The most essential type of biogenetic modification of sediment is because of the boring activities of organisms. Boring by algae, fungi, and bacteria is an especially important process for modifying skeletal fabric and carbonate grains (Boggs, 2009). Even greater intensive boring may also result in the whole micritization of the grain, with the result that all inner textures are destroyed and a type of peloid is created. This process has been affected widely on the Derdere Formation in outcrops and borehole sections, which destroyed the skeletal grains of most fossils. Micritization identified here is an early diagenetic process. Micritic envelopes surround some rudist and echinoderm fragments and wholesale micritization of some benthic foraminifera in bioclastic packstone microfacies makes the recognition of skeletal grains difficult in some intervals.

4.2.2 Dissolution

Dissolution is one of the important diagenetic processes which has a positive impact on porosity and permeability. The secondary porosity is formed by the mechanism of dissolution. Vuggy, mouldic, and interparticle porosity are generated by the process of dissolution, as a result of low stability minerals such as high magnesium calcite. Dissolution occurs within the vadose environment and the upper part of the fresh phreatic environment (Longman, 1980), that is to say, it occurs in shallow environments due to the increase of carbon dioxide which results in the formation of weak acid solutions that dissolve the carbonate components during the passage of this water through the vadose zone. Giles and Marshall (1986) have reported that this process can occur in deep burial environments due to the concentration of CO_2, which is produced because of decay, and decomposition of organic materials in clay–rich facies, in addition to the increase of hydrostatic pressure. Thus, the dissolution process

can occur in shallow environments during early diagenesis processes and in deep burial environments. According to borehole data obtained from porosity logs, porosity in the Derdere Formation varies from 1 to more than 10% in the middle part of the Derdere Formation (Derdere–B). However, the lower part of the Derdere Formation has less than 2% porosity (Derdere–A). Porosity is mainly secondary in nature and dominated by intercrystalline type. Intercrystalline porosity dominantly occurs in dolomite crystals. Vugs are sub–spherical or irregular in shape and reach up to several millimetres in size in core samples (Derdere–C) and a few centimetres in surface sections. Moulds of benthic foraminifera and gastropods are totally or partially filled with calcite cement whereas clay fills some of the vuggy and intercrystalline porosities. Primary porosity is of lesser importance and mostly includes intraparticle porosity. The body cavity of the rudists forms the most important interparticle porosity. It is observed throughout some of the selected study samples in Derdere Formation in the form of either connected vugs or disconnected vugs as a result of cement. The microfacies representing the shoal/ barrier deposits especially rudist rudstone are the most porous intervals in the Derdere Formation, and they contain both primary and secondary porosity. The identified fractures are open to semi–filled with calcite cement. Fracture porosity is widely observed in lime mudstone microfacies of the studied area.

4.2.3 Cementation

The cementation of carbonate sediments is always taken into an important diagenetic process, which gives strength and stability to the rock. Early diagenetic cement precipitates as fibrous aragonite, while granular mosaic cement, drusy cement, and blocky cement precipitate as later diagenetic cement; the latter also indicates that these two types of cement could occur in deep and shallow environments during late diagenesis processes. Based on the petrographic investigation, all types of cement occurred in the Derdere Formation are calcareous; silica cement is absent due to the water–saturated in the cavities with seawater that saturated with calcite and aragonite, following types of calcite cement have been observed in the Derdere Formation.

Equant Granular Cement

This type of cement is characterized by small pore–filling calcite crystals that have no preferred orientation and no substrate control (Flügel, 2004). It is the most observed common cement type in the Derdere Formation in the outcrop and borehole sections.

Drusy Mosaic Cement

This type of cement is characterized by pore–filling calcite crystals increasing in size towards the center of interparticle pores (Flügel, 2004); this type is distinguished by calcite crystals of high transparency and large size with straight edges. This kind of cement has a negative impact on the porosity of the formation. It is present in the bioclastic and wackestone.

Blocky Mosaic Cement

This type of cement is resulted by continuous sedimentation and increased mechanical pressure because of increased sedimentation load; it is characterized by large–size euhedral subhedral calcite crystals (Flügel, 2004). It is the second most observed common type in the Derdere Formation in the outcrop and borehole sections, forming a mosaic of crystals that have roughly the same diameter in all directions. It is thought to form in a freshwater phreatic zone (Longman, 1980).

4.2.4 Neomorphism

The neomorphism described involving all transformations between one mineral and itself or a polymorph (Folk, 1965). Meteoric phreatic conditions are thought to be a lineage of neomorphism in marine sediments (Longman, 1980). Most of the neomorphism is of aggrading type, leading to an increase in crystal size, and this occurs chiefly in fine–grained limestone. On the other hand, degrading neomorphism, leading to a decrease in crystal size, is also present in the studied rocks.

In the Derdere Formation, neomorphism process affects skeletal grains and micritic matrix. Their impact on skeletal grains renders them difficult to determine while in the bioclastic, either as inversion the aragonite into calcite or changing the calcite to another calcite that called recrystallization, both types completed during dissolution and re–precipitation processes (Longman, 1982). In shallow marine environments, the neomorphism process intensifies greatly by the solution under higher temperature and pressure conditions (Flügel, 2004). The intensity in this process is inversely proportional to the ratio of the presence of the muds; whenever the proportions of the muds increase, and the recrystallization process decreased, where the muds impede the recrystallization process (Marschner, 1968).

4.2.5 Dolomitization

It is the process by which the dolomite is formed when magnesium ions replace calcium ions in calcite. The early dolomitization occurs by the replacement of precipitated micrite from seawater rich in magnesium ions and contact sediments before their lithification, where calcium ion is replaced by magnesium ion that existed in the seawater, or through the mixing of interstitial water between the particles with fresh water after the exposure of sediment to the air, resulting in increased magnesium ion and decreased calcium ion, thus dolomite is formed.

Three types of dolomitization were recognized within the Derdere Formation formed by different mechanisms (Xenotopic, Hypidiotopic, and Idiotopic dolomite), this corresponds to the dolomite formed at the dolomitic limestone microfacies in the Derdere Formation, which reflects the shallow conditions which are formed due to the mixing of the cosmic freshwater and the marine water found in the pores of the rocks causing the process of complete dolomitization. Generally, the dolomitization process within Derdere Formation did not clearly affect reservoir quality, because most of the dolomite formed was associated with stylolite.

4.2.6 Stylolites and Dissolution Seams

In the last stage of diagenesis, the compaction increases as a result of overburden pressure or due to tectonic stress. In the initial stages, the process of compaction involves the expulsion of liquids that occupy the pores between the grains and, therefore, reduce the primary porosity of the sediments.

Stylolites are very common in the limestones of the Derdere Formation. Even at first glance, it is evident that in limestones without and/or only with minor amounts of allochems stylolites with very low amplitudes and a stylolite plane parallel to the bedding plane are predominantly developed. By contrast, in limestones with abundant allochems, the spatial distribution and the size of the allochems, in general, seem to influence higher amplitudes and different spatial distribution of stylolites. Furthermore, the varying influences of vertical overburden and of tectonic stress–fields with different orientations influence the types of stylolites markedly.

CHAPTER 5

DEPOSITIONAL ENVIRONMENTS

5.1 Depositional and Palaeoenvironmental Scenario

The overriding controls on carbonate deposition are tectono–eustatic, which are together control fluctuations in sea–level. These settings include a shelf, ramp, epeiric platform, isolated platform, and/or drowned platform. Climate controls water circulation patterns, temperature, salinity, nutrient supply, storm, and current strengths, and wave activity (Tucker and Wright, 1990; Markello et al, 2008). Three major carbonate ramp depositional subenvironments are recognized: (1) wave–dominated inner ramp above fair–weather wave base, (2) middle ramp below fair–weather wave base, and above storm wave base, and (3) outer ramp below the storm–wave base, open marine (Burchette and Wright, 1992), The microfacies characteristics have allowed a good understanding of the Cenomanian–Turonian carbonate ramp, as explained in the figure 5.1.

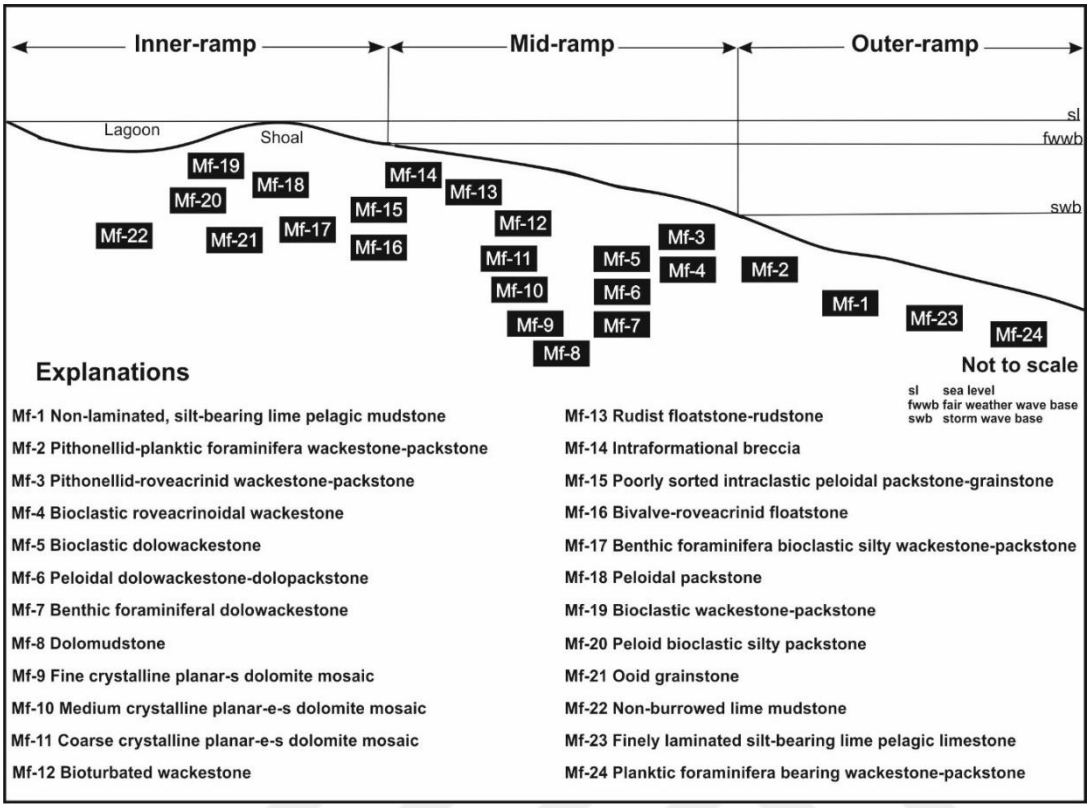


Figure 5.1. Distribution of microfacies types and depositional environments of the Derdere, and Karababa–A Member in the carbonate ramp model.

5.1.1 Middle–Late Cenomanian

All the study boreholes are scattered over SE Turkey; therefore, I can assume that the roveacrinoidal material, found as crumbled and disarticulated pieces within mudstone facies, provides fair and reliable insights about the roveacrinoidal population during the middle Cenomanian: the roveacrinoid skeletons were not transported far away, even stirred by weak bottom currents, and locally dismantled, and scattered within mud–supported sediments. Roveacrinids, as well as saccocomids, were hemipelagic to pelagic organisms, with possible escape response to escape predators. Subsequently to their early planktonic larval stage inducing a wide dispersal of any echinoderm brood, these roveacrinoidal relics can be regarded as potential biostratigraphic index species, and environmental proxies as well (Mülayim et al. 2018). Since they are usually found associated with pithonellids, and their own abundance occurrences are positively correlated with those of first–level, surface carbonate producers (blooms of

calcareous dinocysts, pithonellids, and heterohelicidids; Ferré 1997), they have been regarded as opportunistic organisms. The Upper Cretaceous rocks of SE Turkey show unexpectedly the dual presence of roveacrinids and saccocomids. Since roveacrinids have been found so far over the Arabian Platform more frequently in carbonate–grained, open–ramp marine environments, their co–occurrence advocates for a mixed environment or, at least, supports that saccocomids were swept secondarily from a shallower but quieter environment.

5.1.2 Latest Cenomanian

In the İnişdere stratigraphic section, the Derdere Formation represents typical inner ramp deposits. In the upper part of this formation abundant peloids, intraclasts and shallow–water bioclasts (i.e. benthic foraminifera, bivalves, dasycladalean algae) are present, as well as spar cementing, indicating a shallow water environment. In the upper part of this formation a ramp environment has been inferred from the Derdere Formation microfacies characterized by peloids, and shallow–water bioclasts. In this section, ooids are missing, replaced by peloids and shallow–water bioclasts in the upper part, illustrating the transition from the relatively peloidal shoal. In summary, the microfacies assemblage in the Derdere Formation indicates a rather quiet environment before the drowning event, in relation to the low relative sea–level and broadly flat terrain with a non–slope break at that time.

In the Sabunsuyu stratigraphic section, the most prominent rocks in the stratigraphical interval studied are characterized by rudist–dominated, fine– to coarse–grained lithologies, which are made up of intense fragmentation of bioeroded mollusc shells (Figure 5.2). Hermatypic corals and green algae disappear almost completely at this level (Mülayim et al., 2020). Non–skeletal grains (predominantly peloids) are common. Planktonic foraminifera is generally rare throughout the section, but abundantly present at some levels. The matrix is fine– to coarse–grained and ranges from wackestone to floatstone with a wide range of skeletal particles. These sediments were produced in situ on the ramp on which rudist and bivalves were the primary sediment producers. The rudist–bearing limestones formed under slightly, moderately and strongly agitated water conditions. The presence of limestones with identifiable

rudists, bivalves and roveacrinids, alternating with bioclastic limestones including intensely fragmented shells of rudists, bivalves and gastropods, document occasional changes in energy conditions on the carbonate ramp, triggered by storm activity. Rudists and other bivalves were actively moved by currents, waves and storms, causing fragmentation and transportation, albeit not far from their original environment. The presence of some limestones with planktonic foraminifera illustrates the effects of occasional open–marine connections within the proximal parts of the outer–ramp.

Rudist–bearing limestone sequence of the Sabunsuyu section presents close similarities in terms of features such as alternation and changes of depositional conditions with those of the central Apennines (Carbone et al., 1971) and may also be correlated with the central and eastern regions of the northern Mediterranean Province (Philip, 1980; Özer, 1988; Philip and Mermigis, 1989; Carbone, 1993; Sartorio et al., 1992; Cestari and Sartorio, 1995; Laviano et al., 1998a, b; Steuber, 1999; Di Stefano and Ruberti, 2000; Stössel and Bernoulli, 2000; Korbar et al., 2001; Sarı, 2006a, b; Parente et al., 2007; Sarı and Özer, 2009; Sarı et al., 2009; Cestari and Laviano, 2012; Troya et al., 2011; Frija et al., 2015) and the Gulf of Mexico (Scott, 1990). However, high–energy platform margin depositional environments have been proposed in those studies, rather than the carbonate ramp depositional conditions presented here.

There are lithological similarities of the Sabunsuyu stratigraphic section with those described in previous studies, in southeast Turkey (Cros et al., 1999), but fossil contents of the Derdere and Karababa formations included essentially planktonic foraminifera, but rudists and other taxa were not described nor recorded. Therefore, features of depositional settings in those studies contain missing data for the Derdere and Karababa formations. These units have recently been studied in southeast Turkey by Cros et al. (1999), Mülayim et al. (2018, 2019a) and Özkan and Altıner (2018), who proposed a carbonate ramp process; this shows some resemblances with that of the Sabunsuyu section. However, rudist–bearing limestones were not clearly indicated and determined by those authors; our own observations have documented the presence of identifiable rudists in the same area (Yılmaz et al., 2019; Özer et al., 2019a, b). The lithological and depositional features of the Sabunsuyu section, such as the upper

Cenomanian rudist–bearing, platform–type carbonates and the Turonian pelagic condensed limestone sequence, show clear similarities to those of the İnişdere stratigraphic section in southeast Turkey, recently presented by Mülayim et al. (2019a). The presence of a hardground surface between the upper Cenomanian rudist–bearing limestones and the Turonian pelagic limestones in the Sabunsuyu stratigraphic section can be compared with the "drowning unconformity" of the İnişdere stratigraphic section of Mülayim et al. (2019a), thus illustrating the same change in depositional conditions. A similar hiatus has been recorded from the Arabian Plate (Sharland et al., 2001; Haq and Al–Qahtani, 2005; Haq, 2014) and also Egypt (Bauer et al., 2003). The Bey Dağları Carbonate Platform (BDCP; southwest Turkey) comprises middle–upper Cenomanian rudist–bearing limestones as well. However, the BDCP succession differs from the Sabunsuyu sequence as the Cenomanian rudist–bearing limestones of the former do not show any pelagic incursion and are overlain by Turonian rudist–bearing neritic limestones in the northern part (Sarı et al., 2004, 2009; Sarı, 2006b; Sarı and Özer, 2009), where Turonian neritic limestones are overlain by Coniacian–Santonian pelagic limestones with planktonic foraminifera (Sarı, 2006a, 2009). However, neritic conditions prevailed throughout the Late Cretaceous in the southern part of the platform (Susuzdağ area), which includes Santonian–lower Campanian rudist–bearing limestones (Sarı et al., 2009; Sarı and Özer, 2009) which could be correlated with the Santonian rudist–bearing limestones of the Sabunsuyu succession.

The upper Cenomanian rudist–bearing limestones of the Sabunsuyu section show similarities to those of Jordan (Schulze et al., 2003, 2004; Bandel and Salameh, 2013; Özer and Ahmad, 2015, 2016), Egypt (Bauer et al., 2004; Salama et al., 2016; Farouk et al., 2017; Abdel–Fattah et al., 2018) and Tunisia (Razgallah et al., 1994; Chikhi–Aouimeur et al., 2006). However, the Turonian limestones of the Sabunsuyu section differ from those of the Afro–Arabian platform (Syria, Iraq, Jordan, Iran, Egypt, Tunisia) in the absence of rudists.

5.1.3 Early Turonian

The overlying Karababa–A Member represents an outer ramp environment below the storm wave base, as evidenced by the presence of planktonic foraminifera and pithonellids throughout the member. It is considered herein to be equivalent in Türkoğlu, İnişdere, and Sabunsuyu stratigraphic sections. Thus, this facies indicates that low sedimentation rates and high sea–level, in general, characterized this transitional stage. The palaeotopography has been interpreted as gentler according to the monotonous microfacies. This change probably resulted from a relative sea–level rise. It covered the platform carbonates thickening substantially southwards. Compared with the Derdere Formation, the microfacies changes within the Karababa–A Member are abrupt and pronounced. Importantly, the microfacies in the Karababa–A Member are distinguished from each other mainly according to the types and contents of bioclasts because the environment changed abruptly over a considerable lateral extent.

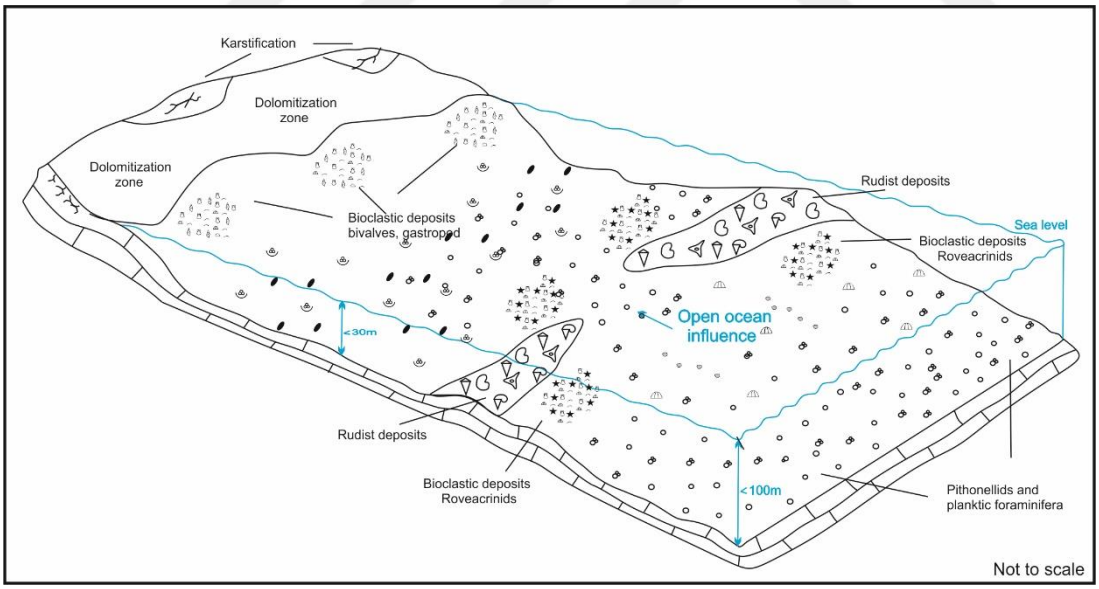


Figure 5.2. Block diagram showing the interpretation of the Cenomanian depositional environments in the study area in SE Turkey in the northwestern part of the Arabian Carbonate Platform.

5.2 Palaeoenviromental Change Across the Cenomanian–Turonian Boundary

There is a close relationship between the changes in the fossil assemblages and the drowning of the northwestern part of the Arabian Carbonate Platform. Carbonate sedimentation is represented by the abundance of large benthic foraminifera, mollusc and calcareous algae. These groups were very important carbonate producers during the Cenomanian time interval. Extensive shallowing during that time, favoring the deposition of intertidal–supratidal facies deposited during short subaerial exposure of some parts of the carbonate ramp platform is observed (Mülayim et al. 2016). Exposure to extensive areas of carbonate ramp platform would have represented a drastic reduction of the habitat of benthic organisms, resulting in competition for space and nutrients. This might have forced some species into extinction, at least on a basinwide scale. The establishment of open marine conditions that occurred with the subsequent relative sea–level rise might have had an additional negative effect on the surviving organism, triggering more extinction. Rates of relative sea–level rise increased during the early stages of the *W. archaecretacea* PRZ.. During that time, the carbonate ramp platform was drowned. These rocks show an increasing proportion of open marine organisms, still under oligotrophic conditions. Few benthic foraminifera survived into this stage. Bioclasts were dominated by mollusc fragments. The lower part of *W. archaecretacea* PRZ probably indicates a transitional (mesotrophic) stage between oligotrophic and eutrophic conditions (Hallock et al 1988). This is mainly represented in the central and eastern parts of the platform, where shallow marine sedimentation continued after the drowning of the northwestern parts. Alternating beds containing a more diverse fossil community with, mollusc, and echinoderm indicate fluctuating nutrient levels. The deposition of facies rich in non–keeled planktonic foraminifera in the northwestern and western part at that time might indicate the invasion of cooler waters that could also affect carbonate producers. Mesotrophic–eutrophic conditions seem to have been established close to the C–T boundary. Abundant pithonellids, non–keeled planktonic foraminifera, and echinoderms dominated sediments deposited during that time (Figure 5.3). This degradation of the environment further affected the carbonate producing benthos and reduced carbonate accumulation rates that, combined with the relative sea–level rise,

forward a deepening of the environment. Pelagic conditions expanded southward during the early Turonian. Poor oxygenation of seawater around the sediment–water interface is interpreted from the lack of bioturbation that preserved a very fine lamination. Hedbergellids, heterohelicids, whiteinellids, and occasionally roveacrinids are the main constituents in these rocks. Toward the middle Turonian, more oligotrophic conditions were established and keeled planktonic foraminifera became more common (Figure 5.3) (Premoli–Silva and Silter, 1994).

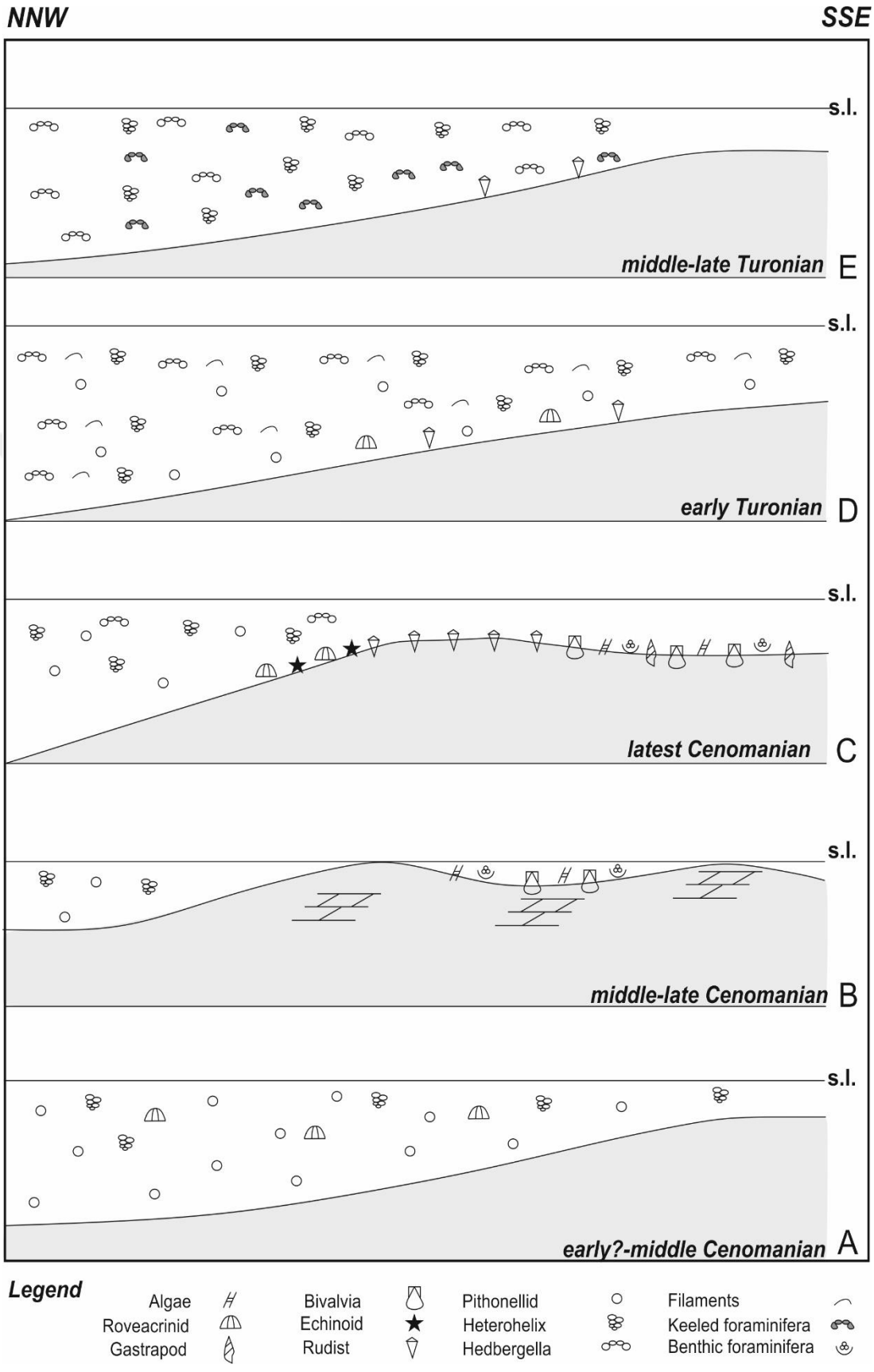

NNW
SSE
s.l.
middle-late Turonian
E
s.l.
early Turonian
D
s.l.
latest Cenomanian
C
s.l.
middle-late Cenomanian
B
s.l.
early?-middle Cenomanian
A
Legend
Algae
Roveacrinid
Gastrapod
Bivalvia
Echinoid
Rudist
Pithonellid
Heterohelix
Hedbergella
Filaments
Keeled foraminifera
Benthic foraminifera

Figure 5.3. Cenomanian–Turonian palaeoecological evolution of the northwestern part of the Arabian Carbonate Platform. A. The establishment of open marine conditions are reflected by the abundance of pithonellids and planktonic foraminifera. B. Short and limited subaerial exposure reduced benthic habitat and might have led to the extinction of several groups of large benthic foraminifera. C. Carbonate sedimentation is represented by the abundance of benthic foraminifera, mollusc and calcareous algae. The restricted open marine condition led to the progressive eutrophication of the shallow environment. D. Extinction and eradication of carbonate producers reduced the sedimentation rate. A relative rise in sea–level led to the deeper of the environment and the deposition of pelagic facies. E. Oligotrophic conditions were established as indicated by the presence of keeled planktonic foraminifera at middle–late Turonian.

CHAPTER 6

SEQUENCE STRATIGRAPHY

A sequence stratigraphic study has been carried out in order to discover the signals of the Cretaceous eustatic event in SE Turkey and eventually improve the chronostratigraphic frame of the Cenomanian–Turonian carbonates. Despite the fact that the depositional features of sedimentary packages in the Cenomanian–Turonian carbonates are sometimes strongly masked by dolomitization enough stratigraphic, paleontologic, and sedimentological data are available to identify the genetically related depositional sequences during sea–level cycles. Among the studied, the Sabunsuyu and İnişdere stratigraphic sections, which comprise the Cenomanian–Turonian carbonates has been selected for the sequence stratigraphic study. In this section eustatic signals have been recognized in the Derdere formation and Karababa–A Member ranging in age from the middle Cenomanian to the late Turonian.

6.1 Sequence Stratigraphy Framework of the Sabunsuyu Section

On different scales, the various sequences may have resulted from fluctuating eustatic sea–levels and local tectonics. The hardground surfaces recorded during fieldwork (i.e., pink ferruginous hard crusts), combined with vertical facies evolution, are here used to interpret sequence boundaries (SB). Moreover, major facies shifts from shallower– to deeper–marine carbonate facies indicate sequence boundaries. In total, three sequence boundaries have been identified in this succession; two in the Cenomanian (SB Ce 1–2) and one in the Turonian (SB Tu 1) (Figure 6.1). These unconformities define a corresponding number of 3rd–order depositional sequences

(sensu Posamentier et al., 1988; Vail et al., 1991) that commonly consist only of transgressive (TST) and highstand systems tracts (HST) due to a lack of accommodation space during falling and low sea–level stands. In the study area, I have subdivided the Cenomanian–Santonian succession into three sequences (Figure 6.2).

6.1.1 Depositional Sequence 1

In the outcrop studied, the base of Sequence 1 (SB 1) is at the upper Albian–middle Cenomanian boundary. This sharp boundary separates the upper Albian–lower Cenomanian Sabunsuyu Formation (very thick dolomitic beds) from the overlying middle–upper Cenomanian Derdere Formation (thinner limestone and calcareous shale beds). This sequence is delineated at the base by the middle–upper Cenomanian sequence boundary (SB 1) (Figure 6.1). where it is overlain by levels with *Asterohedbergella asterospinosa* of middle–late Cenomanian age. The basal sequence boundary (SB 1) is the unconformity between the Sabunsuyu and Derdere formations. This unconformity is characterized by the presence of a sudden facies shift from dolomites to limestone and by the presence of dissolution vugs indicating exposed conditions. In the Cenomanian succession exposed at Kilis city (southeast Turkey), the correlative upper Albian–middle Cenomanian boundary has already been identified by Cros et al. (1999). The TST facies is composed mainly of outer–ramp facies laminated/non–laminated, silt–bearing limy mudstone). The TST is marked by a small influx of siliciclastics that consist of calcareous shale with exogyrine oysters. In the Sabunsuyu section, the HST is composed mainly of limy mudstone and dolostone facies, intercalated with chert bands and nodules. The upper part is represented by aggradational stacking of shallow–ramp facies with quartz–dominated inputs in subfacies. It is marked by the presence of intensive dissolution and dolomitization. The dolostone package resulted from aggradation when accommodation space was filled as rapidly as it was created so that water depth remained relatively constant.

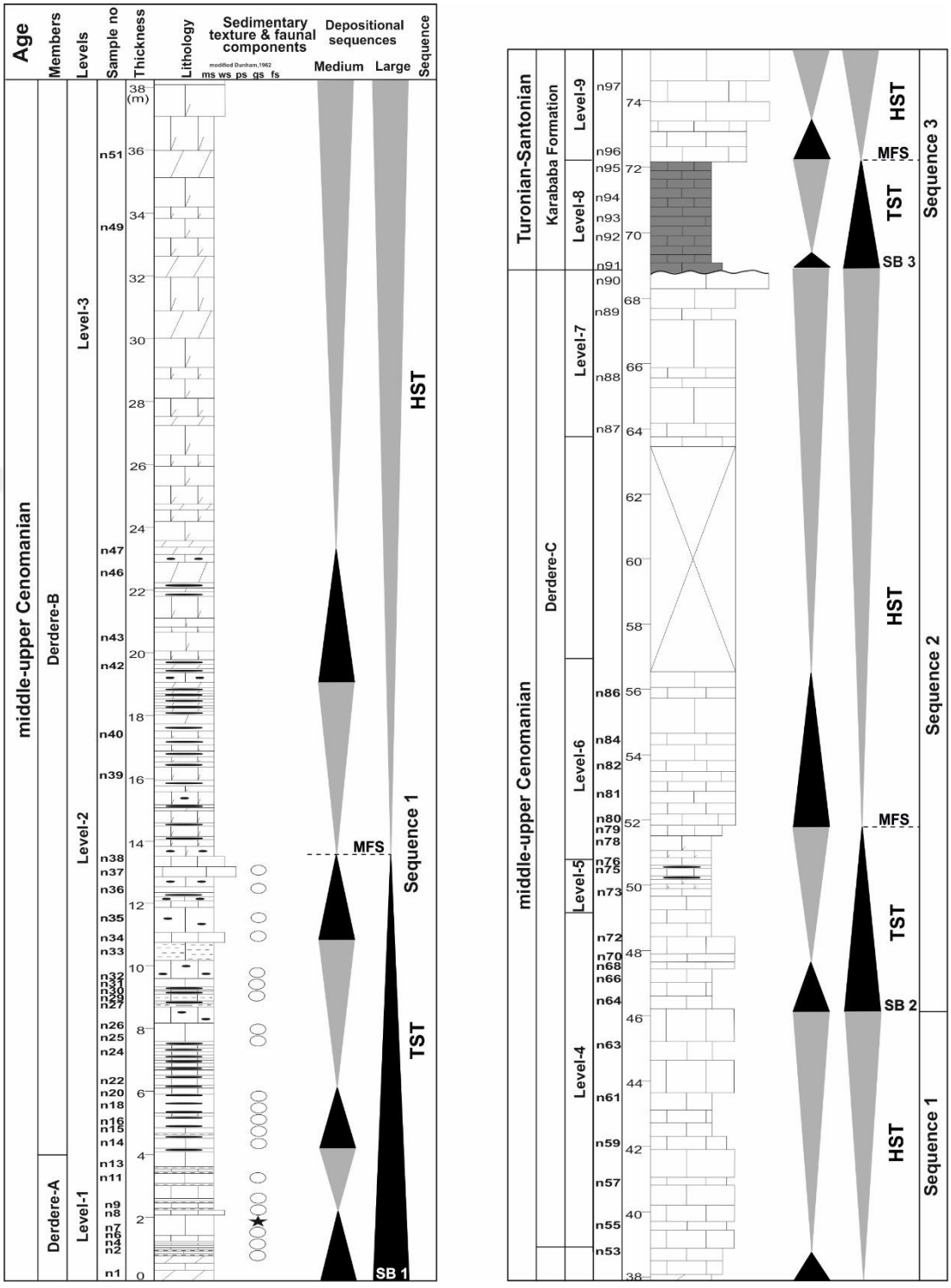


Figure 6.1. Sequence stratigraphical construction of the Sabunsuyu stratigraphic section showing systems tracts, sedimentary packages and important surfaces (from Mülayim et al., 2019a).

6.1.2 Depositional Sequence 2

This sequence is bounded at the base by sequence boundary 2 (SB 2), (Figure 6.1) which is characterised by the presence of rudist rudstone facies. Aggradational to progradational stacking patterns identify the HST in sequence 2. During the HST, the first rudist–bearing cycle formed and prograded basinward. The HST of the large–scale sequence 2 represents the second rudist–bearing cycle during the aggradation of the carbonate ramp. The rudist–bearing cycles are identified within this systems tract and go through an ideal vertical shallowing upwards from slightly low–energy to high–energy mid–ramp facies. Petrographic descriptions for this systems tract show that it comprises two shallowing–upward parasequences. The first rudist–bearing cycle was laid down during progradation and consists of limestone with planktonic foraminifera and roveacrinids, shallowing up into rudist rudstone with benthic foraminifera and gastropods, forming the upper medium–scale sequence (Mülayim et al. 2020). The rudist assemblage in HST of the Sabunsuyu section includes *Sauvagesia* sp., *Durania* sp., *Biradiolites* sp., *Durania acuticostata, Sauvagesia sharpei* and *Bournonia*? sp. (Mülayim et al. 2020). The second rudist–bearing cycle consists of limestone with echinoids and roveacrinids followed by massive rudist–bearing limestone stacked in an aggrading pattern. The foraminifera includes *Meandrospira* sp., *Dorothia* sp., Gavelinellidae, and Lenticulinidae; associated are bivalves and gastropods, all reflecting deposition in shallow water during the HST of sequence 2. In the Sabunsuyu section *Caprinula* sp. (*C.* cf. *sharpei*), *Sauvagesia* sp., *Radiolites* sp. and *Ichthyosarcolites triangularis* are in the HST of the upper sequence 2. The capping rudstone in both rudist–bearing cycles formed under decreased water depths due to either aggradational growth of the rudist lithostrome and/or a sea–level fall. The transition from progradational early highstand to aggradational late highstand is recorded by a hardground surface at the top of a massive rudist–bearing limestone. The rudist accumulation was able to keep up with the increase in accommodation during early highstand sea–level rise. The TST facies begins with bioclastic packstone in the Sabunsuyu section. These facies are overlain by quiet, open rudist floatstone/rudstone facies, which is intercalated with bioclastic wackestone. The MFS is at the top of a highly fossiliferous limestone bed with roveacrinids, echinoids,

pithonellids, and planktonic foraminifera, that indicate relatively deeper mid– to outer–ramp environments.

6.1.3 Depositional Sequence 3

Sequence boundary 3 lies at the base of Sequence 3 between the middle–upper Cenomanian Derdere Formation and the Turonian–Santonian Karababa Formation (Figure 6.1). These deposits comprise the TST of Sequence 3 and are characterized by glauconite, pinkish iron crust, and bioturbation which indicate condensation. In the Sabunsuyu section, the boundary is distinguished by a hardground. The transgressive systems tract is marked by mide to outer–ramp deposits of limestone containing pithonellid and planktonic foraminifera. The drowning of the platform during the early Turonian is interpreted to be the result of a longer–term relative sea–level rise. During the TST, acceleration in the rate of relative sea–level rise led to the deposition of a retrogradational component rich in planktonic foraminifera, pithonellids and roveacrinids of mid– to outer–ramp environments. The change from TST to HST is represented by the transition from retrogradational to progradational sedimentation patterns. The maximum flooding surface in this large–scale sequence is best placed at the top of the mid– to outer–ramp facies of the maximum flooding interval. The highstand systems tract is composed of a shallowing–upwards (prograding) parasequence set that formed due to normal regression during a sea–level highstand. The relative fall/still stand in sea–level led to formation of late HST deposits with shoal facies prograding basinwards. Thus, the HST is characterised by a predominance of high–energy packstone and rudist rudstone facies, which contain numerous skeletal fragments (i.e., *Bournonia excavata*, *Apricardia* sp. and indeterminate bivalves). The HST deposits are mainly peloid silty bioclastic packstone and echinoderm/ benthic foraminifera–bioclastic packstone intercalated with mudstone. These bioclastic packstones, interpreted as storm layers (Aigner, 1985), are common but usually amalgamated with wavy beds of graded bioclastic material. In fact, during these phases of base–level highstand, these deposits contain numerous echinoids which indicate a change from moderate energy of the mid–ramp to high–energy shoal facies.

6.2 Sequence Stratigraphical Comparison for Sabunsuyu Section

The sequence–stratigraphical framework of the middle–upper Cenomanian–Santonian succession in the Sabunsuyu section has been compared with schemes Schulze et al. (2003), Sharland et al. (2004), Haq and AleQahtani (2005), Saber et al. (2009), Haq (2014) and Mülayim et al. (2016) (Figure 6.2). Their correlation incorporates the stratigraphical succession of the Sabunsuyu section and positions of the SBs recognised in the study area. Depositional sequence 1 is the thickest sequences in the middle to upper Cenomanian of the Sabunsuyu section. I interpret this thickness increase to reflect prolonged duration of the sea–level in highstand position on the Arabian Platform due to a 2 nd–order rise of sea–level from the middle to late Cenomanian (Haq, 2014). Thus, this global signal probably controlled the sedimentation rate in this time interval and carbonate production increased in the outer– to mid–ramp highstand carbonate deposits (Mülayim et al., 2016). Despite the thickness reduction and the effect of dolomitization which masked the original depositional texture and composition of the depositional sequences in the Cenomanian, palaeontological data for depositional sequence 1 enabled us to correlate with Haq (2014) and recognise the middle Cenomanian sequence boundary (SB2) in the study area. This is also correlated with SB2 in northern Sinai (Saber et al., 2009), CeJo3 in Jordan (Schulze et al., 2003, 2005) and KCe4 of Haq (2014) (Figure 5.2). Following the mid–Cenomanian regression, sea–level rise during the late Cenomanian and early Turonian led to deposition of transgressive systems tract of the second sequence. This system tract is mainly characterised by mid–outer ramp facies rich in planktonic foraminifera and pithonellids. Depositional sequence 2, well exposed in the field, displays evolution from outer– to mid–ramp deposition and is abruptly overlain by pelagic deposits of the Karababa A and B members, signalling the changing rates of subsidence in the Arabian Platform and the onset of tectonic events. The upper Cenomanian–lower Turonian transgression is assumed here to correlate with the eustatic sea–level rise of Haq (2014) and regional deeping in the adjacent shelf area in Jordan (Schulze et al., 2003, 2005) and the Arabian Peninsula (Sharland et al., 2001). The upper part of this facies (late Cenomanian) was considered by

Mülayim et al. (2019a and b) to reflect the Oceanic Anoxic Event 2 (OAE 2) in the Inişdere and Türkoğlu sections.

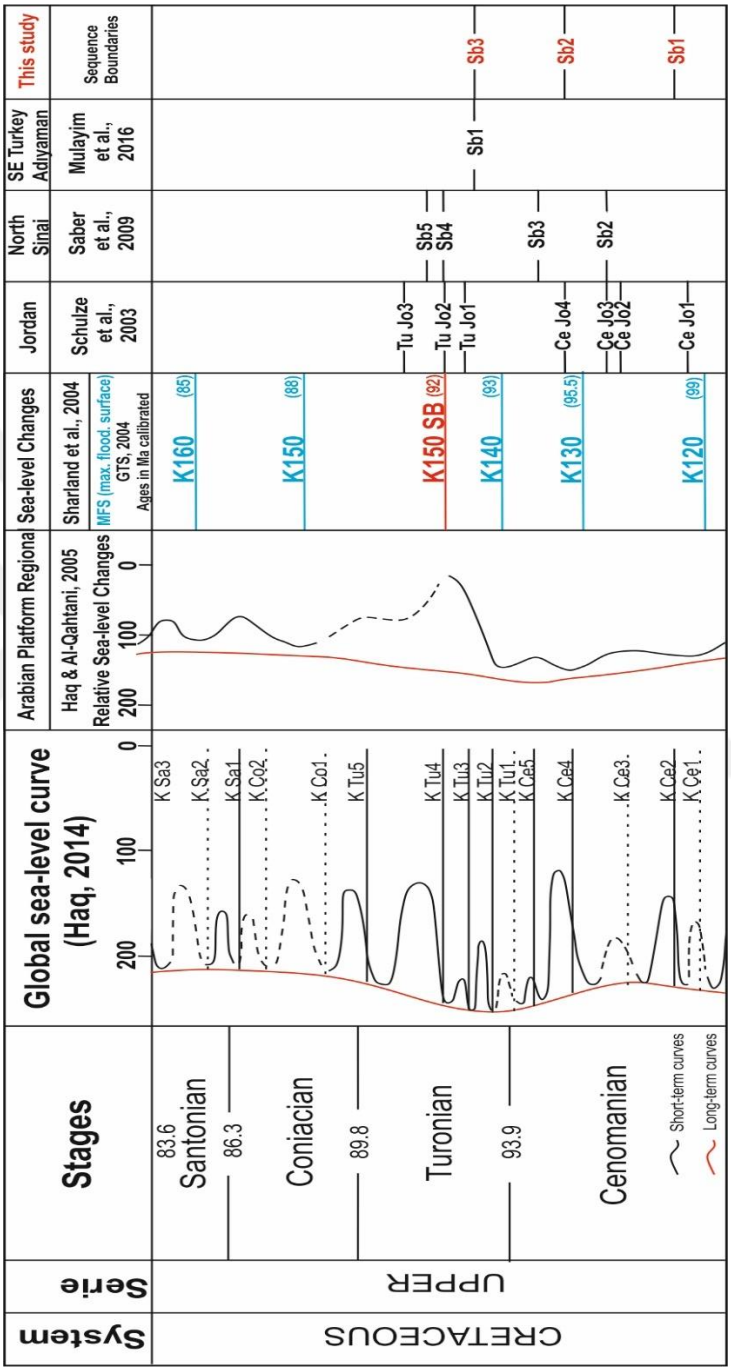


Figure 6.2. Comparison between sequence boundaries of the present study with others in neighbouring areas and with the global eustatic scheme of Haq (2014).

6.3 Sequence Stratigraphy Framework of the İnişdere Stratigraphic Section

A major eustatic rise is generally interpreted to have occurred across the CTBE (Haq et al., 1988; Haq 2014). The changes from benthic dominated biota assemblages to planktonic assemblages near the CTBE suggest that this sea–level rise played a significant role in the drowning of the northern Arabian Platform. The first phase of drowning (initial drowning) is materialized by the lower bedded limestone of the Derdere Formation, rich in benthic foraminifera, mollusc, rudists and dasycladalean algae (Figure 6.3). This indicates deposition in the upper part of the photic zone. Such depositional facies may be controlled by moderately increasing rates of sea–level rise and considered as the upper part of the highstand systems tract (Figure 6.3) in a sequence stratigraphic framework (Catuneanu et al. 2009, 2011). The highstand systems tract in the area is marked by transition from shallow subtidal to intertidal facies, which reflects the overall shallowing–upward trend during this regressive phase. Complete drowning occurred slightly above the CTBE (base of Karababa A–Member) and brought the carbonate platform below the euphotic zone. This drowning is recorded by the upper condensed laminated limestone succession in which planktonic foraminifera predominates (Figure 6.3). Such a depositional facies seems to be related to rapidly increasing rates of sea–level rise, and then represents the upper part of a major transgressive systems tract (TST, Figure 6.3). The TST interval of this sequence consists of sediments including deeper pelagic limestone and foraminifera bearing wackestone/packstone beds. The maximum marine flooding and subsequent total drowning of the carbonate platform were materialized by the accumulation upon the surface of the Karababa–A Member (Mülayim et al. 2019a). According to Mülayim et al. (2016), in SE Turkey, the CTBE coincides with the maximum flooding surface (MFS) between the transgressive systems tract and the highstand systems tracts of a depositional sequence correlative with the third–order eustatic cycle UZA–2.5 of Haq et al. (1988); these systems tracts are respectively represented by the Derdere Formation and Karababa–A Member (Figure 6.3).

The ramp stage in the lowest part of the Karababa–A Member represents the upper part of a TST, with a condensed section, showing that the carbonate platform may have drowned abruptly. The Karababa–A Member was under the control of a regional

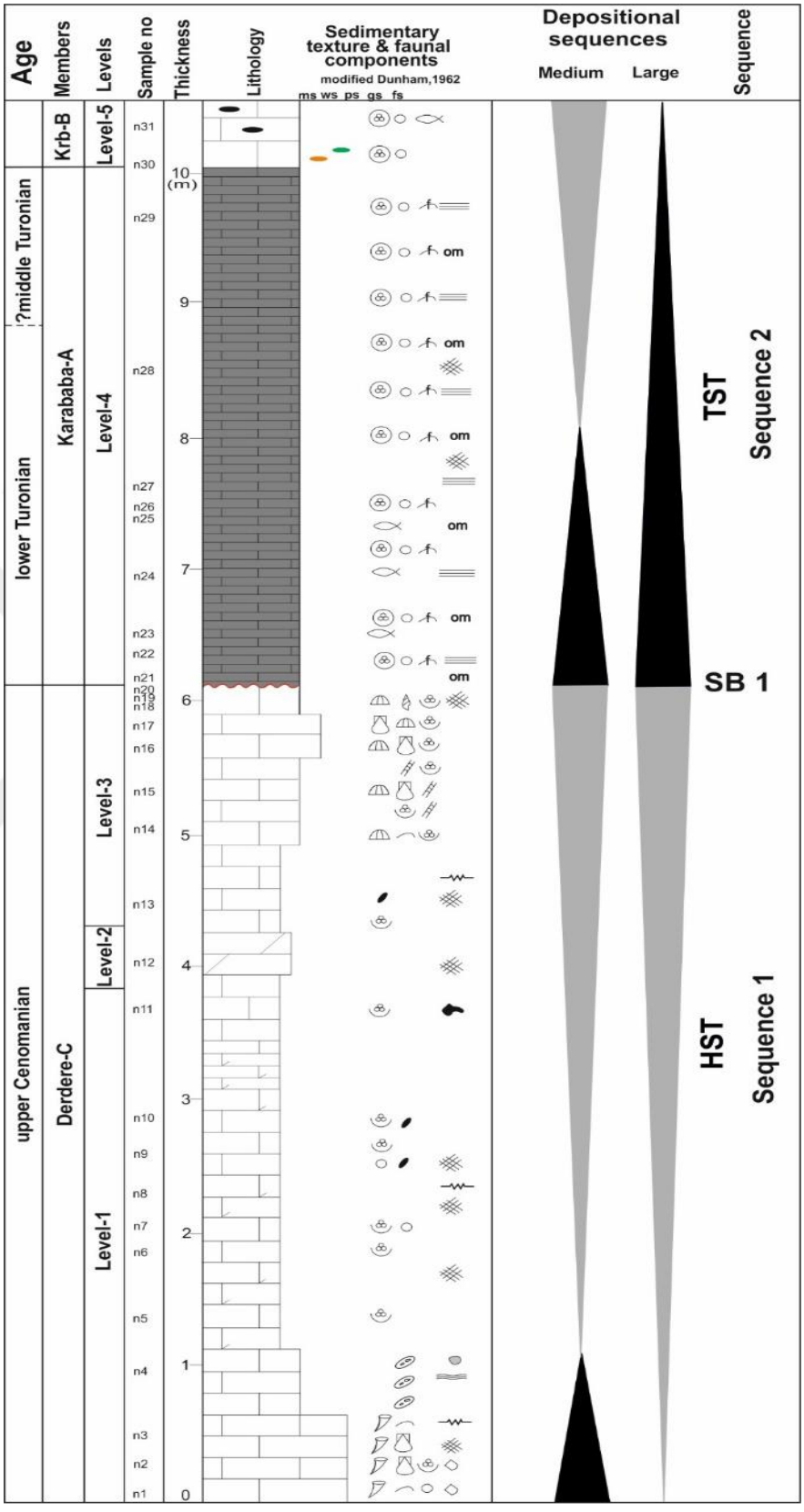


Figure 6.3. Sequence stratigraphical construction of the İnişdere sttratigraphic section showing systems tracts, sedimentary packages and important surfaces.

and even global sea–level fluctuation. Although the tectonic setting changed during this time interval, its effect was probably less and not enough to induce platform drowning (Sharland et al. 2001). More importantly, as mentioned before, the transgressive event at the base of the Karababa–A Member is correlated to a major eustatic sea–level rise above sequence boundary KTu 4 (91.8 Ma (Haq 2014).

6.4 Sequence Stratigraphical Comparison for İnişdere Stratigraphic ection

As in other parts of the Arabian Plate, only spotty age control is available currently for the upper Cenomanian–Turonian rocks in the study area. However, the available palaeontological and stable isotope data show that the Derdere Formation and Karababa–A Member of the Karababa Formation were deposited during the time interval of the late Cenomanian–early Turonian, based on an assemblage of benthic and planktonic foraminifera. The Cenomanian–Turonian interval in the study area has a good match with the sequence stratigraphy of the Arabian Plate (Sharland et al. 2001; Haq and Al–Qahtani 2005) and with the global curve of Haq (2014) (Figure 6.4). The Derdere Formation represents the upper part of the regressive cycle, comprising the whole regressive facies cycles. Based on correlation (Figure 6.4), the MFS is the earliest Turonian

Karababa–A Member MFS and considered here to be equivalent to the MFS K140 (the maximum flooding surface of Sharland et al. 2001). In addition, this surface matches well with the MFS of the depositional sequence KTu 4 in the global curve of Haq (2014) (Figure 6.4). The good match of the recognized sequence stratigraphic surfaces with that of the Arabian Plate (Sharland et al. 2001; Haq and Al–Qahtani 2005) supports their eustatic origin. Differences in dating of these surfaces across the Arabian Plate (Figure 6.4) may be attributed to the scarcity of palaeontological markers owing to lithological control in the strata representing the respective time interval. In addition, any missing middle Turonian sealevel fall event (i.e. KTu 2 of Haq 2014) in SE Turkey may be the result of limited age dating and/or local tectonic effect and/or possible superimposition of several short–time sea–level falls in this time interval.

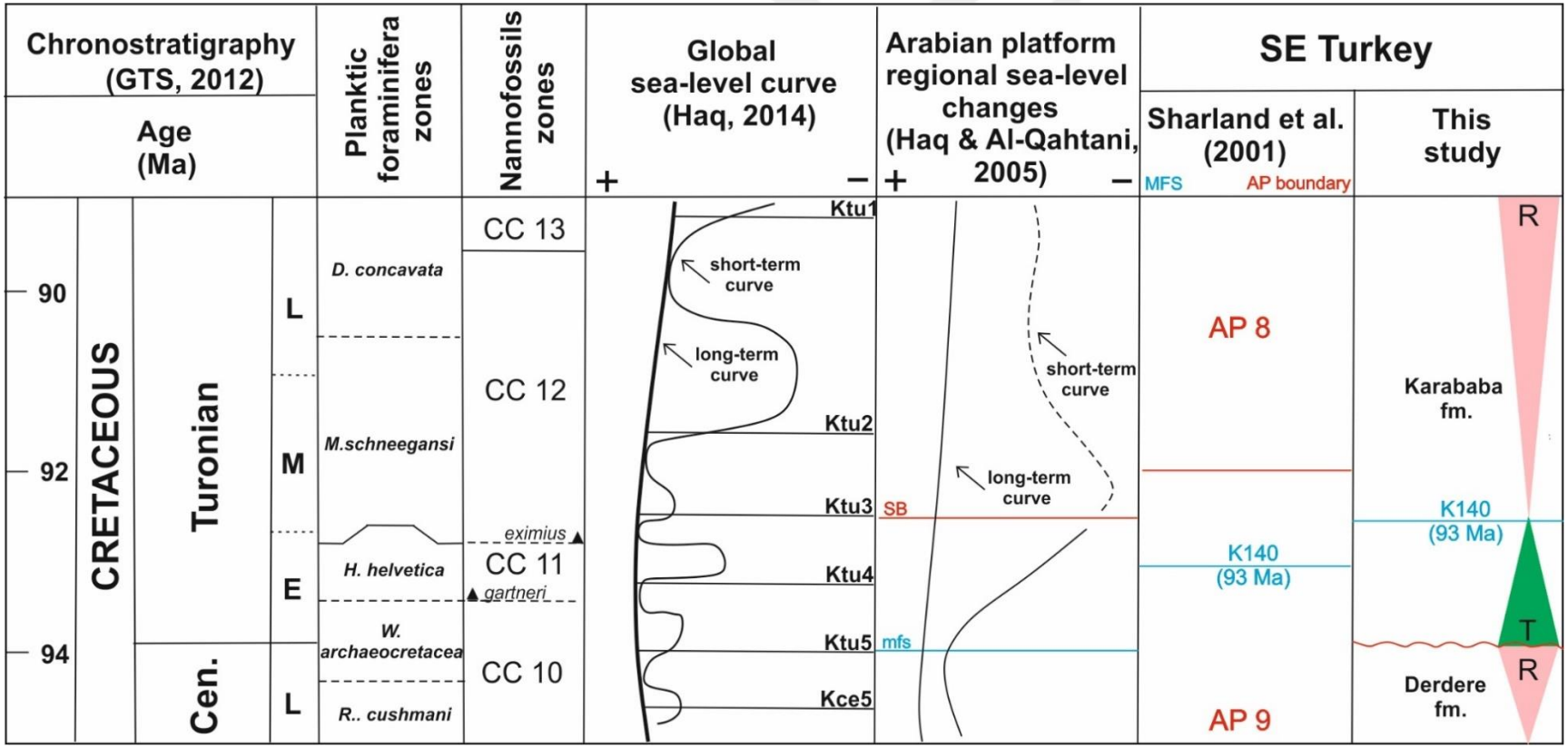

Chronostratigraphy (GTS, 2012)
Age (Ma)
Planktic foraminifera zones
Nannofossils zones
Global sea-level curve (Haq, 2014)
+
–
Arabian platform regional sea-level changes (Haq & Al-Qahtani, 2005)
+
–
SE Turkey
Sharland et al. (2001)
MFS
AP boundary
This study
90
92
94
CRETACEOUS
Turonian
Cen.
L
M
E
L
D. concavata
M.schneegansi
H. helvetica
W. archaeocretacea
R.. cushmani
CC 13
CC 12
CC 11
CC 10
eximius
gartneri
Ktu1
Ktu2
Ktu3
Ktu4
Ktu5
Kce5
short-term curve
long-term curve
short-term curve
long-term curve
SB
mfs
AP 8
AP 9
K140 (93 Ma)
K140 (93 Ma)
R
T
R
Karababa fm.
Derdere fm.

Figure 6.4. Correlation of the Cenomanian–Turonian of the study area with that of SE Turkey, global and Arabian Plate sea–level curve (Sharland et al. 2001; Haq and Al–Qahtani 2005; Haq 2014) and comparison of ages assigned to calcareous nannofossil (CC; Sissingh 1977) and planktonic foraminifer biozones used in Geologic Time Scale (GTS) 2012 (Gradstein et al. 2012). Underscored names to the right are for planktonic foraminifer zonal markers whose ages (in parentheses) are calibrated using biostratigraphic occurrence data from Caron et al. (2006) (from Mülayim et .al., 2019a).

CHAPTER 7

RECORDS OF CRETACEOUS OCEANOGRAPHIC ANOXIC EVENTS ON THE DROWNED ARABIAN PLATFORM

7.1 Drowning Platform

The term ‘drowning unconformity’ was introduced by Schlager and Camber (1986) for an unconformity created by the drowning of a carbonate platform and the subsequent onlap of siliciclastics or other non–platform deeper–water sediments. The concept of drowning unconformities is well established and there are many examples of carbonate platform drowning strata documented from the Mesozoic rock record (Schlager 1981, 1989; Erlich et al. 1990, 1993; Föllmi et al. 1994; Drzewiecki and Simo 1997; Weissert et al. 1998; Blomeier and Reijmer 1999; Ruiz–Ortiz et al. 2004; Föllmi and Gainon 2008; Marino and Santantonio 2010; Masse and Masse 2011; Godet 2013; Kalanat et al. 2015; Brandano et al. 2016; Sulli and Interbartolo 2016; Yılmaz et al., 2018).

Carbonate platforms are complex natural systems that are sensitive to a number of environmental–factors that may contribute to drowning, such as a sudden and rapid rise of relative sea–level. This also relates to recent global warming and the fate of today’s carbonate factories during future sea–level rise. In addition, environmental stresses that may lead to carbonate platform demise and the subsequent formation of drowning unconformities may also include oceanic anoxic events (OAEs), tectonics subsidence, flexural loading, hyper– and hyposalinity, change in carbon dioxide

content of the oceans or atmosphere, change in nutrient supply, temperature, hydrodynamics, turbidity, light penetration and evolutionary modification of biota (Hallock and Schlager 1986; Erlich et al. 1990, 1993; Schlager 1991; Thorne 1992). An abrupt change in lithology and fossil assemblages switch can occur at a single surface, which represents a drowning unconformity horizon (Schlager and Camber 1986; Schlager 1989).

The presenting outcrop evidence analogous to an interpreted drowning unconformity, its timing and the changes of biotic assemblages across the Cenomanian–Turonian Boundary Event(CTBE). Based on the sedimentary facies and stable isotope analysis, a relative sea–level curve for the Cenomanian–Turonian interval has been established. Sedimentological, geochemical and palaeontological data are evaluated in order to determine the effects of OAE 2 and the cause of subsequent carbonate platform drowning.

7.1.1 Drowning Unconformity

Drowning unconformities occur when the rate of sea–level rise exceeds the rate of carbonate production, and the platform is submerged below the photic zone (Schlager and Camber 1986; Schlager 1989, 1991). In this study, 'drowning unconformity' refers to a change from a shallow, benthic biota to a pelagic biota, which was necessarily caused by a relative sea–level rise along the carbonate ramp (Figure 7.1). Drowning unconformities have been interpreted as sequence boundaries by numerous researchers (Schlager 1989, 1991, 1992, 1993; Erlich et al. 1990, 1993; Campbell 1992). Schlager (1991) stated that 'a sequence boundary represents a geometrically manifest change in the pattern of sediment input and dispersal' and suggested that drowning unconformities are sequence boundaries. In the İnişdere section, the sequence boundary is recognized at the top of the Derdere Formation as the base of Karababa–A Member. It separates the shallow carbonate deposits of the upper Cenomanian and the deeper pelagic carbonate deposits of the overlying lower Turonian. This boundary is recognized as a drowning unconformity (Schlager, 1989). Depending on rates of sediment supply and changes in sea–level, drowning unconformities may be time transgressive (Erlich et al. 1990, 1993; Föllmi et al. 1994),

and they are commonly represented by abrupt changes in sediment type. The recognition of this event fills a gap in current knowledge on Late Cretaceous stratigraphy; it seems to correlate well with other similar and coeval drowning unconformities described around the Arabian Carbonate Platform (Figure 7.2).

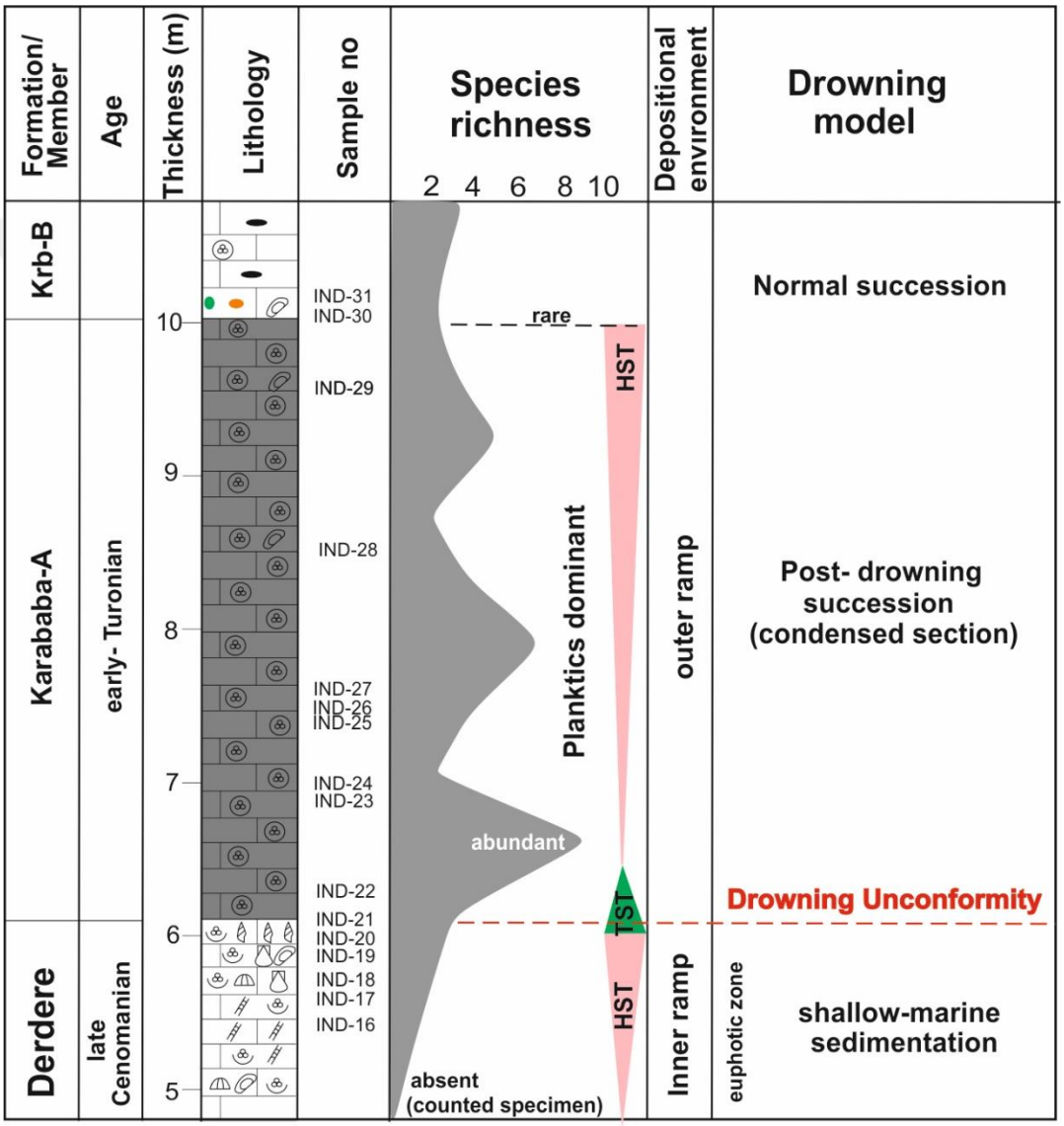


Figure 7.1. The species ranges of planktonic/benthic foraminifera and drowning model in the İnişdere stratigraphic section (after Mülayim et .al. 2019a).

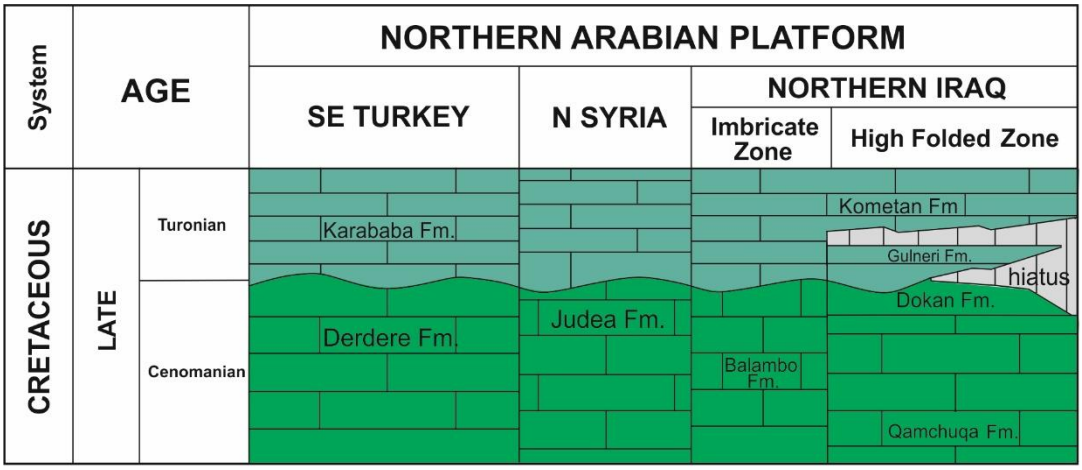


Figure 7.2. Cenomanian–Turonian, stratigraphic correlation of the Derdere Formation and the Karababa–A Member (SE Turkey) with the northern margin of the Arabian Carbonate Platform for Syria and Iraq areas (after Jaff et al. 2015; Mülayim et .al. 2019a).

7.1.2 Anoxia

The Cenomanian–Turonian Boundary Event (CTBE) was a period of pronounced oxygen deficiency in the world's ocean, representing OAE 2 (Schlanger and Jenkyns 1976; Arthur and Schlanger 1979; Waples 1983; Schlanger et al. 1987; Arthur et al. 1988; 1990; Wohlwend et al. 2016). In the Karababa–A sequence, the occurrence of dark grey, laminated, organic–rich sediments near the CTBE in the İnişdere and Türkoğlu sections are evidence of deposition under oxygen–deficient conditions at this time. However, it seems unlikely that oxygen–deficient waters ever flooded the outer ramp. The demise of the SE Turkey carbonate platform during the CTBE may have taken place either during a time of anoxic conditions on the platform representing OAE 2 or when nutrient–rich conditions dominated, leading to eutrophication of the platform. Both anoxia and eutrophication would have been capable of reducing the growth potential of shallow water carbonate, producing benthos (Hallock and Schlager 1986). In SE Turkey, eutrophication and subsequent anoxia is interpreted as the main mechanisms for reducing carbonate production as can be testified by the increase in marine organic matter (total organic carbon average = 2.66%) associated with the Karababa–A organic–rich carbonates (Soylu et al. 2005). As a matter of fact,

it is widely accepted that the late Cenomanian global transgression caused the oxygen minimum zones to spread widely, resulting in an OAE (Arthur et al. 1987; Schlanger et al. 1987; Jarvis et al. 1988), and decreased carbonate productivity. Black shales within the OAE 2 can be observed in lower Turonian deposits following the drowning of the platform. However, black shales of the main phase of OAE 2 are not recorded in the studied section owing to carbonate deposition on the shallower part of the platform, but are represented by excursions of the carbonate $\delta^{13}C$. Thus, the drowning of the carbonate platforms may be diachronic. Wendler et al. (2010) and Frank et al. (2010) stated that the demise of the Levant platform occurred during the phase of decreasing $\delta^{13}C$ values after OAE 2 spanning the early Turonian.

7.2 Stable Isotope Analyses

Carbon–isotope stratigraphy has shown itself to be a powerful tool in the correlation of Cretaceous sedimentary successions. The best–studied interval is that which straddles the Cenomanian–Turonian boundary (CTB) (Kowallis et al., 1995; Voigt and Hilbrecht, 1997). This has been documented isotopically from Europe, North America, Africa, and the Atlantic, Pacific and Indian oceans, (Jenkyns, 1985; Hillbrecht and Hoess, 1986; Schlanger et al., 1987; Jarvis et al., 1988; Kuhnt et al., 1990; Thurow et al., 1992; Jenkyns et al., 1994; Jenkyns et al., 1995; Accarie et al., 1996; Yılmaz et al., 2010; Mülayim et al., 2019a and b). Expanded stratigraphic sequences across this interval show a complex multi–faceted positive carbon–isotope excursion whose profile is conventionally taken to reflect global burial patterns of organic carbon. Certain intervals of geological time were characterized by anomalously high burial rates of organic carbon on a global scale and these have been termed "oceanic anoxic events' or 'OAEs' (Jenkyns, 1980; Arthur et al., 1990). Although the OAE 2 is the best–studied OAE of the whole Mesozoic and has been well documented in pelagic and hemipelagic sequences so far, there have been few attempts to detect the event in shallow water limestones (Drzewiecki and Simo, 1997; Davey and Jenkyns, 1999). However, hiatuses complicate interpretations of the stable isotope stratigraphy in shallow shelf environments, as demonstrated by Jarvis et al. (1988) for limestones displaying anomalous carbon isotope values.

The oxygen isotope composition of a carbonate rock precipitated from water depends primarily on the isotope composition of the water and on temperature. According to Hudson (1977), diagenetically altered limestones are lighter in oxygen than primary carbonate rocks. The isotope composition of limestones changes during diagenesis either by addition of cement generations or by the exchange of allochems or earlier cement already present, or both. As a result, neomorphism can lead to heavier or lighter oxygen isotope compositions. Hilbrecht et al. (1992) and Voigt and Hilbrecht (1997) presented evidence for local primary differences in the amplitude and stratigraphical variations of $\delta^{13}C$ values and significant diagenetic effects in permeable rocks. Sudden shifts in carbon isotope values can be produced by hiatuses. These are confirmed by biostratigraphical evidence, demonstrating that stable isotopes can be used as a means to identify and assess the extent of gaps in the stratigraphical record (Voigt and Hilbrecht, 1997).

Even though the $\delta^{13}C$ values of shallow–water carbonates are more prone to diagenetic effects than pelagic carbonates, major globally well–documented isotope events are proved to be preserved in the carbon isotope records of shallow–water carbonate sequences. Those carbon isotope events include several oceanic anoxic events (OAEs) which are the Mid–Cenomanian Event (MCE1) and Cenomanian/Turonian Event (OAE II). The carbon isotope stratigraphy of shallow–water carbonates can be used as a high–resolution stratigraphic correlation tool as long as the forcing mechanisms of the $\delta^{13}C$ excursions are well–defined.

Here I investigate the Cenomanian–Turonian carbon and oxygen isotope excursion accompanying the OAE 2 as registered in the shallow and overlying deeper–water facies of the Türkoğlu (TRK), İnişdere (IND), Sabunsuyu (SAB), and CM–14 sections.

In this chapter, the results of the stable carbon and oxygen isotope measurements of the bulk carbonate samples are presented. A new stable carbon isotope curve for the Cenomanian–Turonian of the SE Turkey in northern Arabian Plate is constructed, strictly constrained by the stratigraphic profile of the Derdere and Karababa formations. Correlations based on carbon isotope trends with Croatia and outcrops from the USA successions are discussed in detail. A total of 82 samples from the Cenomanian–Turonian boundary beds of Derdere and Karababa formations were derived as presented in Table 7.1 and 7.2. The $\delta^{13}C$ and $\delta^{18}O$ ratios were determined and plotted against lithology.

Table 7.1 $\delta^{13}C$ and $\delta^{18}O$ data from this study. # indicates negative $\delta^{13}C$ values and * indicates samples with relatively lower $\delta^{13}C$ values than those of adjacent samples, displaying as spikes in the carbon isotope curve.

Number	Sample name	^{13}C(‰) vs VPDB	^{18}O(‰) vs VPDB
1	2,84	1,88	–4,00
2	C–2	0,16	–5,33
3	C–7	0,52	–5,95
4	7,66	0,28	–5,28
5	C–8	0,47	–5,10
6	C–9	0,63	–4,66
7	C–10	0,65	–6,28
8	10,22	0,56	–4,21
9	6,24	0,56	–3,99
10	6,97	0,31	–4,37
11	7,41	0,40	–4,87
12	7,46	0,46	–5,06
13	1KB	1,23	–3,17
14	S4A	1,25	–3,04
15	S1A	1,30	–3,27
16	S3A	1,34	–2,74

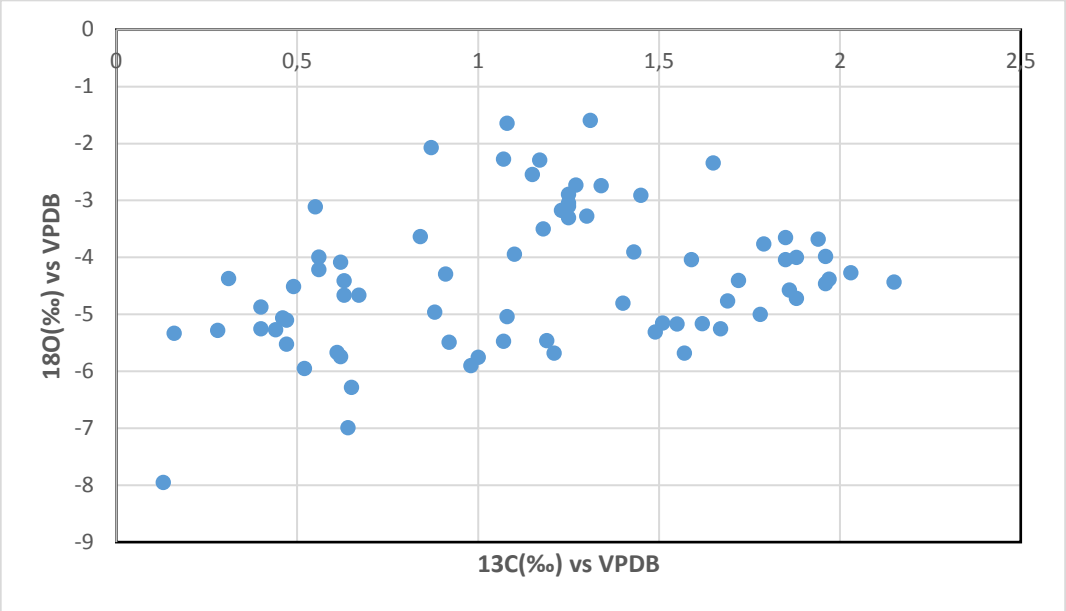
Table 7.1. (continued)

17	S5A #	–0,26	–4,61
18	S2A	1,25	–3,10
19	SF4	1,17	–2,29
20	47,95	1,67	–5,25
21	10,23	0,87	–2,07
22	SF3	1,31	–1,59
23	TKB1	1,94	–3,68
24	8,56	0,49	–4,51
25	6,16	0,88	–4,96
26	6,58	1,62	–5,16
27	5,97	1,72	–4,40
28	5,89	1,79	–3,76
29	1,96	0,64	–6,99
30	6,02	1,86	–4,57
36	2D*	0,84	–3,63
37	0,48	1,08	–5,04
38	9,68*	0,63	–4,41
39	48,57	1,51	–5,15
40	0,85A	1,85	–4,04
41	10,66*	0,55	–3,11
42	48,07	1,53	–5,31
43	2,16A	1,59	–4,04
44	48,82	1,57	–5,68
45	3D	1,25	–3,30
46	10,02*	0,67	–4,66
47	2,06*	0,92	–5,49
48	1,04 #	–0,63	–3,81
49	52,95	1,40	–4,80
50	4D	1,10	–3,94
51	54,27	1,69	–4,76

Table 7.1. (continued)

52	1D	1,18	–3,50
53	49,92	1,78	–5,00
54	54,47	1,96	–4,46
55	51,03	1,88	–4,72
56	14	1,07	–2,27
57	11,72	1,08	–1,64
58	0,07A	1,43	–3,90
59	0,17*	0,13	–7,95
60	54,54	1,97	–4,38
61	SAB1	1,00	–5,75
62	SF2	1,65	–2,34
63	SF1	1,15	–2,54
64	2KB	1,27	–2,73
65	6,92*	0,22	–3,66
66	SAB2*	0,98	–5,90
67	47,37*	0,62	–5,74
68	C4*	0,61	–5,67
69	49,26	1,55	–5,17
70	47,07*	0,21	–2,80
71	C6.2*	0,44	–5,27
72	3,74	1,85	–3,65
73	1,76	1,28	–5,47
74	0,05 #	–0,53	–4,85
75	45,72	1,81	–2,02
76	47,49	1,21	–5,68
77	C6.3*	0,47	–5,52
78	1,41	1,07	–5,47
79	48,97	1,49	–5,31
80	2,76	1,19	–5,46
81	C6.1*	0,40	–5,25
82	1,41A*	0,91	–4,29

Table 7.2 Cross–plot of $\delta^{13}C$ and $\delta^{18}O$ values of all the samples from this study



7.2.1.Türkoğlu Stratigraphic Section–Upper Part

Carbon Isotope: Carbon isotope values are obtained in the Türkoğlu stratigraphic section (TSS). In the Derdere Formation at TRK, the $\delta^{13}C$ values generally range from 1,96% to 0,21% (Figure 7.3). The carbon–isotope curve is defined, with more fluctuations in the upper part of the formation. The Derdere–Karababa boundary interval is marked by generally high $\delta^{13}C$ values (reaching up to +1.97%). Defining a positive peak on the carbon–isotope curve in the middle part of the Derdere Formation, a large shift in the $\delta^{13}C$ values is evident. The Karababa Formation has positive $\delta^{13}C$ values, ranging from +0,91 to +1,94 % (Figure 7.3). A well–defined carbon–isotope curve, with $\delta^{13}C$ values averaging +1.5%, with a possible small positive peak marked by the $\delta^{13}C$ values greater than +1,97%. In the uppermost part of the stratigraphic section, a well–defined curve is maintained, exhibiting a trend of decreasing $\delta^{13}C$ values from +1,59% to +0,91%. In Karababa Formation, carbon isotope values display a negative shift after the boundary as in other European or American curves (Figure 7.3).

Oxygen Isotope: At Türkoğlu stratigraphic section, all $\delta^{18}O$ values are between –5,68% and 3,68% (Figure 7.3). At TRK, the oxygen isotope curve presents a similar trend with carbon isotope curve with some differences. $\delta^{18}O$ values centres around –4,38%. In the lowermost Karababa Formation at TRK, $\delta^{18}O$ values increase slightly and primarily show a peak around –4,29%, which is in contrast to the highly variable $\delta^{13}C$ values of this part of the succession. A small negative peak occurs in both carbon– and oxygen–isotope curves. Above this peak, the $\delta^{18}O$ values gradually increase from –5,31 to –4,38%, (Figure 7.3). The increase in the $\delta^{13}C$ values in the uppermost part of the TK succession coincides with a trend of increasing $\delta^{18}O$ values.

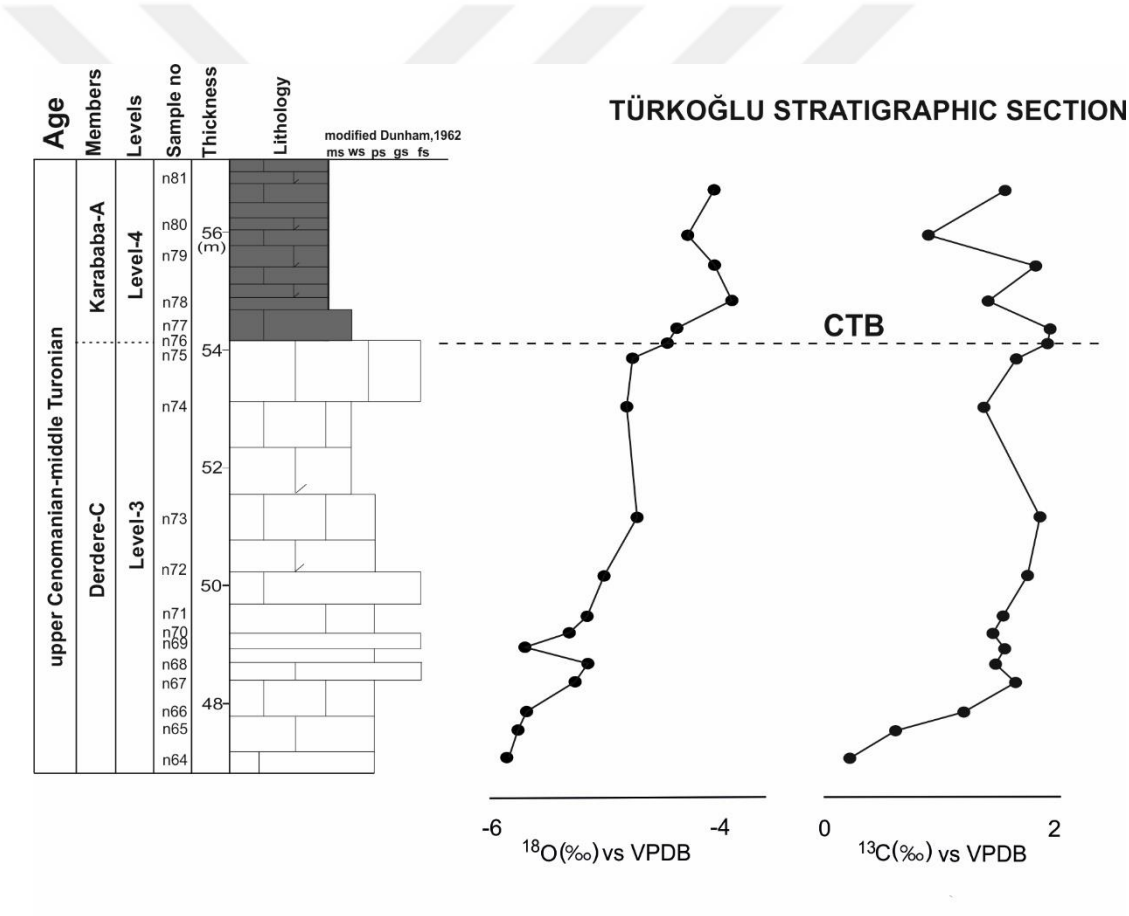


Figure 7.3. Lithostratigraphic section sampled at upper part of the Türkoğlu succession (SE Turkey) with accompanying carbon– and oxygen–isotope data. The position of Cenomanian–Turonian boundary (CTB), according to carbon–isotope values are also indicated (after Mülayim et al. 2019b).

7.1.2 Türkoğlu Stratigraphic Section–Lower Part

Carbon Isotope: Samples were collected for analysis only from the bottom part of the Derdere formation in Türkoğlu stratigraphic section (Figure 7.4). The carbon isotope values are slightly fluctuations throughout the section, with a minimum value of 0.55 ‰ and a maximum value of 1.65 ‰.

Oxygen Isotope: The oxygen isotope curve starts at a value of –5.75 %, followed by a more negative value of –5.9 ‰, a increase to –2.54 ‰ and another increase to values of broadly –1.59 ‰. In the upper part of the succession, the values decrease again to –3.11 ‰. The oxygen isotope trend is similarly proportional to that of the $\delta^{13}C$ curve. The first two $\delta^{18}O$ values vary with an amplitude of more over 2.5 ‰.

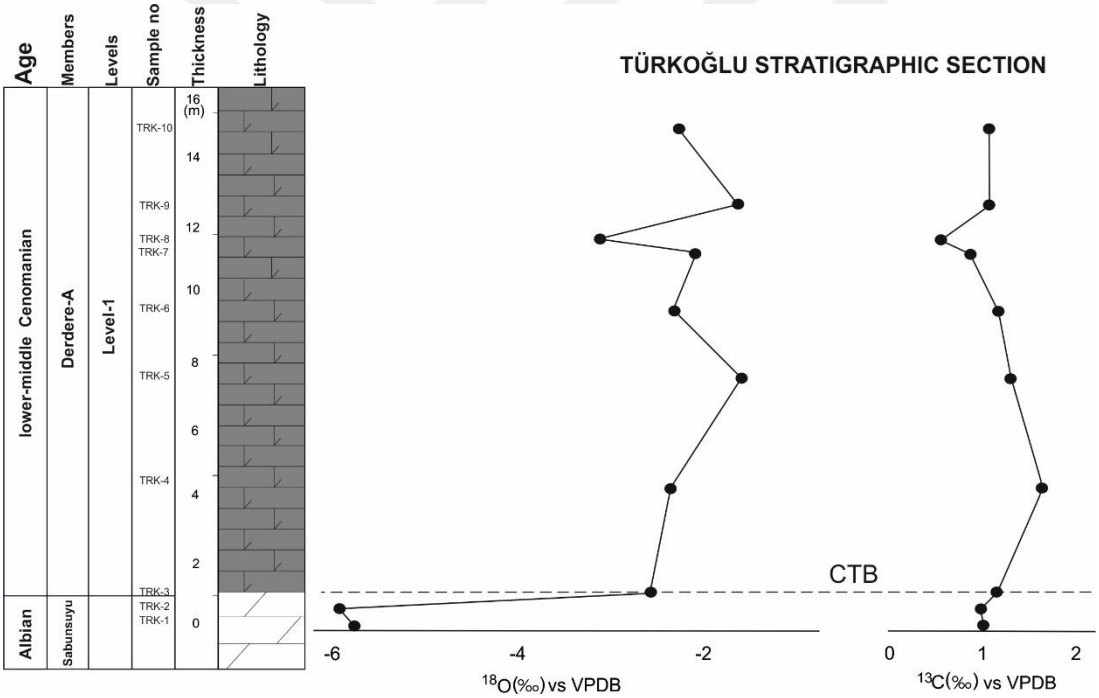


Figure 7.4. Lithostratigraphic section sampled at lower part of the Türkoğlu succession (SE Turkey) with accompanying carbon– and oxygen–isotope data.

7.1.3 İnişdere Stratigraphic Section

Carbon Isotope: Stable carbon isotope ratios from the Inişdere stratigraphic section indicate that $\delta^{13}C$ values from the Derdere Formation generally range from 2.15 to 0.13‰ (Figure 7.5). The carbon–isotope curve is characterized by more prominent fluctuations in the upper part of the formation. The Derdere–Karababa formations boundary interval is marked by generally high $\delta^{13}C$ values reaching+1.86‰. These values define a positive peak of the carbon–isotope curve, followed by significantly decreasing values upsection. In the middle part of the Derdere Formation, a large shift in the $\delta^{13}C$ values is also evident. It exhibits a positive peak. The peaks define prominent a positive plateau with a magnitude of about 2‰. The Karababa Formation displays positive $\delta^{13}C$ values, ranging from +0.40 to +0.88‰ (Figure 7.5). A well–defined carbon–isotope curve, with $\delta^{13}C$ values averaging +0.51‰, with a minor positive peak is marked by the $\delta^{13}C$ values greater than +0.62‰. In the uppermost part of the section, a well–defined curve is maintained, exhibiting a general stable trend with values from +0.22 to +0.88‰.

Oxygen Isotope: Oxygen isotope ($\delta^{18}O$) values are highly negative at the İnişdere stratigraphic section, between −7.95 and −3.65‰ (Figure 7.5). The oxygen isotope curve presents largely similar trends to the carbon isotope curve; $\delta^{18}O$ values centre around −4.83‰. In the lowermost Karababa Formation, $\delta^{18}O$ values increase slightly and primarily show a peak around −3.99‰, which is in contrast to the highly variable $\delta^{13}C$ values of this part of the succession. A small negative peak occurs in both carbon– and oxygen–isotope curves. Above this peak, the $\delta^{18}O$ values gradually increase from −4.08 to −5.28‰, (Figure 7.5). The slight increase in the $\delta^{13}C$ values in the uppermost part o the section coincides with a trend of increasing $\delta^{18}O$ values decreasing values in the up–section. In the middle part of the Derdere Formation, a large shift in the $\delta^{13}C$ values is also evident. It exhibits a positive peak. The peaks define prominent positive plateau with a magnitude of about 2‰. The Karababa Formation displays positive $\delta^{13}C$ values, ranging from +0.40 to +0.88‰ (Figure 7.5). A well–defined carbon–isotope curve, with $\delta^{13}C$ values averaging +0.51‰, with a minor positive peak is marked by the $\delta^{13}C$ values greater than +0.62‰. In the

uppermost part of the section, a well–defined curve is maintained, exhibiting a general stable trend with values from +0.22 to +0.88‰.

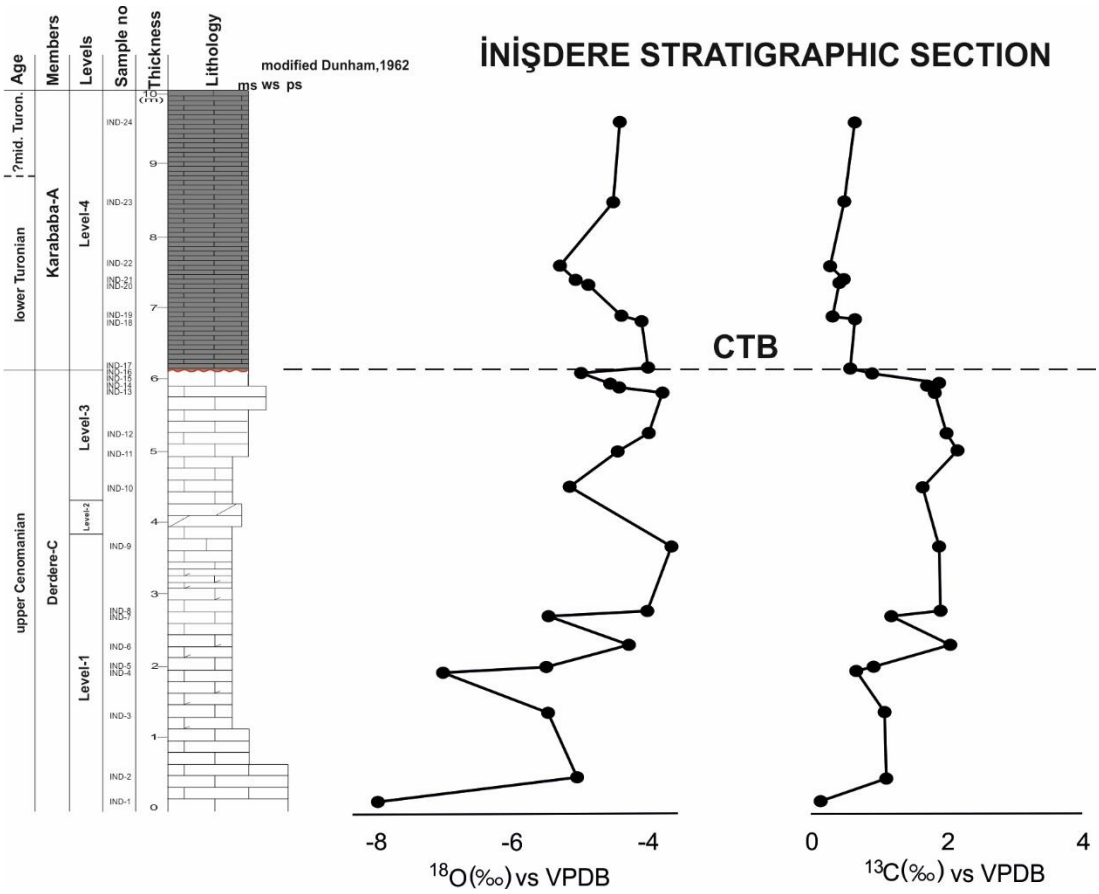


Figure 7.5. Lithostratigraphic section sampled at İnişdere succession (SE Turkey) with accompanying carbon– and oxygen–isotope data. The position of the Cenomanian–Turonian boundary (CTB), according to carbon–isotope values is also indicated (after Mülayim et al. 2019a).

7.1.4 Sabunsuyu Stratigraphic Section

Carbon Isotope: In the Sabunsuyu stratigraphic section, the carbon isotope values fluctuate between a maximum of 1.34 ‰ and a minimum of 0.84 ‰ (Figure 7.6). In the lower part the curve starts at 1.18 ‰, decreases slightly to 0.84 ‰, then increases to 1.25 ‰ and again decreases rapidly to 1.1 ‰. The fluctuations are broader, with a rise to 1.3‰, a decline to 1.25 ‰ and a second rise to 1.34 ‰.

Oxygen Isotope: The stratigraphical trend in oxygen isotope values differs slightly from that of the carbon isotope stratigraphy (Figure 7.6). The values fluctuate only from –3.94 ‰ to –2.74 ‰.

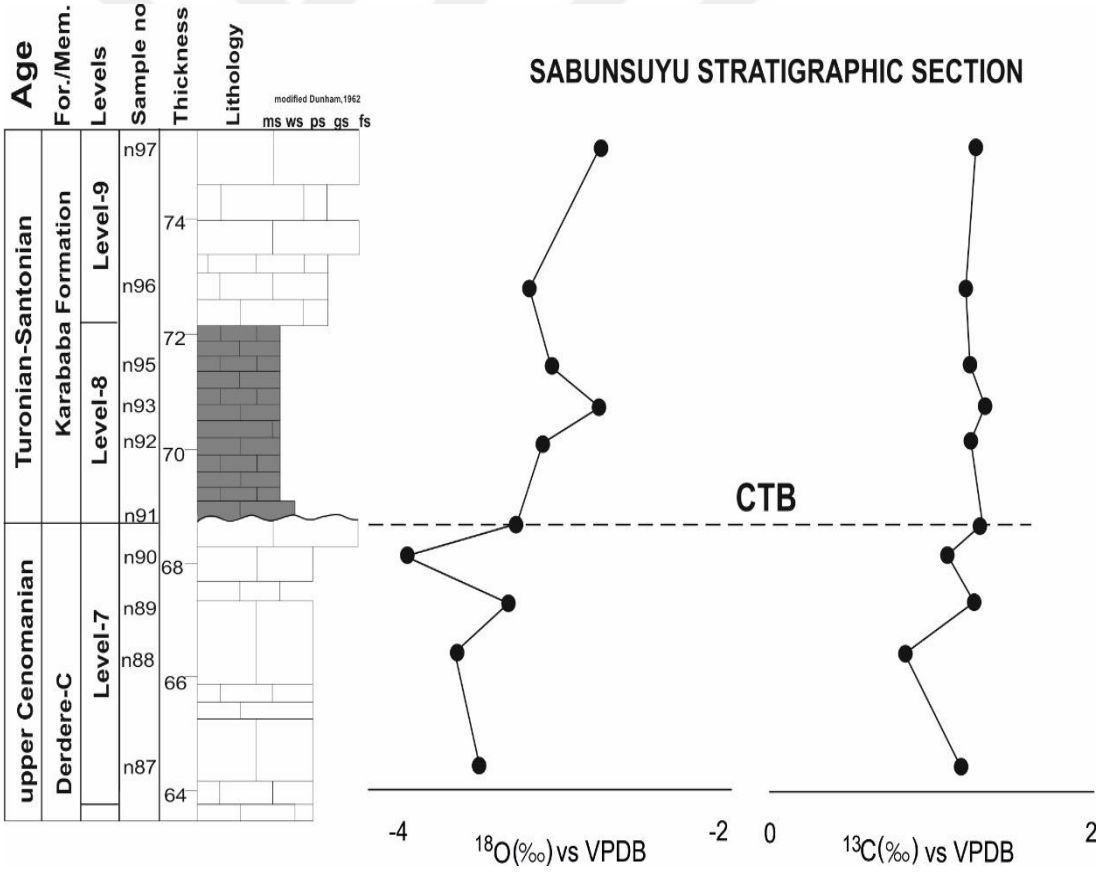


Figure 7.6. Lithostratigraphic section sampled at Sabunsuyu succession (SE Turkey) with accompanying carbon– and oxygen–isotope data. The position of the Cenomanian–Turonian boundary (CTB), according to carbon–isotope values is also indicated.

7.1.5 CM–14 Borehole Section

Carbon Isotope: The amplitude of fluctuation in $\delta^{13}C$ values is small. The carbon isotope values fluctuate but show a slightly negative trend throughout the succession (Figure 7.7). The $\delta^{13}C$ values decrease from 0.65 ‰ to 0.16 ‰, show a positive peak in the upper part of section followed by a decrease to the top of section (0.16 ‰) in the Turonian (Figure 7.7).

Oxygen Isotope: The amplitude of fluctuation in $\delta^{18}O$ values is large. In the lower part of the succession the values remain relatively constant (around –5.67 ‰), increase slightly to the top of section (–4.66 ‰) and then decrease rapidly to values of –6.28 ‰ in the upper part of section (Figure 7.7).

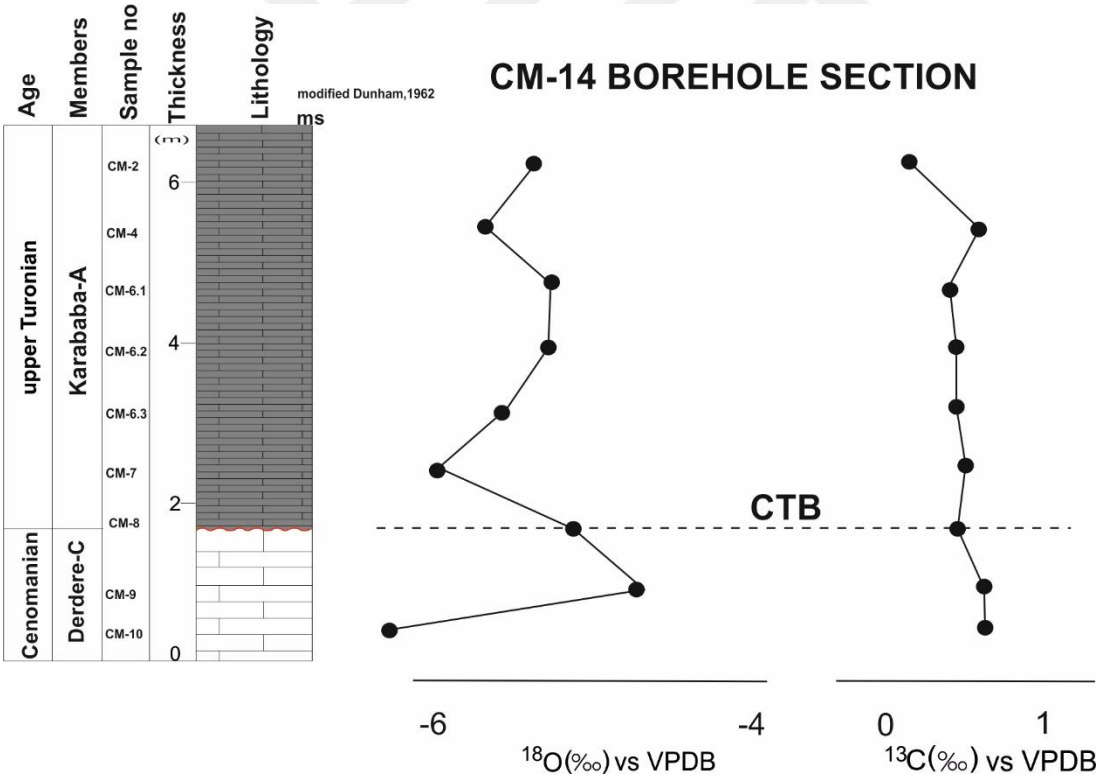


Figure 7.7. Lithostratigraphic section sampled at CM–14 borehole section (SE Turkey) with accompanying carbon– and oxygen–isotope data. The position of the Cenomanian–Turonian boundary (CTB), according to carbon–isotope values is also indicated (from Mülayim et al., 2020b).

7.3 Timing and Correlation Based on the $\delta^{13}C$ Excursion

When compared to the Eastbourne and Pueblo carbon–isotope reference curves (Jarvis et al., 2006; Pearce et al., 2009) the CTB excursion is also observed similarly in TRK (Figure 7.8). The three major excursion peaks (a, b, and c; cf. Pearce et al., 2009) are only tentatively recognized in the more complete. The first peak ‘‘a’’ marks the onset of the Plenus Cold Event, while the second peak ‘‘b’’ directly precedes one of the most severe intra–Cretaceous biotic crisis during the latest Cenomanian (Pearce et al., 2009). Above the possible third peak (tentative peak ‘‘c’’ with $\delta^{13}C$ values. 1,97%) in the upper part of the TRK succession, the trend of decreasing values upsection (from +0,91 to +1,94%) hints at the end of the CTB interval event (Figure 7.8).

Comparison with the carbon–isotope reference curves suggests that the CTB is within the upper part of the succession in TRK and corresponds to the boundary between Derdere Formation and Karababa–A member. This data shows that the youngest part of the Derdere Formation is not younger than the late Cenomanian. (Figure 7.8). The documented distribution of the upper Cenomanian fossils in the Derdere succession, and the results of carbon–isotope stratigraphy suggest that the lowermost possible position of the CTB is in the upper part of the Derdere succession. This placement is in general agreement with the position of the boundary (Pearce et al., 2009; Figure 7.8). The observed small differences in both stratigraphic thickness and lithostratigraphic characteristics of the succession from the CTB interval reflect details in sediment accumulation records across the platform.

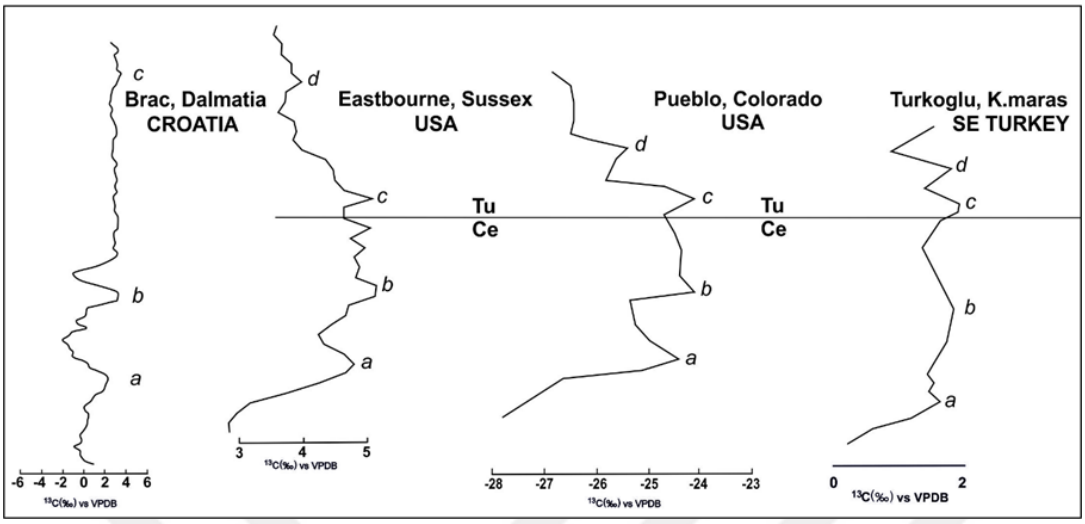


Figure 7.8. Correlation of C–isotope curve of Türkoğlu stratigraphic section with the curves obtained from the Cenomanian–Turonian Eastbourne and Pueblo reference sections and Brac succession. Letters a, b, and c mark the characteristic peaks of Pearce et al, 2009. (after Mülayim et al. 2019b).

When compared with the Eastbourne and Pueblo carbon–isotope reference curves (Kennedy et al. 2005; Jarvis et al. 2006; Pearce et al. 2009) the CTBE carbon isotope excursion is also observed similarly in the İnişdere stratigraphic section (Figure 7.9). Two of the three major excursion peaks (a, b, cf. Pearce et al. 2009) are tentatively recognized in the plateau interval of the studied section. The first peak 'a' marks generally the onset of the Plenus Cold Event (e.g. Jarvis et al. 2006). The extinction of *R. Cushmani* occurred during the third and main cooling phase of this event (Kuhnt et al. 2017). This extinction event occurred during major changes towards poorly oxygenated bottom water conditions and probably were also linked to transient cooling episodes within the Plenus Cold Event (Kuhnt et al. 2017). The environmental context of the main global extinction events of keeled planktonic foraminifera (*R. cushmani*) in the İnişdere stratigraphic section exhibits striking similarities. Comparison with the carbon–isotope reference curves suggests that the CTBE is present within the upper part of the İnişdere stratigraphic section and corresponds largely to the boundary between the Derdere Formation and the Karababa–A Member. According to our data, the youngest part of the Derdere Formation is not younger than

the late Cenomanian (Figure 7.9). The documented distribution of the upper Cenomanian fossils in the Derdere Formation and the results of carbon–isotope stratigraphy suggest that the lowermost possible position of the CTBE is in the uppermost part of the Derdere succession. In the Karababa Formation, carbon isotope values display a negative shift above the formation boundary similar to other sections (e.g. Jarvis et al. 2006). This placement is in general agreement with the position of the Cenomanian–Turonian boundary (Pearce et al. 2009; Figure 7.9). Minor differences observed in both stratigraphic thickness and lithostratigraphic characteristics of the succession from the CTBE interval local influence on sediment accumulation and preservation is recorded across the platform. This also suggests that the topmost part of the Derdere Formation correlates to the OAE 2 interval.

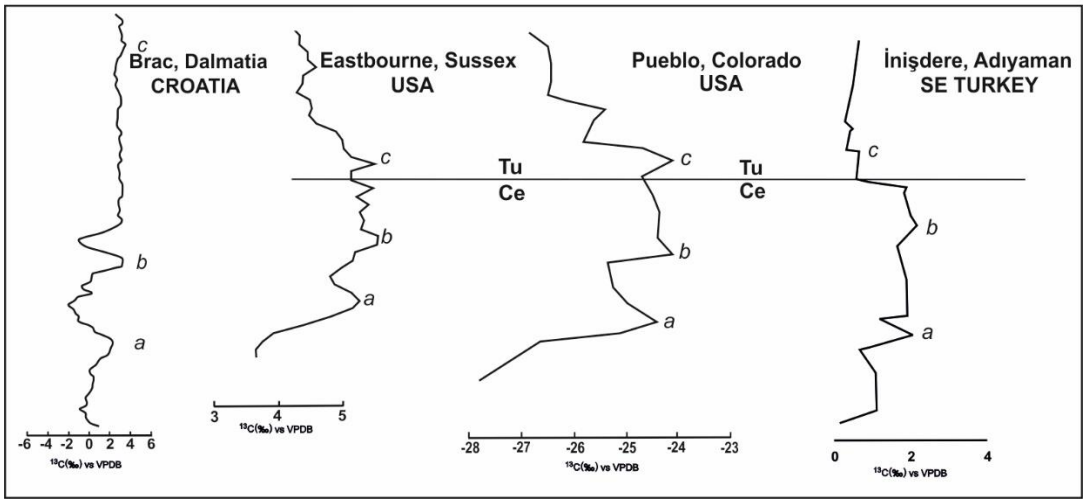


Figure 7.9. Correlation of the C–isotope curve of İnişdere stratigraphic section with the curves obtained from the Cenomanian–Turonian Eastbourne and Pueblo reference sections and Brac succession. Letters a–c mark the characteristic peaks of Pearce et al. (2009) (after Mülayim et al. 2019a).

7.4 Diagenetic Effect

The possibility of diagenetic alteration in carbonates is a major problem in the interpretation of stable isotope data. Scholle and Arthur (1980) noted a drop in $\delta^{18}O$ values at or near the Cenomanian–Turonian boundary. Jarvis et al. (1988) utilized oxygen isotope data only as a means of isolating diagenetically altered samples and to indicate obvious diagenetic trends. They did not ascribe any primary stratigraphical significance to the $\delta^{18}O$ curve. The positive trend of the $\delta^{13}C$ curve observed is in contrast to the negative trend recorded by Hilbrecht and Hoefs (1986). They interpreted their carbon isotope data as indicating falling sea–water temperatures during the latest Cenomanian, an interpretation supported by palaeontological data. Positive $\delta^{13}C$ peak signals are thought to indicate a maximum in productivity (Arthur et al., 1988; Gale et al., 1993). According to Emrich et al. (1970) and Scholle (1974), carbon isotopes are relatively immune to diagenetic modification. This is true for nearly impermeable fine–grained sedimentary rocks. However, in permeable deposits, the primary composition of carbon isotopes changes as a result of migrating pore waters, which transport dissolved $CaCO_3$ through isotopically different areas.

The $\delta^{13}C$ values were plotted against $\delta^{18}O$ values (Figures 7.3 to 7.7) to reveal correlation patterns between the outcrop areas. The İnişdere and Türkoğlu samples plot together and have higher $\delta^{13}C$ values than the samples from the Sabunsuyu area. Nevertheless, the range of $\delta^{18}O$ values of both data sets is comparable (from –5.1 to –3.1 ‰). It is concluded, that the data reflect approximately the same degree of diagenesis in all regions. Consequently, the differences between the $\delta^{13}C$ values must have other causes than purely diagenetic alteration. Therefore, the excursions are interpreted as original trends that may be used for stratigraphical purposes. Strong asymmetries and deviations from the curve shape defined by Gale et al. (1993) and Jenkyns et al. (1994) are a result of local variations in depositional rates (Bralower 1988).

7.5 Biostratigraphy Versus Isotope Stratigraphy

The results of the stable isotope analyses have been integrated with macro– and micropalaeontological data. For individual sections or small areas carbon isotope stratigraphy has limited applications when used alone, although it can be successfully used in combination with palaeontological data (Hilbrecht, 1998). In the Sabunsuyu area, the Cenomanian–Turonian transition does not include the peaks in $\delta^{13}C$ values (Figure 7.10). In general, hiatuses are indicated by sudden changes in the isotopic composition. In the Sabunsuyu stratigraphic section where the *W. archaeocretacea* Zone is missing, this gap in the succession is evidenced by a change in $\delta^{13}C$ values of nearly 1 ‰. Thus, it is likely that the $\delta^{13}C$ peaks fall within the hiatus. The $\delta^{18}O$ Derdere values of the Sabunsuyu stratigraphic section are similar to $\delta^{13}C$ Derdere values but are apparently altered by diagenesis as evidenced by increasingly negative values (cf. Scholle, 1977; Scholle and Arthur, 1980). Nevertheless, the stratigraphical trend for the $\delta^{18}O$ curves resembles that of the $\delta^{13}C$ curves, except for the positive peak in the $\delta^{18}O$ excursion.

The İnişdere $\delta^{13}C$ curve shows multiple peaks and no long term trend can be observed. It is possible that the peaks reflect the different lithologies sampled. Chemostratigraphy and biostratigraphy indicate that the following phenomena are synchronous: drowning of sequence, condensed sedimentation on the ramp, a third–order sea–level rise interpreted by Haq (2014) and the base of the positive $\delta^{13}C$ excursion. The coincidence of the base of the carbon shift and the termination of shallow water production at the boundary between sequences Derdere and Karababa–A suggests that the two phenomena and causally linked. The maximum $\delta^{13}C$ value in the upper part of the section (1.86 ‰) coincides with the occurrence of the planktonic foraminifera *W. archaeocretacea*. at this locality (Figure 7.10). However, in this section, the $\delta^{13}C$ peaks are comparable to those of the Türkoğlu stratigraphic section, where the lithology is clearly different. The excursion appears to cross into sediments from the *H. helvetica* biozone, but a more detailed biostratigraphic and geochemical investigation is needed to confirm this. The $\delta^{13}C$ peaks in the upper part of the Türkoğlu stratigraphic section can be tentatively correlated with those of the Sabunsuyu and CM–14 borehole sections. The $\delta^{13}C$ and $\delta^{18}O$ curves in the Türkoğlu,

Sabunsuyu and CM–14 show different trends to this of the İnişdere stratigraphic section. The tthree sections apparently represent the same stratigraphical level, as indicated by the $\delta^{13}C$ curve and the biostratigraphical markers (Figure 7.10). It thus appears that the $\delta^{13}C$ values reflect original trends. In addition, the correlation pattern of $\delta^{13}C$ and $\delta^{18}O$ shown in Figure 7.9 suggests that the degree of diagenetic alteration was uniform across the study area.

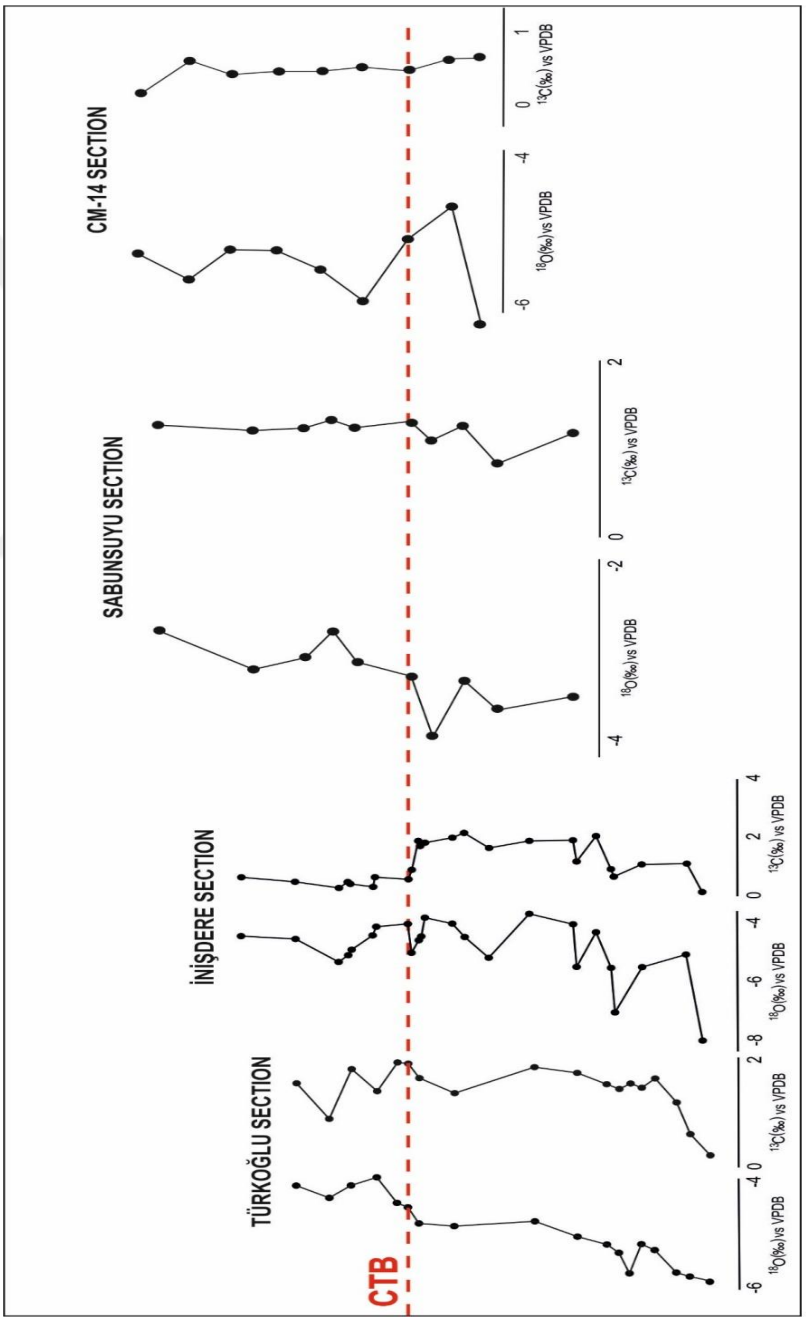


Figure 7.10. Tentative correlation of the $\delta^{13}C$ and $\delta^{18}O$–curves in the studied areas.

7.6 Possible mid–Cenomanian Event in SE Turkey

The middle Cenomanian events are documented from sections in England, Italy, Spain and western USA where they occur in the lower part of the middle Cenomanian as two relatively closely spaced $\delta^{13}C$ excursions (Paul et al., 1994; Rodriguez–Lazaro et al., 1998; Coccioni and Galeotti, 2003; Jarvis et al., 2006; Gale et al., 2008). The $\delta^{13}C$ excursions in the lower middle Cenomanian of the Sabunsuyu stratigraphic section may corroborate these observations. During the early Cenomanian, sea–level steadily increased followed by a major sea–level fall at the early/middle Cenomanian boundary (Gale et al., 2002, 2008). Similar sea–level trends can be observed at Sabunsuyu during the early to middle Cenomanian, including low–amplitude, short–term sea–level falls leading to oyster deposition. At Sabunsuyu, oyster deposition prevents full characterization of MCE event (Figure 7.11), although a 1‰ excursion is observed in the overlying shale. During the late Cenomanian, this major sea–level rise is observed at Sabunsuyu by decreasing the detrital influx and increasing HI values. The most noticeable sea–level fall is observed in the Sabunsuyu stratigraphic section prior to OAE 2. A small gravity–flow marks the sea–level low at Sabunsuyu. This sea–level fall is also recorded in shallow sequences of Central Europe with an estimated 5 to 10 m decrease prior to OAE 2 (Gale et al., 2002; Wilmsen, 2003; Voigt et al., 2006).

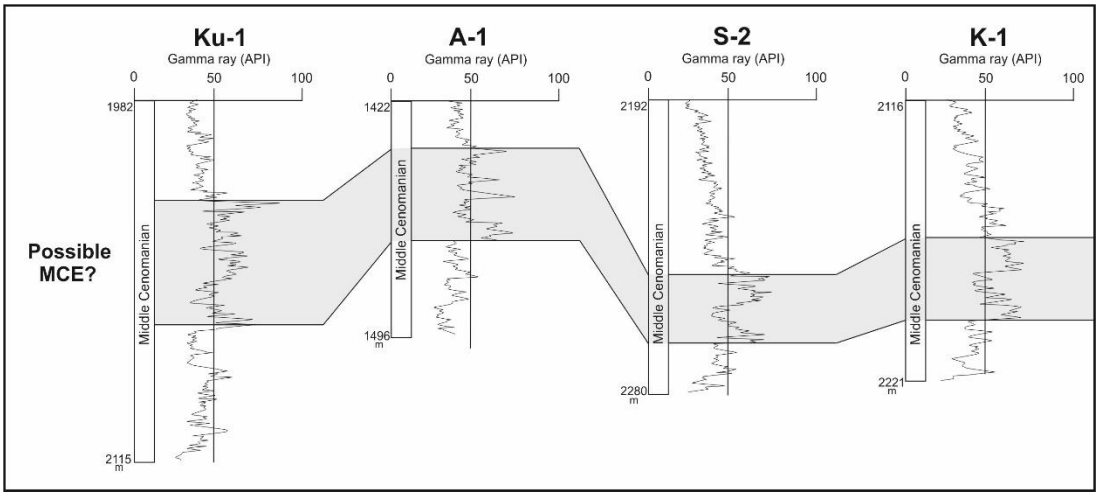


Figure 7.11. Correlation of the gamma–ray curves and possible mid–Cenomanian event (MCE) zone in the borehole sections.

7.6 Biotic Contributions to Records of Anoxic Events

In biotic changes in the Sabunsuyu stratigraphic section is more difficult to quantify due to the sporadic occurrence of marine microfossils and rarity or absence of age diagnostic species, however, some environmental inferences can be drawn. A key feature of the Sabunsuyu stratigraphic succession is the presence of oysters (exogyras) in limestone beds during the middle and late Cenomanian. Benthic foraminiferal assemblages are rare in subtidal environments but increase in inner neritic ramp settings. At Sabunsuyu stratigraphic section, benthonic abundance and diversity increases across and above the OAE 2, correlative with the sea–level rise and species assemblages, which consist mainly of abundant low oxygen–tolerant species (for example, Gavelinellidae); this suggests dysoxic bottom waters. By contrast, benthic foraminifera in deeper marine environments is generally absent due to anoxic bottom waters (Keller et al., 2001, 2004; Keller and Pardo, 2004a; Wagner et al., 2004; Kuhnt et al., 2005).

CHAPTER 8

PALAEO–ENVIRONMENTAL PROXIES AND CORRELATION TO ADJACENT AREAS: TAPHONOMIES AND PALEOECOLOGY

8.1 Paleoenvironmental Significance of Pithonellids

The pithonellids are considerable contributors to the nanno– and microfossil limestones of Upper Cretaceous depositional sequences worldwide (Wendler et al., 2002b). The most of the grains of carbonate ramp facies are composed of these phytoplankton organisms in the lower–middle Cenomanian of the northern Arabian platform, SE Turkey. Most of the pithonellids have a long stratigraphic range and cannot be used in biostratigraphy. However, they have the potential to be used for palaeo–environmental reconstruction, and as such I use them to interpret conditions prevailing on the northern Arabian Plate SE Turkey. The present study is the first to report a pithonellids assemblages from the Cretaceous Tethyan realm of SE Turkey. A comprehensive review of studies on pithonellids and an overview of the global distribution and palaeoecology of the pithonellids was given by Dias–Brito (2000). This thessi provides the first overview of pithonellids, from the lower–middle Cenomanian carbonate deposits of the Derdere Formation in SE Turkey.

8.1.1 Nutrient Availability and Water Depth

Along the ramp, the distribution of the pithonellids can be related to nutrients and water depth. Jarvis et al. (1988) suggest that the pithonellids appear to have been an opportunistic group, their abundance probably reflecting an increased nutrient supply. Wendler et al. (2002b) stated that the water depth or the availability of nutrients are

depended on the distribution of pithonellids on the shelf. The pithonellids are also associated with small simple morphologies of r–strategist planktonic foraminifera which are restricted to surface–dwelling species such as *Heterohelix* sp., the low salinity tolerance of hedbergellids and low oxygen–tolerant heterohelicids (Hart, 1980a;b, 1999; Jarvis et al. 1988; Leckie, 1987; Leckie et al. 1998; Leckie et al. 2002; Keller and Pardo, 2004). The pithonellids and small morphology r–strategists planktonic foraminifera are adapted to eutrophic environments (Leckie, 1987; Premoli Silva and Sliter, 1994; Coccioni and Luciani, 2004; Caron et al. 2006). Wendler et al. (2002b) stated that the pithonellids show temporal changes in abundance related to nutrient availability; thus *Pithonella sphaerica* has been interpreted as a species indicative of eutrophic conditions. Dias–Brito (2000) and Wiese et al. (2015), concluded that the pithonellids are typical of distal, most likely nutrient–depleted, shelf environments. Here marked a change of pithonellid dominated assemblages during the Cenomanian transgression. I also observe a marked change towards pithonellid dominance during the earliest Cenomanian transgression in the study area. Zügel (1994) interpreted increased abundances of *Pithonella ovalis* to indicate transgressive episodes (Figure 8.1). A relationship between *P. ovalis* increase and transgression has been widely observed in the Cenomanian of Western Europe (Villain, 1975; Keupp, 1987, 1991; Wendler et al. 2002a) and the Tethys (Dali–Ressot, 1987). Thus, a bathymetry–related zonation across the shelf/ramp appears to be a consistent feature of the distribution of the pithonellids, *P. sphaerica* being dominant in marginal shelf areas and *P. ovalis* preferring somewhat deeper outer shelf/ramp environments. Because of the life strategy of these planktonic organisms that inhabited the surface water, it is difficult to explain, however, how water depth itself could control their spatial distribution. It appears more plausible that environmental differences such as gradients in nutrient availability controlled the spatial differences in pithonellid assemblages.

8.1.2 Upwelling Relations

Considering that an abundant and diversified pithonellid biota is a good indicator of sedimentation in the transitional neritic–oceanic zone (Spadini et al. 1988), and taking into account that during the mid and late Cretaceous numerous areas in both western and eastern margins of the continents were influenced by coastal upwelling (Parrish and Curtis, 1982; Patzkowsky et al., 1991; Wendler et al., 2002b). Pithonellid–rich deposits have been as being genetically associated with mid–Cretaceous upwellings (Robaszynski et al., 1993; Dias–Brito, 1992b, 1996a; Saıdi et al., 1997). Accordingly, I hypothesize that the studied area also represents an upwelling region. *Pithonella sphaerica* dominated the area in which the influence of the upwelling, presumably cool, water masses is assumed. However, it cannot be interpreted as a cool–water species, because throughout the Tethyan Realm it was widely distributed throughout waters which were reconstructed to have had high temperatures (Alsenz et al.,2013). Dias–Brito (2000) stated that pithonellids were thermophilic, planktonic organisms their restriction to the Tethyan Realm. Therefore, the cool waters must have mixed with the warm Tethyan waters sufficiently to remain in the temperature range required by the pithonellids. Hence, *P. sphaerica* was best adapted to temperature changes which represent the most opportunistic of the pithonellids. It has also required the highest nutrient concentrations. To conclude, the abundance and spatial distribution of *P. sphaerica* and *P. ovalis* in the studied material indicate that the limestones of the Derdere Formation were deposited under eutrophic conditions in well–mixed surface waters (Figure 8.1).

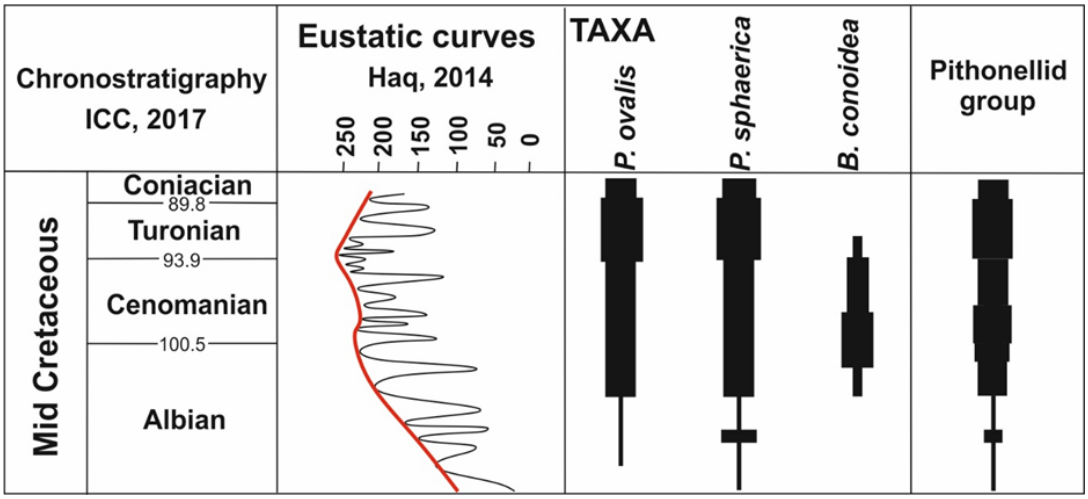


Figure 8.1. Schematic and tentative semi–quantitative distribution of pithonellids in the fossil record and its relationship to global sea–level fluctuations. (after Dias–Brito, 2000). Chronostratigraphy and eustatic curves after Haq, (2014).

8.2 Palaeo–Environmental Significance of Filament Marker Beds

'Filaments' (thin elongate shelly plates of calcitic nature) have been widely mentioned from Triassic to Cretaceous carbonate deposits. Whereas Triassic occurrences were attributed to halobiid bivalves (Colom, 1955; Flügel, 2004), Jurassic ones are thought to be protoconchs or juvenile shells of posidoniid (*Bositra, Posidonia*) bivalves (Jefferies and Minton 1965; Navarro et al., 2009) and/or crinoid thecal plates (Ferré and Dias–Brito, 1999: Ferré et al., 1999). Rivas et al. (1997) suggested that pectinid bivalves of the Entolium group could also produce thin, filament–like shells. 'Filaments' (thin bivalve shells or crinoidal plates) occur massively or discretely in several distinct levels worldwide throughout the C–TB interval and above (Razgallah et al., 1994; Naili et al., 1995; Accarie et al., 1996; Nederbragt and Fiorentino, 1999; Van Buchem et al., 2002; Wan et al., 2003; Ettachfini and Andreu, 2004; Amédro et al., 2005; Caron et al., 2006; Zagrarni et al., 2008; Robaszynski et al., 2010; Negra et al., 2011; Bomou et al., 2013; Useche et. al., 2016). However, in the present state of the art, Cretaceous 'filaments' have not been so far assigned to a precise taxonomic group, but have been used as a potential source of marker levels based on morphological aspects.

The studied thin bivalve shells at hand come as thin–sections of core samples collected from the Karababa–A Member of the Mardin Group in the Arabian plate, SE Turkey. This member is located between the underlying Cenomanian shallow–water carbonates of the Derdere Formation (Fig. 1) and the overlying (Coniacian–Santonian) hemipelagic deposits of the Karababa–B Member (Mülayim et al., 2019a). Most 'filament' event beds occur around the CTB. These levels were spotted along their respective core section and dated by means of planktonic foraminiferal biostratigraphy for further potential local, regional and global correlations. A carbon isotopic ($\delta^{13}C$) analysis was also performed to support the biostratigraphic correlation (Mülayim et al., 2019a, and b).

The present study aims to present the petrogenetic contribution of 'filaments' and the potential use of their mass–occurrence/event beds in palaeo–environmental interpretation and in regional/global stratigraphic correlation.

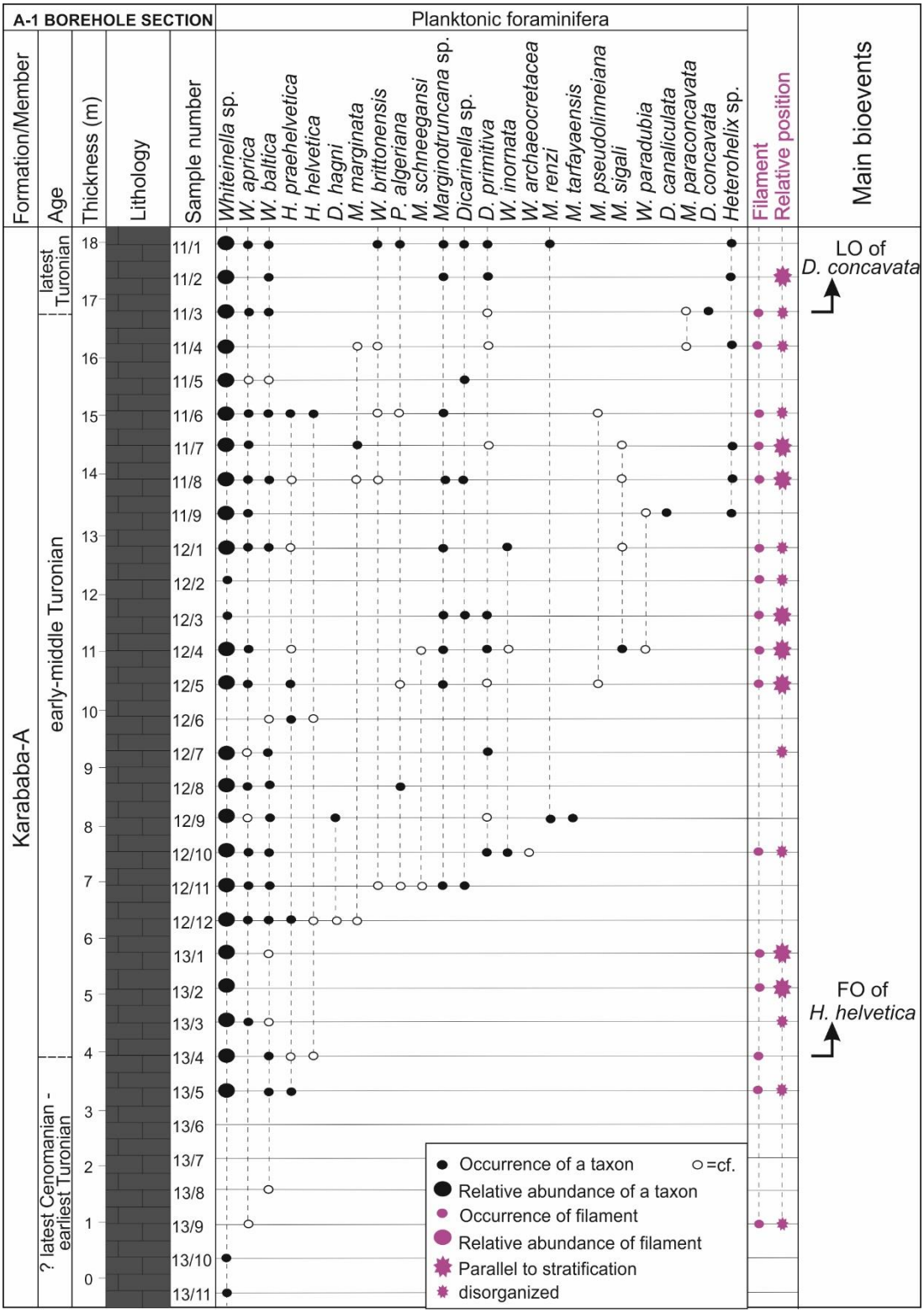


Figure 8.2. Stratigraphic column of the A–1 borehole succession showing the stratigraphic distribution of the planktonic foraminifera and filaments in the Karababa–A Member.

BS-1 SECTION
Formation/Member
Karababa-A
Epoch
early Turonian
middle Turonian
late Turonian
Thickness (m)
Lithology
Sample number
W. africa
W. baltica
H. helvetica
H. praehelvetica
Dicrinella sp.
M. pseudolinneiana
D. concavata
W. archaeocretacea
A. cretacea
Whiteinella sp.
Heterohelix sp.
Effelithus eximius
Lucianorhabdus maleformis
Quadrum gartneri
Filament
KM-1 SECTION
Formation/Member
Karababa-A
Epoch
early Turonian
middle late Turonian
Thickness (m)
Lithology
Sample number
H. praehelvetica
W. africa
A. cretacea
Marginotruncana sp.
W. paradubia
W. baltica
D. hagni
F. maslakovae
Dicarinella sp.
M. marginata
H. helvetica
Whiteinella sp.
Heterohelix sp.
Quadrum gartneri
Filament
Relative position
CM-14 SECTION
Formation/Member
Karababa-A
Epoch
middle Turonian
late Turonian
Thickness (m)
Lithology
Sample number
W. baltica
P. algeriana
W. africa
M. coronata
Whiteinella sp.
M. sigali
Heterohelix sp.
Lucianorhabdus maleformis
Filament
Relative position
Occurrence of a taxon
=cf.
Relative abundance of a taxon
Occurrence of filament
Relative abundance of filament
Parallel to stratification
disorganized
CM-14
ADIYAMAN
BS-1
KM-1
N
15 km

Figure 8.3. Stratigraphic correlations between three borehole sections including the Cenomanian–Turonian boundary in the Adıyaman district. Stratigraphic distribution of some planktonic foraminifera, calcareous nannofossils and filaments are given on the right– hand side of each log. (after Mülayim et al. 2019a).

8.2.1 Petrographic Characteristics

Microscopically, all core sections (Figures 8.4 and 8.5) display planktonic foraminifera–bearing wackestone/packstone microfacies within an argillaceous matrix; abundant planktonic foraminifera, as the most skeletal allochems, are usually recrystallized and thickly packed, associated with widespread pithonellids, bivalve filaments and rare phosphatized grains (fish bones), and roveacrinid plates. Detailed observations of 'filaments' were conducted in four core sections (Figures 8.4 and 8.5). Some 'filaments' are scattered, straight to gently curved shelly sections regularly present in carbonate mudstone facies. Some others are longer and show a preferential orientation parallel to stratification (Figures 8.4 and 8.5). Partly, long 'filaments' indicate undulated forms loosely packed with globular planktonic foraminifers. All this suggests some faint compaction process that had weakly affected these 'filaments'. In other cases, the 'filaments' are smaller, like broken pieces, isolated, and show varied orientations. Except for fragmentation, the shells do not display any taphonomic features (e.g. encrustations or borings). Entire or almost complete shells/plates and large fragments are commonly preferentially oriented parallel to bedding. In some other thin–sections of the lower part of the core sections, pyrite occurs whereas phosphatic grains were also occasionally observed near the top of these same core sections.

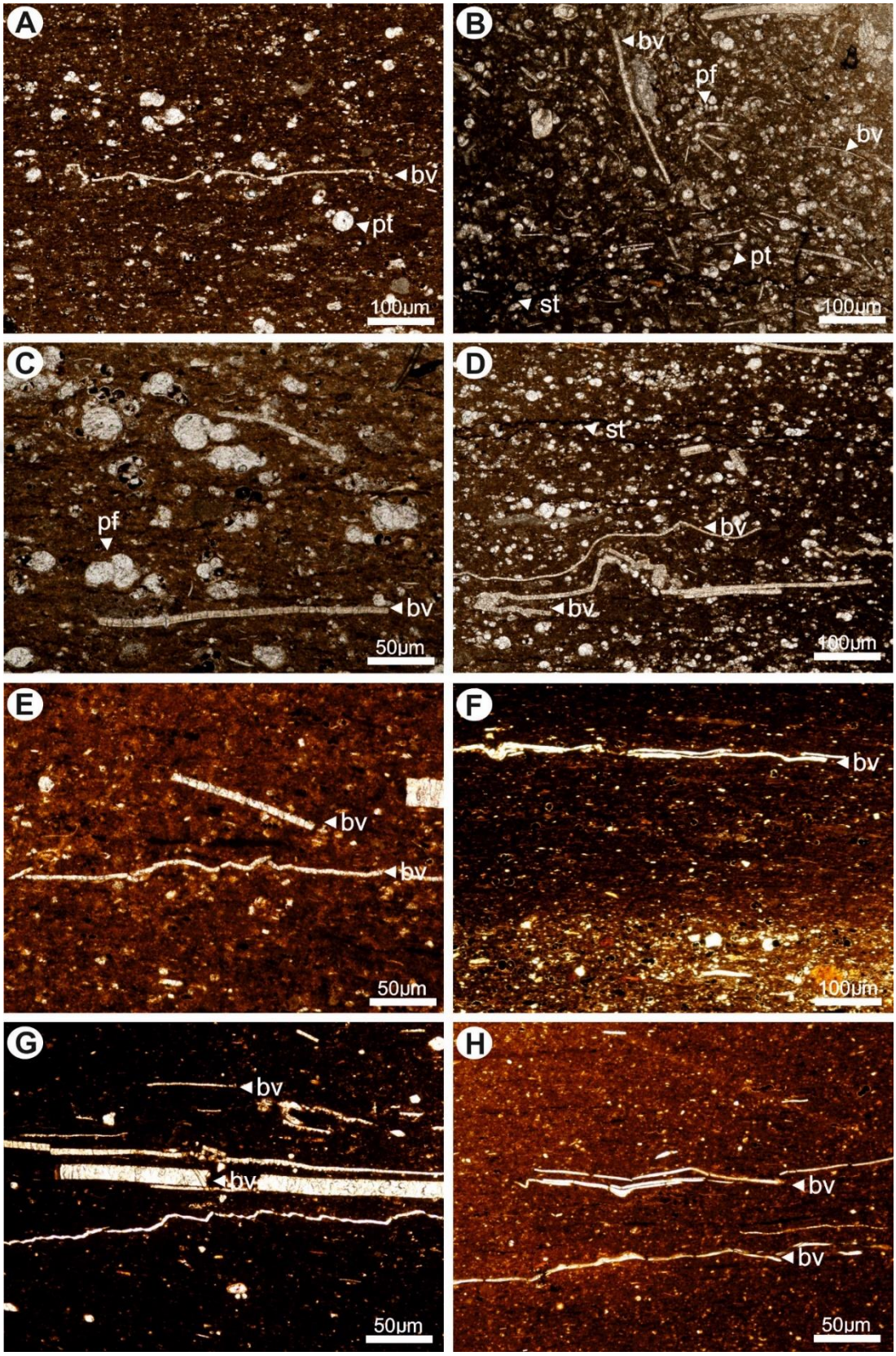

A
bv
pf
100µm
B
bv
pf
bv
pt
st
100µm
C
pf
bv
50µm
D
st
bv
bv
100µm
E
bv
bv
50µm
F
bv
100µm
G
bv
bv
50µm
H
bv
bv
50µm

Figure 8.4. Microfacies photographs of the Karababa–A Member, A–1 core section, Adiyaman district, SE Turkey. A. Slightly deformed and diagenetically compressed, smooth bivalve shell valve, sample P1011637. B. Most probably scattered fragments of a smooth bivalve shell valve, sample P1011681. C. 'Large' fragments of prismatic bivalve shell valve (possibly some inoceramid relative), sample P1011636. D. Diagenetically compressed, smooth bivalve shell valve, sample P1011642. E. Possibly some inoceramid relative, sample P1011645. F. Diagenetically compressed bivalve shell, sample P1011704. G. The thicker 'filament' resembles a transverse section of some echinoid plate test, the thinner ones are definitely transverse sections of smooth bivalve shell valves, sample P1011647. H. Diagenetically compressed huge fragments of smooth bivalve shell valve, sample P1011668. bv: bivalve pl: planktonic foraminifera.

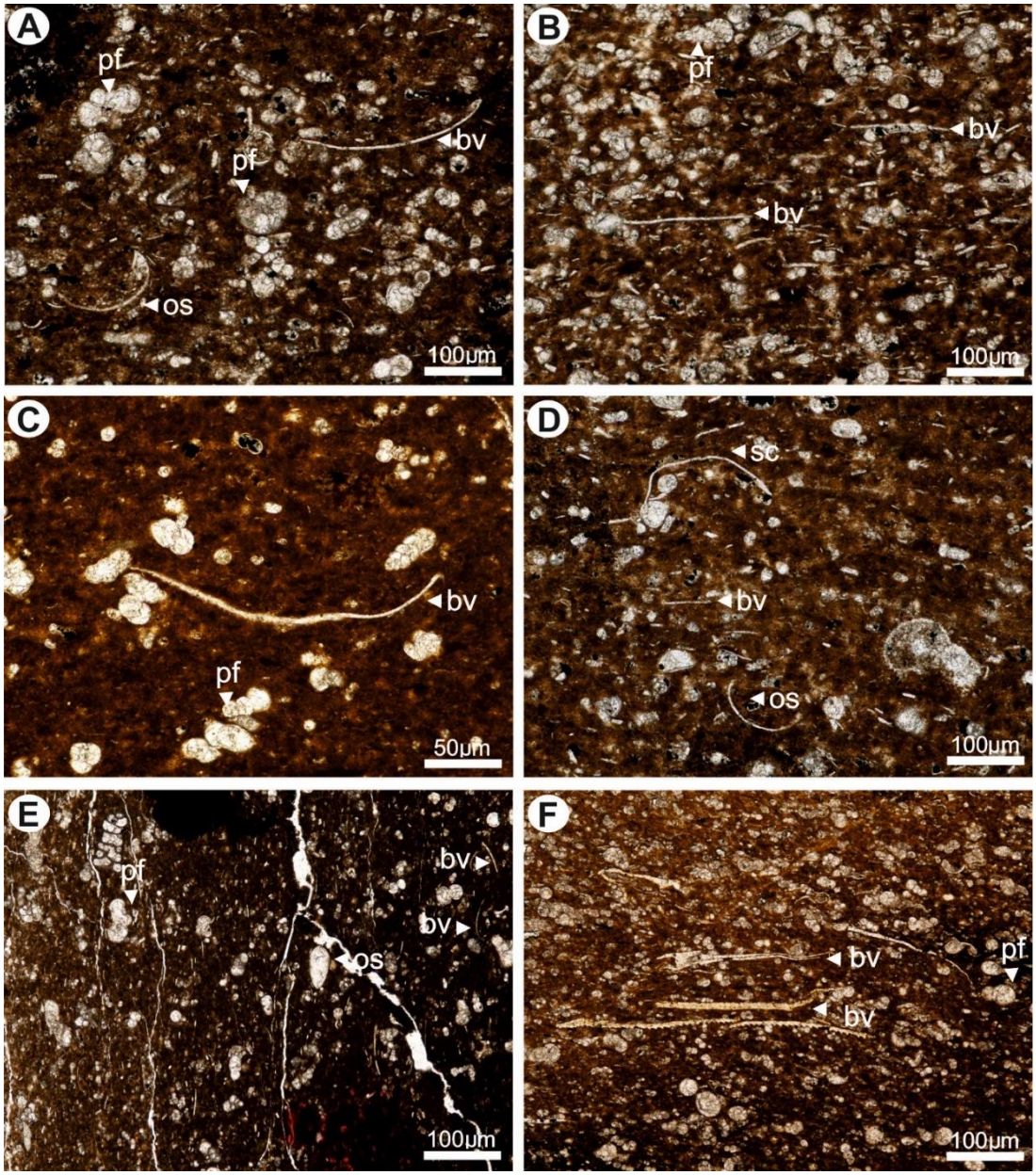


Figure 8.5. Microfacies photographs of the Karababa–A Member, Adiyaman district, SE Turkey. A. In the lower–left corner an isolated ostracode valve. In the upper right corner a transverse section of a smooth bivalve shell (with a hint of a hinge), sample P1011848, CM–14 borehole section. B. Many transverse sections of smooth bivalve shell fragments lying conformably to bedding, distal outer–ramp environment, sample P1011850, CM–14 borehole section. C. Right in the middle a transverse section of a smooth bivalve shell (bow–like), from outer–ramp environment, sample P1011814, KM–1 borehole section. D. In the lower–left corner a longitudinal axial section of a juvenile valve of *Bairdia* sp. In the lower middle part a transverse section of an

ostracode valve (*Cytherella* sp.). In the upper left corner a transverse section of a thecal plate (TS–Theca) of a saccocomid (*Applinocrinus* sp.) and smooth bivalve shell debris, sample P1011775, KM–1 borehole section. E. Right in the middle of the photograph a complete ostracode shell with both valves connected (*Cytherella parallela*). Interspersed in the facies some small and thin fragments/debris of smooth bivalve shell conformable to bedding from an outer–ramp environment, sample P1011296, İnişdere stratigraphic section. F. Five bivalve shell valves: the central one may be attributed to buchiids, but the lower two show some crenulation, sample P1011753, BS–1 borehole section. bv: bivalve pl: planktonic foraminifera, os: ostracod.

8.2.2 'Filaments', Depositional Environment, Sea–Level Change, and OAE 2

The studied sections are substantially homogenous in terms of lithological characteristics, but minor shifts in the depositional environment and faunal assemblages suggest a major change in such a pelagic setting. The shape, length, and orientation of the 'filaments' are linked to the depositional setting. supported by microfacial analysis Wackestone textures involved well–preserved pelagic bivalve shells and/or crinoidal plates reflect a low–energy depositional environment below fair–weather wave base (FWWB): settling of shells and plates down on the seafloor led to their orientation parallel to bedding. Negra et al (2011) stated that most bivalve shells were remobilized and broken into fragments during storms. Presumably, the smaller the broken fragments, the longer the transport distance from the source to final deposition. Rivas et al. (1997) pointed out that compaction causes the breaking of thin bivalve shells. However, deposition and burial must have been rapid since shells indicate neither micritization, nor bio–perforation, nor encrustation.

One of the major global sea–level rises is known to be initiated have occurred just before the C–TB and culminated around the early/middle Turonian boundary (Haq, 2014). In such a situation of eustatic fluctuation, recurrent 'filament' events are regarding successive transgressive pulses at the onset of a transgressive interval, announcing the "return to normal" marine conditions (Negra et al., 2011; Kędzierski et al., 2012; Mülayim et al., 2019a, and b). Considering the position and repeated

occurrences of ‘filament’ events, the transgressive phase should be imputed to the lowermost part of the Karababa–A Member. The maximum of transgression may coincide with the major filament event bed (Figure 8.6). These repeated occurrences of ‘filaments’ also reflect a global event, most likely corresponding to the progressive transgression related to the major Turonian sea–level rise. In general, the biofacial change at the C–TB has been attributed to a combination of factors including climatic change, change in oceanic current, enhanced bio–productivity, oxygen starvation, and organic–matter accumulation (Caron et al., 1999). Mülayim et al. (2019a) stated that the Arabian platform in SE Turkey was drowned around the C–TB as a result of changing environmental conditions in the Karababa–A Member. High sea–level conditions for this interval triggered repeated oxygen–depleted conditions that favoured deposition and preservation of organic–rich sediments.

Major biological changes emphasize environmental crises–induced during the OAE 2 in the study area A ‘filament’ event bed situated close to the end of the *W. archaeocretacea* Zone is interpreted as the product of mass mortality of thin shell bivalves (Figure 8.5). During their coming down in the water column, they may have gone through an oxygen–deficient water mass causing their suffocation (Bomou et al., 2013); then these organisms died in great numbers before maturity, their small valves falling on the seafloor wide open. This may explain such repeated occurrences of a catastrophic hecatomb of juvenile bivalves, likewise concerning the pelagic crinoid banks; such bio–events seem to have been global (Caron et al., 2006). This relative abundance of ‘filaments’ is coherent with the organic–rich facies of the Karababa–A Member: deposition and preservation of organic matter being favoured by the ascent of the oxygen minimum zone in SE Turkey (Mülayim et al., 2019a).

Such ‘filament’ event beds are observed at the coeval position in C–TB sections worldwide (e.g., Anglo–Paris Basin: Jefferies, 1962, 1963; Gale et al., 1993; Ferré and Breton 1995; Algeria: Naili et al., 1995; South Tibet: Wan et al., 2003; Morocco: Ettachfini et al., 2004; USA: Caron et al., 2006; Tunisia: Zagrarni et al., 2008; Negra et al., 2011) and constitute valuable marker proxies for constraining the position of the C–TB (Figure 8.6). The main ‘filament’ event bed falls above the C–T precision interval in the A–1 core section and a few meters above the equivalent level in the

İnişdere stratigraphic section. I propose to use the ‘filament’ event bed as a proxy marker for the C–TB for its very close position.

8.2.3 Filament Event and Carbon–Isotope Correlation

‘Filament’ events offer an additional tool to correlate the Karababa–A Member and its lateral equivalents at the regional scale (African Plate, Arabian Plate) but also at the global scale, as the expression of oceanic communication between different oceans, (e.g.: Tethys, Western Interior Seaway,…) and eustatic change, around and after C–TBE (Figure 8.7).

Carbon isotopic values are obtained from the CM–14 core section. In the Karababa–A Member (CM–14 core section), the $\delta^{13}C$ values generally range from 0.65 to 0.16‰. This gradual decline continues into the lower Turonian. In comparison to most Tethysian and central Atlantic sections, these $\delta^{13}C$ values are relatively low (Figure 8.7). In the CM–14 core section, this interval is associated with several ‘filament’ mass–occurrence levels. In the CM–14 core section, none of these features are particularly clearly visible. Some organic enrichment might be only visible in the expanded İnişdere and Türkoğlu stratigraphic sections (Mülayim et al., 2019a, and b). Since values are consistently ‘lighter’ than those from supposedly unaltered profiles, the carbon isotope excursion may be here mostly masked by diagenesis; however, the overall shape of the curve may record an original, pre–diagenetic signal. The broad positive plateau, visible in the more carbonated İnişdere stratigraphic section, is comparable to those recorded from most expanded/complete sections.

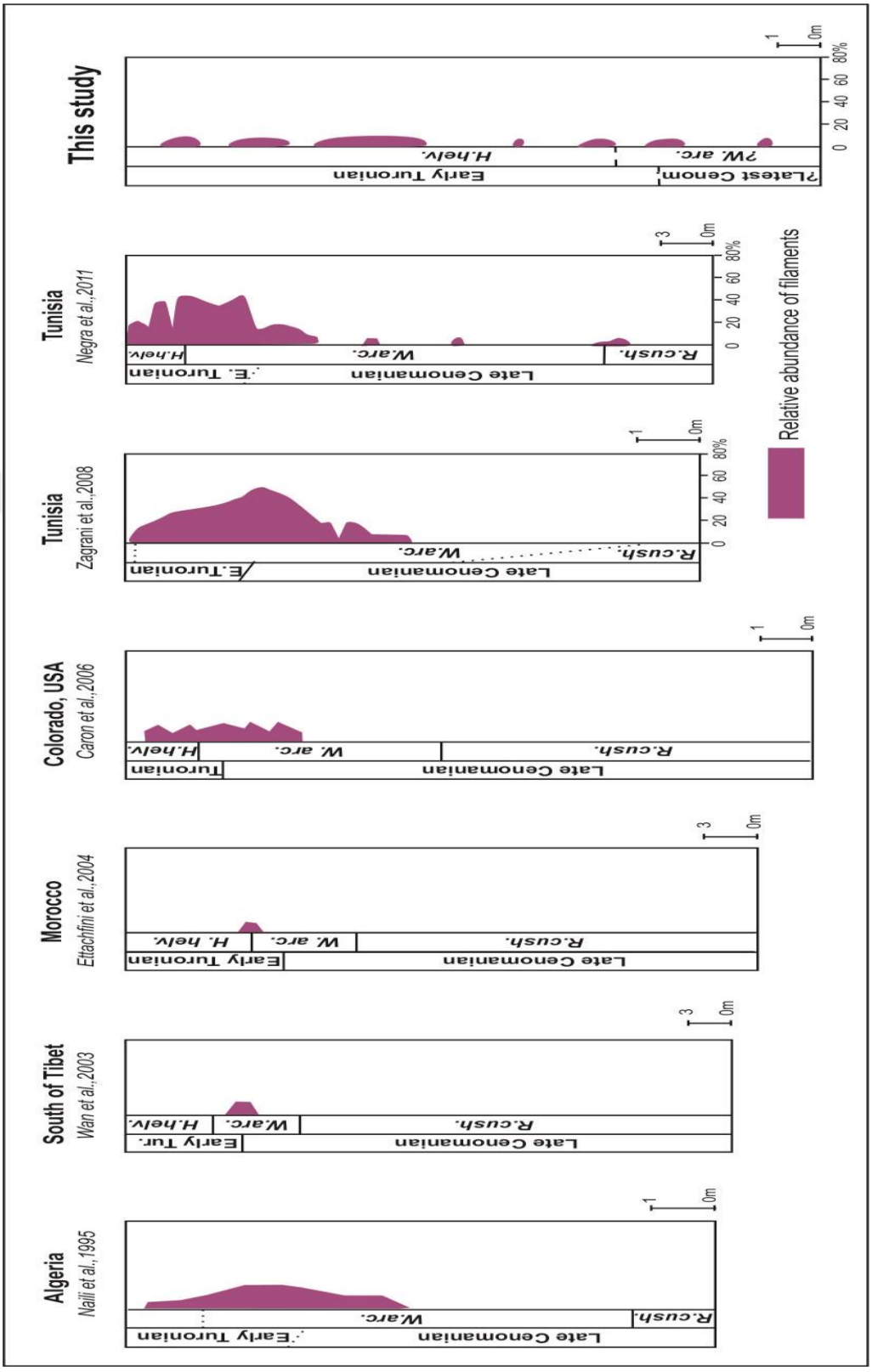


Figure 8.6. A relative abundance of the filaments in the Cenomanian–Turonian successions at global correlation.

The ‘filament’ event beds highlight stressful environmental conditions during the OAE 2 turnover in every studied sections. The repeated heterohelicid blooms (as surface–dwellers opportunists) reflect the better adaptation of these organisms to abrupt high–productivity environmental change and generally underline a dramatic oxygenation decrease in the water column below (Caron et al., 2006; Reolid et al., 2015). The wealth of ‘filament’ is interpreted as resulting either from the mass mortality of planktonic bivalve larvae (Caron et al., 2006; Kędzierski et al., 2012; Bomou et al., 2013) and/or from the disintegration of pelagic bivalves by high–energy events (Negra et al., 2011), or even trophic blooms of pelagic crinoids followed by their mass accumulation, scattering and winnowing (Ferré et al., 2018). They are interpreted as being related to heightened marine productivity and oxygen–deficient water masses. Such event beds have been observed worldwide in coeval biostratigraphic position (around the CTB –namely the Plenus Beds– and above) in the Western Interior Seaway (USA, Caron et al., 2006), the Boreal Realm (Anglo–Paris Basin: Jefferies, 1962, 1963; Gale et al., 1993; Ferré and Breton, 1995) and the Tethys (Tibet: Bomou et al., 2013; Tunisia: Caron et al., 2006) (Figure 8.6). For the first time, I report in SE Turkey the record of the ‘filament’ event beds as potential marker beds around and above the C–T boundary. Moreover, the occurrence of ‘filament’ beds below the FO of *H. helvetica* may constitute a first–order correlative tool to anticipate or precise the CTB, above–mentioned the restoration of keeled planktonic foraminifera.

This 'filament event' may indicate a regional and global eustatic sea–level rise. Leckie et al., (2002) mentioned that this global sea–level change as a transition time within the Middle Cretaceous oceanic –climate system. Tectonic and volcanic activities that occurred in the earliest Turonian had an impact on the greenhouse effect and sea–level rise, causing global climate change (Leckie et al., 2002). Meanwhile, a global–scale, higher frequency (3rd–order), the sea–level change could be induced the production of ‘filament’ event beds in the organic–rich limestones of the Karababa–A Member. As in other basins, the ‘filament’ event beds occur during high sea–level conditions around and immediately above the C–TB (Haq, 2014); these high sea–level conditions are prone to bottom anoxia in some restricted areas and, subsequently, to the accumulation of organic–rich deposits such as the Karababa–A Member. From a

palaeoecological point of view, the mass occurrence of ‘filaments’ close to the C–TB may also express enhanced marine productivity (Negra et al., 2011). Gale et al. (2000) suggested that the species change that occurred at the end of the Cenomanian was due to a decrease in productivity due to the increase in sea–level, due to the impact of nutrient–poor ocean waters. Such a mechanism can be applied in relatively shallow waters, where tens of meters of sea–level variation can have significant effects on paleo–environments. This could be the prevailing mechanism in SE Turkey since the Karababa–A Member recorded shallower–water depositional environments (Mülayim et al., 2019a)

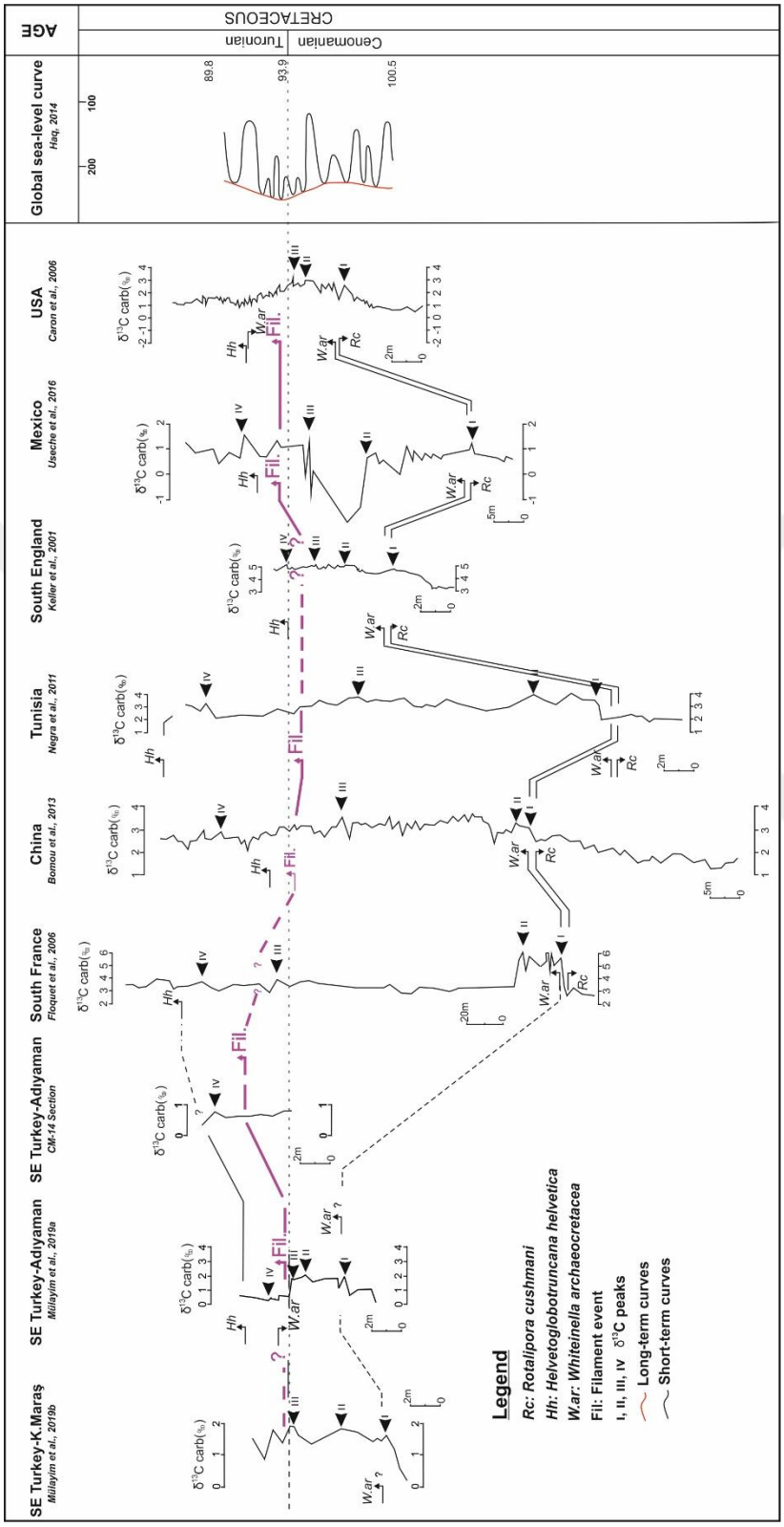


Figure 8.7. Correlation of the studied section with the various sections with first and last occurrences of zone marker taxa, filament events, sea–level variations, and carbon isotope peaks.

8.3 Stratigraphic Meaning and Potential of Roveacrinid

The roveacrinoidal assemblages of SE Turkey display no direct stratigraphic inference of index species. Nevertheless, these assemblages are rather diversified and comparable with the other lower Cenomanian assemblages found in adjacent countries. But I must stress out that these are less diversifed than the coeval assemblages from the US Gulf Coast (Peck 1943, 1948; Hess 2015; Gale 2017), and mainly consist in weakly ornamented species. Despite this lack of specific stratigraphic value, their recurring occurences can be used to define abundance levels (environmental and/or eustatic meaning) correlatable between boreholes on a intra–basinal scale, or at a wider scale (Arabian Platform, E–W Tethysian–wide correlations, etc.). Further works will have to focus on a detailed compiling of such abundance levels both in cores and field sections, within the scope of framing a comprehensive list of successive biostratigraphic events, among which roveacrinid abundance levels would have a lead part, as they are having nowadays in northern Africa (Benyoucef et al. 2017; Ferré et al. 2017).

8.3.1 Palaeo–Environmental Proxies and Correlation to Adjacent Areas

All the study boreholes are scattered over SE Turkey; therefore, I can assume that the roveacrinoidal material, found as crumbled and disarticulated pieces within mudstone facies, provides fair and reliable insights about the roveacrinoidal population during the early Cenomanian: the roveacrinoid skeletons were not transported far away, even stirred by weak bottom currents, and locally dismantled, and scattered within mud–supported sediments. Roveacrinids, as well as saccocomids, were hemipelagic to pelagic organisms, with possible escape response to escape predators. Subsequently to their early planktonic larval stage inducing a wide dispersal of any echinoderm brood, these roveacrinoidal relics can be regarded as potential biostratigraphic index species, and environmental proxies as well. Since they are usually found associated with calcisphere blooms, and their own abundance occurrences are positively correlated with those of first–level, surface carbonate producers (blooms of calcareous dinocysts, calcispheres, and heterohelicidids; Ferré 1997), they have been regarded as

opportunistic organisms. The Upper Cretaceous rocks of SE Turkey show unexpectedly the dual presence of roveacrinids and saccocomids. Since roveacrinids have been found so far over the Arabian Platform more frequently in carbonate–grained, open–ramp marine environments, their co–occurrence advocates for a mixed environment or, at least, supports that saccocomids were swept secondarily from a shallower but quieter environment. Furthermore, I may wonder about their potential role (HMC echinodermal plates as enhancing agent) in the dolomitization further south and the poronecrosis of potential reservoir rocks (Figure 8.8).

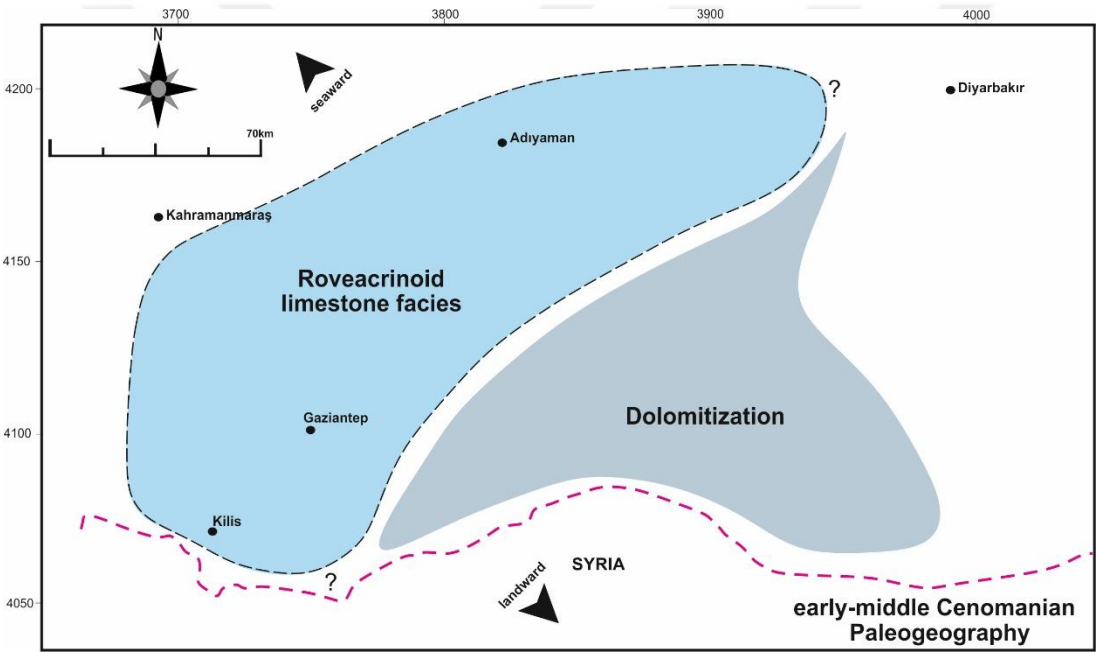


Figure 8.8. Geographic distribution of roveacrinid facies over SE Turkey.

8.4 Rudist Shell Concentrations

Rudists constitute exclusive bioclasts, characterized mainly by radiolitid species in the middle part of the Derdere Formation. Most of the calcitic outer shell layer of bioclasts is completely recrystallized and commonly unbroken. The cellular prismatic structure of this layer can be partly observed in some fragments. The aragonitic inner shell layer of radiolitids is unprotected due to dissolution. In some cases, the shells are disoriented and assume multiple superimposed orientations in the same layer. Isolated individuals

are also common; small bouquets are rare. Bioerosion may have led to the formation of elongated fragments found both in bioclastic fractions, together with large fragments, where they appear oriented. It appears in this section that rudists are associated with bioclastic levels composed almost exclusively of comminuted rudist shells, lodged even in between close–set individuals. The bioclasts derive from rudist, bivalve and roveacrinid shells and appear to be bioeroded and moderately abraded. They laterally interfinger with small–bioclastic to large–scale limestone beds in which the bioclasts consist of poorly sorted, bioeroded and fairly abraded rudist, bivalve and echinoid shell fragments in a silty–bioclastic wackestone matrix. In some cases, grading appears well developed, suggesting that the final deposition of skeletal elements was caused by high–energy events such as storm flows. A small number of holes in the bioclasts were observed in field studies and also in studies of thin–section. These are very rare and small, probably bored by algae and fungi. Physical breakdown seems to be the main piece of evidence of bioerosion.

In the Derdere Formation, sheet–like and tabular bodies are usually associated with monospecific rudist associations at the top of the unit. These do not exhibit horizontal orientation. The rudist shells, in upright growth position, appear either clustered or as isolated individuals. The top of this tabular body may be associated with an incipient hardground. Bedding is often evidenced by such surfaces which are observed especially at the Cenomanian–Turonian boundary. This type of shell accumulation characterizes the top bed of the Derdere Formation (upper Cenomanian). Grain sorting is poor and bioclasts are bioeroded and moderately abraded; shells are packed. However, rudist–rich levels appear to be concentrated in the upper two metres, whereas they become rare upsection; rudists often form levels. In other cases, they appear as oriented, dispersed, toppled individuals of pristine preservation or slightly reworked. The upper shell bed is associated with a sharp basal contact with the Karababa Formation. Most of the rudist shell beds in the Derdere Formation are composed of large numbers of shells that are oriented parallel to subparallel with respect to bedding. These beds have a discontinuous shell distribution laterally. The broadly spaced, imbricated stacking of the radiolitid shells implies originally loosely clustered shells. Storm waves may have been caused by toppling and dense stacking of shells.

In the Karababa Formation, shell beds are horizontal, in lateral view orientation. Most shells show signs of bioerosion; they are highly abraded, while some of them are still articulated. Shell fragments dominate over complete shells; fragmentation and abrasion are abundant and shells are comminuted beyond taxonomic recognition. Their orientation is random, while species diversity is low. These monospecific shell beds are thick. Rudists in growth position are rare; most of them appear to have toppled and locally oriented, but may have been reworked. Rudist–rich beds are frequent in the uppermost part of the series, whereas they become rarer in the middle but are abundant and thicker in the middle–upper part of the Karababa Formation. Good shell preservation is indicative of a more energetic environment but the presence of unbroken shells suggests that water circulation was not so effective in destroying shells. Differences in shell orientation recognised at some levels suggest variations in current direction. Species diversity is low. The removal of finer matrix produced by bioerosion and in–situ reworkings of skeletal elements, rather than transport, are linked to periods of prolonged exposure and low sedimentation rates.

8.4.1 Taphonomic Aspects of Rudists

In the Sabunsuyu succession, rudists represent a greater proportion of fossil assemblages from Cenomanian– Santonian limestones. Taphonomic observations yield many data on the sedimentary processes in operation. Rudists occurred in three palaeoecological morphotypes, i.e., elevators, clingers and recumbents (Gili et al., 1995; Skelton and Gili, 2002) and their palaeoecological characters have recently been reviewed by Gili and Götz (2018). It seems that rudists were rarely fossilized in life position because of storms that could cause toppling of shells. However, the conical and cylindro–conical upright position of elevator radiolitids observed may indicate growth position. In a few cases, the small cylindro–conical radiolitid shells show an upward curvature. The recumbent ichthyosarcolitids (Skelton and Gili, 2002; Gili and Götz, 2018) were not observed in any life position. The body cavities of rudists are usually infilled by the surrounding finer bioclastic sediments and/or more commonly by peloids.

CHAPTER 9

CONCLUSIONS

The present thesis presents an improved stratigraphic framework, mainly based on additional biostratigraphic data, stable isotopic ($\delta^{13}C$ and $\delta^{18}O$) analysis, and a newly established sequence stratigraphic scheme. The thesis also worked out faunal assemblages and microfacies analysis that can be correlated with adjacent platform areas and that enable the reconstruction of palaeoenvironmental changes in interaction with sea–level fluctuations and palaeogeographical development.

The following key conclusions can be drawn from this study:

OAE 2 and Drowning Carbonate Platform

- Around the CTBE, the carbonate platform in SE Turkey drowned under the euphotic zone owing to rapid eustatic sea–level rise and local tectonic effects. The $\delta^{13}C$ excursion provides a direct correlation between the late Cenomanian–early Turonian OAE2, the Cenomanian–Turonian boundary, and the drowning of the SE platform. This indicates that prevailing oxygen–poor environmental conditions during OAEs may be responsible for periods of carbonate platform drowning. The rate of accumulation after the drowning unconformity is very low, and this may produce a short condensed section. The drowning of the platform coincided approximately with the widely documented Cenomanian–Turonian OAE and sea–level rise.

- The drowning below the euphotic zone and the resulting shutdown of the carbonate productivity coincided with a substantial change in the microfossil assemblages, manifested by a major and rapid decline in species diversity and abundance, particularly the foraminifera.

Lithostratigraphy and Biostratigraphy

- Timing of the Cenomanian–Turonian platform succession is improved, mainly based on new biostratigraphic data of detailed planktonic and benthic foraminifera investigations and rudist and calcareous nannofossils findings. These results can be integrated into over regional biozonation–schemes. In particular, the position of the Cenomanian–Turonian boundary can be determined in many cases and the termed Derdere Formation can be subdivided. The enhanced stratigraphy allows north to south correlations within the entire study area and with successions in the Arabian Plate.

- During the early Turonian, the carbonate deposition in SE Turkey recovered contemporaneously with the development and diversification of various planktonic foraminifera groups in deeper-water records (e.g. *Dicarinella, Marginotruncana*, and *Helvetoglobotruncana*). However, biostratigraphic interpretation of shallow-water sequences is inherently more challenging because of the generally low species diversity, the sporadic microfossil occurrences, and the low diversity and endemism in macrofossils. These difficulties are also apparent in the studied sections. However, sufficient age control can be obtained for the Cenomanian–Turonian transition by integrated microfossil biostratigraphy.

- Rudists are here described from the Sabunsuyu succession for the first time. The biostratigraphical data obtained from these provide a valuable contribution to a better understanding of the Derdere and Karababa formations in the Sabunsuyu succession. The biogeography and correlation of rudists identified here show a low diversity in comparison to those of the northern

Mediterranean Tethys, but are similar to recorded occurrences from the southern margin and to the distribution and diversity of these species towards the eastern part of the Arabian Platform.

Sequence Stratigraphy

- A sequence stratigraphic model containing three sequence boundaries, three sedimentary sequences, the related systems tracts, and maximum flooding surfaces is newly established and correlated over the entire study area. The recent scheme is compared with a global model and the Arabian Plate. Differences predominantly result from minor order sea–level changes and local/regional tectonic events. A comparison of the sequence stratigraphical framework with that for adjacent areas (northern Sinai, Gulf of Suez, and Jordan) and with the global scheme of Haq (2014) reveals a few differences in the timing of sequence boundaries, which may be related mainly to local/regional tectonic events that affected deposition in the study area, as well as to minor sea–level fluctuations. It is concluded here that the depositional history of the Cenomanian–Turonian sequence examined was controlled by the global eustatic sea–level change (Haq and Al–Qahtani, 2005; Haq, 2014) and a regional to local tectonic effect (i.e., trusting and crustal loading) of the development in the northern Arabian continental margin in southeast Turkey that began during the late Cenomanian– early Turonian.

Paleoecological Proxies

- The roveacrinid assemblages of southeastern Turkey show noticeable discrete differences, among which the faint presence of saccocomids, and the high morphological diversity of roveacrinids. Some simple occurrence or accumulation levels can be used as baseline marker beds for local datation, inner–field, or even inter–regional correlation depending on the relative abundance of roveacrinid remains. Such abundance and/or accumulation

levels are suitable for worldwide correlation, all correlatable with eustatic changes.

- Pithonellids–rich deposits of the Derdere Formations are the result of paleoenvironmental conditions related to an early phase of the transgression that flooded the northern Arabian Carbonate Platform (SE Turkey) in the earliest Cenomanian. Pithonellids have been interpreted to be opportunistic organisms that inhabited eutrophic, ramp environments together with other opportunist forms such as r or r–k strategists planktonic foraminifera and roveacrinids.

- Filament event is characterized in Karababa–A Member by the abundance of r–species (e.g. *Whiteinella*), Local paleoenvironmental conditions may be influenced by the turnover and consequently, the *W. archaeocretacea* PRZ could have a variable duration in the study area. South Tethyan realm of the paleontological record is poor as well as the C–T boundary in SE Turkey filaments can be used as a biomarker as a stratigraphic level. These 'filament' event beds are also correlated on a global scale in worldwide.

REFERENCES

Abdel–Fattah, Z.A., Kora, M.A., and Raafat, S.A. 2018. Depositional environments and sequence stratigraphy of a mixed siliciclastic–carbonate ramp. An example from the Cenomanian to Turonian Galala Formation in the northern Eastern Desert, Egypt. Journal of African Earth Sciences 147, 352–373.

Accarie, H., Emmanuel, L., Robaszynski, F., Baudin, F., Amédro, F., Caron, M., and Deconinck, J. F. 1996. La géochimie isotopique du carbone ($\delta^{13}C$) comme outil stratigraphique. Aplication à la limite Cénomanien–Turonien en Tunisie central. C. R. Acad. Sci. Paris 322, 579–586.

Aigner, T. 1985. Storm depositional systems. Dynamic stratigraphy in modern and ancient shallow marine sequences. Springer, Berlin, 174 p.

Ala, M., and Moss, B. 1979. Comparative petroleum geology of SE Turkey and NE Syria. Journal of Petroleum Geology. 1.3–27.

Alsenz, H., Regnery, J., Ashckenazi–Polivoda, S., Meilijson, A., Ron–Yankovich, L., Abramovich, S., Illner, P., Almogi–Labin, A., Feinstein, S., Berner, Z. and Püttmann, W. 2013. Sea surface temperature record of a Late Cretaceous tropical southern Tethys upwelling system, Palaeogeography, Palaeoclimatology, Palaeoecology, 392, 350–358.

Alsharhan, A.S., and Nairn, A.E.M., 1997. Sedimentary basins and petroleum geology of the Middle East. Elsevier, Amsterdam, 878 p.

Amedro, F., Accarie, H., and Robaszynski, F. 2005. Position de la limite Cénomanien–Turonien dans la formation Bahloul de Tunisie centrale: apports intégrés des ammonites et des isotopes du carbone (δ13C). Eclogae geol. Helv., 98, 151–167.

Andrawis, S.F., Faris, M., and El Sheikh, H. 1986. Biostratigraphic studies on the Upper Cretaceous (Senonian) Rocks of East Mubarak, Well No. 1, Western Desert, Egypt. Egyptian Journal of Geology, 30, 121–130.

Anthonissen, D.E., and Ogg, J. G., (compilers) 2012. Appendix 3: Cenozoic and Cretaceous biochronology of planktonic foraminifera and calcareous nannofossils. In: Gradstein, F. M., Ogg, J. G., Schmitz, M. D., and Ogg, G. M., (eds.) The Geologic Time Scale 2012, 2. Amsterdam, Elsevier, 1083–1127.

Arthur, M. A., and Schlanger, S. O. 1979. Cretaceous 'oceanic anoxia events' as causal factors in the development of reef reservoirs giant oil fields. American Association of Petroleum Geologists Bulletin, 63, 870–885.

Arthur, M. A., Dean, W. E., and Pratt, L. M. 1988. Geochemical and climatic effects of increased marine organic carbon burial at the Cenomanian/Turonian boundary. Nature, 335, 714–717.

Arthur, M. A., Zachos, J.C., and Jones, D. S. 1987. Primary productivity and the Cretaceous/Tertiary boundary event in the oceans. Cretaceous Research, 8, 43–45.

Arthur, M. A., Schlanger, S. O., and Jenkyns, H. C. 1987. The Cenomanian–Turonian Oceanic Anoxic Event II. Palaeoceanographic controls on organic matter production and preservation. In: Marine petroleum source rocks (eds Brooks, J. and Fleet, A.J.). Geological Society of London, Special Publication 26, 401–420.

Arthur, M. A., Jenkyns, H. C., Brumsack, H. J., and Schlanger, S. O. 1990. Stratigraphy, geochemistry, and paleoceanography of organic carbon–rich Cretaceous sequences. In: Ginsburg, R.N. and Beaudoin, B. (eds.) Cretaceous Resources, Events and Rhythms Background and Plans for Research. Kluwer Academic, 75–119.

Baccelle, L., and Bosellini, A., 1965. Diagrammi per la stima visive Della composizione percentuale nelle rocce sedimentarie. Annali Della Università di Ferrara, Sezione IX, Science Geologiche Paleontologiche, 1, 59–62.

Bandel, K., and Salameh, H., 2013. Geologic development of Jordan. Evolution of its rocks and life. The University of Jordan Press, Amman, 278 p.

Barrier, E., and B. Vrielynck (Contributors: Bergerat, F., Brunet, M.F., Mosar, J., Poisson, A. and S. Sosson), 2008, Palaeotectonic Maps of the Middle East. Tectono–SedimentaryPalinspastic Maps from Late Norian to Piacenzian:

Commission for the Geological Map of the World (CGMW)/UNESCO (http://www.ccgm.org), scale 1:18 500 000, 14 sheets.

Bauer, J., Kuss, J., Steuber, and T. 2003. Sequence architecture and platform configuration (Late Cenomanian–Santonian), Sinai, Egypt. Sedimentology 50, 387–414.

Bauer, J., Steuber, T., Kuss, J., and Heimhofer, U. 2004. Distribution of shallow–water benthics (rudists, calcareous algae, benthic foraminifera) in the Cenomanian–Turonian carbonate platform sequences of Sinai, Egypt. In: Hofling, R. (eds.), Contributions to the 5th International Congress on Rudists, Erlangen, Germany 247, 207–232.

Benyoucef, M., Mebarki, K., Ferré, B., Adaci, M., Bulot, L.G., Desmares, D., Villier, L, Bensalah, M., Frau, C., Ifrim, C., and Malti, F. Z. 2017. Litho– and biostratigraphy, facies patterns and depositional sequences of the Cenomanian–Turonian deposits in the Ksour Mountains (Saharan Atlas, Algeria). Cretaceous Research 78, 34–55.

Benzaggagh, M., Homberg, C., and Ben Abdesselam–Mahdaouid, S. 2018. Saccocomid crinoid sections and biozones of the upper Jurassic in the western Tethyan realm. In: Villaseñor Martínez A–B, Rosales Domínguez C, Olóriz–Sáez F (eds.) 10th International Congress on the Jurassic System, San Luis Potosí, Mexico, 3, 20–24.

Berberian, M., and King, G.G.P. 1981. Towards a paleogeography and tectonic evolution of Iran: Canadian Journal of Earth Sciences, 18, 210–265.

Blomeier, D. P., and Reijmer, J. J. 1999. Drowning of a Lower Jurassic carbonate platform: Jbel Bou Dahar, High Atlas, Morocco. Facies, 41, 81–110.

Boggs, S. J., 2009. Petrology of Sedimentary Rocks. 2nd Edition, Cambridge University Press, New York, 600 p.

Bomou, B., Adatte, T., Tantawy, A. A., Mort, H., Fleitmann, D., Huang, Y., and Föllmi, K.B. 2013. The expression of the Cenomanian–Turonian oceanic anoxic event in Tibet. Palaeogeography, Palaeoclimatology, Palaeoecology, 369, 466–481.

Bornemann, A., and Norris, R. D. 2007. Size–related stable isotope changes in Late Cretaceous planktonic foraminifera: implications for paleoecology and photosymbiosis. Marine Micropaleontology, 65, 32–42.

BouDagher–Fadel, M. K. 2012. Biostratigraphic and geological significance of planktonic Foraminifera. Developments in Palaeontology and Stratigraphy 22. Elsevier, Amsterdam, 312 p.

Bozcu, A., Baudin, F., Danelian, T., Vrielynck, B., Bozcu, M., and Poisson, A, 2011. New evidence for the record of the Cenomanian–Turonian oceanic anoxic event (OAE 2) in the Pamphylian basin (Akdoğan Section, Antalya Nappes, SW Turkey): Comparison with surrounding basinal settings. Cretaceous Research, 32 (6), 823–832.

Brandano, M., Corda, L., Tomassetti, L., and Tagliavento, M., 2016. Frequency analysis across the drowning of a lower Jurassic Carbonate Platform: the Calcare Massiccio Formation (Apennines, Italy). Marine and Petroleum Geology, 78, 606–620.

Buchbinder, B., Benjamini, C., and Lipson–Benitah, S., 2000. Sequence development of Late Cenomanian–Turonian carbonate ramps, platforms and basins in Israel– Cretaceous Research 21, 813–843.

Burchette, T.P., and Wright, V.P. 1992. Carbonate Ramp Depositional Systems. Sedimentary Geology, 79, 3–57.

Burnett, J.A. 1998. Upper Cretaceous. In: Bown, P.R. (eds.) Calcareous Nannofossil Biostratigraphy (British Micropalaeontological Society Publications Series). Chapman and Kluwer Academic Publishers, London, 132–199.

Caffau, M., Pugliese, N., and Plenicar, M. 1996. The development of the mollusc fauna in the Cenomanian of the stratigraphic sequence of Visogliano (Karst of Triest, Italy). Geologija 37/38.

Campbell, A. E. 1992. Unconformities in Seismic Records and Outcrops. PhD thesis, Vrije Universiteit, Amsterdam 187 p.

Carbone, F. 1993. Cretaceous depositional systems of the evolving Mesozoic carbonate platform of central Apennine thrust belt, Italy. Geologica Romana 29, 31–53.

Carbone, F., Praturlon, A., and Sirna, G. 1971. The Cenomanian shelf edge facies of Rocca di Cave. Geologica Romana, 10, 131–198.

Caron, M. 1985. Cretaceous Planktonic Foraminifera. In: Bolli, H.M., Saunders, J.B. and Perch Nielsen, K. (eds.) Plankton Stratigraphy. Cambridge University Press, Cambridge, 17–86.

Caron, M., and Homewood, P. 1983. Evolution of early planktonic foraminifera. Marine Micropaleontology, 7, 453–462.

Caron, M., Dall'agnolo, S., Accarie, H., Barrera, E., Kauffman, E.G., Amedro, F., and Robaszynski, F. 2006. High–resolution stratigraphy of the Cenomanian–Turonian boundary interval at Pueblo (USA) and Wadi Bahloul (Tunisia): stable isotopes and bioevents correlation. Géobios, 39, 171–200.

Carter, D.J., and Hart, M. 1977. Aspects of mid–Cretaceous stratigraphical micropalaeontology. Bulletin of the British Museum, Natural History (Geology), 29, 1–135.

Cater, J.M.L., and Gillcrist, J.R. 1994. Karstic reservoirs of the mid–Cretaceous Mardin Group, SE Turkey: tectonic and eustatic controls on their genesis, distribution, and preservation. Journal of Petroleum Geology, 17, 253–278.

Catuneanu, O., and Abreu, V.E.A.L. 2009. Towards the standardization of sequence stratigraphy. Earth–Science Reviews, 92, 1–33.

Catuneanu, O., Galloway, W.E., Kendall, C.G.St.C., Miall, A.D., Posamentier, H.W., Strasser, A., and Tucker, M.E. 2011. Sequence stratigraphy: methodology and nomenclature. Newsletters on Stratigraphy, 44, 173–245.

Cestari, R. 2008. Los rudistas (Bivalvia, Hippuritoidea) en el Appenino centroemeridional (Italia): analisis de las associaciones de Radíolitidos en context de plataforma calcarea en el SupereGreenhouse climate del Cretacico

Superior. Unpubl. PhD thesis. Universitat Autonoma de Barcelona, Bellaterra, 198 p.

Cestari, R., and Laviano, A, 2012. Rudist facies distribution in the Late Cretaceous of Cilento and western Basilicata (southern Italy). Rivista Italiana di Paleontologia Stratigrafia 118, 277–294.

Cestari, R., and Sartorio, D. 1995. Rudists and facies of the periadriatic domain. Agip, S. Donato Milanese, 207 p.

Cestari, R., Pons, J. M., and Sirna, G. 1998. Undescribed Ichthyosarcolites from Sicily belonging to Gemmellaro's Collection. In: Masse, J.–P., Skelton, P.W. (eds.), Quatrieme Congres international sur les Rudistes. Geobios, Memoire special 22, 69–73.

Chikhi–Aouimeur, F. 2010. L'Algerie a travers son patrimoine paleontologique. Les rudistes. Sarl Baosem, 269 p.

Chikhi–Aouimeur, F., Abdallah, H., Pons, J. M., and Vicens, E., 2006. The Cenomanian–Turonian rudists of the Gafsa region, Tunisia. In: Malchus, N., Pons, J.–M. (eds.), Organisms diversity and evolution 6. Electronic supplement 16, Abstracts and posters of the "International Congress on Bivalvia" at the Universitat Autonoma de Barcelona, Spain.

Coccioni, R., and Galeotti, S. 2003. The mid–Cenomanian Event: prelude to OAE 2. Palaeogeography, Palaeoceanography, Palaeoecology 190, 427–440.

Coccioni, R., and Premoli Silva, I. 2015. Revised Upper Albian–Maastrichtian planktonic foraminiferal biostratigraphy and magnetostratigraphy of the classical Tethyan Gubbio section (Italy). Newsletters on Stratigraphy, 48, 47–90.

Colom, G. 1955. Jurassic–Cretaceous pelagic sediments of the western Mediterranean zone and the Atlantic area. Micropaleontology, 1, 109–124.

Coşkun, B. 1992. Oil possibilities of the Mardin Group around the Adıyaman, Çemberlitşs and Bölükyayla. PhD Thesis, Ankara University, 200 p.

.Coşkun, B., 1996. Tectonic controls on the evolution of porosity in the Cretaceous Mardin Group carbonates, Adıyaman oilfields, SE Turkey. Journal of Petroleum Geology 19, 4, 445–460.

Cros, P., Dercourt, J., Günay, Y., Fourcade, E., Bellier, J.P., Lauer, J.P., Manivit, H., and Kozlu, H. 1999. The Arabian Platform in southeastern Turkey: an Albian–Cenomanian carbonate ramp collapsed during the Senonian. TAPG Bulletin 11,1, 55–77.

Çelikdemir, E. M., Dülger, S., Görür, N., Wagner, C., and Uygur, K., 1991. Stratigraphy, sedimentology, and hydrocarbon potential of the Mardin Group, SE Turkey. Special Publications of the European Association of Petroleum Geoscientists 1, 439–454.

Çoruh, T., Yakar, H., and Ediger, V.S. 1997. Güneydoğu Anadolu Bölgesi otokton istifinin biyostratigrafi atlası (Atlas of biostratigraphy for the autochthonous succession of the southeastern Anatolian Region). TPAO Araştırma Merkezi Grubu, Eğitim Yayınları, Ankara 30, 401p.

Dali–Ressot, M.D. 1987. Les Calcisphaerulidae des terrains Albien–Maastrichtien de Tunisie centrale (J. Bireno et J. Bou el Ahneche): interets systematique, stratigraphique et pale´oge´ographique. PhD thesis, University of Tunis, p. 191.

Davey, S.D., and Jenkyns, H.C. 1999. Carbon–isotope stratigraphy of shallow–water limestones and implications for the timing of Late Cretaceous sea–level rise and anoxic events (Cenomanian–Turonian of the peri–Adriatic carbonate platform, Croatia). Eclogae Geologicae Helvetiae, 92, 163–170.

Demirel, I. H., and Güneri, S. 2000. Cretaceous carbonates in the Adıyaman region, SE Turkey: an assessment of burial history and source–rock potential. Journal of Petroleum Geology, 23, 91–106.

Desmares, D., Grosheny, D., Beaudoin, B., Gardin, S., and Gauthier–Lafaye, F. 2007. High–resolution stratigraphic record constrained by volcanic ash beds at the Cenomanian–Turonian boundary in the Western Interior Basin, USA. Cretaceous Research, 28, 561–582.

Desmarest, A.G. 1817. Memoire sur deux genres de coquilles fossiles cloisonnees et a siphon. Journal de Physique, de Chimie et d'Histoire naturelle 85, 42–51.

Dhondt, A.V. 1973. Systematic revision of the subfamily Neitheinae (Pectinidae, Bivalvia, Mollusca) of the European Cretaceous. Memoires de l'Institut royal des Sciences naturelles de Belgique 176, 1–101.

Dias–Brito, D. 1992. Ressurgencia neo–albiana a eoturoniana na costa leste da America do Sul: evideˆncias a partir de estudos microbiofaciologicos na Bacia de Campos, Brasil. 2º Simposio sobre as Bacias Cretacicas Brasileiras, Resumos expandidos, 35–37.

Dias–Brito, D. 1996. A evolucao do geossistema mesocretaceo da margem sudeste–leste do Brasil, como sugerida por estudos microfaciolo´ gicos. Boletim do 4o Simpo´sio sobre o Creta´ceo do Brasil, 21–31.

Dias–Brito, D. 2000. Global stratigraphy, paleobiogeography and paleoecology of Albian–Maastrichtian pithonellid calcispheres: impact to Tethys configuration: Cretaceous Research, 21, 315–349.

Di Stefano, P., and Ruberti, D. 2000. Cenomanian rudist–dominated shelf–margin limestones from the Panormide carbonate platform (Sicily, Italy): facies analysis and sequence stratigraphy. Facies 42, 133–160.

Douville, H. 1888. Etudes sur les caprines. Bulletin de la Societe Geologique de France 16 (3), 699–730.

Drzewiecki, P.A. and Simo, J.A. 1997. Carbonate platform drowning and oceanic anoxic events on a mid–Cretaceous carbonate platform, south–central Pyrenees, Spain. Sedimentary Research, 67, 698–714.

Dunham, R. J. 1962. Classification of carbonate rocks according to depositional textures. In: Ham, W.E. (eds.) Classification of Carbonate Rocks. American Association of Petroleum Geologists, Tulsa, OK, Memoirs, 108–121.

Duran, O., and Aras, M. 1990. Yeniköy Petrol Sahası (GD Anadolu) Mardin Grubu karbonatları çökel fasiyes ve rezervuar özellikleri. Turkey 8. Petroleum Congress Geology Bulletin, 272–281.

d'Orbigny, A. 1847. Sur les brachiopodes ou palliobranches. Comptes Rendus hebdomadaires des Seances de l'Academie des Sciences Paris 25, 266–269.

d'Orbigny, A. 1850. Paleontologie Française, Terrains cretaces 4, Brachiopodes. Masson, Paris, 105–328.

Embry, A.F., and Klovan, J. E. 1971. A Late Devonian reef tract on northeastern Banks Island, Northwest Territories. Bulletin Canadian Petroleum Geology, 33, 730–781.

Emrich, K., Enhalt, D. H., and Vogel, J. C. 1970. Carbon isotope fractionation during the precipitation of calcium carbonate. Earth Planet. Sci. Lett., 8: 363–371.

Erlich, R.N., Barrett, S.F., and Guo, B.J. 1990. Seismic and geologic characteristics of drowning events on carbonate platforms. American Association of Petroleum Geologists Bulletin, 74, 1523–1537.

Erlich, R. N., Longo, A. P., and Hyare, S. 1993. The response of carbonate platform margins to drowning: evidence of environmental collapse. In: Loucks, R.G. and Sarg, J.F. (eds.) Carbonate Sequence Stratigraphy. American Association of Petroleum Geologists, Tulsa, OK, Memoirs, 57, 241–266.

Ettachfini, E.M. and Andreu, B. 2004. Le Cénomanien et le Turonien de la plate–forme Préafricaine du Maroc. Cretaceous Research, 25, 277–302.

Falzoni, F., Petrizzo, M.R., Jenkyns, H.C., Gale, A.S., and Tsikos, H. 2016. Planktonic foraminiferal biostratigraphy and assemblage composition across the Cenomanian–Turonian boundary interval at Clot Chevalier (Vocontian Basin, SE France). Cretaceous Research, 59, 69–97.

Falzoni, F., Petrizzo, M. R., and Valagussa, M, 2018. A morphometric methodology to assess planktonic foraminiferal response to environmental perturbations: the case study of Oceanic Anoxic Event 2, Late Cretaceous. Bollettino della Società Paleontologica Italiana, 57, 103–124.

Farinacci, A., and Manni, R. 2003. Roveacrinids from the Northern Arabian Plate in SE Turkey. Turkish Journal of Earth Science, 12, 209–214.

Farouk, S., Ahmad, F., and Powell, J. H. 2017. Cenomanian–Turonian stable isotope signatures and depositional sequences in northeast Egypt and central Jordan. Journal of Asian Earth Sciences 134, 207–230.

Ferré, B., and Berthou, P.Y. 1993. Roveacrinidal remains from the Cotinguiba formation (Cenomanian–Turonian) of the Sergipe Basin (NE Brazil). In: 13º Congresso Brasileiro de Paleontologia, 1º Simposio Paleontologico do Cone Sul, Sao Leopoldo, Brazil, Boletim de Resumos, 119 p.

Ferré, B, and Berthou, P.Y. 1994. Roveacrinidal remains from the Cotinguiba formation (Cenomanien–Turonien) of the Sergipe Basin (NE Brazil). Acta Geol. Leopold XVIII (39–1), 299–313.

Ferré, B., and Breton, G. 1995. First evidence of starfish ossicles of the family Asteriid in the Cenomanian to Coniacian chalks of the Paris Basin (France). Revue de Micropaléontologie, 38 (4):299–309.

Ferré, B., Cros, P., and Fourcade, É. 1997. Tethyan Mid–Cretaceous (Cenomanian–Turonian) Roveacrinids (Roveacrinida, Crinoidea) as stratigraphical and paleobiogeographical tools. In: Final Regional Meeting of IGCP Project 362 BTethyan and Boreal Cretaceous^, Stara Lesna, Slovakia, Mineralia Slovaca, Bratislava 29 (4–5), 267–268.

Ferré, B., and Granier, B. 1997a. The Albian stemless microcrinoids (Roveacrinidae, Crinoidea) of the Congo Basin (Angola). Gaea Heidelbergensis, 3, 129–130.

Ferré, B., and Granier, B. 1997b. Roveacrinus berthoui, nov. sp., the earliest representative of the family Roveacrinidae (Roveacrinida, Crinoidea) in the lower Hauterivian of Busot (Alicante, Spain). In: Final Regional Meeting of IGCP Project 362 BTethyan and Boreal Cretaceous^, Stara Lesna, Slovakia, Mineralia Slovaca, Bratislava 29 (4–5), 338–339.

Ferré, B., and Dias–Brito, D. 1999. Microfacies recognition of Roveacrinid families Lom–bardia, Eothrix, Globochaete and other strains. In: Dias–Brito, D., de Castro, J.C., Rohn, R. (eds.), Boletim do 5◦Simposio sobre o Cretaceo do Brasil, 651–659.

Ferré, B., Fernandez–Gonzalez, M., and Dias–Brito, D., 1999. New insight into Microcalam–oides Bonet, 1956–Revised systematics and subsequent bearings.

In: Dias–Brito, D., de Castro, J.C., Rohn, R. (eds.), Boletim do 5oSimposio sobre o Cretaceo do Brasil, 661–668.

Ferré, B., and Granier, B. 2000. Roveacrinus berthoui nov. sp., Early Hauterivian representative of Roveacrinidae (Roveacrinida, Crinoidea) of Busot (Alicante, Spain). Geol Carpath 51, 101–107.

Ferré, B., and Granier, B. 2001. Albian roveacrinids from the southern Congo Basin, off Angola. Journal of South America Earth Science 14, 219–235.

Ferré, B., Mebarki, K., Benyoucef, M., Villier, L., Bulot, L.G., Desmares, D., Benachour, H.B., Marie, L., Sauvagnat, J., Bensalah, M., Zaoui, D., and Adaci, M., 2017. Roveacrinids (Crinoidea, Roveacrinida) from the Cenomanian–Turonian of Southwest Algeria (Saharan Atlas and Guir Basin). Ann Paléontol 103, 3, 185–196.

Ferré, B., Granier, B., Gorzelak, P., and Salamon, M. A. 2018. Cretaceous Roveacrinids from Mexico revisited overcoming the taxonomic misidentifications and subsequent biostratigraphic abuse. Bol. Soc. Geol. Mexico 70, 2, 499 – 530.

Flexer, A., Rosenfeld, A., Lipson–Benitah, S., and Honigstein, A. 1986. The Cretaceous Tethys: Sedimentary Cycles, Biometry, Unconformities and Interregional Sea–Level Changes. In Abstracts, Annual Meeting, Ma'alot, Jerusalem: Israel Geological Society, 37–39.

Flügel, E. 2004. Microfacies of carbonate rocks: analysis, interpretation and application. Springer–Verlag. 976 p.

Folk, R. L. 1965. Some Aspects of Recrystallization in Ancient Limestones. In: Pray LC, Murray RC (eds.) Dolomitization and Limestone Diagenesis. Society for Sedimentary Geology, Special Publications, 13, 14–48.

Fontaine, J.M., Monod, O., Braud, J., and Perincek, D. 1989. The Hezan Units: a fragment of the south neo–Tethyan passive continental margin in SE Turkey. Journal of Petroleum Geology 12, l, 29–50.

Föllmi, K.B., and Gainon, F. 2008. The demise of the northern Tethyan Urgonian carbonate platform and subsequent transition towards pelagic conditions: the sedimentary record of the Col de la Plaine Morte area, central Switzerland. Sedimentary Geology, 205, 142–159.

Föllmi, K. B., Weissert, H., Bisping, M., and Funk, H. 1994. Phosphogenesis, carbon–isotope stratigraphy, and carbonate–platform evolution along the Lower Cretaceous northern Tethyan margin. Geological Society of America Bulletin, 106, 729–746.

Frank, R., Buchbinder, B., and Benjamini, C. 2010. The mid–Cretaceous carbonate system of northern Israel: facies evolution, tectonoestratigraphy configuration and global control on the central Levant margin of the Arabian plate. In: Homberg, C., Bachmann, M. (eds.), Evolution of the Levant Margin and western Arabian platform since the Mesozoic, Geological Society, London, Special Publication, 341, 133–170.

Frija, G., Parente, M., Di Lucia, M., and Mutti, M. 2015. Carbon and strontium isotope stratigraphy of the Upper Cretaceous (Cenomanian–Campanian) shallow–water carbonates of southern Italy: chronostratigraphic calibration of larger foraminifera biostratigraphy. Cretaceous Research 53, 110–139.

Gale, A. S., Jenkyns, H. C., Kennedy, W.J., and Corfield, R.M. 1993. Chemostratigraphy versus biostratigraphy: Data from around the Cenomanian–Turonian boundary: Geological Society of London Journal, 150, 29–32.

Gale, A.S., Hardenbol, J., Hathway, B., Kennedy, W.J., Young, J.R., and Phansalkar, V., 2002. Global correlation of Cenomanian (Upper Cretaceous) sequences: evidence for Milankovitch control on sea–level. Geology, 30, 291–294.

Gale, A.S., Voigt, S., Sageman, B.B., and Kennedy, W.J. 2008. Eustatic sea–level record for the Cenomanian (Late Cretaceous)–extension to the Western Interior Basin, USA. Geology, 36, 859–862.

Gale, A.S. 2016. Roveacrinida (Crinoidea, Articulata) from the Santonian–Maastrichtian (Upper Cretaceous) of England, the US Gulf Coast (Texas, Mississippi) and southern Sweden. Pap Palaeontol 2, 489–532.

Gale, A.S. 2017. An integrated microcrinoid zonation for the lower Campanian chalks of southern England, and its implications for correlation. Cretaceous Research 87, 312–357.

Gebhardt, H., Friedrich, O., Schenk, B., Fox, L., Hart, M.B., and Wagreich, M. 2010. Paleoceanographic changes at the northern Tethyan margin during the Cenomanian–Turonian oceanic anoxic event OAE 2. Marine Micropaleontology, 77, 25–45.

Giles, M.R., and Marshall J.D. 1986. Constraints on the development of secondary porosity in the subsurface: re–evaluation of processes. Marine and Petroleum Geology 3, 243–255.

Gili, E., and Götz, S. 2018. Paleoecology of rudists. Part N2, Chapter 26B. Treatise Online 103, 1–29.

Gili, E., Masse, J. P., Skelton, P.W. 1995. Rudists as gregarious sediment–dwellers, not reef–builders, on Cretaceous carbonate platforms. Palaeogeography, Palaeoclimatology, Palaeoecology 118, 245–267.

Godet, A. 2013. Drowning unconformities: palaeoenvironmental significance and involvement of global processes. Sedimentary Geology 293, 45–66.

Gossage, D. W. 1956. Compiled progress report on the geology part of Petroleum District VI, Southeast Turkey.N. V. Turkse Shell Report no: 2, 22 p.

Görür, N., Çelikdemir, E., and Dülger, S. 1991. Carbonate platforms developed on passive continental margins: Cretaceous Mardin carbonates in southeast Anatolia as an example. Bulletin of the Technical University of Istanbul 44, 301–324.

Gradstein, F.M., J.G. Ogg, A.G. Smith, F.P. Agterberg, W. Bleeker, R.A. Cooper, V. Davydov, P. Gibbard, L. Hinnov, M.R. House, L. Lourens, H–P. Luterbacher, J. McArthur, M.J. Melchin, L.J. Robb, J. Shergold, M. Villeneuve, B.R. Wardlaw, J. Ali, H. Brinkhuis, F.J. Hilgen, J. Hooker, R.J. Howarth, A.H. Knoll, J. Laskar, S. Monechi, J. Powell, K.A. Plumb, I. Raffi, U. Röhl, P. Sadler, A. Sanfilippo, B. Schmitz, N.J. Shackleton, G.A. Shields, H. Strauss, J. Van Dam, J. Veizer, Th. van Kolfschoten and D. Wilson. 2004. A Geologic Time Scale 2004. Cambridge University Press, 589 p.

Gradstein, F.M., Ogg, J.G., Schmitz, M., and Ogg, G. 2012. The Geologic Time Scale, 1–2. Elsevier, Oxford, 1176.

Gregg, J.M. and D.F. Sibley 1984. Epigenetic dolomitization and the origin of xenotopic dolomite texture. Journal of Sedimentary Research, 54, 908–931.

Güven, A., Dinçer, A., Tuna, E. M., and Çoruh, T. 1991. Stratigraphic evolution of the Campanian–Paleocene autochthonous succession of the South Anatolia. Ozan Sungurlu Symposium Proceedings, 238–261.

Hallock, P. 1988. The role of nutrient availability in bioerosion: Consequences to carbonate buildups. Palaeogeography, Palaeoclimatology, Palaeoecology 63, 1–3, 275–291.

Hallock, P., and Schlager, W. 1986. Nutrient excess and the demise of coral reefs and carbonate platforms. Palaios, 1, 389–398.

Hamaoui, M. 1965. On a new subgenus of Hedbergella (Foraminiferida). Israel Journal of Earth Sciences 13, 133–142.

Hancock, J. M. 1993. Sea–level changes around the Cenomanian–Turonian boundary. Cretaceous Research, 14, 553–562.

Hancock, J.M., and Kauffman, E.G., 1979. The great transgressions of the Late Cretaceous. Journal of the Geological Society 136, 175–186.

Handfield, R. W., Bryant, G. F., and Keskin, C., 1959. Measured section, Korudağ (American Overseas Petroleum). TPAO Exploration Group, 523.

Haq, B.U., Hardenbol, J., and Vail, P.R. 1988. Mesozoic and Cenozoic chronostratigraphy and cycles of sea–level change. In: Wilgus, C.K., Hastings, B.S., Posamentier, H., Van Wagoner, J., Ross, C.A. and Kendall, C.G. St C. (eds.) Sea–level Changes: An Integrated Approach. Society of Economic Paleontologists and Mineralogists, Houston, Special Publications, 42, 71–108.

Haq, B. 2014. Cretaceous eustasy revisited. Global Planet Change, 113, 44–58.

Haq, B., and Al–Qahtani, A.M. 2005. Phanerozoic cycles of sea–level change on the Arabian Platform. GeoArabia 10, 127–160.

Haq, B. 2017. Jurassic Sea–Level Variations: A Reappraisal. GSA Today, 28, 1.

Harris, P.M., Frost, S.H., Seigle, G.A., and Schneidermann, N. 1984. Regional unconformities and depositional cycles, Cretaceous of the Arabian Peninsula. In: Schlee, J.S. (eds.), International unconformities and hydrocarbon accumulation. American Association of Petroleum Geologists Memoir 36, 67–80.

Hart, M.B., and Weaver, P.P.E. 1977. Turonian microbiostratigraphy of Beer, SE Devon. Proceedings of the Ussher Society, 4, 86–93.

Hart, M.B., and Bailey, H.W. 1979. The distribution of planktonic Foraminiferida in the mid–Cretaceous of NW Europe. In: Wiedmann, J. (eds.) Aspekte der Kreide Europas. IUGS, Stuttgart, Series A, 6, 527–542.

Hart, M.B. 1980a. The recognition of mid–Cretaceous sea–level changes by means of foraminifera: Cretaceous Research, 1, 289–297.

Hart, M.B. 1980b. A water depth model for the evolution of the planktonic foraminifera: Nature, 286, 252–254.

Hart, M.B. 1999. The evolution and biodiversity of Cretaceous planktonic foraminifera. Geobios, 32, 247–255.

Hart, M.B. 2008. Cretaceous foraminifera from the Turonian succession at Beer, southeastern Devon, England. Cretaceous Research, 29, 1035–1046.

Hess, H. 2015. Roveacrinids (Crinoidea) from the mid–Cretaceous of Texas: ontogeny, phylogeny, functional morphology and lifestyle. Swiss J Palaeont 134, 77–107.

Hilbrecht, H., and Hoers, J. 1986. Geochemical and palaeontological studies of the $\delta^{13}C$ anomaly in Boreal and North Tethyan Cenomanian Turonian sediments

m Germany mad adjanced areas. Palaeogeography, Palaeoclimatology, Palaeoecology 53, 169–189.

Hilbrecht, H., Hubberten, H.W., and Oberhfinsli, H, 1992. Biogeography of planctonic foraminifera and regional carbon isotope variation: productivity and water masses in Late Cretaceous Europe. Palaeogeography, Palaeoclimatology, Palaeoecology 92, 407–421.

Hilbrecht, H. 1998. Late Cretaceous carbon isotope stratigraphy: Potential contribution of carbonate dissolution and taxonomic effects. Zentralblatt der Geologie Paläontologie 1, 1245–1254.

Horstink, J. 1971. Late Cretaceous and Tertiary geological evolution of Eastern Turkey. Proceedings of 1 st Turkish Petroleum Congress, Ankara, Turkey, 25–41.

Huber, B.T., and Petrizzo, M.R. 2014. Evolution and taxonomic study of the Cretaceous planktonic foraminiferal genus *Helvetoglobotruncana* Reiss, 1957. Journal of Foraminiferal Research, 44, 40–57.

Huber, B.T., Petrizzo, M.R., Watkins, D.K., Haynes, S.J., and Macleod, K.G. 2017. Correlation of Turonian continental margin and deep–sea sequences in the subtropical Indian Ocean sediments by integrated planktonic foraminiferal and calcareous nannofossil biostratigraphy. Newsletters on Stratigraphy, 50, 141–185.

Hudson, J. D. 1977. Stable isotopes and limestone lithification. Journal of the Geological Society of London 133, 637–660.

Jaff, R.B.N., Wilkinson, I. P., Lee, S., Zalasiewicz, J., Lawa, F., and Williams, M. 2015. Biostratigraphy and palaeoceanography of the early Turonian–early Maastrichtian planktonic foraminifera of NE Iraq. Journal of Micropalaeontology, 34, 105–138.

Jagt, J.M.W. 1999. Late Cretaceous–Early Palaeogene echinoderms and the K/T boundary in the southeast Netherlands and northeast Belgium Part 1: Introduction and stratigraphy, Part 2: Crinoids. Scr. Geol. 116, 1–155.

Janofske, D., and Keupp, H. 1992. Mesozoic and Cenozoic ‘‘calcispheres’’ update in systematics. International Nannoplankton Association Newsletter 14, 14–16.

Jarvis, G.A., Carson, M.K.E., Cooper, M.B., Hart, P. N. Leary, B.A. Tocher D. Horne, and Rosenfeld, A. 1988. Microfossil assemblages and the Cenomanian–Turonian (Late Cretaceous) Oceanic Anoxic Event. Cretaceous Research, 9, 3–103.

Jarvis, I., Gale, A.S., Jenkyns, H.C., and Pearce, M.A. 2006. Secular variation in Late Cretaceous carbon isotopes: a new $\delta^{13}C$ carbonate reference curve for the Cenomanian–Campanian (99.6–70.6 Ma). Geological Magazine, 143, 561–608.

Jeffenes, R.P.S. 1962. The palaeoecology of the *Actinocamax plenus* Subzone (lowest Turonian) in the Anglo Paris Basin. Palaeontology 4, 609–647.

Jefferes, R.P.S. 1963. The stratigraphy of the *Actinocamax plenus* Subzone (Turonian) in the Anglo–Paris Basin. Proceedings of the Geologists' Association 74, 1–34.

Jefferies, R.P.S., and Minton, P. 1965. The mode of life of two Jurassic species of 'Posidonia' (Bivalvia). Palaeontology, 8, 1, 156–185.

Jenkyns, H.C. 1980. Cretaceous anoxic events: from continents to oceans. Jour. Geological Society of London 137, 171–188.

Jenkyns, H.C., Gale, A.S., and Corfield, R.M. 1994. Carbon– and oxygen–isotope stratigraphy of the English Chalk and Italian Scaglia and its palaeoclimatic significance. Geological Magazine 131, 1–34.

Jenkyns, H.C., Mitterlose, J., and Sliter, W.V. 1995. Upper Cretaceous carbon and oxygen isotope stratigraphy of deep–water sediments from the north–central Pacific, Site 869, flank of Pikinni–Wodejebato, Marshall Islands, in: Winterer, E.L. Sager, W.W., Firth, J.V., Sinton, J. M. (eds.), Proceedings of the Ocean Drilling Program, Scientific Results, 143, Ocean Drilling Program, College Station, Texas, 105–108.

Jenkyns, H.C. 1999. Mesozoic anoxic events and palaeoclimate. Zentralblatt für Geologie und Paläontologie Teil I 7–9, 943–949.

Kalanat, B., Vahidinia, M., Moghaddam, H.V., and Gharaie, M.H.M. 2015. A Cenomanian–Turonian drowning unconformity on the eastern part of Kopet–Dagh Basin, NE Iran. Arabian Journal of Geoscience, 8, 8373–8384.

Karabulut, A., Köylüoğlu, M., and Sayılı, A. 1992. Güneydoğu Anadolu platform bölgesinde (X. Petrol bölgesi) Mardin Grubu ve Karaboğaz Formasyonu rezervuarlarının değerlendirimi. Türkiye 9. Petrol Kongresi Jeoloji Bildirileri. 471–478.

Kedzierski, M., Machaniec, E., Rodríguez–Tovar, F.J., and Uchman, A. 2012. Bio–events, foraminiferal and nannofossil biostratigraphy of the Cenomanian/Turonian boundary interval in the Subsilesian Nappe, Rybie Section, Polish Carpathians. Cretaceous Research 35, 181–198.

Keller, G., Han, Q., Adatte, T., and Burns, S. J. 2001. Palaeoenvironment of the Cenomanian–Turonian transition at Eastbourne, England. Cretaceous Research 22, 391–422.

Keller, G., Berner, Z., Adatte, T., and Stueben, D. 2004. Cenomanian–Turonian and delta C–13, and delta O–18, sea–level and salinity variations at Pueblo, Colorado. Palaeogeography, Palaeoclimatology, Palaeoecology 211, 19–43.

Keller, G., and Pardo, A. 2004a. Age and paleoenvironment of the Cenomanian–Turonian global stratotype section and point at Pueblo, Colorado. Marine Micropaleontology 51, 95–128.

Kennedy, W.J., Walaszczyk, I., and Cobban, W.A. 2005. The global boundary stratotype section and point for the base of the Turonian stage of the Cretaceous: Pueblo, Colorado, U.S.A. Episodes, 28, 93–104.

Keupp, H. 1987. Die kalkigen Dinoflagellaten–Zysten des Mittelalb bis Untercenoman von Escalles/Boulonnais (N–Frankreich). Facies 16, 37–88.

Keupp, H. 1991. Kalkige Dinoflagellatenzysten aus dem Eibrunner Mergel (Cenoman–Turon–Grenzbereich) bei Abbach/ Su¨ ddeutschland. Berliner Geowissenschaftliche Abhandlungen A 134, 127–145.

Khazaei, A.R., Skelton, P.W., and Yazdi, M. 2010. Maastrichtian rudist fauna from Tarbur Formation (Zagros region, SW Iran). Preliminary observations. In: Özer, S., Sarı, B., Skelton, P.W. (eds.), Jurassic–Cretaceous rudists and carbonate platforms, Part (A), 8 th International Rudist Congress, Turkish Journal of Earth Sciences, 19, 703–719.

Koop, W., and Stoneley, R. 1982. Subsidence History of the Middle East Zagros Basin, Permian to Recent. Philosophical Transactions of the Royal Society A, 305, 149–168.

Korbar, T., Fucek, L., Husinec, A., Vlahovic, I., Ostric, N., Maticec, D., and Jelaska, V. 2001. Cenomanian carbonate facies and rudists along shallow intraplatform basin margin –the Island of Cres (Adriatic Sea, Croatia). Facies 45, 39–58.

Kowallis, B.J., Christiansen, E.H., Deino, A.L., Kunk, M.J., and Heaman, L.M. 1995. Age of the Cenomanian–Turonian boundary in the Western Interior of the United States: Cretaceous Research, 16, 109–129.

Köylüoğlu, M. 1986. Chronostratigraphy, microfacies and microfossils of the autochthonous units of the SE Anatolia. TPAO Exploration Group, Report No: 1986.

Kuhnt, W., Herbin, J.P., Thurow, J., and Wiedmann, J. 1990. Distribution of Cenomanian–Turonian organic facies in the Western Mediterranean and along the adjacent Atlantic margin, in: Huc, A.Y. (eds.) Deposition of Organic Facies. AAPG Studies in Geology 30, 133–160.

Kuhnt, W., Nederbragt, A., and Leine, L. 1997. Cyclicity of Cenomanian–Turonian organic carbon–rich sediments in the Tarfaya Atlantic coastal basin (Morocco). Cretaceous Research 18, 587–601.

Kuhnt, W., Luderer, F., Nederbragt, S., Thurow, J., and Wagner, T. 2005. Orbital–scale record of the late Cenomanian–Turonian oceanic anoxic event (OAE 2) in the Tarfaya Basin (Morocco). Int. J. Earth Sci. (Geol. Rundsch.), 94, 147–159.

Kuhnt, W., A.E. Holbourn, S. Beil, M. Aquit, T. Krawczyk, S. Flogel, E.H. Chellai, and H. Jabour, 2017. Unraveling the onset of Cretaceous Oceanic Anoxic Event 2 in an extended sediment archive from the Tarfaya–Laayoune Basin, Morocco. Paleoceanography, 32, 923–946.

Laviano, A., Maresca, M.G., and Tropeano, M. 1998a. Stratigraphic organization of rudist biogenic beds in the Upper Cenomanian successions of the western Murge (Apulia, southern Italy). In: Masse, J.P., Skelton, P.W. (eds.), Quatrieme Congres International sur les Rudistes. Geobios, Memoire Speciale 22, 159–168.

Laviano, A., Sirna, G., and Facchini, G. 1998b. Rudist facies distribution in the centralesouthern Apennines and Apulia, Italy. In: Masse, J.P., Skelton, P.W. (eds.), Quatrieme Congres International sur les Rudistes. Geobios, Memoire Speciale 22, 169–180.

Leckie, R.M. 1987. Paleoecology of mid–Cretaceous Planktonic foraminifera: A comparison of open sea and Epicontinental Sea assemblages: Micropaleontology, 33, 164–176.

Leckie, R.M., Yuretrich R.F., West O.L.O., Finnkelstein D., and Schmidt T.M. 1998. Paleoceanography of the southwestern Western Interior Sea during the time Cenomanian–Turonian boundary (Late Cretaceous), in Dean, W., Arthur, M.A. (eds.), Stratigraphy and Paleoenvironments of the Cretaceous Western Interior Seaway, Society of Economic Paleontologists and Mineralogists, Concepts in Sedimentology and Paleontology, 6, 101–126.

Leckie, R.M., Bralower T.J., and Cashman R. 2002. Oceanic anoxic events and plankton evolution: Biotic response to tectonic forcing during the mid–Cretaceous: Paleoceanography, 17, 3, 13–27.

Loeblich Jr., A.R., and Tappan, H. 1988. Foraminiferal genera and their classification. Van Nostrand Reinhold Company, New York, 970 p.

Lombard, A. 1937. Microfossiles d'attribution incertaine du Jurassique supérieur alpin. Eclogae Geol Helv 30, 320–331.

Lombard, A. 1945. Attribution de microfossiles du Jurassique supérieur alpin à des Chlorophycées. Eclogae. Geol. Helv. 38, 163–173.

Longman, M.W. 1980. Carbonate diagenetic textures from nearsurface diagenetic environments. American Association of Petroleum Geologists Bulletin 64 461–487.

Longman, M, 1982. Carbonate diagenesis as a control on stratigraphic traps (with examples from the Williston Basin): AAPG Education Course Note Series No. 21. Tulsa, Oklahoma.

Lowery, C.M., and Leckie, R.M. 2017. Biostratigraphy of the Cenomanian–Turonian Eagle Ford Shale of South Texas. Journal of Foraminiferal Research, 47, 105–128.

Lucena Santiago, G., 2014. Revision de la fauna de rudistas de les Collades de Basturs (Lleida, Pirineos Centro–Meridionales). Unpubl. PhD Thesis. Universitat Autonoma de Barcelona, Bellaterra, 290 p.

Lucia, F.J. 1995. Rock–fabric petrophysical classification of carbonate pore space for reservoir characterization. Bulletin of the American Association of Petroleum Geologists, 79, 1275–1300.

Macé–Bordy, J. 2007. Revision des rudistes cretaces (Bivalvia) de la Paleontologie Française d'Alcide d'Orbigny. Deuxieme partie. Annales de Paleontologie 93, 67–105.

Machel, H.G. 2004. Concept and models of dolomitization: a critical reappraisal. In C.J. Braithwaite, G. Rizzi and G. Darke (editors), The geometry and petrophysics of dolomite hydrocarbon reservoir. Geological Society of London Special Publication no. 235, 7–63.

Marino, M., and Santantonio, M. 2010. Understanding the geological record of carbonate platform drowning across rifted Tethyan margins: examples from the Lower Jurassic of the Apennines and Sicily (Italy). Sedimentary Geology, 225, 116–137.

Markello, J.R., Koepnick, R. B., Waite, L. E., and Collins, J. F. 2008. The carbonate analogs through time (catt) hypothesis and the global atlas of carbonate fields—a systematic and predictive look at phanerozoic carbonate systems. Controls on Carbonate Platform and Reef Development SEPM Special Publication No. 89.

Marschner, H. 1968. Relationship between carbonate grain size and non–carbonate content in carbonate sedimentary rocks. In: Recent developments in carbonate sedimentology in Central Europe. Springer Verlag, 55–57.

Marzouk, A.M., and Lüning, S. 1998. Comparative biostratigraphy of calcareous nannofossils and planktonic foraminifera in the Paleocene of Eastern Sinai, Egypt. Neues Jahrbuch für Geologie und Paläontologie, 207, 77–105.

Masse, J.P., and Masse, M.F. 2011. Drowning discontinuities and stratigraphic correlation in platform carbonates. The late Barremian–early Aptian record of southeast France. Cretaceous Research, 32, 659–684.

Meriç, E., Oktay, F.Y., Toker, V., Tansel, İ., and Duru, M. 1987. Sedimentary geology and biostratigraphy (foraminifera, nannoplankton and ostracods) of the Upper Cretaceous–Eocene sequence in the Adıyaman area, southeast Turkey, Turkish Geological Society Bulletin, 30, 19–32.

Mülayim, O. 2013. Microfacies analysis, depositional environments and sequence stratigraphy of the Late Cretaceous Karababa and Derdere formations in the Cemberlitas oilfield, Adıyaman, southeastern Turkey. MSc Thesis, University of Alabama, Tuscaloosa, AL, USA.

Mülayim, O., Mancini, E., Çemen, İ., and Yilmaz, İ. Ö, 2016. Upper Cenomanian–Lower Campanian Derdere and Karababa formations in the Çemberlitaşoil field, southeastern Turkey: their microfacies analyses, depositional environments, and sequence stratigraphy. Turkish Journal of Earth Sciences, 25, 46–63.

Mülayim, O., Yilmaz, İ.Ö., and Ferre, B. 2018. Roveacrinid microfacial assemblages (Roveacrinida, Crinoidea) from the Lower–Middle Cenomanian of the Adıyaman area (SE Turkey). Arabian Journal of Geosciences, 11, 545.

Mülayim, O., Yilmaz, I.Ö., Sarı, B., Taslı, K., and Wagreich, M. 2019a. Cenomanian–Turonian drowning of the Arabian Carbonate Platform, the İnişdere section, Adıyaman, SE Turkey. In: Wagreich, M., Hart, M.B., Sames, B., Yilmaz, I.O. (eds.), Cretaceous climate events and shorteterm sea–level changes. Geological Society of London, Special Publication.

Mülayim, O., Yilmaz, İ.Ö., Sarı, B., and Taslı, K. 2019b. Carbon–isotope stratigraphy of the Cenomanian–Turonian carbonate succession of the Türkoğlu section (SE Turkey): implications for the timing of Late Cretaceous sea–level rise and anoxic event. IESCA 2019, Conference Abstracts.

Mülayim, O., Yılmaz, İ.Ö., Özer, S., Sarı, B., and Taslı, K. 2020. A Cenomanian–Santonian rudist–bearing carbonate platform on the northern Arabian Plate, Turkey: facies and sequence stratigraphy. Cretaceous Research, 110.

Naili, H., Belhadj, Z., Robaszynski, F. and Caron, M. 1995. Présence de roches mère à faciès Bahloul vers la limite Cénomanien–Turonien dans la région de Tébessa (Algérie orientale). Notes du Service Géologique de Tunisie, 61, 1–12.

Navarro, V., Molina, J.M., and Ruiz–Ortiz, P.A. 2009. Filament lumachelle on top of Middle Jurassic oolite limestones: event deposits marking the drowning of a Tethysian carbonate platform (Subbetic, southern Spain). Facies, 55, 89–102.

Nederbragt, A.J., and Fiorentino, A. 1999. Stratigraphy and paleoceanography of the Cenomanian–Turonian boundary event in Oued Mellegue, northwestern Tunisia. Cretaceous Research, 20, 47–62.

Negra, M. H., Zagrarni, M. F., Hanini, A., and Strasser, A. 2011. The filament event near the Cenomanian–Turonian boundary in Tunisia: filament origin and environmental signification. Bulletin Society of Géologist, France. 182, 6, 507–519.

Nishi, H., Takashima, R., Hatsugai, T., Saito, T., Moriya, K., Ennyu, A., and Sakai, T. 2003. Planktonic foraminiferal zonation in the Cretaceous Yezo Group, Central Hokkaido, Japan. Journal of Asian Earth Sciences, 21, 867–886.

Norris, R.D., and Wilson, P.A. 1998. Low–latitude seasurface temperatures for the mid–Cretaceous and the evolution of planktonic foraminifera. Geology, 26, 823–826.

Okay, A. I., and Tüysüz, O. 1999. Tethyan sutures of northern Turkey. In: Durand. B., Jolivet, L., Horvath, E and Seranne, M. (eds.) The Mediterranean Basins: Tertiary Extension within the Alpine Orogen. Geological Society, London, Special Publications, J56 475–515.

Okay, A. I., Tüysüz, O., Satır, M., Özkan–Altıner, S. D. Altıner, S. Sherlock, R. H. Eren. 2006. Cretaceous and Triassic subduction–accretion, HP/LT metamorphism and continental growth in the Central Pontides, Turkey, Geol. Soc. Am. Bull., 118, 1247–1269.

Özer, S. 1988. Descriptions de quelques rudistes a canaux dans le Cenomanien de Turquie. Geologie Mediterraneanne 15, 159–167.

Özer, S. 1992. Relationships between Anatolian and Arabian plates during the Maastrichtian related to the rudist fauna. Proceedings 9th Petroleum Congress of Türkiye, 255–262.

Özer, S. 2005. Two new species of canaliculate rudists (Dictyoptychidae) from southeastern Turkey. Geobios 38, 235–245.

Özer, S. 2010a. *Dictyoptychus* Douville: taxonomy, revision, phylogeny and biogeography. In: Özer, S., Sarı, B., Skelton, P.W. (eds.), Jurassice Cretaceous rudists and carbonate platforms, Part (A), 8 th International Rudist Congress, Turkish Journal of Earth Sciences, 5, 19, 583–612.

Özer, S. 2010b. Campanian–Maastrichtian *Pseudosabinia* from Turkey: descriptions and taxonomic problems. In: Özer, S., Sarı, B., Skelton, P.W. (eds.), Jurassic–Cretaceous rudists and carbonate platforms, Part (A), 8 th International Rudist Congress, Turkish Journal of Earth Sciences, 19, 643–669.

Özer, S., and Ahmad, F. 2015. Cenomanian–Turonian rudist (Bivalvia) lithosomes from NW of Jordan. Journal of African Earth Sciences 107, 119–133.

Özer, S., and Ahmad, F. 2016. *Caprinula* and *Sauvagesia* rudist faunas (Bivalvia) from the Cenomanian of NW Jordan. Stratigraphy and taxonomy. Cretaceous Research 58, 141–159.

Özer, S., and El–Sorogy, A.S. 2017. New record of *Durania cornupastoris* (rudist) from the Campanian of the Aruma Formation, Riyadh, Saudi Arabia: description and biogeographic remarks. Journal of African Earth Sciences 129, 380–389.

Özer, S., and Kahrıman, H.H. 2019. Cenomanian canaliculated rudists (Bivalvia) from the Geyik Dağı–Hadim area (Central Taurides, S Turkey): systematic paleontology, stratigraphic importance and depositional environments. Cretaceous Research 104–161.

Özer, S., Meriç, E., Görmüş, M., and Kanbur, S. 2009. Biogeographic distributions of the rudists and benthic foraminifera: an approach to Campanian–Maastrichtian paleobiogeography of Turkey. Geobios 42, 623–638.

Özer, S., Karim, K.H., and Sadiq, D.M. 2013. First determination of rudists (Bivalvia) from NE Iraq: systematic palaeontology and palaeobiogeography. Bulletin of the Mineral Research and Exploration 147, 31–55.

Özer, S., El–Sorogy, A.S., Al–Dabbagh, M.E., and Al–Kahtany, K. 2019a. Campanian–Maastrichtian unconformities and rudist diagenesis, Aruma Formation, Central Saudi Arabia. Arabian Journal of Geosciences 12, 1–17.

Özer, S., Yilmaz, I.O., Mülayim, O., Sarı, B., Hosgör, I., and Tasli, K. 2019b. Upper Cretaceous rudist carbonate ramp facies in the SE Anatolia, Turkey: a comparison with the Arabian platform facies. In: 34th IAS Meeting of Sedimentology Conferences, Roma, Italy, 27.

Özkan, R., and Altiner, D. 2019. The Cretaceous Mardin Group carbonates in southeast Turkey: lithostratigraphy, foraminiferal biostratigraphy, microfacies, and sequence stratigraphic evolution. Cretaceous Research, 98, 153–178.

Özkaya, S. I., Dölek, T., Yapan, K., and Durukan, B.A. 2019. Controls on Fracture Flow Potential In A Tight Carbonate Reservoir: Sayindere Formation (Campanian), West Adiyaman Basin, SE Turkey. Journal of Petroleum Geology, 42 2, 207–228.

Parente, M., Frijia, G., and Di Lucia, M. 2007. Carboneisotope stratigraphy of Cenomanian–Turonian platform carbonates from the southern Apennines (Italy): a chemostratigraphic approach to the problem of correlation between Shallow–water and deep–water successions. Journal of the Geological Society London 164, 609–620.

Parlak, O., Rızaoğlu, T., and Bağcı, U. 2009. Tectonic Significance of the Geochemistry and Petrology of Ophiolites in Southeast Anatolia, Turkey. Tectonophysics, 473, 173–187.

Parrish, J. T., and Curtis, R. L. 1982. Atmospheric circulation, upwelling, and organic–rich rocks in the Mesozoic and Cenozoic eras. Palaeogeography, Palaeoclimatology, Palaeoecology 40, 31–66.

Patzkowsky, M. E., Smith, L. H., Markwick, P. J., Engberts, C. J., and Gyllenhaal, E. D. 1991. Applications of the Fujita–Ziegler paleoclimate model: Early Permian and Late Cretaceous examples. Palaeogeography, Palaeoclimatology, Palaeoecology 86, 67–86.

Paul, C.R.C., Mitchell, S.F., Marshall, J.D., Leary, P.N., Gale, A.S., Duane, A.M., and Ditchfield, P.W., 1994. Palaeoceanographic events in the Middle Cenomanian of Northwest Europe. Cretaceous Research 15, 707–738.

Pearce, M.A., Jarvis, I., and Tocher, B.A. 2009. The Cenomanian–Turonian event, OAE 2 and palaeoenvironmental change in epicontinental seas: new insights from the dinocyst and geochemical records. Palaeogeography, Palaeoclimatology, Palaeoecology, 280, 207–234.

Peck, R.E. 1943. Lower Cretaceous crinoids from Texas. J Paleontol 17 5, 451–475.

Peck, R.E. 1948. A Triassic crinoid from Mexico. J Paleontol 22 1, 81–84.

Perinçek, D., Duran, O., Bozdoğan, N., and Çoruh, T. 1991. Stratigraphy and paleogeography evolution of the autochthonous sedimentary rock in the SE Turkey (Güneydoğu Türkiye'de otokton sedimanter kayaların stratigrafisi ve paleocoğrafik evrimi). Ozan Sungurlu Symposium Proceedings 274–305.

Peryt, D., and Wyrwicka, K. 1991. The Cenomanian–Turonian anoxic event in SE Poland. Cretaceous Research 12, 65–80.

Petrizzo, M.R. 2000. Upper Turonian–lower Campanian planktonic foraminifera from southern mid–high latitudes (Exmouth Plateau, NW Australia: biostratigraphy and taxonomic notes. Cretaceous Research, 21, 479–505.

Petrizzo, M.R. 2001. Late Cretaceous planktonic foraminifera from Kerguelen Plateau (ODP Leg 183): new data to improve the Southern Ocean biozonation. Cretaceous Research, 22, 829–855.

Petrizzo, M.R. 2002. Palaeoceanographic and palaeoclimatic inferences from Late Cretaceous planktonic foraminiferal assemblages from the Exmouth Plateau (ODP Sites 762 and 763, eastern Indian Ocean). Marine Micropaleontology, 45, 117–150.

Petrizzo, M.R. 2003. Late Cretaceous planktonic foraminiferal bioevents in the Tethys and in the Southern Ocean record: an overview. Journal of Foraminiferal Research, 23, 330–337.

Philip, J. 1980. Cretace superieur de Provence. Geobios. Memoire Special 4, 99–109

Philip, J., and Airaud–Crumiere, C. 1991. The demise of the rudist–bearing carbonate platforms at the Cenomanian–Turonian boundary: a global control. Coral Reefs, 10, 115–125.

Philip, J., and Mermigis, A. 1989. Bioconstructions et plateseformes carbonatees a rudistes du Cretace superieur des zones ophiolitiques: le Massif de l'Akros (Argolide, Grece). Geologie Mediterraneenne 16, 145–153.

Pleničar, M., and Jurkovšek, B. 2000. Rudists from the Cenomanian bioherms of Hrusice and Nanos, Slovenia. Geologija 42, 69–116.

Polšak, A. 1967. Macrofaune cretacee de l'Istrie meridionale (Yougoslavie). Palaeontologica Jugoslavica 8, 1–219.

Pons, J.M., Vicens, E., and Tarlao, A. 2011. Cenomanian radiolitid bivalves from Malchina, Karst of Trieste, Italy. Cretaceous Research 32, 647–658.

Posamentier, H.W., Jervey, M.T., and Vail, P.R. 1988. Eustatic controls on clastic deposition, I. Conceptual framework. In: Wilgus, C.K., Hastings, B.S., Kensall, C.G.S.C., Posamentier, H.W., Ross, C.A., Van Wagoner, J.C. (eds.), Seaelevel changes: an integrated approach, vol. 42. Society of Economic Paleontologists and Mineralogists, Special Publication, 109–124.

Premoli Silva, I., and Sliter, W.V. 1995. Cretaceous planktonic foraminiferal biostratigraphy and evolutionary trends from the Bottaccione section, Gubbio, Italy. Palaeontograph Italy, 82, 1–89.

Premoli Silva, I., and Sliter, W.V. 1999. Cretaceous paleoceanography: evidence from planktonic foraminiferal evolution. In: Barrera, E. and Johnson, C.C. (eds.) The Evolution of the Cretaceous Ocean–Climate System. Geological Society of America, Special Papers, 332, 301–328.

Premoli Silva, I., and Verga, D. 2004. Practical Manual of Cretaceous Planktonic Foraminifera. In: Verga, D. and Rettori, R. (eds.) International School on Planktonic Foraminifera. Universities of Perugia and Milano, Tipografia Pontefelcino, Perugia, 283–462.

Razgallah, S., Philip, J., Thomel, G., Zaghbib–Turki, D., Chaabani, F., Ben Haj Ali, N., and M'Rabet, A. 1994. La limite Cenomanien–Turonien en Tunisie centrale et meridionale: biostratigaphie et paleoenvironnements. Cretaceous Research 15, 507–533.

Rider, M. H. 1996. The geological interpretation of well logs, Whittles Publishing, 280 p.

Rider, M. H. 1990. Gamma–ray log shape used as a facies indicator: critical analysis of an oversimplified methodology, Eds; Hurst, A., Lovell, M. A. and Morton, A. C., in; Geological Applications of Wireline Logs, Geological Society Special Publication, 48, .27–37.

Rigo de Righi, M., and Cortesini, A. 1964. Gravity tectonics in Foothills Structure Belt of southeast Turkey. AAPG Bulletin, 1911–1937.

Rineau, V., and Villier, L. 2018. Taxonomic revision of the genus *Ichthyosarcolites* Demarest, 1812, and description of a new canaliculate rudist from the Cenomanian of Slovenia: Oryxia sulcata gen. et sp. nov. (Bivalvia, Hippuritida). Cretaceous Research 90, 60–79.

Rivas, P., Aguırre, J., and Braga, J.C. 1997. Entolium beds: Hiatal Shell concentrations in starved pelagic settings Middle Liassic, SE Spain. Eclogae geol. Helv., 90, 293–301.

Robaszynski, F, and Caron, M. (coordinators), 1979. Atlas de Foraminiferes planctoniques du Cretace moyen. Parts 1–2. Cahiers de Micropaleontologie, 1–2, 1–181.

Robaszynski, F., Amédro, M., and Caron, M. 1993. La limite Cénomanien–Turonien et la Formation Bahloul dans quelques localités de Tunisie Centrale. Cretaceous Research 14, 477– 486.

Robaszynski, F., and Caron, M. 1995. Cretaceous planktonic foraminifera: comments on the Europe–Mediterranean zonation. Bulletin de la Société Géologique de France, 166, 681–692.

Robaszynski, F., Caron, M., Dupuis, C., Amedro, F., Gonzales Donoso, J.M., and Linares, D., 1990. A tentative integrated stratigraphy in the Turonian of Central Tunisia: formations, zones, and sequential stratigraphy in the Kalaat Senan Area. Bulletin du Centre de recherches Elf–Aquitaine, 14, 213–384.

Robaszynski, F., Zagrarni, M. F., Caron, M., and Amedro, F. 2010. The global bio–events at the Cenomanian–Turonian transition in the reduced Bahloul Formation of Bou Ghanem (central Tunisia). Cretaceous Research 31, 1–15.

Robertson, A.H.F. 1998. Mesozoic–Tertiary tectonic evolution of the Easternmost Mediterranean area: integration of marine and land based evindence. In Proceedings of the Ocean Drilling Program, Scientific Results, Robertson AHF, Emeis K-C, Richter C, Camerlenghi A (eds.).160, 723–782.

Robertson, A.H.F., Parlak, O., Yıldırım, N., Dumitrica, P., and Taslı, K. 2015. Late Triassic rifting and Jurassic–Cretaceous passive margin development of the Southern Neotethys: evidence from the Adıyaman area, SE Turkey.) Int J Earth Sci (Geol Rundsch) 105, 167–201.

Robertson, A.H.F., Boulton, S.J., Taslı, K., Yıldırım, N., Inan, N., Yıldız, A., and Parlak, O. 2016. Late Cretaceous–Miocene sedimentary development of the Arabian continental margin in SE Turkey (Adıyaman region): implications for regional palaeogeography and the closure history of southern Neotethys. Journal of Asian Earth Sciences 115, 571–616.

Rodriguez–Lazaro, J., Pascual, A., and Elorza, J. 1998. Cenomanian events in the deep western Basque Basin: the Leioa section. Cretaceous Research 19, 673–700.

Ruban, D., Al–Husseini, M., and Iwasaki, Y. 2007. Review of Middle East Paleozoic Plate tectonics. GeoArabia. 12. 35–56

Ruiz–Ortiz, P.A., Bosence, D.W.J., Rey, J., Nieto, L.M., Castro, J.M., and Molina, J. M. 2004. Tectonic control of facies architecture, sequence stratigraphy and drowning of a Liassic carbonate platform (Betic Cordillera, Southern Spain). Basin Research, 16, 235–257.

Saber, G.S., Salama, Y.F., Scott, R.W., Abdel–Gawad, G.I., and Aly, M.F. 2009. Cenomanian–Turonian rudist assemblages and sequence stratigraphy on the North Sinai carbonate shelf, Egypt. GeoArabia 14, 113–134.

Salama, Y.F., Abdel–Gawad, G.I., Saber, S.G., El–Shazly, S.H., Grammer, G.M., and Özer, S. 2016. Chemostratigraphy of the Cenomanian–Turonian shallow–water carbonate: new correlation for the rudist levels from North Sinai, Egypt. Arabian Journal of Geosciences 9, 755.

Sarı, B. 2006a. Upper Cretaceous planktonic foraminiferal biostratigraphy of the Bey Dağları autochthon in the Korkuteli area, western Taurides, Turkey. Journal of Foraminiferal Research 36, 241–261.

Sarı, B. 2006b. Foraminifera–rudist biostratigraphy, Sr–C–isotope stratigraphy and microfacies analysis of the Upper Cretaceous sequences of the Bey Dağları Autochthon (western Taurides, Turkey). Unpubl. PhD Thesis. Dokuz Eylul University İzmir, 436 p.

Sarı, B., and Özer, S. 2009. Upper Cretaceous rudist biostratigraphy of the Bey Dağları carbonate platform, western Taurides, SW Turkey. Geobios 42, 359–380.

Sarı, B., Steuber, T., and Özer, S. 2004. First record of Upper Turonian rudists (Mollusca, Hippuritoidea) in the Bey Dağları carbonate platform, Western Taurides (Turkey): taxonomy and strontium isotope stratigraphy of Vaccinites praegiganteus (Toucas, 1904). Cretaceous Research 25, 235–248.

Sarı, B., Taslı, K., and Özer, S. 2009. Benthonic foraminiferal biostratigraphy of the Upper Cretaceous (Middle Cenomanian–Coniacian) sequences of the Bey Dağları Carbonate Platform, western Taurides, Turkey. Turkish Journal of Earth Sciences 18, 393–425.

Sartorio, D., Tunis, G., Venturini, S., 1992. Open circulation facies in the Cenomanian of the northeastern margin of the Friuli Platform: the Iudrio Valley Case (NE Italy). Geologia Croatica 45, 87–93.

Saıdi, F., Ben Ismaıl, M.H., and M'Rabet, A., 1997. Le Turonian de Tunisie centro–occidentale: facies, paleogeographie et stratigraphie sequentielle dune plate–forme carbonatee ennoyee. Cretaceous Research 18, 63–85.

Schlager, W. 1981. The paradox of drowned reefs and carbonate platforms. Geological Society of America Bulletin, 92, 197–211.

Schlager, W. 1989. Drowning unconformities on carbonate platforms. In: Crevello, R.D., Sarg, J.F., Read, J.F. Wilson, J.L. (eds.) Controls on Carbonate Platform to Basin Development. Society of Economic Paleontologists and Mineralogists, Los Angeles, Special Publications, 44, 15–25.

Schlager, W. 1991. Depositional bias and environmental change important factors in sequence stratigraphy. Sedimentary Geology, 70, 109–130.

Schlager, W. 1992. Sedimentology and Sequence Stratigraphy of Reefs and Carbonate Platforms. American Association of Petroleum Geologists, Tulsa, OK, Continuing Education Course Note Series, 34.

Schlager, W. 1993. Accommodation and supply + a dual control on stratigraphic sequences. Sedimentary Geology, 86, 111–136.

Schlager, W, and Camber, O. 1986. Submarine slope angles, drowning unconformities and self–erosion of limestones escarpments. Geology, 14, 762–765.

Schlanger, S.O., and Jenkyns, H.C. 1976. Cretaceous oceanic anoxia events: causes and consequences. Geologie en Mijnbouw, 55, 179–184.

Schlanger, S.O., Arthur, M.A., Jenkyns, H.C., and Scholle, P.A. 1987. The Cenomanian– Turonian Oceanic Anoxia Event. I. Stratigraphy and distribution of organic carbon–rich beds and the marine d13C excursion. In: Brooks, J. and Fleet, A.J. (eds.) Marine and Petroleum Source Rocks. Geological Society, London, Special Publications, 26, 371–399.

Schneider, H.L. 1987. Zur Kelchmorphologie und Systematik der Roveacrininae PECK, 1943 (Crinoidea, Oberkreide). Neues Jb Geol Paläontol Abh 175, 181–206.

Schneider, H. L. 1989. Zur Morphologie und Ontogenese von Roveacrinus geinitzi n. sp. (Crinoidea, Oberkreide). Neues Jb Geol Paläontol Abh 178, 167–181.

Scholle, P.A. 1974. Diagenesis of Upper Cretaceous chalks from England, Northern Ireland and the North Sea, in Hsu, K.J., and Jenkyns, H.C., eds., Pelagic Sediments: on Land and under the Sea: Oxford, International Association of Sedimentologists Special Publication 1, 177–210.

Scholle, P.A. 1977. Chalk diagenesis and its relation to petroleum exploration: oil from chalks, a modern miracle? American Association of Petroleum Geologists Bulletin 61, 982–1009.

Scholle, P. A., and Arthur, M. A. 1980. Carbon isotope fluctuations in Cretaceous pelagic limestones: potential stratigraphic and petroleum exploration tool. American Association of Petroleum Geologists Bulletin, 64 1, 67–87.

Schulze, F., Lewy, Z., Kuss, J., and Gharaibeh, A. 2003. CenomanianeTuronian carbonate platform deposits in west central Jordan. International Journal of Earth Sciences (Geologische Rundschau) 92, 641–660.

Schulze, F., Marzouk, A., Bassiouni, M.A.A., and Kuss, J. 2004. The upper Albian to Turonian carbonate platform succession of west central Jordanestratigraphy and crisis. Cretaceous Research 25, 709–737.

Schulze, F., Kuss, J., and Marzouk, A. 2005. Platform configuration, microfacies and cyclicities of the upper Albian to Turonian of westecentral Jordan. Facies 50, 505–527.

Scotese, C. R. 2014. Atlas of Late Cretaceous Maps, PALEOMAP Atlas for ArcGIS, volume 2, The Cretaceous, Maps 16–22, Mollweide Projection, PALEOMAP Project, Evanston, IL.

Scott, R.W., Root, S.A., Tenery, J.H., and Nestell, M. 1977. Morphology of the Cretaceous microcrinoid Poecilocrinus (Roveacrinidae). J Paleontol 51, 343–349.

Scott, R.W. 1990. Models and stratigraphy of mid–Cretaceous reef communities, Gulf of Mexico. Society of Economic Paleontologists and Mineralogists, Concepts–in Sedimentology and Paleontology 2, 102.

Sharland, P. R., Archer, R., Casey, D.M., Davies, R.B., Hall, S.H., Heward, A.P., Horbury, A.D., and Simmons, M.D. 2001. Arabian plate sequence stratigraphy, vol. 2. GeoArabia, Special Publication 371 p.

Sharland, P.R., Casey, D.M., Davies, R.B., Simmons, M.D., and Sutcliffe, O.E. 2004. Arabian plate sequence stratigraphy revisions to SP2. GeoArabia 9, 199–214.

Sibley, D. F., and Gregg, J.M. 1987. Classification of dolomite rock textures. Journal of Sedimentary Petrology, 57, 967–975.

Simmons, M.D., Vicedo, V., Yilmaz, İ. Ö., Hoşgör, İ., Mülayim, O., and Sarı, B., 2020. Micropalaeontology, Biostratigraphy and Depositional Setting of the Mid–Cretaceous Derdere Formation at Derik, South–East Turkey. Journal of Micropaleontology. (In press).

Sinanoğlu, E., and Erkmen, U. 1980. Güneydoğu Anadolu Apsiyen–Aptiyen palinostratgirafisi ve bölgenin Alt Kretase palinoprovensleri içindeki yeri. Proceedings of Fifth petroleum congress of Turkey. 51–59.

Sissingh, W. 1977. Biostratigraphy of Cretaceous calcareous nannoplankton. Geologie en Mijnhomv, 56, 37–50.

Skelton, P.W., and Gili, E. 2002. Palaeoecological classification of rudist morphotypes. In: Proceedings of the 1 st International Conference of Rudists, Belgrad 1988. Serbian Geological Society, Special Publication, 265–287.

Slišković, T. 1966. Zwei neue Arten der Gattung Ichthyosarcolites aus der Oberkreide (Ablagerungen der Südherzegowina). Conseil des Academies des Sciences et des Arts de la RSF de Yougoslavie. Bulletin scientifique A12, 177–178.

Sliter, W.V. 1989. Biostratigraphic zonation for Cretaceous planktonic foraminifera examined in thin–section. Journal of Foraminiferal Research, 19, 1–19.

Soylu, C., Yalçın, M.N., Horsfield, B., Schenk, H.J., and Mann, U. 2005. Hydrocarbon Generatıon Habıtat of Two Cretaceous Carbonate Source Rocks in SE Turkey. Journal of Petroleum Geology, 28, 67–82.

Spadini, A. R., Esteves, F. R., Dias–Brito, D., Azevedo, R. L. M., and Rodrigues, R. 1988. The Macae´ Formation, Campos Basin, Brazil: its evolution in the context of the initial history of the South Atlantic. Revista Brasileira de Geociencias 18, 261–272.

Stampfli, G. and Borel, G.D. 2002. A plate tectonic model for the Paleozoic and Mesozoic constrained by dynamic plate boundaries and restored synthetic oceanic isochrons. Earth and Planetary Science Letters. 196 p.

Steuber, T. 1999. Cretaceous rudists of Boeotia, central Greece. Special Papers in Palaeontology 61, 1–229.

Steuber, T. 2002. Web Catalogue of the Hippuritoidea (rudist bivalves). http://www.paleotax.de/rudists/index.htm.

Steuber, T., Özer, S., Schlüter, M., and Sarı, B. 2009. Description of *Paracaprinula syriaca* Piveteau (Hippuritoidea, Plagioptychidae) and a revised age of ophiolite obduction on the African–Arabian Plate in southeastern Turkey. Cretaceous Research 30, 41–48.

Stocklin, L. and Setudehnia, A.O. 1972. Lexique Stratigraphique internationale de l' Iran; 3, 9b, 311.

Stössel, I., and Bernouilli, D. 2000. Rudist lithosome development on the Maiella carbonate platform magrin. In: Insalaca, E., Skelton, P.W., Palmer, T.J. (eds.), Carbonate platform systems: components and interactions, Geological Society, London, Special Publication, 177–190.

Sulli, A., and Interbartolo, F. 2016. Subaerial exposure and drowning processes in a carbonate platform during the Mesozoic Tethyan rifting: the case of the

Jurassic succession of Western Sicily (central Mediterranean). Sedimentary Geology, 331, 63–77.

Summerhayes, C.P. 1987. Organic–rich Cretaceous sediments from the North Atlantic. In: Marine petroleum source rocks (eds. by Brooks, J., Fleet, A. J.,). Geological Society of London Special Publication 26, 301–316.

Sungurlu, O. 1974. Geology of the northern part of Petroleum district–Vl). In: Okay, H. and Dilekôz, E. (eds.) 2nd Petroleum Congress of Turkey, Proceedings, Ankara, Turkey. Turkish Association of Petroleum Geologists, Ankara, 85–107.

Şenel, M. 2002. 1/500000 scaled geology map of Turkey, Adana sheet. Ankara, Turkey: General Directorate of Mineral Research and Exploration.

Şengör, A.M.C., and Yılmaz, Y. 1981. Tethyan evolution of Turkey: a plate tectonic approach. Tectonophysics 75, 181–241.

Tardu, T. 1991. A sequence stratigraphic approach to the Mardin Group: tectonics and hydrocarbon potential of Anatolia and surrounding regions. In: Proceedings of Ozan Sungurlu Symposium. Turkish Association of Petroleum Geologists, Ankara, 306–332.

Thorne, J.A. 1992. An analysis of the implicit assumptions of the methodology of seismic sequence stratigraphy. In: Watkins, J.S., Kenneth, F.Z. Mcmillen, J. (eds.) Geology Geophysical Continental Margins. American Association of Petroleum Geologists, Texas, Memoirs, 53, 375–394.

Thurow, J., Brumsack, H.J., Rullkötter, J., Litke, R., and Meyers, P. 1992. The Cenomanian–Turonian boundary event in the Indian Ocean–a key to understand the global picture, In Duncan, R.A., Rea, D.K., Kidd, R.B., von Rad, U., Weissel, J.K. (eds.), The Indian Ocean: A Synthesis of Results from the Ocean Drilling Program. American Geophysical Union, Geophysical Monograph 70, 253–273.

Toucas, A. 1907. Etudes sur la classification et sur l'evolution des Radiolitides. Premiere partie: Agria et Praeradiolites. Memoires de la Societe geologique de France 36 (14), 5–46.

Troya, L., Vicens, E., Pons, J. M., and Lucena, G. 2011. Cenomanian rudists from platform margin to lower slope settings, p. 18. Sant GervaseSopeira area, south–central Pyrenees, Spain. In: The Ninth International Congress on Rudist Bivalves, Kingston, Jamaica. Abstracts, Articles and Field Guides.

Troya Garcia, L. 2015. Rudistas (Hippuritida, Bivalvia) del Cenomaniense–Coniaciense (Cretacico superior) del Pirineo meridionalecentral. Paleontologia i biostratigrafia. Unpubl. PhD thesis. Universitat Autonoma de Barcelona, Bellaterra, 497 p.

Tucker, M.E., and Wright, V.P. 1990. Carbonate Sedimentology. Blackwell, Oxford, 482 p.

Tuna, D. 1974. Lithostratigraphic nomenclature of units of Districts VI, SE Turkey. Proceedings of 2nd Turkish Petroleum Congress, Ankara, Turkey 183–187.

Tunis, G., Özer, S., Radoicic, R., Sasaran, L., Tarlao, A., and Tentor, M. 2013. The state of the knowledge of the genus Pseudopolyconites. Caribbean Journal of Earth Science 45, 107–118.

Useche, F.N., Canet, C, Barragán, R., and Alfonso, P. 2016. Bioevents and redox conditions around the Cenomanian–Turonian anoxic event in Central Mexico. Palaeogeography, Palaeoclimatology, Palaeoecology 449, 205–226.

Usta, D., Ateş, Ş., Beyazpirinç, M., and Kanar, F. 2015. New Data on the Stratigraphy of the Central and Northern Amonous Mountains (Osmaniye–Gaziantep–K. Maraş), TAPG Bulletin, 27, 1, 57–98.

Uzunçimen, S., Tekin, U.K., Bedi, Y., Perinçek, D., Varol, E., and Soycan, H. 2011. Discovery of the Late Triassic (Middle Carnian–Rhaetian) radiolarians in the volcano–sedimentary sequences of the Koçali Complex, SE Turkey: correlation with the other Tauride units. Journal of Asian Earth Sci 40, 180–200.

Vail, P. R., Audemard, F., Bowman, S.A., Eisner, P.N., and Perez–Cruz, C. 1991. The stratigraphic signatures of tectonics, eustasy and sedimentology–an overview. In: Einsele, G., Ricken, W., Seilacher, A. (eds.), Cycles and events in stratigraphy. Springer–Verlag, Berlin, 617–659.

Van Buchem, F.S.P., Razin, P., Homewood, P.W., Oterdoom, W. H., and Philip, J. 2002. Stratigraphic organization of carbonate ramps and organic–rich intrashelf basins: Natih Formation (Middle Cretaceous) of northern Oman. AAPG Bull., 86, 21–53.

Varol, E., Bedi, Y., Tekin, U.K., and Uzunçimen, S. 2011. Geochemical and petrological characteristics of Late Triassic basic and volcanic rocks from the Koçali Complex, SE Turkey: implications for the Triassic evolution of Southern Tethys. Ofioliti 36, 101–115.

Velić, I. 2007. Stratigraphy and palaeobiogeography of Mesozoic benthic foraminifera of the Karst Dinarides (SE Europe). Geologica Croatica, 60, 1–113.

Verniory, R. 1954. Eothrix alpina Lombard, Algue ou Crinoïde? Arch Sci Geneva 7 (4): 327.

Verniory, R. 1955. Extension géographique et stratigraphique du genre Saccocoma Agassiz dans le Dauphiné méridional et en Provence. Arch Sci Geneva 8, 225–226.

Verniory, R. 1956. La création du genre Lombardia Brönnimann est–elle justifiée? Arch Sci Geneva 9 (1), 86.

Verniory, R. 1960. Présence (et variétés) de Saccocoma tenella Goldfuss à Talloires (Haute–Savoie). Arch Sci Geneva 13, 250–257.

Verniory, R. 1961. Présence de Saccocoma quenstedti Doreck (in coll.) dans les gorges de la Méouge (Sisteron Provence). Arch Sci Geneva 14, 315–320.

Verniory, R. 1962. Une nouvelle forme de Saccocoma (Montbrand, Hautes–Alpes, France). Arch Sci Geneva 15, 391–397.

Villain, J. M. 1975. ‘‘Calcispherulidae’’ (incertae sedis) du Cretace´ superieur du Limbourg (Pays–Bas), et d’autre regions. Palaeontographica A 149, 193–242.

Voigt, S., and Hilbrecht, H. 1997. Late Cretaceous carbon isotope stratigraphy in Europe: Correlation and relations with sea–level and sediment stability. Palaeogeography, Palaeoclimatology, Palaeoecology 134, 39–60.

Voigt, A., Gale, A.S., and Voigt, T. 2006. Sea–level change, carbon cycling and palaeoclimate during the Late Cenomanian of northwest Europe: an integrated palaeoenvironmental analysis. Cretaceous Research 27, 836–858.

Wagner, C., and Pehlivanlı, M. 1987. Geological control in the distribution of source rocks reservoirs in upper Cretaceous carbonates of southeast Turkey. J Petrol Sci Eng 2: 105–114.

Wagner, T., Sinninghe Damste, J., Hofmann, P., and Beckmann, B. 2004. Euxinia and primary production in Late Cretaceous eastern equatorial Atlantic surface waters fostered orbitally driven formations of marine black shales. Volume Paleoceanography 19, 4.

Wan, X., Wıgnall, P.B., and Zhao, W. 2003. The Cenomanian–Turonian extinction and oceanic anoxic event: evidence from southern Tibet. Palaeogeography, Palaeoclimatology, Palaeoecology 199, 283–298.

Waples, D.W. 1983. Reappraisal of anoxia and organic richness, with emphasis on Cretaceous of North Atlantic. American Association of Petroleum Geologists Bulletin, 67, 963–978.

Weissert, H., Lini, A., Föllmi, K.B., and Kuhn, O. 1998. Correlation of early cretaceous carbon isotope stratigraphy and platform drowning events: a possible link? Palaeogeography, Palaeoclimatology, Palaeoecology, 137, 189–203.

Wendler, J.E., Gräfe K.U., and Willems, H. 2002a. Reconstruction of mid Cenomanian orbitally forced paleoenvironmental changes based on calcareous dinoflagellate cysts: Palaeogeography, Palaeoclimatology, Palaeoecology, 179, 19–41.

Wendler, J.E., Gräfe, K.U., and Willems, H. 2002b, Paleoecology of calcareous dinoflagellate cysts in the mid–Cenomanian Boreal Realm: implications for the reconstruction of paleoceanography of the NW European shelf sea: Cretaceous Research, 23, 213–229.

Wendler, J., and Willems, H. 2004. Pithonelloid wall–type of the Late Cretaceous calcareous dinoflagellate cyst genus *Tetratropis*. Review of Palaeobotany and Palynology 129, 133– 140.

Wendler, J.E., Lehmann, J., and Kuss, J. 2010. Orbital time scale, intra–platform basin correlation, carbon isotope stratigraphy and sea–level history of the Cenomanian–Turonian Eastern Levant platform, Jordan. In: Homberg, C. and Bachmann, M. (eds.) Evolution of the Levant Margin and Western Arabia Platform Since the Mesozoic. Geological Society, London, Special Publications, 341, 171–186.

Wiese, F., Zobel K., and Keupp, H. 2015. Calcareous dinoflagellate cysts and the Turonian nutrient crisis –Data from the upper Turonian of the Lower Saxony Basin (northern Germany). Cretaceous Research 56 673–688.

Wilmsen, M. 2003. Sequence stratigraphy and palaeoceanography of the Cenomanian Stage in northern Geremany. Cretaceous Research 24, 525–568.

Wohlwend, S., Hart, M., and Weissert, H. 2016. Chemostratigraphy of the Upper Albian to mid–Turonian Natih Formation (Oman) – how authigenic carbonate changes a global pattern. The Depositional Record, 2, 97–117.

Yılmaz, I. Ö, Altiner, D., Tekin, U. K., Tuysuz, O., Ocakoğlu, F., and Açıkalın, S. 2010. Cenomanian–Turonian Oceanic Anoxic Event (OAE 2) in the Sakarya Zone, northwestern Turkey: Sedimentological, cyclostratigraphic, and geochemical records. Cretaceous Research 31, 207–226.

Yılmaz, I.O., Hoşgör, I., Mülayim, O., Özer, S., Sarı, B., and Tasli, K. 2019. Development of pelagic phase after drowned Arabian Platform, SE Turkey. In: 34th IAS Meeting of Sedimentology Conferences, Roma, Italy, 42.

Yılmaz, Y. 1993. New evidence and model on the evolution of the southeast Anatolian Orogen. Bulletin of the Geological Society of America 105, 251–271.

Yılmaz, Y. 2011. New Data Interpretation on the Development of the Southeast Anatolian Orogenic Belt (Güneydoğu Anadolu Orojenik Kuşağının Evrimine Yeni Verilerle Yeni Bir Bakış) 18 th International Petroleum and Natural Gas Congress and Exhibition of Turkey.Abstract.

Yılmaz, E., and Duran, O. 1997. Güneydoğu Anadolu Bölgesi otokton ve allokton birimler stratigrafi adlama kılavuzu ('Lexicon' guide for stratigraphic nomenclature of the autochthonous and allochthonous units in the southeast Anatolian region). Turkish Petroleum Company, Educational Publication 31, 460 p.

Young, J. R., Bergen, J.A., Bown, P.R., Burnett, J.A., Fiorentino, A., Jordan, R.W., Kleijne, A., van Niel, B.E., Romein, A.J.T., and von Salis, K. 1997. Guidelines for coccolith and calcareous nannofossil terminology. Palaeontology 40, 875–912.

Yurtsever, T.S., Tekin, U.K., and Demirel, I H. 2003. First evidence of the Cenomanian– Turonian boundary event (CTBE) in the Alakir Çay Nappe of the Antalya Nappes, southwest Turkey. Cretaceous Research 24, 41–53.

Zagrarni, M. F., Negra, M. H., and Hanini, A. 2008. Cenomanian–Turonian facies and sequence stratigraphy, Bahloul Formation, Tunisia. Sedimentary Geology 204, 18–35.

Zügel P. 1994. Verbreitung kalkiger Dinoflagellaten–Zysten im Cenoman/Turon von Westfrankreich und Norddeutschland. Courier Forschungsinstitut Senckenberg 176, 1–159.

APPENDICES

Appendix I: Published Research Papers

Arabian Journal of Geosciences (2018) 11:545
https://doi.org/10.1007/s12517-018-3901-z

ORIGINAL PAPER



Roveacrinid microfacial assemblages (Roveacrinida, Crinoidea) from the Lower-Middle Cenomanian of the Adıyaman area (SE Turkey)

Oguz Mulayim[1] · Ismail Omer Yilmaz[2] · Bruno Ferré[3]

Received: 7 June 2018 / Accepted: 5 September 2018
© Saudi Society for Geosciences 2018

Abstract
In the northwestern part of the Arabian Platform, the Adıyaman district (SE Turkey) displays some Lower-Middle Cenomanian deep-marine sediments of the Derdere Formation. These sediments are yielding abundant echinodermal remains, among which some thecal and brachial plates are assignable to roveacrinids. Routine microfacies analysis of the Lower-Middle Cenomanian part of the Derdere Formation revealed unexpected early Cenomanian assemblages of roveacrinoidal ossicles, comparable with those formerly reported further south in the Cenomanian-Turonian of the Arabian Platform. For the first time, genuine and undisputable Roveacrinidae are illustrated for SE Turkey. Seven borehole sections were scrutinized in search of microcrinoidal sections, most especially within carbonate microfacies. Within the scope of better constraining the position of the Lower-Middle Cenomanian, we had been compiling the successive occurrence of respective identified roveacrinid remains. These roveacrinidal assemblages are consisting in: *Roveacrinus communis* Douglas (1908) (= *R. derdereensis* Farinacci & Manni); *Roveacrinus* cf. *alatus* Douglas (1908); *Roveacrinus spinosus* Peck (1943); *Roveacrinus* sp.; Roveacrinidae indet.; *Applinocrinus* sp.; and Saccocomidae indet. These specimens provide significant clues to constrain the palaeogeographic reconstruction of Tethyan seaways, and represent potential fossil index candidates for the Lower Cenomanian stratigraphy of the Adıyaman district.

Keywords Roveacrinida · Roveacrinidae · Saccocomidae · Cretaceous · Cenomanian · Turkey

Cenomanian–Turonian drowning of the Arabian Carbonate Platform, the İnişdere section, Adıyaman, SE Turkey

O. MULAYIM[1]*, O. I. YILMAZ[2], B. SARI[3], K. TASLI[4] & M. WAGREICH[5]

[1]*Turkish Petroleum Corporation, Adıyaman District Management, Adıyaman, Turkey*

[2]*Middle East Technical University, Department of Geological Engineering, Ankara, Turkey*

[3]*Dokuz Eylul University, Department of Geological Engineering, Izmir, Turkey*

[4]*Mersin University, Department of Geological Engineering, Mersin, Turkey*

[5]*University of Vienna, Department of Geodynamics and Sedimentology, Vienna, Austria*

OM, 0000-0003-3283-8070; BS, 0000-0002-2389-2772; MW, 0000-0002-8828-0857

**Correspondence: omulayim@tpao.gov.tr*

Abstract: The Cenomanian–Turonian carbonate ramp in the Adıyaman Region of SE Turkey (Northern Arabian Platform) records an abrupt shift from benthic carbonate deposits to pelagic deposits near the Cenomanian–Turonian boundary event (CTBE) in the İnişdere stratigraphic section and surrounding borehole sections. A positive $\delta^{13}C$ excursion of up to 2.15% is recorded in carbonate and organic carbon deposited around the CTBE and provides evidence of a direct link between the CTBE and oceanic anoxic events and the demise of the shallow carbonate production in the Derdere Formation. The microfacies analyses, biostratigraphic dating and palaeoenvironmental interpretations suggest that the platform was drowned near the CTBE as a result of changing environmental conditions. The microfacies indicating significant deepening show a contemporaneity to equivalent surfaces globally and thus strongly support an isochronous formation of Cenomanian–Turonian facies by eustatic sea-level changes. Anoxia spreading over the platform drastically reduced the carbonate production as observed in the studied sections and, therefore, resulted in a reduction in carbonate accumulation rates. Regional/local subsidence and a coeval sea-level rise during the late Cenomanian to early Turonian interval were the cause of the drowning of the platform, including regional anoxia at the northern Arabian platform linked to the Cenomanian–Turonian oceanic anoxic event (OAE2).

Carbon–isotope stratigraphy of the Cenomanian–Turonian carbonate succession of the Türkoğlu section (SE Turkey): implications for the timing of Late Cretaceous sea–level rise and anoxic event

Oğuz Mülayim [1]

İsmail Ömer Yılmaz [2]

Bilal Sarı [3]

Kemal Taslı [4]

(1) TPAO Adıyaman District Management, Geology Division, Adıyaman, Turkey
(2) Middle East Technical University, Department of Geological Engineering, Çankaya, Ankara, Turkey
(3) Dokuz Eylül University, Department of Geological Engineering, Tınaztepe, Buca, İzmir, Turkey
(4) Mersin University, Department of Geological Engineering, Yenişehir, Mersin, Turkey

E–mail: omulayim@tpao.gov.tr

ABSTRACT

A carbon–isotope stratigraphy of the upper Cretaceous shallow and deeper water Cretaceous limestones from Türkoğlu section, SE Turkey, has enabled an accurate definition of the Cenomanian–Turonian boundary. Carbon–isotope stratigraphy of this succession revealed a positive shift $\delta^{13}C$ values that reached +1,97% and represent the CTB interval excursion (OAE2). The sediments close to the boundary show pelagic influence registered by the presence of planktic foraminifera. These results spotlight the potential use of carbon isotopes as a dating and high–resolution correlative tool in shallow–water carbonate rocks and help to elucidate the timing of oceanographic events affected the area that we studied. In particular, it is suggested that the highest rate of a relative, possibly eustatic sea–level rise took place during the latest Cenomanian, that was followed by the global oceanic anoxic event during Cenomanian–Turonian boundary (CTB) interval, and that peak transgression or maximum flooding was achieved during the early Turonian in this region.

Keywords: Carbon–isotope stratigraphy, sea–level rise, Cenomanian–Turonian boundary (CTB), OAE2

Cretaceous Research 110 (2020) 104414

Contents lists available at ScienceDirect

Cretaceous Research

journal homepage: www.elsevier.com/locate/CretRes

A Cenomanian–Santonian rudist–bearing carbonate platform on the northern Arabian Plate, Turkey: facies and sequence stratigraphy

Oğuz Mülayim [a, *], İsmail Ömer Yılmaz [b], Sacit Özer [c], Bilal Sarı [d], Kemal Taslı [e]

[a] TPAO, Turkish Petroleum Corporation, Adıyaman Directorate, Adıyaman, 02040, Turkey
[b] Middle East Technical University, Department of Geological Engineering, Ankara, 06800, Turkey
[c] 6349 Sok. 9/7, Atakent–Karşıyaka, İzmir, 35540, Turkey
[d] Dokuz Eylül University, Department of Geological Engineering, Buca, İzmir, 35370, Turkey
[e] Mersin University, Department of Geological Engineering, Mersin, 33342, Turkey

ARTICLE INFO

Article history:
Received 10 September 2019
Received in revised form
5 January 2020
Accepted in revised form 5 February 2020
Available online 11 February 2020

Keywords:
Cenomanian–Santonian
Carbonate ramp
Bivalves
Mediterranean

ABSTRACT

Recent studies have shown that Cenomanian–Santonian carbonate sedimentary rocks rich in rudists are widespread throughout southeastern Turkey. The Derdere and Karababa formations have been analysed in the Sabunsuyu section (Kilis Province). On a field scale, we can distinguish rudist–rich beds that rhythmically alternate with bioclastic levels composed of bivalves, gastropods and roveacrinids in these formations. Although pelagic faunal elements (predominantly planktic foraminifera and pithonellids) are documented in the lowermost part of the series, the rudist–rich facies are represented mainly in the Derdere and Karababa formations. Rudists, benthic and planktic foraminifera indicate middle–late Cenomanian and Turonian–Santonian ages for the Derdere and Karababa formations, respectively. Based on studied facies, five microfacies have been recognised and categorised in three facies groups: inner ramp, mid ramp and outer ramp. Evidence such as gradual changes in facies and absence of extensive uninterrupted barrier reefs indicate that the Derdere Formation was deposited in a ramp depositional system. The sedimentology and taphonomic signature of the rudist shell beds have been described in order to obtain a better understanding of the depositional environment and the physical processes that controlled Cenomanian–Santonian sedimentation. Monospecific tabular beds characterise mainly the upper part of the series (topmost part of Derdere Formation and Karababa Formation); more complex rudist concentrations, characterised by moderate species diversity, increase upsection. The rudist levels are associated with highstand systems tract deposits because of the suitability of trophic conditions in the rudist–dominated ramp.

© 2020 Elsevier Ltd. All rights reserved.

The pithonellid calcitarchs in the Cenomanian of the Derdere Formation in the Northern Arabian Plate (SE Turkey): A paleoenvironmental significance

Turkish Journal of Earth Science 2020) in review

Mülayim, O., Yilmaz I. O., Wendler, J.

Abstract

A pithonellid calcitarchs acme has been investigated on the northern Arabian Carbonate Platform in the Adıyaman, SE Turkey. The studied interval includes organic rich limestones of the Derdere Formation. Their large quantity is interpreted as an indicator of changes in primary productivity associated with a major transgressive episode. We observed the pithonellid calcitarchs Bonetocardiella conoidea, Pithonella ovalis, and P. sphaerica which are considered to be indicators of high nutrient content under strongly fluctuating paleoenvironmental conditions. We attribute their great abundance to increased nutrient supply following the lower – middle Cenomanian global transgression which also affected the northern Arabian Carbonate Platform (SE Turkey). The blooms appear to be coeval with oceanographic change. They may reflect an event–like episode of upwelling and/or eutrophic conditions, typically found in ramp settings globally.

Filament marker beds in the Karababa–A Member (Cenomanian–Turonian boundary) of the SE Turkey: Palaeo–environmental significance, stratigraphy and correlation

Proceeding of the Geologists' Association (2020) in review

Mülayim, O., Yilmaz, I. O., Sari, B., Ferré, B

Abstract

A 'filament' event bed/level corresponds to the abundant occurrence of thin elongate shells of pelagic, bivalve or crinoidal, origin, within pelagic, laminated, and organic–matter rich limestones. These organic–rich limestones had been deposited under anoxic conditions in an outer–ramp environment. These thin elongate, bivalve shells, or crinoidal plates, are found broken in small pieces, disintegrated, or simply preserved parallel to bedding as complete specimens. Such 'filament' beds were spotted in deposits, namely the Karababa–A Member in SE Turkey, around the Cenomanian–Turonian boundary (CTB) and above. On a global scale, these filament event beds illustrate sea–level rise related to eustacy and/or climatic change. The abundance of filaments close to the CTB is a biological marker of high organic productivity resulting from a climatic change to warmer conditions. The prevailing higher sea–level conditions were then favourable to the accumulation and preservation of organic–rich facies, characteristic of the Oceanic Anoxic Event 2 (OAE 2). Using both biostratigraphic and carbon isotopic data, those deposits were dated the latest Cenomanian–earliest Turonian age. Filament event beds were recorded in the same order, except for some small differences. A good number of these bio–events are global. Consequently, at global scale, they are susceptible to constrain the C–TB with a significant degree of confidence.

CURRICULUM VITAE

PERSONAL INFORMATION

Surname, Name: Mülayim, Oğuz
Nationality: Turkish (TC)
Date and Place of Birth: 6 November 1985, Köyceğiz/Muğla
Marital Status: Married
Phone: +90 416 212 52 47
email: e199439@metu.edu.tr

EDUCATION

Degree	Institution	Year of Graduation
MS	University of Alabama Geosciences	2013
BS	DEU Geological Engineering	2009
High School	Köyceğiz Anadolu High School, Muğla	2003

WORK EXPERIENCE

Year	Place	Enrollment
2013–Present	Turkish Petroleum Corporation	Sn. Wellsite Geologist
2009–2010	Pontid Mining Co.	Exploration Geologist
2008 August	Eti Elektrometalurji Chromium Processing, Co.	Intern Geo. Student
2007 August	Komurcuoğlu Marble Co.	Intern Geo. Student

FOREIGN LANGUAGES

Advanced English, Beginner German

PUBLICATIONS

Mülayim, O., Yılmaz, I. O., Sarı, B., Ferré, B. Filament marker beds in the Karababa–A Member (Cenomanian–Turonian boundary) of the SE Turkey: Palaeo–environmental significance, stratigraphy and correlation. Proceeding of the Geologists' Association, (2020 in review)

Mülayim, O., Yilmaz I. O., Wendler, J. The pithonellids in the early–middle Cenomanian interval from Adıyaman district in the Northern Arabian Plate (SE Turkey): Paleoenvironmental significance. Turkish Journal of Earth Science, (2020 in review)

Mülayim, O., Yılmaz, İ.Ö., Özer, S., Sarı, B. and Taslı, K. A Cenomanian–Santonian rudist–bearing carbonate platform on the northern Arabian Plate, Turkey: facies and sequence stratigraphy. Cretaceous Research, 110 (2020)

Mülayim, O., Yilmaz, İ.Ö., Sarı, B., Taslı, K. and Wagreich, M., Cenomanian–Turonian drowning of the Arabian Carbonate Platform, the İnişdere section, Adıyaman, SE Turkey. In: Wagreich, M., Hart, M.B., Sames, B. and Yilmaz, İ.Ö. (eds.) Cretaceous Climate Events and Short–Term Sea–Level Changes Geological Society, London, Special Publications, 498 (2019)

Mülayim, O., Yilmaz, İ.Ö., Sarı, B., Taslı, K., Carbon–isotope stratigraphy of the Cenomanian–Turonian carbonate succession of the Türkoğlu section (SE Turkey): implications for the timing of Late Cretaceous sea–level rise and anoxic event. IESCA 2019, Conference Abstracts (2019)

Mülayim, O., Yilmaz, İ.Ö. and Ferré, B., 2018. Roveacrinid microfacial assemblages (Roveacrinida, Crinoidea) from the Lower–Middle Cenomanian of the Adıyaman area (SE Turkey). Arabian Journal of Geosciences, 11 (18), 545 (2018)

Mülayim, O., Mancini, E., Cemen, I. and Yilmaz, İ.Ö. 2016. Upper Cenomanian–Lower Campanian Derdere and Karababa formations in the Çemberlitaş oil field, southeastern Turkey: their microfacies analyses, depositional environments, and sequence stratigraphy. Turkish Journal of Earth Sciences, 25, 46–63 (2016)